ROLE OF THE LYSOSOMAL INTEGRAL MEMBRANE PROTEIN TYPE 2 (LIMP-2/SCARB2) IN LIPID TRANSPORT AND BEYOND

Dissertation

In fulfillment of the requirements for the degree “Dr. rer. nat.”
of the Faculty of Mathematics and Natural Sciences
at Kiel University

submitted by

SASKIA HEYBROCK

Kiel, August 2020

REFEREE:	Prof. Dr. Paul Saftig
CO-REFEREE:	Prof. Dr. Eric Beitz
DATE OF THESIS DEFENSE:	29th October 2020

1. Introduction

1.1. Cholesterol metabolism

Cells need different groups of macromolecules to maintain proper function and vitality. Besides proteins and carbohydrates, lipids represent an essential and diverse class of molecules that are needed for the formation of lipid bilayers separating the inside of the cell from the external environment as well was allowing the formation of sub-cellular compartments. Furthermore, many lipid species function as signaling molecules and as energy stores in the form of lipid droplets (van Meer *et al.* 2008). Lipid subgroups include fatty acids, which are also a major component of many lipid species, phospholipids, mono-, di- and triglycerides, sphingolipids and sterols, among others. Membrane lipids can be grouped into three main categories, glycerophospholipids, sphingolipids and sterols (Harayama and Riezman 2018). The sterol cholesterol is an integral structural component of all vertebrate membranes and sterol analogs exist in plants and fungi (Figure 1-1 A). This hydrophobic molecule consists of 27 carbon atoms which are arranged in four fused rings (the sterane backbone) and an aliphatic side-chain. Additionally, cholesterol contains a hydroxyl group, making this part of the molecule polar (Bloch 1965, Ohvo-Rekila *et al.* 2002). The amphipathic nature of cholesterol influences its orientation in membranes (Figure 1-1 B): in parallel to the fatty acid chains of the phospholipids and the hydroxyl group interacts with the hydrophilic head groups of neighboring phospholipids (Yeagle 2004). In membranes, cholesterol modulates membrane properties such as fluidity, curvature, permeability and function of various integral membrane proteins (Burger *et al.* 2000, Jafurulla and Chattopadhyay 2013, Levitan *et al.* 2014).

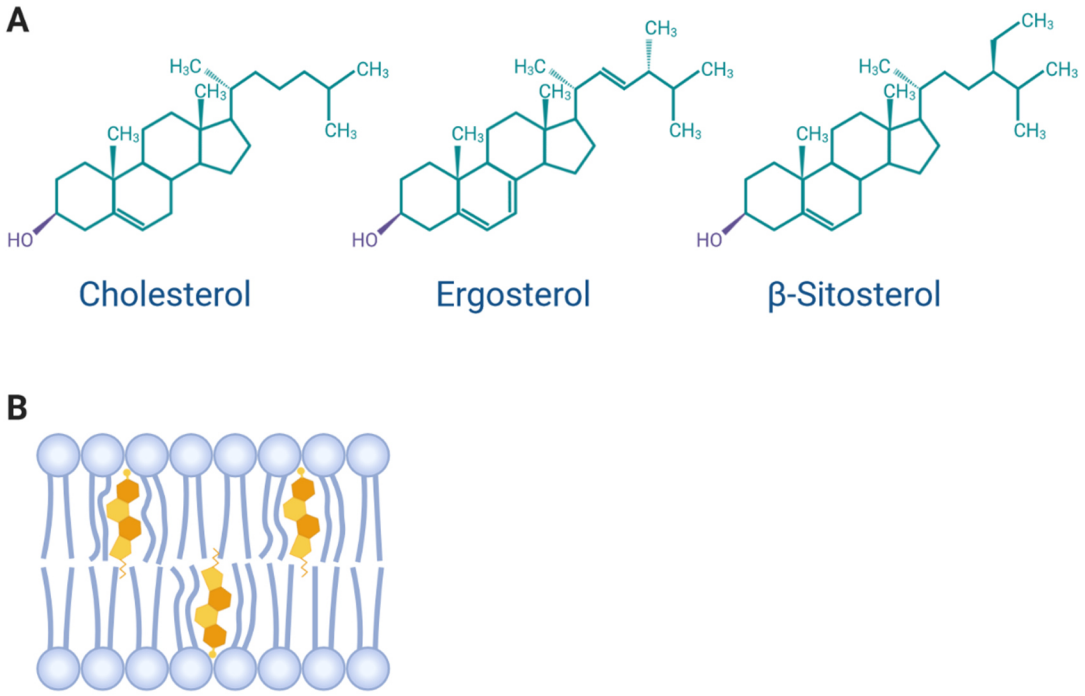

Figure 1-1: Cholesterol structure and membrane orientation A Main group of sterols in different species. Structure of cholesterol and the sterol analogs of yeast and plants, ergosterol and β-sitosterol, respectively. Ergosterol differs from cholesterol by the addition of two double bonds and one methyl group, while β-sitosterol has a modified side chain in comparison to cholesterol. Structures based on (Korber *et al.* 2017). **B** Orientation of cholesterol in the phospholipid bilayer. The polar hydroxyl group of cholesterol interacts with the head groups of the phospholipids while the steroid rings and carbon tail are buried within the unipolar center of the membrane. The presence of the bulky steroid core of cholesterol that is oriented perpendicular to the plane of the membrane disturbs the dense packing of phospholipid, thereby modifying membrane properties, i.e. increasing rigidity. Scheme based on (Berg *et al.* 2018)

Cholesterol is not distributed homogeneously throughout the different cellular membrane systems. On the contrary, as depicted in Figure 1-2, the plasma membrane harbors the majority of membranous cholesterol, 30-40 mol% of lipids (Ikonen 2018). In certain membrane microdomains, lipid rafts, cholesterol constitutes up to 50 % of the membrane lipids (Pike 2004). In the endoplasmic reticulum (ER), in contrast, cholesterol concentration exceeding a threshold of about 1-5 mol% of total ER lipids (depending e.g. on the cell type) triggers a negative feedback loop that acts on the ER-residing cholesterol sensing and regulating machinery to downregulate cholesterol uptake and de-novo synthesis (Radhakrishnan *et al.* 2008). In relation to the total cellular cholesterol pool, the ER harbors 0.5 % - 1% cholesterol (Lange and Steck 1997, Lange *et al.* 1999).

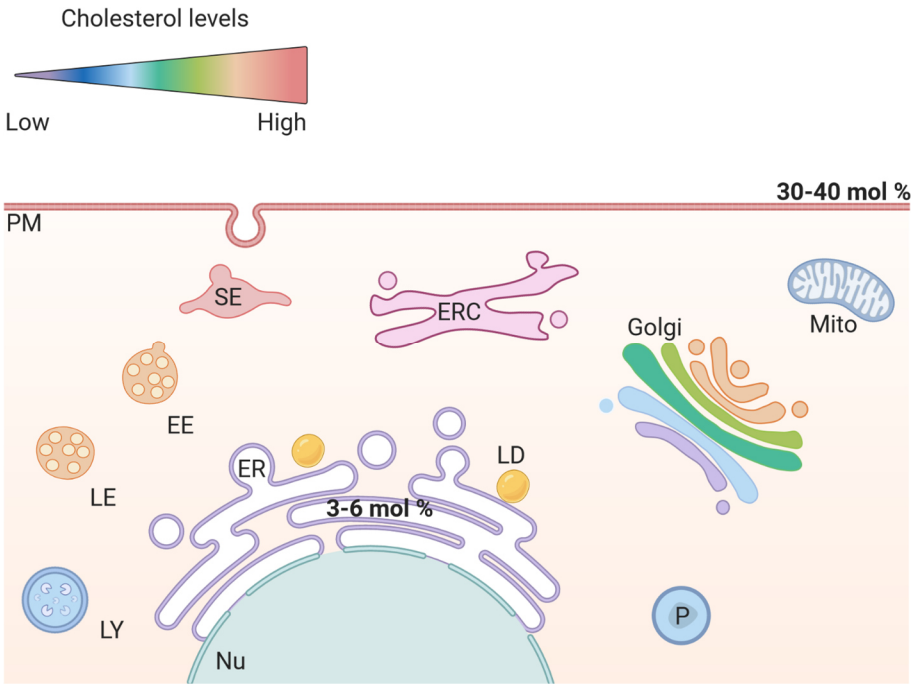

Figure 1-2: Cholesterol levels throughout cellular membranes. Cholesterol content of organelles and membranes varies. In the plasma membrane (PM), cholesterol is estimated to make up 30-40 mol% of the total lipids. Organelles that also have a high cholesterol content include the endocytic recycling compartment (ERC), sorting endosomes (SE) as well as the *trans* Golgi network, whereas *cis* Golgi, mitochondria (Mito), lysosomes (LY) and peroxisomes (P) have lower cholesterol levels. The lowest amount of cholesterol can be found in endoplasmic reticulum (ER) membranes, where 3-6 mol% of total levels consist of cholesterol. Excess cholesterol is stored in lipid droplets (LD) which bud off from the ER. EE, early endosome; LE late endosomes; Nu, nucleus. Scheme based on information provided by (Maxfield *et al.* 2016, Ikonen 2018).

As mentioned above, cholesterol is of vital importance for the cells, however, it can also be lethal if its cellular levels surpass a critical threshold. Therefore, cellular cholesterol levels underlie strict sensing and regulation. Cholesterol levels are being sensed in the ER and in response a sophisticated cellular machinery adjusts pathways regulating exogenous and endogenous cholesterol supply (Brown and Goldstein 1997, Goldstein *et al.* 2006). The transcription factor sterol-regulatory element binding protein 2 (SREBP2) is a key factor in this machinery (illustrated in Figure 1-3 A). While under conditions of ample cholesterol supply, SREBP2 is bound by ER-retention proteins sterol regulatory element-binding protein cleavage-activating protein (SCAP) and insulin-induced gene 1 (INSIG1), upon cholesterol depletion, the binding of the SCAP/SREBP2 complex to INSIG1 is removed and SCAP/SREBP2 translocates to the Golgi in COPII-coated vesicles. There, SREBP2 is sequentially cleaved by site 1 and site 2 proteases (S1P and S2P, respectively) and the emerging N-terminal fragment (nSREBP2) translocates to the nucleus where it binds to a specific DNA sequence called sterol regulatory element (SRE) in the promoter region of certain genes and thus activates the transcription of the target genes which encode proteins involved in low-density lipoprotein (LDL) uptake and endogenous cholesterol synthesis, i.e. low-density lipoprotein receptor (LDLR) and 3-hydroxy-methyl-glutaryl-COA reductase (HMGCR), respectively (see also Figure 4-12 A). Acquisition of cholesterol is accomplished by two different pathways in

mammalian cells, either by uptake from external sources or by endogenous de-novo synthesis from acetyl-CoA (Bloch 1965, Goldstein and Brown 1990), which are described in detail below.

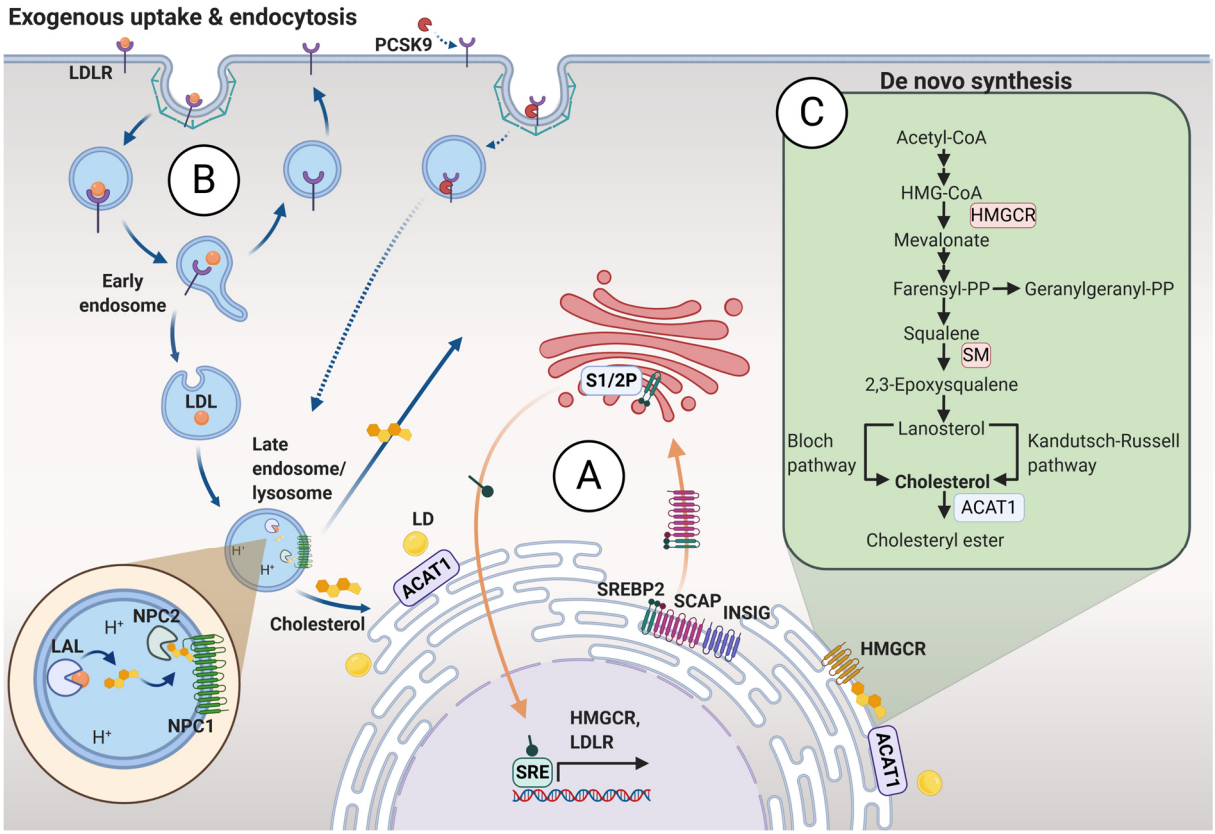

Figure 1-3: Cholesterol homeostasis underlies complex and sophisticated regulatory mechanisms. A Cholesterol levels are being sensed in the ER where the transcriptions factor sterol-regulatory element binding protein 2 (SREBP2) is being retained by sterol regulatory element-binding protein cleavage-activating protein (SCAP) and insulin-induced gene 1 (INSIG1). Low levels of cholesterol cause translocation of SREBP2 to the Golgi where it undergoes cleavage by site 1 and site 2 proteases (S1P, S2P) the resulting fragment consequently translocates to the nucleus, binds to sterol regulatory element 1 (SRE-1) and activates transcription of genes needed for re-supply of cholesterol, e.g. 3-hydroxy-methyl-glutaryl-COA reductase (HMGCR) and Low-density lipoprotein receptor (LDLR), respectively. **B** Circulating LDL particles are bound by the LDLR at the plasma membrane and the complex is endocytosed. After the ligand-receptor complex dissociates, LDLR is recycled back to the cell surface for additional rounds of LDL binding. Alternatively, it is bound by the protease proprotein convertase subtilisin/kexin type 9 (PCSK9) and both are targeted to lysosomes for degradation (dashed lines) The lipid core of LDL particle is hydrolyzed by lysosomal acid lipase (LAL) in lysosomes and cholesterol is liberated. The hydrophobic lipid is then bound by Niemann-Pick Type C2 protein (NPC2) which delivers it to the membrane protein Niemann-Pick type C1 (NPC1) for export from lysosomes. Cholesterol then redistributes to the plasma membrane as well as to the ER by mechanisms not completely elucidated, although the importance of membrane contacts has been demonstrated**. C** Cholesterol can also be synthesized in the ER from two molecules acetyl-Coenzyme A (CoA) The pathway involves more than 30 steps. Important intermediates are depicted. The rate-limiting enzymes HMGCR and squalene monooxygenase (SM) are highlighted in red. Since excess free cholesterol is toxic for the ER, it is subsequently esterified by the ER-resident protein Acyl-CoA:cholesterol acyltransferase (ACAT1) and stored in lipid droplets (LD). Scheme based on (Ikonen 2008, Luo *et al.* 2020).

1.1.1. Cellular cholesterol uptake

The bulk of the cellular cholesterol is derived from external sources like nutritional uptake or breakdown of lipoprotein particles that circulate in the blood stream. These lipoproteins exist in various compositions of protein and lipid abundances as well as size (Figure 1-4), impacting their density (Schumaker and Adams 1969). The liver synthesizes triacylglycerol (TAG)- and cholesterol-rich very low-density lipoproteins (vLDLs) which undergo conversion to

intermediate-density lipoproteins and are further modified to yield LDL. Besides their lipid content, these three lipoproteins characteristically contain apolipoprotein B (apoB) (Chen *et al.* 2019). Among these different lipoprotein particle species, LDL particles are the major type of lipoprotein circulating in the blood stream and are characterized by an enrichment of cholesterol and cholesterol esters and a diameter of 20-25 nm. Many cells express the protein LDLR which clusters in clathrin-coated pits on the cell surface (Goldstein *et al.* 1979). LDL particles bind to this receptor via apoprotein B-100 (Brown and Goldstein 1986). Recruitment of clathrin adaptor proteins like Low Density Lipoprotein Receptor Adaptor Protein 1 (LDLRAP1; only in polarized cells like hepatocytes), Disabled homolog 2 (DAB2) and adaptor protein 2 (AP-2) which recognize the endocytic sorting motif NPVY in the cytoplasmic domain of LDLR subsequently lead to clathrin-mediated endocytosis of the LDL-particle-LDLR complex (Chen *et al.* 1990, Chen *et al.* 2019). Consequently, LDL is transported along the endocytic flux towards lysosomes which are the degradation centers of the cell, the process of which is illustrated in Figure 1-3 B. The decreasing endosomal pH causes conformational changes in the LDLR which cause its dissociation from the LDL particle. The LDLR is recycled back to the plasma membrane by the endosomal recycling complex COMMD (copper metabolism MURR1 domain)– CCDC22 (coiled-coil domain containing 22)– CCDC93 (coiled-coil domain containing 93) in order to bind to additional LDL particles (Bartuzi *et al.* 2016, Fedoseienko *et al.* 2018). Alternatively, it is bound by the protease proprotein convertase subtilisin/kexin type 9 (PCSK9) which prevents its recycling to the plasma membrane, thus ensuring the degradation of LDLR (and PCSK9) in lysosomes (Lagace *et al.* 2006, Kwon *et al.* 2008, Lagace 2014). Once the LDL particles reach the acidic lysosomes, they are degraded by the enzyme lysosomal acid lipase (LAL) which liberates the lipids in the core of the LDL particles, cholesterol esters and triglycerides. LAL hydrolyzes the ester bond, creating free cholesterol (Goldstein *et al.* 1975). The hydrophobic lipid is then bound by the small soluble protein Niemann-Pick C2 (NPC2). Besides NPC2, lysosomal associated membrane protein type 1 and type 2 (LAMP1 and LAMP2) have been recently described as acceptors for free cholesterol (Li and Pfeffer 2016). In order to reach other cellular destinations like the ER, where the cholesterol sensing machinery resides, cholesterol must cross the lysosomal limiting membrane whose luminal face is lined with a thick carbohydrate layer, the glycocalyx, thus protecting it from the acidic milieu of the lysosomal lumen. The transit across this impermeable layer is facilitated with the help of the lysosomal membrane protein Niemann-Pick C1 (NPC1) which accepts cholesterol from NPC2 in a mechanism termed ‘hydrophobic hand-off’ and shuttles it across the membrane. While the molecular details of this mechanism remained enigmatic for a long time, recent crystallographic studies revealed the existence of a hydrophobic cavity connecting the N-terminal domain (NTD) and the sterol sensing domain (SSD) of NPC1(Gong *et al.* 2016, Li *et al.* 2016, Winkler *et al.* 2019). This intramolecular tunnel serves as a channel through which cholesterol is transported. As the driving force of this

transport a proton-relay network was discussed (Winkler *et al.* 2019) which could lead to pincer-like movement of cholesterol through the tunnel. Mutations in or loss of either NPC1 or NPC2 lead to critical accumulation of cholesterol and other lipids in lysosomes, thereby causing a fatal disease, Niemann Pick disease (NPC). The pathology includes hepatosplenomegaly and neurodegeneration, which is ultimately lethal (Sturley *et al.* 2004).

Upon its arrival in the lysosomal limiting membrane, cholesterol is distributed to other subcellular compartments to maintain cholesterol homeostasis. A portion of lysosomal cholesterol is rapidly trafficked to the plasma membrane, where it is needed for maintenance of structure and fluidity of the phospholipid bilayer (Brasaemle and Attie 1990, Johnson *et al.* 1990). It is estimated that approximately 30 % of LDL-derived cholesterol is directly transported to the ER (Neufeld *et al.* 1996, Underwood *et al.* 1998). Since cholesterol is insoluble in the aqueous cytoplasm, transport to these various destinations has to be accomplished by vesicular and non-vesicular pathways (Maxfield and van Meer 2010). According to recent research, non-vesicular transport involving cholesterol-transport proteins is the major pathway for cholesterol distribution (Prinz 2007, Lev 2010, Ikonen 2018). Proteins and mechanisms that are involved in these processes are describe below (1.5).

Dietary free cholesterol is absorbed in the intestine by enterocytes that line the inner surface of the gut. These specialized cells express the protein NPC1-like 1 (NPC1L1) on their apical membrane that mediates selective uptake of unesterified cholesterol via clathrin-mediated endocytosis (Brown *et al.* 2007, Ge *et al.* 2008). Cholesterol is then esterified by Acyl-CoA:cholesterol acyltransferase 2 (ACAT2) (Chang *et al.* 2001) and subsequently – together with TAGs- released to the blood and lymph as the core of chylomicrons (also referred to as ultra-low density lipoproteins, ULDL) which in turn are delivered to the liver, the main organ for cholesterol synthesis (Chen *et al.* 2019, Luo *et al.* 2020).

The liver as well as the gut also have a key role in the removal of excess cholesterol from the body. On a cellular level cholesterol efflux is mediated by members of the ATP-binding cassette (ABC) transporter family and class B scavenger receptor family member SR-BI. The ABC subfamily G members 5 and 8 (ABCG5 and ABCG8) are expressed at the apical surface of enterocytes and hepatocytes and mediate the excretion of cholesterol into the intestinal lumen and bile where it is processed into bile salts (Fitzgerald *et al.* 2010).

In peripheral tissues excess cholesterol is removed in a process called reverse cholesterol transport (Rosenson *et al.* 2012). This process involves the generation of high-density lipoprotein (HDL), which is schematically depicted in Figure 1-4. ABC subfamily A member 1 (ABCA1) is a plasma membrane-localized protein that is especially important in macrophages where it translocates cellular cholesterol to the blood (Attie 2007). Cholesterol then binds to apolipoprotein A-I (apoA-I). This leads to the generation of nascent HDL that then in turn

accepts further cholesterol leading to the maturation of HDL (Gelissen *et al.* 2006). Cholesterol-loaded HDL eventually reaches the liver where it binds the highly expressed cholesterol transporter SR-BI at the plasma membrane of hepatocytes which extracts cholesterol from HDL without internalization of HDL, this process is referred to as selective cholesterol uptake (Rigotti *et al.* 2003). As mentioned above, cholesterol is metabolized and excreted from the body via bile acids and the gut. HDL-derived cholesterol also serves as an important pre-cursor for the synthesis of steroid hormones in the adrenal glands, ovaries and testes (Hu *et al.* 2010).

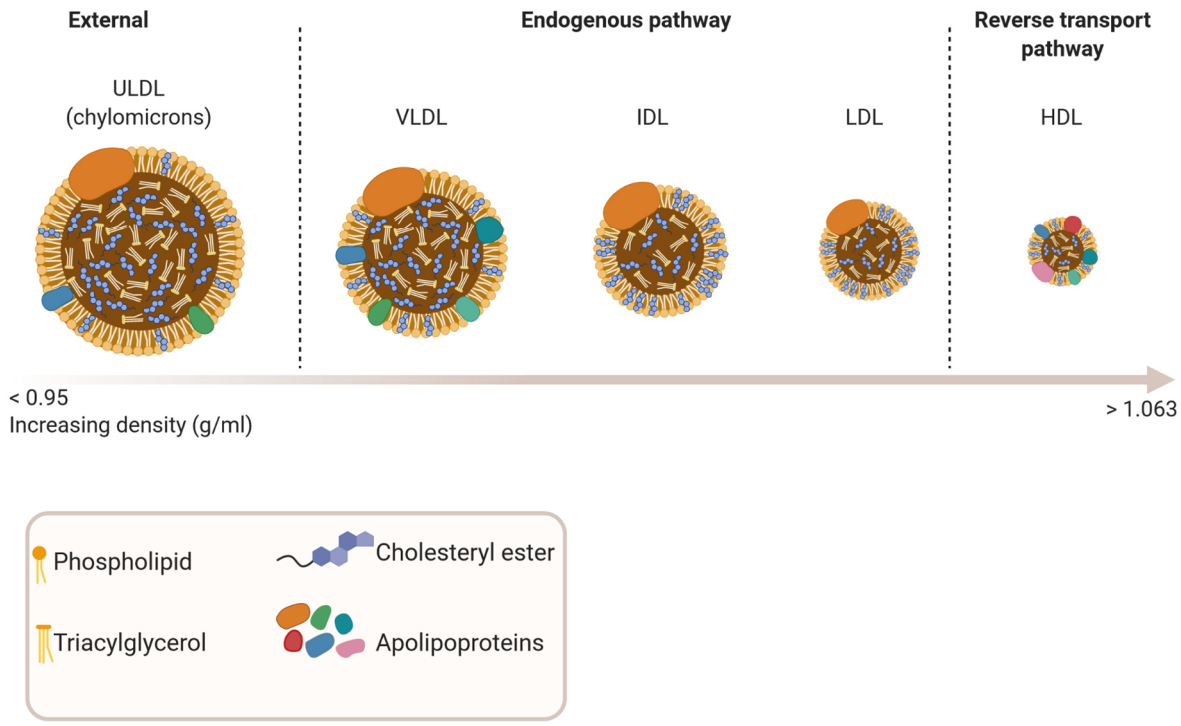

Figure 1-4: Classification and composition of lipoprotein particles. Lipoprotein particles can be differentiated according to their protein and lipid content which impacts their size and density. The largest lipoprotein particle species are ultra-low density lipoprotein (ULDL), which are formed in the small intestine and contain dietary triglycerides and other lipids. Synthesis starts with very-low density lipoprotein (VLDL) particles, which then transit to lipoproteins of intermediate density (IDL) and finally form low-density lipoprotein (LDL) particles, the most abundant lipoprotein particle species in the circulation and the source of external cholesterol for cells. High-density lipoprotein particles, on the other hand, are utilized to remove excess cholesterol from peripheral tissues via transport to the liver and bile ducts and eventual excretion in the form of bile acids. Besides their characteristic lipid content, the lipoprotein particle species carry different apolipoproteins in their limiting membrane. Except for HDL, apolipoprotein B-100 (orange) is characteristically present. Further apolipoproteins such as apolipoprotein B-48, apolipoprotein A, C and E are present in the membranes of ULDL, VLDL and HDL, respectively.

1.1.2. De-novo cholesterol biosynthesis

While all animal cells have the ability to produce cholesterol, the bulk synthesis occurs in the liver. The synthesis of cholesterol is a complex biochemical process involving more than 30 steps, as summarized in Figure 1-3 C. The majority of this process is conducted in the ER, but starts in the cytoplasm with the basic building block acetyl-Coenzyme A (acetyl-CoA) (Bloch 1965). Two acetyl-CoA molecules condense and the condensation between these and a third

acetyl-CoA molecule yield 3-hydroxyl-3-methylglutaryl (HMG-)-CoA. The ER-resident enzyme HMG-CoA reductase (HMGCR) catalyzes the conversion of HMG-CoA to mevalonate, an essential cellular lipid that is also a precursor for non-sterol isoprenoids (Goldstein and Brown 1990). This process is the rate-limiting step of cholesterol synthesis. Inhibition of HMGCR by statins, a group of antihyperlipidemic agents, has proven beneficial for patients at risk of developing cardiovascular disease (Stancu and Sima 2001). Mevalonate is subsequently metabolized to farnesyl pyrophosphate in a series of phosphorylation, decarboxylation and condensation reactions. Condensation of two molecules of farnesyl pyrophosphate by the enzyme squalene synthase yield squalene which is afterwards cyclized by oxidosqualene cyclase to produce lanosterol. This triterpenoid is the first intermediate of the pathway consisting of a steroid nucleus. To produce cholesterol, lanosterol is then further modified via the Bloch (Bloch 1965) or Kandutsch-Russell (Kandutsch and Russell 1960, Kandutsch and Russell 1960) pathway (Figure 1-3), which differ in chronological order of the step that leads to the reduction of the double bond at C24 in the side chain, or in a combinatory pathway involving steps from both. The preference for the different pathways seems to be tissue dependent as suggested by a recent in vivo study (Mitsche *et al.* 2015), with the Bloch pathway being the dominant pathway utilized in testis and spleen for instance, while the bulk of cholesterol synthesized in brain and skin follows a mixture of Bloch and Kandutsch-Russell pathway. The reason for the existence for these parallel pathways might lie in the generation of distinct intermediate products which in turn have distinct effects on cellular processes such as cholesterol homeostasis (Yang *et al.* 2006), fatty acid production and inflammation (Spann *et al.* 2012).

Cholesterol is subject to various modifications which alter its physical properties, such as solubility. The occurrence of glucosylated cholesterol β-cholesterylglucoside (1-*O*-cholesteryl-*β*-D-glucopyranoside, *β*-GlcChol) has been demonstrated in mammalian cells (Kunimoto *et al.* 2000, Akiyama *et al.* 2013) and a recent study confirmed the existence in mammalian tissues as well. While the physiological role of this cholesterol species remains to be elucidated, it was speculated that GlcChol could be utilized as a transport form of cholesterol since it is far more water soluble than free cholesterol (Marques *et al.* 2016). Moreover, the plant-type sterylglucoside *β*-sitosterylglucoside (1-*O*-sitosteryl-*β*-D-glucopyranoside (*β*-GlcSito)) and an additional, unidentified sterylglucoside were isolated from embryonic chicken brain (Akiyama *et al.* 2016). While previously all sterylglycosides found in vertebrates were thought to contain glucose as carbohydrate component, Akiyma and colleagues recently confirmed the presence of *β*-cholesterylgalactoside (1-*O*-cholesteryl-*β*-D-galactopyranoside, *β*-GalChol), in rodent and fish brain tissue (Akiyama *et al.* 2020).

1.1.3. Impact of abnormal cholesterol homeostasis

The intricate and sophisticated cellular machinery and mechanisms that evolved to maintain proper cholesterol homeostasis underline the necessity of balanced cholesterol levels. Indeed, malfunction in either the acquisition or removal of cholesterol is associated with a variety of severe diseases such as atherosclerosis, Alzheimer's disease and cancer.

The most wide-spread chronic inflammatory disease is atherosclerosis which can lead to myocardial infarction and ischemic stroke and currently is estimated to be associated with up to 50 % of deaths in westernized society (Pahwa and Jialal 2020). Initially, natural LDL and oxidized, acetylated or aggregated LDL particles accumulate in the subendothelium of arteries, particularly at branch points, leading to the activation of inflammatory processes in these areas which are characterized by the invasion of blood monocytes that migrate through the epithelial layer and subsequently differentiate into macrophages. The macrophages ingest the accumulating lipoprotein particles consequently triggering the formation of foam cells. Once the accumulation of LDL-derived free cholesterol surpasses a critical threshold, the foam cells undergo apoptosis and cell death and the cellular remnants contribute to the formation of a necrotic core that results in the formation of stenotic lesions in the affected arteries. As the disease progresses, vascular occlusion or disruption of necrotic plagues might cause lethal complications (Tabas 2004, Maxfield and Tabas 2005, Moore *et al.* 2013).

Alterations in cholesterol levels or distribution in the brain were suggested to modulate the formation of amyloid deposits which are a hallmark of Alzheimer's disease. The apoE4 isoform of apolipoprotein E (apoE) is associated with increased activation of microglia and pro-inflammatory cytokine production which may increase pathology, although the details about how the apoE isoform modulates neuroinflammation remain to be elucidated (Tai *et al.* 2015, Stephen *et al.* 2019). Moreover, polymorphisms in other cholesterol-related genes have been genetically linked to the age of onset in this disease (Wolozin 2004).

Intracellularly, disturbance of the re-distribution of LDL-derived free cholesterol and its consequent accumulation is causative for the severe lysosomal storage disorder Niemann-Pick disease type C (Vanier *et al.* 2016) which is described in section 1.3.2. Defects in the enzyme lysosomal acid lipase (LAL) are causative for a two rare lysosomal storage diseases, Wolman's disease (WD), as well as Cholesteryl ester storage disease (CESD) (Anderson *et al.* 1999). In humans, WD is lethal within the first year of life due to complete loss of LAL and consequential rapid accumulation of unhydrolyzed cholesteryl-esters. CESD, in contrast, has a later onset of disease owing to 1-5 % residual LAL activity (Goldstein *et al.* 1975, Anderson *et al.* 1999).

Loss or malfunction of the serine hydrolase LAL has been identified as the cause for a rare fatal lysosomal storage disease, Wolman's disease (WD), as well as Cholesteryl ester storage disease (CESD), which in contrast to WD has a later onset of disease owing to 1-5 % residual LAL activity (Goldstein *et al.* 1975, Anderson *et al.* 1999).

While the association of increased serum cholesterol with development of certain cancer types has been debated controversially in epidemiologic studies (Nielsen *et al.* 2012, Allott *et al.* 2014, Ravnskov *et al.* 2015), there is increasing evidence for a role of deregulated intracellular cholesterol levels in cancer development and progression (Kuzu *et al.* 2016). For example, in a breast cancer cell culture model an altered cholesterol balance was found to be associated with cancer progression (Vassilev *et al.* 2015) and mutated p53, which is the most frequent target for mutations in tumors (Vogelstein *et al.* 2000), was shown to upregulate the mevalonate pathway in a cell culture model of breast epithelial cells, causing drastic morphological changes in these cells (Freed-Pastor *et al.* 2012). Furthermore, cholesterol metabolites such as oxysterols and steroids like estrogen were associated with the development of various forms of cancer (Fox *et al.* 2009, York and Bensinger 2013), illustrating the fundamental influence cholesterol has on cellular function and physiology.

1.2. Lysosomes: Structure and function

Underappreciated after it was first discovered in 1955 (De Duve *et al.* 1955), the lysosome (vacuole in yeast) has now emerged as a center for nutrient exchange and as a metabolic signaling hub with the capacity of modulating vital cellular processes such as gene regulation and immunity, thereby establishing it an integral compartment of all eukaryotic cells except erythrocytes (Settembre *et al.* 2011, Settembre *et al.* 2012, Visvikis *et al.* 2014, Lawrence and Zoncu 2019, Ballabio and Bonifacino 2020).

While other organelles like the endoplasmic reticulum (ER) or Golgi apparatus have a neutral pH, the stand-out feature of the lysosome is its acidic lumen (pH 4.5-5) which is separated from the cytosol by a 7-10 nm thick phospholipid bilayer (Ohkuma and Poole 1978, Eskelinen *et al.* 2003, Saftig 2010). The acidity is mediated by the vacuolar ATPase (V-ATPase) which is located in this lysosomal limiting membrane and translocates protons from the cytosol to the lysosomal lumen (Forgac 1999). The low pH is the prerequisite for the correct function of the more than 60 hydrolases and other soluble proteins which are resident inside the lysosomes (Saftig 2006). These enzymes, including proteases like cathepsins, phosphatases and lipases as well as and non-enzymatic proteins like the sphingolipid-activator proteins saposins A, B , C and D (SAPs), are involved in the degradation of macromolecules such as carbohydrates, proteins, lipids and nucleic acids (Kishimoto *et al.* 1992, Saftig and Klumperman 2009, Ballabio

and Bonifacino 2020). Deficiency of these hydrolases is cause for severe disease (Saftig *et al.* 1995, Marques *et al.* 2020).

The cargo destined for degradation reaches the lysosome by several different pathways: Extracellular fluid and small nutritional particles are internalized by endocytic vesicles that form by invaginations of the plasma membrane, mature into multi-vesicular bodies (MVBs) and follow the endocytic pathway to lysosomes (Huotari and Helenius 2011). Pathogens are targeted for degradation by engulfment in plasma membrane-derived phagosomes which fuse with lysosomes and thus develop into phagolysosomes (Vieira *et al.* 2002). The (macro)autophagy pathway ensures delivery of damaged intracellular membrane and organelle components as well as aggregated proteins to lysosomes for recycling by engulfing them in autophagosomes which subsequently fuse with endosomes or lysosomes to form amphisomes or proteolytically active autolysosomes, respectively (McEwan and Dikic 2011). Furthermore, the acidic environment is needed for ligand-receptor uncoupling and also plays a role in viral infection and spreading of some toxins (Smith and Helenius 2004, Lozach *et al.* 2011, Gruenberg 2020).

In order to prevent premature degradation of membrane components by the hydrolases, the inside of the lysosomal membrane is lined by a dense layer of carbohydrates, termed glycocalyx. The glycocalyx is formed by integral membrane proteins that are resident in the lysosomal membrane and have a carbohydrate- rich domain protruding into the lysosomal lumen (Fukuda 1991, Peters and von Figura 1994), like lysosomal-associated membrane protein 1 and 2 (LAMP1 and LAMP2) (Eskelinen *et al.* 2002), Glycosylated Lysosomal Membrane Protein (GLMP) (Schieweck *et al.* 2009, Massa Lopez *et al.* 2019) and the lysosomal integral membrane protein type 2 (LIMP-2/SCARB2) (Barriocanal *et al.* 1986, Ogata and Fukuda 1994, Schwake *et al.* 2013).

The third group of lysosomal proteins are cytosolic localized proteins which are not permanently part of lysosomes, but dynamically interact with lysosomal membrane proteins and lipids in response to the cell's needs. For instance, availability of amino acids and lipids triggers the lysosomal recruitment and subsequent activation of the mammalian target of rapamycin complex 1 (mTORC1) protein kinase which is the master growth regulator and upon activation triggers downstream pathways for biomass production and suppression of catabolic processes (Kim *et al.* 2008, Sancak *et al.* 2010, Zoncu *et al.* 2011, Castellano *et al.* 2017). In the case of small ruptures in the lysosomal limiting membrane the endosomal sorting complex required for transport (ESCRT) machinery is recruited to restore membrane integrity and prevent the degradation of the damaged organelle by lysophagy, a selective form of autophagy (Skowyra *et al.* 2018). Members of the major lysosomal membrane proteins and classes of luminal enzymes are depicted schematically in Figure 1-5:

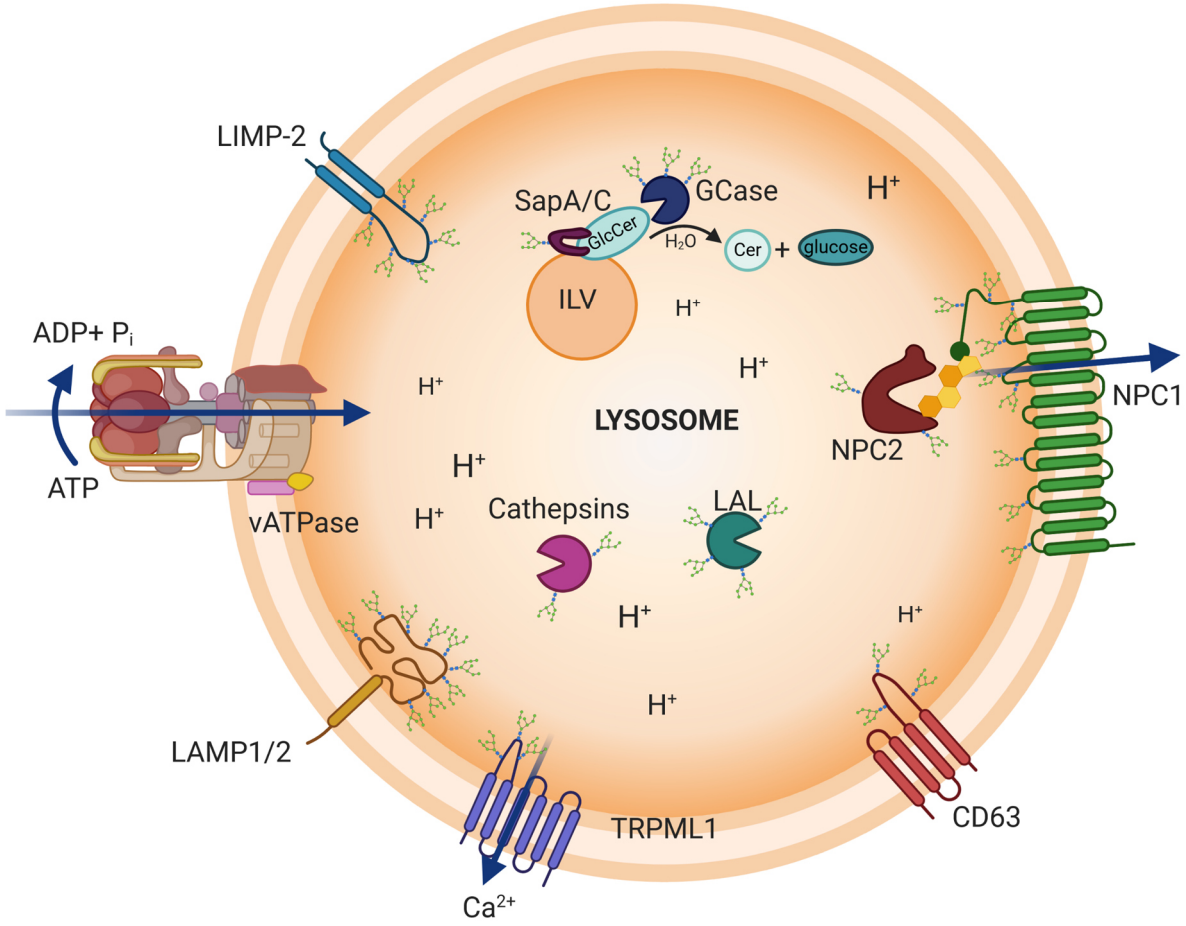

Figure 1-5: Major lysosomal membrane proteins and lysosomal enzymes. The proteins residing in the limiting lysosomal membrane are heterogeneous and fulfill various functions such as transport of small molecules and ions (transient receptor potential cation channel, mucolipin subfamily, member 1, TRPML1), acidification (Vacuolar-type H+-ATPase, vATPase), lipid export (Niemann-Pick Type C1, NPC1), maintenance of lysosome stability (LAMPs/LIMP-2/Cluster of differentiation 63, CD63) and more. Common to all is their glycosylation (indicated as green branches). Together, the membrane proteins form the glycocalyx that protects the limiting membrane from the acidic lumen**.** Here, about 60 different enzymes are degrading their respective substrates, such as proteases (cathepsins), lipases (lysosomal acid lipase, LAL) and hydrolases (beta-glucocerebrosidase, GCase and co-factor saposin A/C (Sap A/C)). Lipid substrates like glucosylceramide (GlcCer) are contained in the membranes of intraluminal vesicles (ILV). The small soluble protein Niemann-Pick Type2 (NPC2) acts as cholesterol transfer protein. Schematic depictions based on (Eskelinen *et al.* 2003, Ballabio and Bonifacino 2020).

1.3. Lysosomal storage diseases (LSDs) & enzymes

Malfunction of lysosomes is causative for several severe human diseases, termed lysosomal storage diseases (LSDs). Although they are clinically heterogeneous, these disorders are commonly characterized by a multisystemic phenotype that is progressing over time and often involves early-onset neurodegeneration (Marques and Saftig 2019, Ballabio and Bonifacino 2020). The impairment of lysosomal function, i.e. degradation and recycling of macromolecules, consequently leads to progressive accumulation of non-degraded material in the lysosomal lumen, thereby impairing further processes such as signaling and ion exchange (Platt *et al.* 2018).

1.3.1. β-glucocerebrosidase and Gaucher disease

The acid hydrolase β-glucocerebrosidase (also termed glucosylceramidase or β-glucosidase, GCase) is a lysosomal enzyme that catalyzes the hydrolysis of the glycosphingolipid glucosylceramide (or glucocerebroside, GlcCer) to ceramide and glucose (Weinreb *et al.* 1968) (Figure 1-5). It is encoded by the *GBA1* gene and the protein consists of 497 amino acids with four N-linked glycans (Erickson *et al.* 1985, Grabowski *et al.* 1990). A non-lysosomal β-glucocerebrosidase exists as well which is encoded by the *GBA2* gene. This enzyme is a membrane-associated protein localized to ER and Golgi membranes, thus providing a lysosome-independent route for degradation of GlcCer (Korschen *et al.* 2013).

Unlike most soluble lysosomal enzymes, GCase does not follow the mannose-6-phosphate receptor pathway, but instead is bound by the lysosomal integral membrane protein type 2 (LIMP-2) in the ER by interaction of hydrophobic helical interfaces on both proteins (Zunke *et al.* 2016). The LIMP-2-GCase complex is then routed to lysosomes via the Golgi and interaction with adapter proteins where the low pH causes the dissociation of both proteins (Reczek *et al.* 2007). The acidic pH is a prerequisite for optimal hydrolytic activity of GCase (Aerts *et al.* 2003). Degradation of GlcCer is enhanced by negatively charged lipids and the activator proteins saposins A and C (Grabowski *et al.* 1990, Kolter and Sandhoff 2010). Saposin C provides access to the membrane-embedded GlcCer by creating perturbed bilayer edges and thereby exposing the substrate to the soluble GCase (Alattia *et al.* 2007).

In addition to its deglycosylation activity towards GlcCer, GCase was recently reported to act as a transglycosidase being able to generate glucosylated cholesterol (GlcChol) as well as catalyze the reverse reaction (Akiyama *et al.* 2013, Marques *et al.* 2016). In addition, it can generate galactosylated cholesterol (GalChol) by transferring the galactosyl moiety from galactosylceramide to cholesterol (Akiyama *et al.* 2020).

Malfunction or deficiency of GCase is the underlying cause for one of the most common lysosomal storage diseases, Gaucher disease (GD, OMIM #230800, ORPHA355), that has a prevalence of 1:40,000-60,000 live births, albeit the occurrence is significantly higher in the Ashkenazi Jewish population (Horowitz and Zimran 1994, Mehta 2006). A hallmark of disease progression is the development of Gaucher cells, enlarged macrophages accumulating lysosomal GlcCer, which are associated with clinical manifestations like hepato- and splenomegaly as well as hematological abnormalities, including anemia and thrombocytopenia, and defective bone development (Brady *et al.* 1966, Lee 1968, Zhao and Grabowski 2002). Clinical manifestation of GD is highly variable in terms of phenotypic manifestation and severity and various mutations in the *GBA1* gene have been identified.

Besides the symptoms describe above, some mutations lead to neurological damage or lethal impairment of skin barrier function (Sidransky *et al.* 1992, Eblan *et al.* 2005).

Mutations in *GBA1* have recently been demonstrated to considerably increase the risk for developing Parkinson's disease (PD) and Lewy body dementia (LBD). While the underlying cause for this remains subject of investigation, it is noteworthy that decreased activity of enzymes degrading various sphingolipids were observed in PD patients and mouse models (Sidransky *et al.* 2009, Boer *et al.* 2020). For instance, GCase levels were reduced and lipid substrates were accumulating in aging neurons of PD patients (Rocha *et al.* 2015). The hallmark for PD, accumulation of protein aggregates like α-synuclein, was observed to correlate with decrease in GCase activity and overexpression of aggregating α-synuclein negatively impacts GCase protein levels. Supplementation of GCase, on the other hand, prevented accumulation of lipid substrates and reduced accumulation of α-synuclein aggregates, suggesting a direct interaction between these proteins (Mazzulli *et al.* 2011, Sardi *et al.* 2011, Mazzulli *et al.* 2016).

1.3.2. Niemann-Pick type C1 and C2 (NPC1 and NPC2)

As mentioned above (Figure 1-3), the integral membrane protein Niemann-Pick type C1 (NPC1) and the soluble protein Niemann-Pick type C2 are essential factors involved in lysosomal cholesterol handling and export and dysfunction or absence of either NPC1 or NPC2 lead to critical accumulation of cholesterol and glycosphingolipids in lysosomes, thereby causing a fatal disease, Niemann Pick type C disease (NPC disease) (Pentchev *et al.* 1985, Sokol *et al.* 1988, Sturley *et al.* 2004). In patients, 95 % of the cases of NPC were found to be associated with mutations in NPC1 and 5 % with mutations in NPC2 (Vanier and Millat 2004).

NPC1 consists of 1278 amino acids including 13 transmembrane domains (TMDs) (Davies and Ioannou 2000). The N-terminal domain protrudes into the lumen of lysosomes and interacts with NPC2 during cholesterol exchange (Gong *et al.* 2016, Li *et al.* 2016, Winkler *et al.* 2019). In addition, NPC1 harbors a sterol-sensing domain (SSD) consisting of TMDs 2-7 that can bind cholesterol as well.

NPC2 is a soluble 130-amino acid glycoprotein which binds sterols with high affinity (Ko *et al.* 2003). The mechanistic details of how NPC2 and NPC1 participate in lysosomal cholesterol export have remained enigmatic for a long time. The first crystal structure of NPC2 was obtained in 2003 and revealed the existence of a hydrophobic pocket that could fit a cholesterol molecule (Friedland *et al.* 2003). Indeed, in 2007 a second crystal structure of NPC2 was published by the same group where the cholesterol analog cholesterol-3-O-sulfate was bound to NPC2 (Xu *et al.* 2007). Further studies on NPC2 and NPC1 elucidated the mechanism of cholesterol transfer between these proteins and several crystal structures of NPC1 revealed

the existence of a hydrophobic tunnel through which cholesterol is likely transported to the outer leaflet of the lysosomal membrane. These findings are recapitulated in section 1.1.1

1.4. Class B scavenger receptor family

The class B scavenger receptor protein family comprises three homologous proteins, the plasma membrane proteins CD36 and SR-BI and the lysosome-located protein LIMP-2/SCARB2. While LIMP-2 is abundantly expressed in a broad spectrum of cell types and tissues, CD36 is mostly found in hematopoietic cells such as platelets, monocytes and macrophages, as well as in insulin-responsive cells and SR-BI is highly expressed in liver and steroidogenic cells like adrenocortical cells. They have a common topological structure, with each protein spanning the membrane twice and harboring a large extracellular/ luminal loop which is heavily N-linked glycosylated (PrabhuDas *et al.* 2017). Despite its unique cellular location, LIMP-2 shares approximately 33 % amino acid sequence identity as well as 55 % amino acid similarity with its family members CD36 and SR-BI, respectively (Neculai *et al.* 2013).

1.4.1. Lysosomal Integral Membrane Protein Type 2 (LIMP-2/SCARB2)

As mentioned previously, the lysosomal integral membrane protein type2 (LIMP-2, previously named LGP85; gene name SCARB2) is an important structural component and together with LAMPs 1 and 2 constitutes one of the most abundant proteins of the lysosomal limiting membrane (Marsh *et al.* 1987). The 478 amino acid protein is comprised of two transmembrane domains that are connected by a large luminal loop. This loop is glycosylated (11 and 10 potential sites in mouse and human, respectively), resulting in a total protein size of 85 kDa, and thus contributes to the formation of the glycocalyx (Fujita *et al.* 1991). The amino- and carboxyterminus of the protein consist of small stretches of amino acids and are facing the cytosol. While LIMP-2 primarily resides in the lysosomal membrane, it can also be found at the plasma membrane to some extent where it serves as a receptor for enterovirus 71 and coxsackievirus 61 (Kobayashi and Koike 2020).

Transport of LIMP-2 to lysosomes is facilitated by adaptor protein complexes 1 and 3 (AP-1, AP-3) which recognize a di-leucine motif in the C-terminus of LIMP-2 (Vega *et al.* 1991, Ogata and Fukuda 1994) and, following synthesis and glycosylation in the ER and Golgi, mediate the packaging of LIMP-2 into clathrin-coated vesicles and subsequent transport to lysosomes (Honing *et al.* 1998, Janvier *et al.* 2003, Braulke and Bonifacino 2009).

The first crystal structure of the luminal domain of LIMP-2 (PDB: 4F7B) was determined in 2013 (Neculai *et al.* 2013) and revealed features important for LIMP-2 function: A helical bundle face close to the apex of LIMP-2 contains exposed alpha-helices α5 and α7 that are important

for binding of GCase. Furthermore, the luminal domain contains a hydrophobic tunnel that transverses the entire length of this domain (Figure 1-6) and is similar to hydrophobic structures that have been identified in the extracellular domains of CD36 and SR-BI, respectively (Canton *et al.* 2013, Neculai *et al.* 2013, Pepino *et al.* 2014). The function of the tunnel remains to be elucidated. During the work on this thesis, a new crystal structure of LIMP-2's luminal loop was published with bound cholesterol and phosphatidylcholine molecules, suggesting a role of LIMP-2 in lipid transport (Conrad *et al.* 2017).

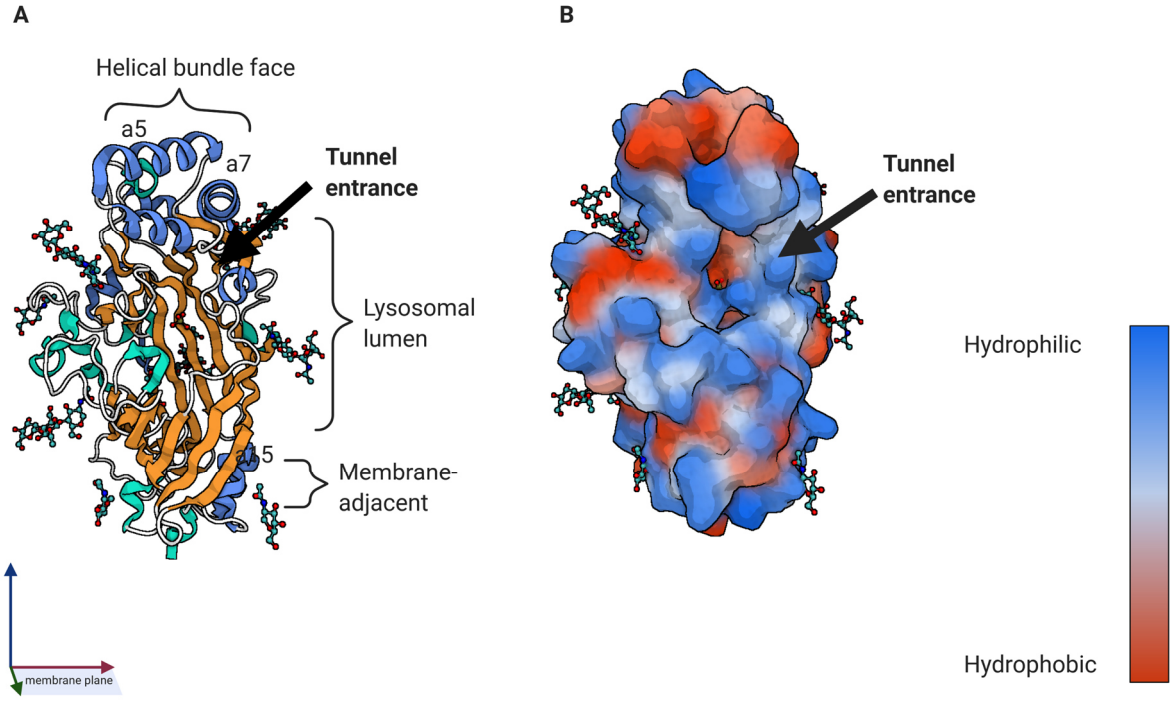

Figure 1-6: Structural model of LIMP-2's luminal domain. A Ribbon presentation of the luminal domain of LIMP-2. The color scheme indicates the secondary structure (blue: alpha-helix, orange: beta-strand, turquoise: beta-turn, white: coil). The helical bundle face contains the alpha-helices important for binding of GCase, α5 and α7. The opening of the hydrophobic cavity is indicated by the black arrow. Carbohydrates are shown in ball and stick format. **B** Solvent-excluded surface (SES) depiction with indication of hydrophobic and hydrophilic regions of the protein. The opening of the hydrophobic cavity is indicated by the black arrow. Inside the tunnel, part of a polyethylene glycol molecule from the crystallization buffer can be seen. Reference coordinates show the orientation of the luminal domain in relation to the membrane. The green and red arrows are in parallel to the membrane plane, while the blue arrow is perpendicular. The structural illustration was performed with Biorender (PDB: 4F7B) based on the crystal structure published by (Neculai *et al.* 2013).

1.4.1.1. Known functions of LIMP-2

In agreement with the pleiotropic phenotypes observed in mice and humans lacking the protein (1.4.1.2), LIMP-2 exerts different functions in the cell. It plays a role in lysosome biogenesis (Kuronita *et al.* 2002), binds the adhesive glycoprotein thrombospondin-1 (Crombie and Silverstein 1998), and is utilized for cell entry by certain viruses like coxsackievirus A16 and enterovirus 71, the causative viruses for hand, foot, mouth disease (HFMD) (Yamayoshi *et al.* 2009, Yamayoshi *et al.* 2012, Kobayashi and Koike 2020). While HFMD often presenting as a mild disease course involving vesicular enanthema in hands, feet and oral mucosa, patients

can also suffer from neurological complications including aseptic meningitis and acute encephalitis (McMinn 2002).

The so far best characterized function of LIMP-2 is its participation in a unique lysosome-targeted transport pathway for the acid hydrolase β-glucocerebrosidase (GCase) that is independent of the mannose 6-phosphate receptor-mediated transport utilized by most soluble lysosomal enzymes. Without LIMP-2, GCase is retained in the ER and the majority of the enzyme is subsequently secreted (Reczek *et al.* 2007). The binding sites for LIMP-2 in GCase vice versa were recently described in more detail(Blanz *et al.* 2010, Zunke *et al.* 2016). Mutagenesis studies mapped the binding site for GCase to helix 5 in the apical bundle of LIMP-2's luminal loop, and using a similar experimental approach, the binding region for LIMP-2 in GCase comprises a helical interface formed by residues 86-96 in helix 1a, residues 99-110 in helix 1b and residues 150-168 in helix 3 which together form a hydrophobic patch (Blanz *et al.* 2010, Zunke *et al.* 2016). A prerequisite for the binding of LIMP-2 and GBA1 is the neutral pH environment of the ER, whereas the acidic pH of lysosomes most likely leads to dissociation of the two proteins (Reczek *et al.* 2007, Zachos *et al.* 2012).

1.4.1.2. Loss of LIMP-2

Loss or malfunction of LIMP-2 was found to be causative for a fatal disease in humans, Action Myoclonus Renal Failure Syndrome (AMRF; OMIM#254900) (Balreira *et al.* 2008, Berkovic *et al.* 2008, Dibbens *et al.* 2016). This disease mainly affects children and young adults and leads to death in the second decade of life. The disease progression is characterized by progressive myoclonus, accumulation of storage material in the brain, ataxia, seizures and usually, but not always, renal dysfunction, ultimately leading to kidney failure (Dibbens *et al.* 2009). Some of these symptoms are also found LIMP-2 knockout (KO) mouse model which was described in 2003 (Gamp *et al.* 2003) and further characterized in 2008 (Berkovic *et al.* 2008). Additionally, the LIMP-2 KO mice develop a peripheral neuropathy caused by defects in the Schwann cells which are generating the protective myelin layer around the axons in the peripheral nerves. This pathology has also been described in some AMRF patients (Dibbens *et al.* 2011, Hopfner *et al.* 2011). LIMP-2-deficient mice also suffer from hearing loss which is linked to missorting of proteins in marginal cells of the *stria vascularis*, indicating a role for LIMP-2 in controlling localization of these proteins (Knipper *et al.* 2006). Figure 1-7 describes tissues and organs heavily affected by lack of LIMP-2. Since LIMP-2 is responsible for the trafficking of GCase to lysosomes, loss of LIMP-2 is accompanied by a reduction in lysosomal GCase levels (Blanz *et al.* 2010, Zachos *et al.* 2012). Intriguingly, tissue-specific differences have been observed regarding residual GCase activity and correlating increase in GlcCer. While in liver extracts from LIMP-2 KO mice, GCase activity was reduced to 20 % in comparison to WT mice, in the brain residual GCase activity was 60 % of the activity measured in WT mice (Reczek *et al.*

2007). In contrast to the pathology in GD patients, there is no occurrence of lipid-laden macrophages in AMRF patients or LIMP-2 KO mice (Gaspar *et al.* 2014). While the exact reason for this is unclear, a potential explanation could lie in the fact that GCase is secreted in these cells and might reach the lysosome by endocytosis (Balreira *et al.* 2008).

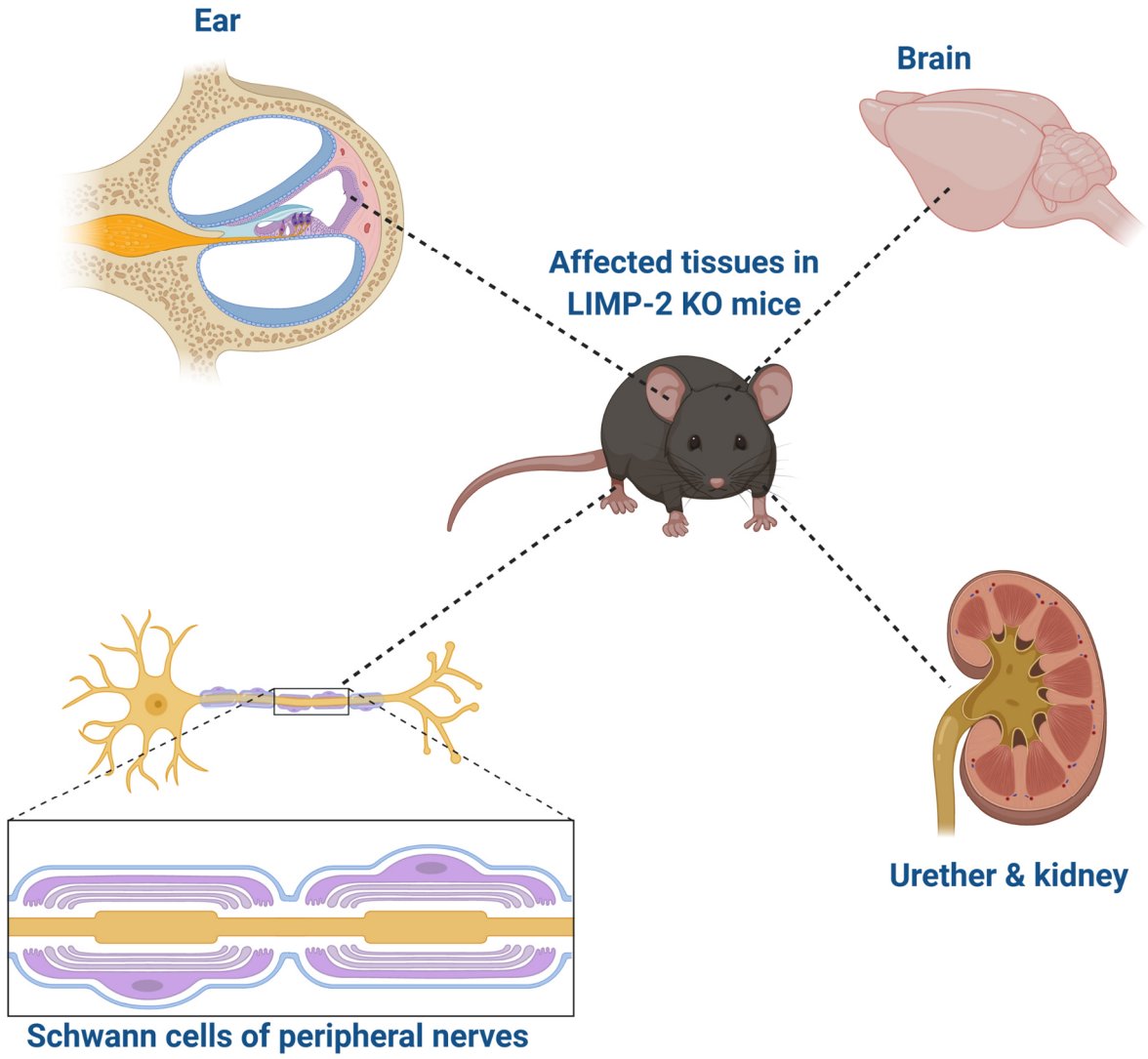

Figure 1-7: Loss of LIMP-2 results in heterogeneous cellular pathology in mice, suggesting pleiotropic functions for LIMP-2. Deafness of LIMP-2 mice is caused by progressive decline of the spiral ganglia in the cochlea and associated degeneration of the *stria vascularis*. In the brain, accumulation of unidentified storage material was observed and the mice exhibit further signs of CNS dysfunction, i.e. ataxia and hind-limb clasping. A hallmark of LIMP-2 KO mice pathology is the development of uni- or bilateral hydronephrosis for which an obstruction of the ureteropelvic junction is causative. Peripheral demyelination was observed in LIMP-2 KO mice due to defects in Schwann cells, responsible for forming the insulating myelin layer around peripheral axons, likely due to miss-trafficking and degradation of peripheral myelin proteins.

1.4.2. Cluster of differentiation 36 (CD36)

Cluster of differentiation 36 (CD36), also known as platelet glycoprotein 4, was identified as a modulator of angiogenesis and cell-to-cell-interactions (Asch *et al.* 1987) and several additional functions for this diverse protein have since been uncovered. It participates in and

directs processes such as macrophage migration and signaling, foam cell formation in the context of inflammation. CD36 is an important factor in defense against pathogenic fungi and bacteria (Ockenhouse and Chulay 1988, Silverstein and Febbraio 2009, Xu *et al.* 2018).

In the context its involvement in several cellular functions, CD36 binds several lipids including oxidized LDL, HDL and fatty acids (Endemann *et al.* 1993, Nozaki *et al.* 1995, Coburn *et al.* 2000, Drover *et al.* 2008). Recently, the ability of the CD36 homologue sensory neuron membrane protein (SNMP) to translocate fatty acid-derived pheromones through its ectodomain was discovered in Drosophila (Gomez-Diaz *et al.* 2016).

1.4.3. Scavenger receptor class B type I (SR-BI)

Scavenger receptor class B type I (SR-BI) is a surface receptor that mediates the selective uptake and transport of cholesterol and cholesteryl esters from HDL into cells, hence participating in the reverse cholesterol pathway (summarized in 1.1.1) (Shen *et al.* 2018). In addition, it is known to bind anionic phospholipids and triglycerides protects against development of atherosclerosis to some extent (Rigotti *et al.* 1995, Acton *et al.* 1996, Braun *et al.* 2002). SR-BI's cholesterol uptake function is especially crucial in the adrenal glands, where HDL-derived cholesterol is utilized for steroidogenesis (Rigotti *et al.* 2003). Recent work by Grinstein and colleagues elucidated the behavior of native SR-BI at the plasma membrane using a highly specific single-chain variable fragment (ScFv) recombinant antibody (Marques *et al.* 2019). In this study, the authors could demonstrate that SR-BI forms large homo-multimers at the plasma membrane and thus avoids rapid internalization as is the case for other scavenger receptors. Thus SR-BI is able to selectively take up cholesterol from HDL particles and release the lipid-poor particles back to the bloodstream for further rounds of transport (Marques *et al.* 2019).

1.5. Membrane contact sites

Although many different membrane-enclosed organelles exist in a cell that exert distinct functions, they don't exist as isolated and independent compartments, but are constantly interacting with each other through physical connections called membrane contact sites (MCS). These MCS serve the purpose of interorganellar exchange of molecules as well as regulation of organelle dynamics and communication. Subcellular regions where the membranes of two distinct organelles are within a distance of approximately 30 nm or less (although in some cases the gap may be wider) of each other are considered as MCS and they can occur as stable association or be dynamically regulated, respectively (Gatta and Levine 2017, Di Mattia *et al.* 2020).

Especially the endoplasmic reticulum (ER) forms an extensive network of contact sites throughout the cell and with various other organelles such as mitochondria, the Golgi apparatus, peroxisomes and the endolysosomal compartments (Wu *et al.* 2018). Formation of inter-organelle contact sites is mediated by specialized scaffold proteins in the respective organelle's membranes which either interact with proteins or lipids in the opposing membrane and hence form a tether (Eisenberg-Bord *et al.* 2016). One of the first described tether complexes consist of the yeast ER-resident protein nucleus-vacuole junction protein (Nvj1) and the vacuolar membrane protein vacuolar protein 8 (Vac8) which were shown to form nucleus-vacuole junctions (Pan *et al.* 2000). The most-well described ER-resident tethers are vesicle-associated membrane protein-associated proteins (VAP) A and B, and motile sperm domain containing protein 2 (MOSPD2), which interact with surface-anchored proteins from various organelles, thus modulating the ER's extensive contact site network. While their interaction partners are specialized and distinct proteins, most of them harbor a FFAT amino acid motif in a cytosolic and therefore accessible domain which is recognized by VAP A and B and MOSPD2, respectively (Loewen *et al.* 2003, Murphy and Levine 2016, Di Mattia *et al.* 2018). Well-characterized examples for these interactors include members of a highly conserved protein family of oxysterol-binding proteins (OSBP)/ OSBP-related proteins (ORP), e.g. OSBP1L, ORP5, and ORP6, as well as StAR Related Lipid Transfer Domain Containing 3 (STARD3), which belongs to the steroidogenic acute regulatory protein (StAR)-related lipid-transfer proteins (START). Recently, the protein GRAM (glucosyltransferases, Rab-like GTPase activators and myotubularins) Domain Containing 1B (GRAMD1B)/AsterB, a member of the Lipid transfer proteins anchored at a membrane contact site (LAM) family of lipid transporters, was revealed to establish membrane contact sites between the ER and the plasma membrane (PM) in response to excess PM cholesterol by virtue of its GRAM domain that binds phosphatidylserine in the inner leaflet of the plasma membrane (Horenkamp *et al.* 2018, Sandhu *et al.* 2018).

1.5.1. Lysosome - ER contact sites

Organelles of the endocytic pathway, namely early and late endosomes as well as lysosomes, are closely associated with ER tubules. In Cos-7 cells, about 60-80 % of early endosomes form contact sites with the ER and this number increases to almost 90% with the maturation of endosomes to lysosomes (Friedman *et al.* 2013, Valm *et al.* 2017). Endosomes and lysosomes are highly mobile and dynamic organelles and their spatial location is influenced by availability of nutrients. While a dispersed distribution of endolysosomes is connected to nutrient abundance, starvation induces re-localization and clustering in the perinuclear area (Korolchuk *et al.* 2011), a process which is controlled by the late endosomal cholesterol-sensing protein ORP1L. Cholesterol-dependent conformational changes of ORP1L modulate contact site

formation and interaction between lysosomes and the ER or microtubule network, thus determining lysosomal positioning (Johansson *et al.* 2007, Rocha *et al.* 2009).

ER-lysosome contact sites are of particular importance for the fate of LDL-derived cholesterol (Figure 1-8). Increasing evidence suggests that 30 % of this pool of cholesterol is directly transferred from lysosomes to the ER (Neufeld *et al.* 1996, Underwood *et al.* 1998). In this regard proteins that could fulfill the dual functions of binding cholesterol and residing at or creating LY-ER membrane contact sites have received increasing attention. The endolysosomal protein STARD3 binds VAP proteins via its cytosolic FFAT motif and utilizes its hydrophobic START domain to shuttle cholesterol between opposing membranes (Wilhelm *et al.* 2017).

Although the mechanistic details remain to be elucidated, Höglinger and colleagues could demonstrate an important role for the ER-contact site protein GRAMD1B and lysosomal cholesterol exporter NPC1 in regulating the transfer of LDL-derived cholesterol to the ER membrane (Hoglinger *et al.* 2019).

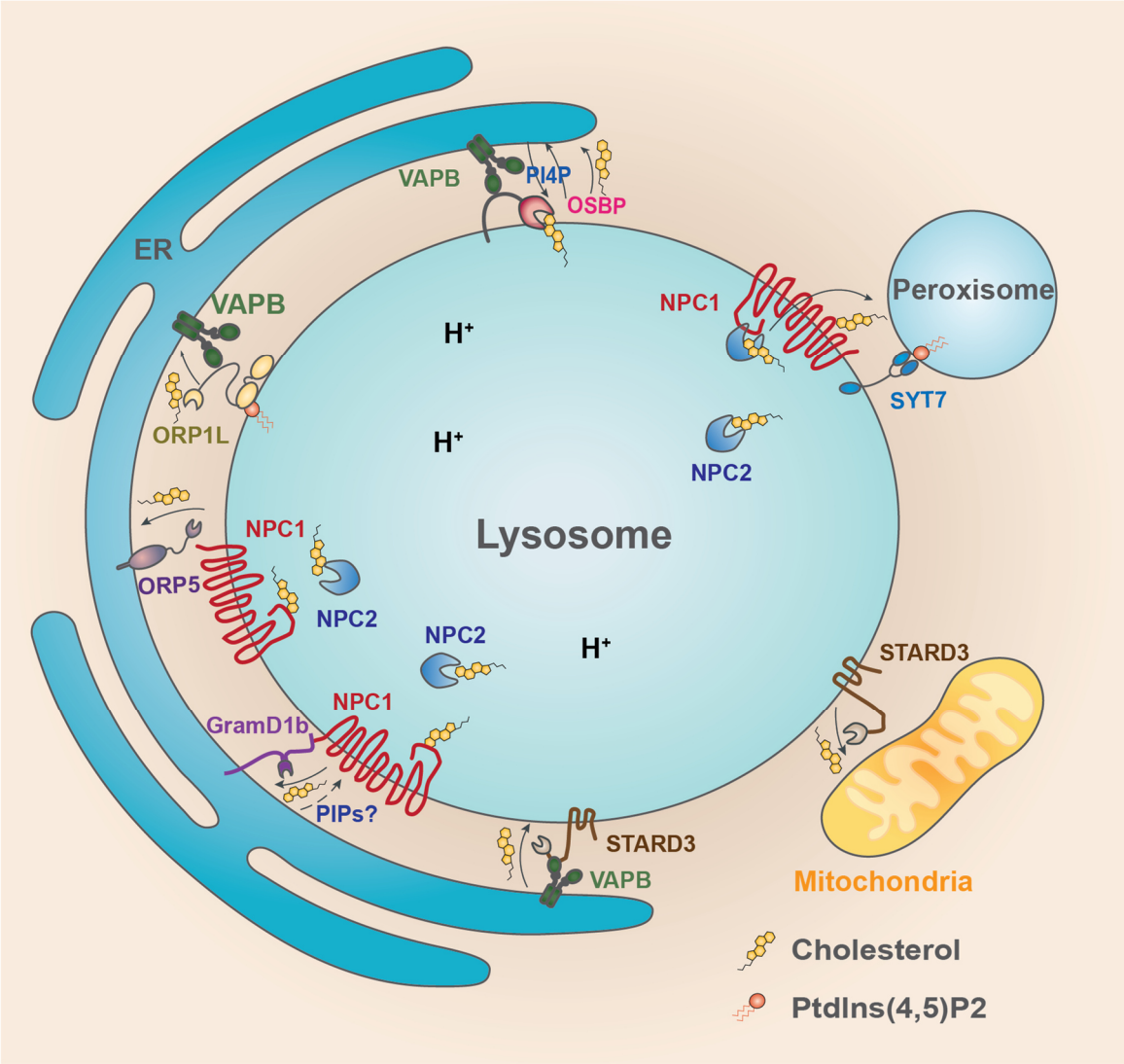

Figure 1-8: Overview of interaction network formed by lysosomal membrane proteins at membrane contact sites in the context of lipid transfer. Several routes for lipid, and especially cholesterol, export operate in parallel. NPC1 interacts with both OSBP-related protein 5 (ORP5) as well as GRAM domain containing 1B (GRAMD1B) to mediate cholesterol transfer to the ER. Furthermore, it mediates lysosome-peroxisome lipid exchange by interaction with synaptotagmin VII (SYT7) and phosphatidylinositol-4,5-bisphosphate [PtdIns(4,5)P2]. VAMP-associated protein (VAP) is another ER-resident protein that exchanges cholesterol with phosphatidylinositol 4-phosphate (PI4P) by interacting with oxysterol-binding protein (OSBP) as well as OSBP-related protein 1L (ORP1L). The endolysosomal START-domain protein STARD3 is thought to mediate cholesterol transfer to contacting organelles like the ER and mitochondria. More players involved in lysosomal membrane contact sites are likely to be discovered in this highly dynamic field of research. Figure slightly modified from (Meng *et al.* 2020).

1.6. Lipidation of proteins

While the functions of proteins were initially thought to only depend on their amino acid composition and secondary and tertiary structure, research of the past decades overturned this view by revealing the existence of a myriad of possible co- as well as post-translational (CTMs and PTMs, respectively) modifications that proteins can transiently or permanently be subjected to, underlining the dynamic nature of cellular processes needed to adapt to an ever-changing environment. Different types of PTMs include phosphorylation, ubiquitination, glycosylation and acetylation which are of importance in signaling cascades and protein quality

control as well as in regulation of protein function and turnover (Duan and Walther 2015). A class of modifications that have come into focus in recent years are the so-called lipidations, where fatty acyl or polyisoprenyl groups are transiently or permanently attached to designated amino acid residues, usually to the nucleophilic side chains of e.g. lysine, cysteine and serine residues, in the target protein via a covalent linkage. They can also occur at the NH_2 group of a protein's N-terminus. This can regulate protein-protein interaction, protein-membrane interaction, alter the stability of proteins and regulate enzymatic activity (Jiang *et al.* 2018). Dependent on the chain length of the attached fatty acid, these modifications are called myristoylation (C_{14}), palmitoylation (C_{16}), prenylation (C_{15} or C_{20}, respectively) and occur mostly on N-terminal glycine (myristoylation) or cysteine residues (prenylation, palmitoylation). In addition, lipid modification on serine residues (O-acylation), lysine residues (N-acylation) and C-terminal cholesterol esterification have been reported, however, too few proteins have been identified so far that undergo these modifications to assess preferred prevalence of these lipidations. Of these lipid modifications, only myristoylation occurs co-translationally as well as post-translationally, whereas the other modifications occur only post-translationally. While prenylation and myristoylation appear to be permanent modifications, palmitoylation is reversible and transient. It is also not unusual for several of these modifications to occur on the same protein and even simultaneously, either serving different functions or having an additive effect. Common lipid modifications on amino acid residues are schematically depicted in Figure 1-9 and discussed in detail in the following chapters.

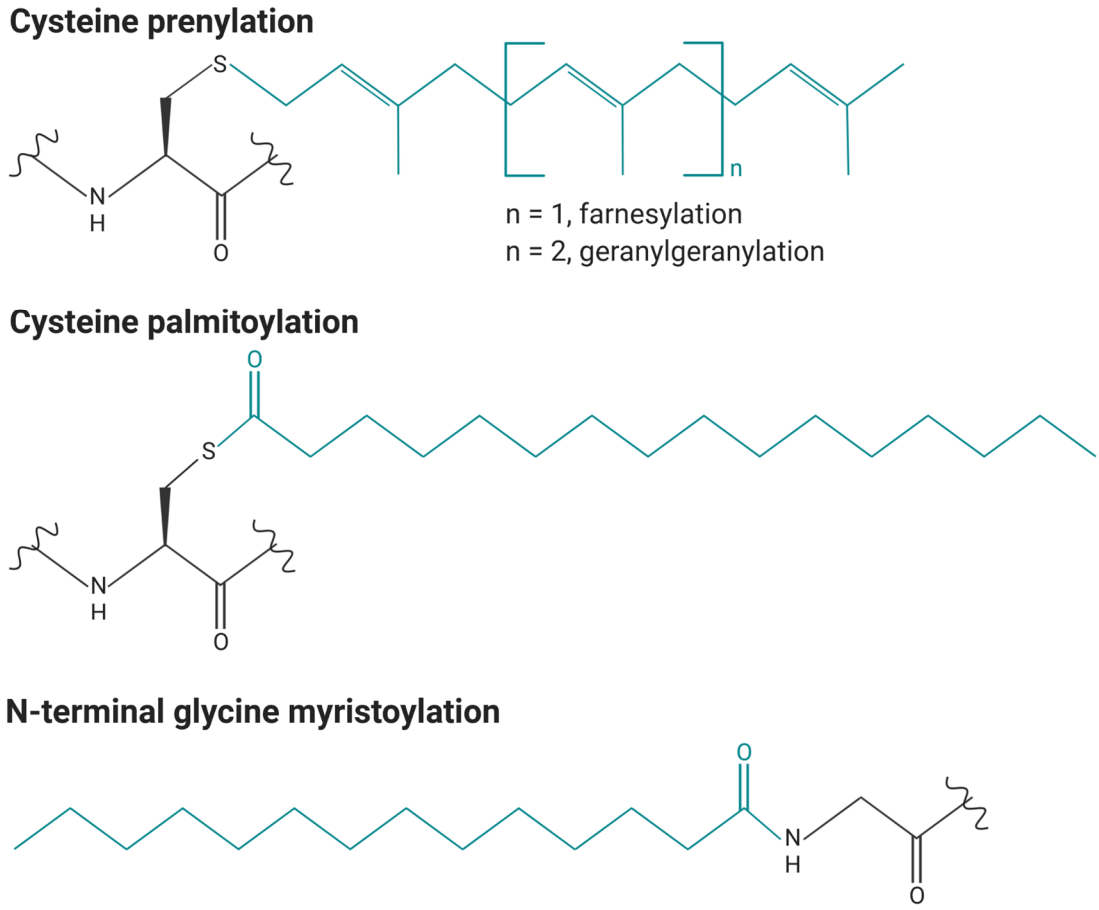

Figure 1-9: Common lipid modifications. Cysteine residues can be modified with fatty acid chains (indicated in green) that differ in length, resulting in farnesylation (C_{15}) or geranylgeranylation (C20; both prenylations) or palmitoylation (C_{16}). Myristoylation (C_{14}), occurs only at the N-terminus of glycine residues during translation or after proteolytic cleavage of a polypeptide chain. Figure adapted from (Jiang *et al.* 2018).

1.6.1. Myristoylation

The attachment of myristoyl, a C_{14} fatty acyl group, mostly occurs co-translationally at a glycine residue at position two of the nascent amino acid chain. Moreover, it can occur post-translationally at a glycine after intermembrane cleavage which is why this process is also referred to as N-terminal glycine myristoylation. In contrast to other lipidations like palmitoylation, myristoylation modifies a protein irreversibly (Gordon *et al.* 1991, Boutin 1997). The reaction is catalyzed by myristoyl-CoA:protein N-myristoyltransferase (NMT) whose expression is widespread in eukaryotes. While lower eukaryotes possess only one NMT, two distinct genes encoding NMTs, NMT1 and NMT2, were identified in higher eukaryotes such as plants, mice and humans (Giang and Cravatt 1998). NMT1 and NMT2 are primarily localized in the cytosol and contain a stretch of basic amino acids, termed K box motif, at their N-terminus that enables them to associate with ribosomes (Takamune *et al.* 2010). A prerequisite for co-translational myristoylation is excision of the initial methionine by methionine aminopeptidase (MetAP) in the nascent amino acid sequence to reveal the N-terminal glycine residue (Giglione *et al.* 2015).

The attachment of a fatty acid enhances the hydrophobicity of the target protein and can thus mediate the targeting of the modified protein to membranes of various subcellular organelles. Myristoylation represents a critical regulatory mechanism involved in signal transduction, apoptosis and pathological processes induced by viruses, fungi and parasites (Johnson *et al.* 1994, Zha *et al.* 2000, Patwardhan and Resh 2010, Tate *et al.* 2014, Wright *et al.* 2014) . While myristoylation alone does not enable membrane association of a soluble protein (which usually requires additional lipidations like cysteine palmitoylation or cysteine prenylation), the specific location of integral transmembrane proteins can be influenced by myristoylation (Maurer-Stroh *et al.* 2004).

1.6.2. Prenylation

The attachment of several isoprene units to C-terminal cysteine residues of proteins is termed prenylation. Farnesylation comprises the addition of three isoprene units (C_{15}), whereas with geranylgeranylation four isoprene units (C_{20}) are added. The latter is the dominant form of prenylation in mammalian cells (Epstein *et al.* 1991). While the presence of a prenylcysteine lyase in lysosomes may lead to the degradation of prenylated proteins (Tschantz *et al.* 2001), so far no enzyme has been described to dynamically remove prenylation from functional proteins (Jiang *et al.* 2018). This, together with the fact that the prenylation group is connected to the cysteine residues via a stable thioether bond has led to the conclusion that prenylation is an irreversible modification. Approximately 2 % of all proteins in mammalian cells are subject to prenylation (Epstein *et al.* 1991). Farnesylation is mediated by farnesyl transferase (FT) and geranylgeranyl transferase (GGT-1). They transfer the geranylgeranyl group from geranylgeranyl diphosphate (GGPP) to proteins. A third protein prenylationtransferase, Rab geranylgeranyl transferase (RGGT or GGT-2) modifies a double cysteine motif in the C-terminus of Rab proteins by transferring two geranylgeranyl groups from GGPP (Jiang *et al.* 2018). Prenylation influences protein function mainly in two different aspects, protein-protein interaction and subcellular membrane localization.

1.6.3. Palmitoylation

Palmitoylation can be divided into two subgroups, based on the amino acid residue that is being modified. While S-palmitoylation, also referred to as S-acylation (Greaves and Chamberlain 2014), occurs at cysteine residues (via thioester linkage), lysine as well as N-terminal cysteine residues can be subject to N-palmitoylation (via amide linkage) (Buglino and Resh 2012, Zaballa and van der Goot 2018). Of the two, S-palmitoylation has been in the spotlight of research so far and while even here scientists are only being to unravel the molecular details, even less is currently known about N-palmitoylation. Henceforth, S-palmitoylation will be referred to as ‘palmitoylation’. The carbonyl carbon of the lipid moiety

reacts with the thiol group of the cysteine residue resulting in a labile, and hence reversible, thioester bond (Zaballa and van der Goot 2018). While for other lipid modifications such as glycine N-myristoylation there are prerequisites that determine which protein can be subject to this lipidation, palmitoylation lacks a consensus motif that allows easy prediction of potential targets. It has, however, been noted that cysteines in juxtamembrane position or within a transmembrane domain have a higher likelihood of undergoing palmitoylation and previous lipid modifications, i.e. myristoylation are often followed by palmitoylation (Jiang *et al.* 2018).

Mass-spectrometry- based high-throughput analyses have drastically increased the number of potentially palmitoylated proteins. The comprehensive palmitoylation database Swisspalm (www.swisspalm.org) combines the knowledge from these datasets, thus enabling the comparison of a protein of interest against almost 10,000 palmitoylation candidates from 55 organisms that were initially reported in 661 studies (Zaballa and van der Goot 2018).

1.6.3.1. Palmitoyl transferases and thioesterases

The enzymes catalyzing the attachment of palmitate to a protein's cysteine residue are named DHHC protein S-acyltransferases (DHHC PATs) based on a characteristic highly conserved Asp-His-His-Cys tetrapeptide motif embedded in a cysteine-rich domain (CRD) that is a prerequisite for enzyme activity. In addition to the CRD, three short motifs are conserved between different S-acyltransferases: The large cytosolic loop connecting TMD 2 and 3 contains an Asp-Pro-Gly (DPG) sequence close to TMD2 and the C-terminal cytosolic sequence harbors a Thr-Thr-Xxx-Glu motif (TTxE, x can be any amino acid) as well as a Palmitoyltransferase Conserved C-terminal motif (PaCCT) which consists of 16 amino acids (Figure 1-10 A). Beyond these motifs, DHHC PAT family members share little sequence homology (Mitchell *et al.* 2006, Gonzalez Montoro *et al.* 2009).

The first step in catalysis consists of autoacylation of DHHC PATs at the cysteine in the DHHC motif. The fatty acid needed for the formation of this transient acyl-enzyme intermediate is donated by acyl-Coenzyme A (CoA). Intriguingly, the autoacylated intermediate could not be detected for all DHHCs (e.g. yeast DHHC PATs Swf1 and Pfa4 and human DHHC17) which argues for the existence of an alternative mechanism for fatty acid transfer (Gonzalez Montoro *et al.* 2015, Verardi *et al.* 2017). The fatty acid is then transferred to the target cysteine of a protein substrate (Figure 1-10 B) and leading to the release of the substrate (Jennings and Linder 2012). A DHHC PAT can also be a substrate of another DHHC PAT as a regulatory mechanism on a cysteine not included in the DHHC motif. Abrami and co-workers demonstrated the requirement of C-terminal acylation of DHHC6 by DHHC16 for the catalytic activity of DHHC6 (Abrami *et al.* 2017).

DHHC PATs are present in different numbers in eukaryotes with five to seven different PATs encoded in yeast, approximately 20 - 22 PATs in *Caenorhabditis elegans* and *Drosophila melanogaster* (Bannan *et al.* 2008, Edmonds and Morgan 2014, Rana *et al.* 2019) and up to 23 family members in mammals (Jiang *et al.* 2018, Zaballa and van der Goot 2018). Prokaryotes on the other hand do not contain palmitoyltransferases albeit bacterial virulence proteins, e.g. from *Salmonella* and *Legionella* can be subjected to palmitoylation in eukaryotic hosts during infection (Hicks *et al.* 2011, Lin *et al.* 2015). Common to all DHHC PATs is the cytosolic orientation of the DHHC-CRD meaning that DHHC-PAT-mediated palmitoylation can only take place in the cytosol. The 23 mammalian DHHC PATs consist of mostly four transmembrane domains (TMDs), although some are predicted to have five (zDHHC4 and zDHHC24) or six (zDHHC13, zDHHC17 and zDHHC23) TMDs, respectively. The enzymes also display a variable subcellular distribution and tissue specificity of some family members might also impart an additional level of regulation (Fukata *et al.* 2004, Ohno *et al.* 2006). The low copy number of DHHC PATS in cells have made it difficult to determine their exact subcellular localization et an endogenous level. However, heterologous overexpression of tagged DHHC PATs demonstrated that ER and Golgi apparatus are the most common endomembrane spots for the enzymes, while a few were also found at the plasma membrane and within vesicular membranes (Ohno *et al.* 2006, Gorleku *et al.* 2011, Greaves *et al.* 2011, Brigidi *et al.* 2015, Abrami *et al.* 2017). An overview of the location of the different human DHHC enzymes is provided in Figure 1-11.

Since palmitoylation is a dynamic and reversible protein modification and often serves a regulatory function, the palmitoyl moiety can be removed from a palmitoylated protein without necessity for degradation/ recycling of the protein. The depalmitoylation reaction is catalyzed by acyl protein thioesterases (APTs) which are part of the metabolic serine hydrolase superfamily (mSH) (Long and Cravatt 2011). Two catalytically active cytosolic thioesterases have been identified, APT1 and APT2 (Duncan and Gilman 1998, Rocks *et al.* 2005, Rusch *et al.* 2011) that mediate the thioester hydrolysis, thereby separating substrate protein and fatty acid. Both enzymes harbor cysteine residues in their N-terminus that can be palmitoylated which likely regulates their subcellular localization and association with the cytosolic face of membranes belonging to the plasma membrane, Golgi apparatus and mitochondria (Yang *et al.* 2010, Won *et al.* 2018). Since the diversity and number of palmitoyltransferases is much higher than the number of thioesterases, it is likely that APT1 and APT2 have a broad substrate spectrum. However, a detailed characterization of their substrate specificity and recognition awaits further research.

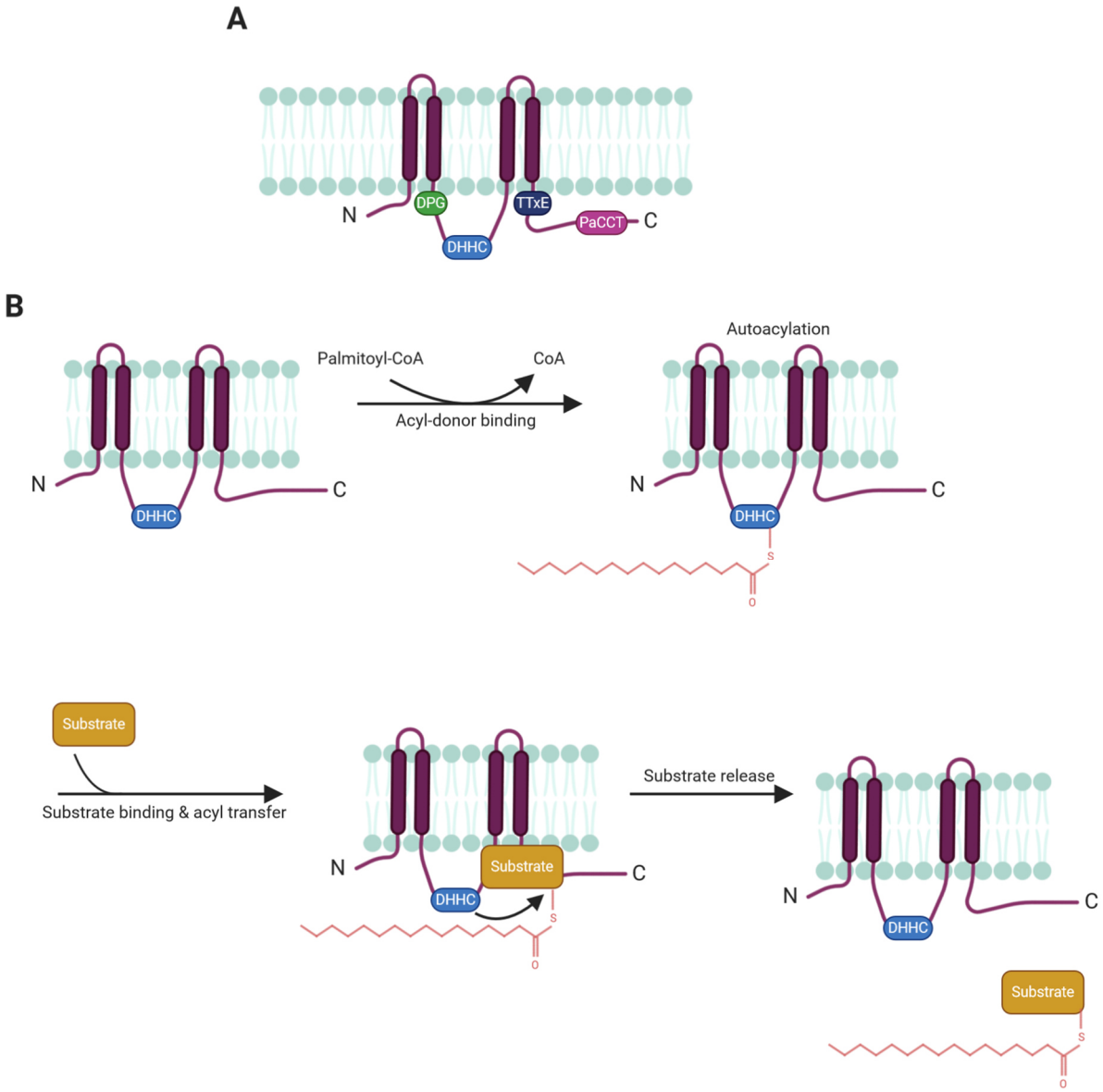

Figure 1-10: General structure of palmitoyltransferases (DHHCs) and palmitoylation process. A Structure of DHHCs highlighting conserved domains and motifs. The catalytic activity is dependent on an Asp-His-His-Cys (DHHC) motif that resides within a cysteine-rich domain (CRD) of about 50 amino acids. While the 23 human enzymes share little additional sequence homology, there are three short conserved motifs in the cytosolic loops: An Asp-Pro-Gly (DPG) sequence is located upstream of the DHHC motif and the C-terminus harbors a Thr-Thr-Xxx-Glu motif (TTxE, where x can be any amino acid) as well as the Palmitoyltransferase Conserved C-terminal (PaCCT) motif. **B** Principle of DHHC-mediated palmitoylation of a substrate protein. DHHCs undergo autoacylation in which palmitate from a donor (palmitoyl-CoA) is transferred to the DHHC motif of the palmitoyltransferase. Upon substrate binding, the fatty acid is transferred from the DHHC protein to the substrate, followed by the release of the substrate. The newly palmitoylated protein is often anchored to membranes (not depicted). Figure slightly adapted from (Jiang *et al.* 2018, Zaballa and van der Goot 2018).

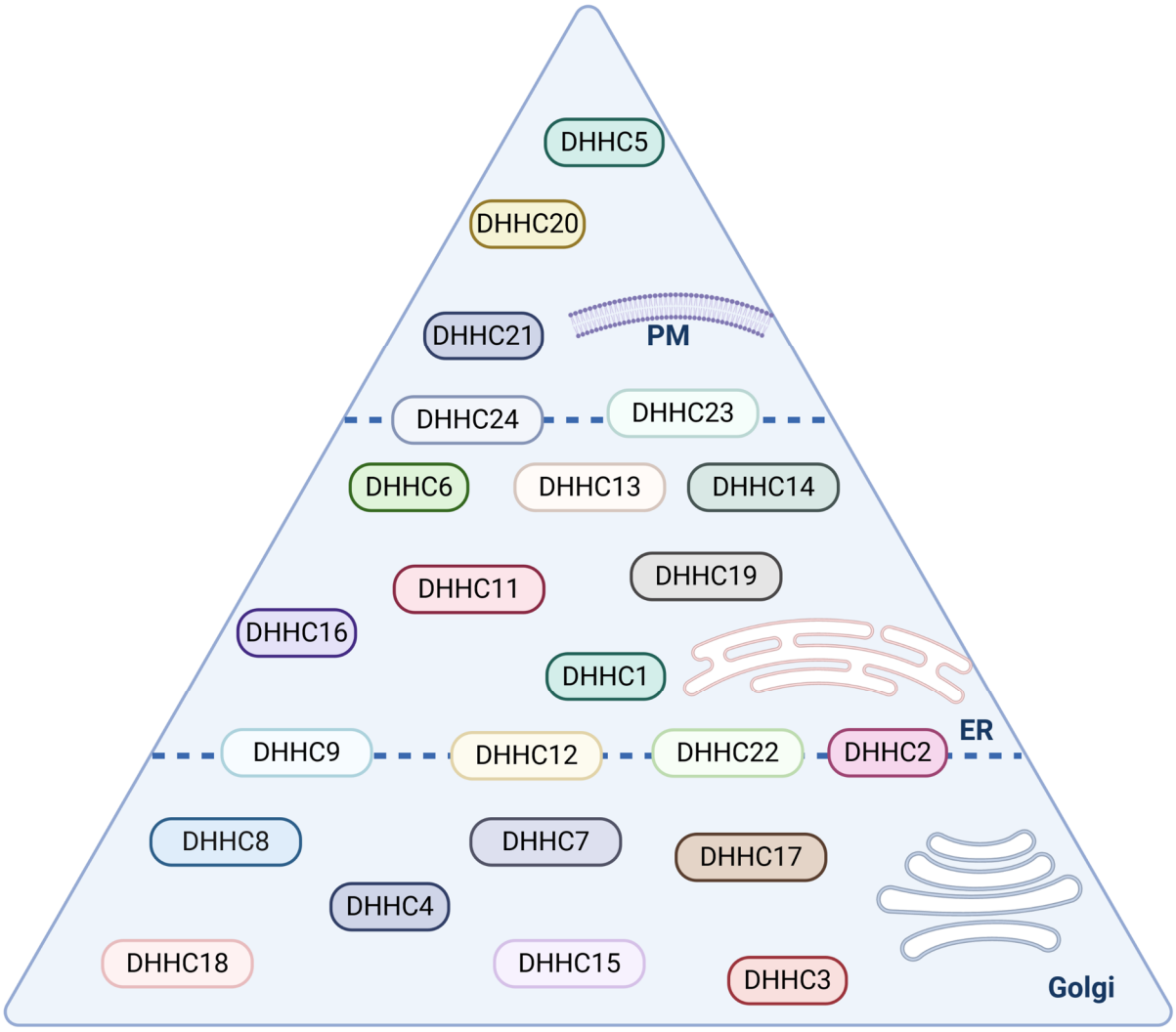

Figure 1-11: Subcellular distribution of human palmitoyltransferases (DHHC PATs). While most DHHC PATs reside in one cellular compartment, i.e. the Golgi, endoplasmic reticulum (ER) or plasma membrane (PM), some enzymes can be found in two organelles, e.g. DHHC9 is located both in the ER and Golgi and DHHC24 can be found in the ER as well as at the PM.

1.6.3.2. Functions and (patho)physiological relevance of palmitoylation

While many aspects of palmitoylation-related biology remain to be investigated to uncover the true significance of palmitoylation, it is already emerging as a vital and widespread regulatory mechanism that affects many areas of cellular homeostasis. The hallmark of this lipidation, its reversibility, makes palmitoylation a powerful modulator of physiological processes. It may alter association of substrate proteins with membrane or membrane microdomains like lipid-rich rafts, tilt transmembrane domains by anchoring cytosolic domains to membranes thereby inducing conformational changes in the target protein or either enhance or inhibit protein-protein interaction, among others (Charollais and Van Der Goot 2009).

One of these tightly regulated processes is protein turnover, which is initiated by ubiquitination. Attachment of ubiquitin molecules designates proteins for proteasomal or lysosomal

degradation. S-acylation prevents ubiquitination and thus premature degradation of a protein in several ways: In the yeast SNARE protein Tlg1 S-acylation diminished access of the E3 ubiquitin ligase to lysine residues nearby the S-acylation site, thus preventing ubiquitination (Valdez-Taubas and Pelham 2005). Altered subcellular localization due to S-acylation can also prevent premature degradation as was shown for the anthrax toxin receptors TEM8 and CMG2 which, once S-acylated, do not associate with lipid rafts and thus escape ubiquitination and targeting to lysosomes for degradation (Abrami *et al.* 2006).

Palmitoylation of proteins has an influence on host-pathogen interactions. Some viruses like influenza and HIV exploit the host's palmitoylation machinery to associate with plasmalemmal lipid-rich microdomains important for viral budding (Blanc *et al.* 2013) and this lipidation has an important role in innate immunity as well. For instance, antiviral activity exerted by interferon-induced transmembrane protein 3 (IFITM3) is dependent on palmitoylation by DHHC3, DHHC7 and DHHC20 at three conserved cysteine residues (Yount *et al.* 2010, Chesarino *et al.* 2014, McMichael *et al.* 2017).

Regulation of cellular metabolism by palmitoylation has been gaining increasing attention in recent years. Proteins involved in insulin signaling and homeostasis such as glucose transporter 4 (Glut4) and cytoplasmic linker proteins (CLIP)-family member ClipR-59 require palmitoylation by DHHCs 7 and 17, respectively, to function properly and DHHC7 activity was found to be increased upon stimulation with insulin (Ren *et al.* 2013, Ren *et al.* 2015, Du *et al.* 2017). Mice deficient for DHHC7, on the other hand, were observed to develop hyperglycemia and glucose intolerance (Du *et al.* 2017).

DHHC PATs are among the many proteins found to be dysregulated in oncogenic cells (Greaves and Chamberlain 2014, Zaballa and van der Goot 2018). While in some cancers, certain DHHC enzymes are upregulated (e.g. DHHC11 in cancers of bladder (Yamamoto *et al.* 2007) and lung (Kang *et al.* 2008); DHHC9 in colorectal tumors (Birkenkamp-Demtroder *et al.* 2002)), a decrease in expression of some palmitoyltransferases was also linked to cancer as in the case of DHHC2 expression in gastric adenocarcinoma (Yan *et al.* 2013) and colorectal cancers (Greaves and Chamberlain 2014) and of DHHC14 in testicular germ cell tumors and prostate cancer (Yeste-Velasco *et al.* 2014). Hence, it is of vital interest for the development of new cancer-targeting therapies to remedy the current lack of understanding the molecular mechanisms that underlie the relationship between different palmitoyltransferases and development as well as progression of cancer.

While not comprehensive, the functions and involvement of DHHC PATs in cellular processes described in this section illustrate the enormous potential and relevance of palmitoylation/ S-acylation for health and disease and future research will undoubtedly uncover even more intriguing roles for palmitoyltransferases, thioesterases and their relation to protein substrates.

2. Objectives

The lysosomal integral membrane protein type 2 (LIMP-2) is an abundant component of the lysosomal membrane and different tasks have been attributed to this protein. The so far best characterized function is its role as an intracellular transporter for the acid hydrolase β-glucocerebrosidase (GCase) from the ER to lysosomes.

The major aim of this thesis was to investigate functions of LIMP-2 that it fulfils in addition to transporting GCase. To this end, a knock-in mouse model was generated and analyzed that expresses a mutant form of LIMP-2 incapable of binding GCase. Analytic comparison of the phenotypic traits of this LIMP-2.Y163D knock-in mouse to those observed in a LIMP-2 KO mouse was utilized to dissect between the phenotypic alterations caused solely by absence of LIMP-2 and those caused by additional decrease in GCase, which in absence of LIMP-2 is not arriving at lysosomes.

A hydrophobic tunnel inside LIMP-2's luminal domain that is also present in the protein family members CD36 and SR-BI suggested a potential role for LIMP-2 in lysosomal lipid transport. Specifically, the question whether cholesterol could be a substrate for LIMP2 was addressed. Experimental approaches to investigate these questions included the use of cross-linkable lipids and microscale thermophoresis in combination with purified recombinant luminal domain of LIMP-2 as well as lipid binding and transport assays analyzed by live-cell imaging in various cell lines. LIMP-2 knockout HeLa cell lines as well as NPC1-LIMP-2 double deficient cells were generated with the CRISPR toolkit to assess the cells' susceptibility to cholesterol storage in comparison to WT and NPC1-deficent HeLa cells. Biochemical techniques such as Western Blot and cholesterol esterification assays were employed to elucidate the physiological relevance of LIMP-2 as a putative lipid transport protein.

Moreover, functions of LIMP-2 at the cytosolic face of lysosomes were assessed. LIMP-2 has two cytosolic domains, the amino- and carboxy-terminus. Their role and characteristics in terms of posttranslational modification (i.e. palmitoylation) and presence at membrane contact sites was established by electron microscopy, co-immunoprecipitation studies and immunofluorescence experiments.

3. Materials and Methods

3.1. Materials

3.1.1. Chemicals and buffers

Table 3-1: Overview of chemicals used in this study.

Chemical	Manufacturer
1 X Trypsin/EDTA	PAA-Laboratories
2-Mercaptoethanol (p.a.)	Roth
30 % (w/v) Acrylamide/ bisacrylamide Rotiphorese® Gel 30 (37.5:1)	Roth
LE Agarose	Biozym
Ammonium Persulfate (APS)	Roth
Bromphenol blue	Canalco
cOmplete™ protease inhibitor cocktail	Roche
Coomassie Brilliant Blue R-250	Bio-Rad
DABCO (1,4-Diazobicyclo[2.2.2]octane)	Sigma Aldrich
DAPI (4‘,6-Diamidine-2-phenylindol)	Sigma Aldrich
Desoxyribonucleosidetrisphosphates (dNTPs) (2 mM/ 10 mM)	Thermo Fisher Scientific
DirectPCR® Lysis Reagent (Mouse Tail)	Viagen Biotech
DMSO (Dimethylsulfoxide)	Roth
DNA-Ladder (100 bp, 1 kb)	Roche
DNA-Loading Dye	Thermo Fisher Scientific
DTT (Dithiothreitol)	Sigma Aldrich
Dulbecco´s Modified Eagle Medium (DMEM)	Gibco
DMEM/F-12	Gibco
Dynabeads	Invitrogen
Ethanol 99,8% p.a.	Roth
Ethidiumbromide	Roth
Ethylendiamintetra acetic acid (EDTA)	Roth
Filipin (F9765)	Sigma Aldrich
Fetal bovine/calf serum (FBS/FCS)	PAA, Laboratories
Glycerol	Sigma Aldrich
Glycine	Roth
Hydrogen peroxide (30 % H_2O_2)	Merck
INTERFERin® siRNA transfection reagent	Polyplus Science
Isopropanol (p.a.)	Roth
Magnesium chloride	Merck
Methanol (p.a.)	Roth
Milk powder	Roth
Mowiol	Calbiochem
mPEG-5k (Methoxypolyethylene glycol maleimide Mn5) #63187	Sigma Aldrich
NP-40	Calbiochem
N,N,N',N'-Tetramethylethylendiamine (TEMED) (p.a.)	Roth
Page Ruler Prestained Protein Ladder Plus	Thermo Fisher Scientific
Paraformaldehyde	Fluka
Penicillin/Steptomycin	PAA-Laboratories
Sodium dodecyl sulfate (SDS)	Roth

Thiosepharose Beads	Sigma Aldrich
Tris(hydroxymethyl)-aminomethane (TRIS)	Roth
Triton X-100	Sigma Aldrich
Trypan blue 0.4 %	Invitrogen
Trypsin/EDTA	Invitrogen
Turbofect® transfection reagent	Thermo Fisher Scientific
Tween 20	Sigma Aldrich
U18666A	Cayman Chemicals

Any additional chemicals that are not included in the list above were purchased from Merck (Sigma-Aldrich), Roth or Thermo Fisher in lab quality (pro analysis, p.a., grade).

Table 3-2: Frequently used buffers

Buffer	Ingredients
Phosphate buffered saline (PBS)	100 mM Na_2HPO_4 18 mM KH_2PO_4 1.37 M NaCl 27 mM KCl pH 6.8
Phosphate buffer (PB)	19 % (v/v) 0.2 M NaH_2PO_4 81 % (v/v) 0.2 M Na_2HPO_4 pH 7.4
50x Tris-Acetat-EDTA (TAE) Puffer	2 mM Tris/HCl 5.5 % (v/v) acetic acid 50 mM EDTA pH 8.0
10x TBS	400 g NaCl 10 g KCl 150 g Tris Base Fill up to 5 l with ddH2O, pH 7.4
TBS-T	Dilute 10x TBS 1:10 with ddH2O and add 1 % Tween 20
PBS with cOmplete™ protease inhibitor cocktail	One tablet of cOmplete™ protease inhibitor cocktail (Roche Diagnostic GmbH) in 50 ml PBS
5x Laemmli buffer (modified from (Laemmli 1970))	10 % SDS 500 mM DTT 50 % Glycerol 250 mM Tris-HCl 0.5 % bromophenol blue dye, pH 6.8, in ddH2O

3.1.2. Kits

All kits were used according to the manufacturer's protocol.

Table 3-3: List of kits.

Description	Company
BCA-Protein Assay Kit	Pierce; Thermo Fisher Scientific, Waltham, US
ECL Advanced/Plus Western Blot Detection Kit	GE Healthcare, Munich, DE
High Pure PCR-Purification Kit	Roche, Mannheim, DE
PureYield Plasmid Midiprep System	Promega, Mannheim, DE
Plasmid Miniprep Kit	Thermo Fisher Scientific, Waltham, US

3.1.3. Cell lines

Name	Description	Origin/ Supplier
LIMP-2 KO MEFs (E5)	Primary murine embryonic fibroblasts; LIMP-2 deficient	(Reczek *et al.* 2007)
LIMP-2 KO MEFs (583-2)	Primary murine embryonic fibroblasts; LIMP-2 deficient	Dr. J. Schröder, laboratory of Prof. Saftig,University of Kiel; (Blanz *et al.* 2010)
WT MEFs (583-3)	Wild-type murine embryonic fibroblasts	Dr. J. Schröder, laboratory of Prof. Saftig CAU Kiel; (Blanz *et al.* 2010)
CHO K1		established cell line, ATCC® CCL-61™
A431		ATCC (CRL-1555)
Cos7	Kidney cell line from African green monkey; SV40 immortalized	ATCC / DSMZ, established cell line
HeLa	Cervical carcinoma cells (Henrietta Lacks)	Deutsche Sammlung von Mikroorganismen und Zellkulturen (DSMZ), established cell line
HeLa NPC1 KO	CRISPR/Cas9-mediated knockout of NPC1 in HeLa WT cells	(Tharkeshwar *et al.* 2017)
HeLa LIMP-2 KO	CRISPR/Cas9-mediated knockout of LIMP-2 in HeLa WT cells	This work
HeLa NPC1/LIMP-2 KO	CRISPR/Cas9-mediated knockout of LIMP-2 in HeLa NPC1 KO cells	This work
Niemann-Pick Type C (NPC) fibroblasts	Human fibroblasts from biopsy of NPC-1 patients	(Millard *et al.* 2000)

3.1.4. Bacteria

Table 3-4: Strains of bacteria used for amplification of plasmid DNA

Organism	Strain	Genotype	Reference
Escherichia coli	XL1-blue	*recA1 endA1 gyrA96 thi -1 hsdR17, supE44 relA1 lac-* [F´pro AB lacIqZΔM15 Tn10(tetr)]	Agilent technologies

For plasmid preparation of all constructs mentioned in this work bacteria were grown on solid and in liquid lysogeny broth (LB)-media, respectively, after sterilization by applying 121 °C and high pressure. To ensure the selective raise of bacteria, sterilized antibiotics according to the resistance encoded on the respective plasmid were added before inoculation.

Liquid LB medium	
1 % (w/v)	tryptone
0.5 % (w/v)	yeast extract
0.1 % (w/v)	glucose
0.5 % (w/v)	NaCl
pH 7.3	

Solid LB medium		
10	g	tryptone
5	g	yeast extract
10	g	NaCl
15	g/l	bacto-agar
ad 1 l ddH_2O; ph7, autoclave, pour warm liquid into 10 cm sterile dishes		

Table 3-5: Antibiotics used for selective raise of bacteria

Antibiotic	Solvent	Stock solution	Final concentration in *E. coli*
Ampicillin	ddH_2O	100 mg/ml	100 µg/ml
Kanamycin	ddH_2O	100 mg/ml	100 µg/ml

3.1.5. Mouse strains

In this study, a strain of LIMP-2 KO mice (full name of mouse strain Eli II 24 +/- RK) was utilized that was first described and established by Gamp and colleagues and additionally analyzed by Berkovic and co-workers (Gamp *et al.* 2003, Berkovic *et al.* 2008). The mice were subsequently backcrossed into C57BL/6N from Charles River as described in (Rothaug *et al.* 2014, Zunke *et al.* 2016).

The LIMP-2-Y163D knock-in mice generated in the framework of this study are described in 3.6.2.

Animal housing is described in 3.6.1. Animal handling and care were performed in agreement with the German animal welfare law according to the guidelines of the Christian-Albrechts University of Kiel. Experiments involving animals were approved by the Ministry of Energy, Agriculture, the Environment and Rural Areas Schleswig-Holstein under the reference number V312-72241.121-3.

3.1.6. List of plasmids and constructs

The plasmids and constructs used in this work are listed below:

Table 3-6: Plasmids

Plasmid	Description	Reference
pXJ40.mVAPA.GFP	murine VAPA with GFP-tag; Amp^R	Prof. D. Neculai
pXJ40.mVAPB.Flag	murine VAPA with Flag-tag; Amp^R	Prof. D. Neculai
pEGFP.hSTARD3.HA	Human STARD3; the GFP-tag of the vector was exchanged for HA; Kan^R	Prof. D. Neculai
mGramd1b.GFP	murine Gramd1b with GFP-tag; Kan^R	Prof. D. Neculai
pFROG.mLIMP-2.WT.myc	murine LIMP-2.WT with myc-tag, Amp^R	generated by Dr. M. Schwake
pFROG.mLIMP-2.G379W/V415W.myc	murine tunnel mutant of LIMP-2 with myc-tag; Amp^R	generated by Dr. M. Schwake
pFROG.LIMP-2.C4S.myc	single palmitoylation mutant of LIMP-2, denoted LIMP-2.P3x; Amp^R	This work
pFROG.LIMP-2.C5S.myc	single palmitoylation mutant of LIMP-2, denoted LIMP-2.P3x; Amp^R	This work
pFROG.LIMP-2.C458S.myc	double palmitoylation mutant of LIMP-2, denoted LIMP-2.P3x; Amp^R	This work
pFROG.LIMP-2.C4,5,458S.myc	triple palmitoylation mutant of LIMP-2, denoted LIMP-2.P3x; Amp^R	This work
pmCherryN1.mLIMP-2.WT.mCherry	murine LIMP-2.WT with mCherry-tag; Kan^R	This work
pmCherryN1.mLIMP-2.G379W/V415W.myc	murine tunnel mutant of LIMP-2 with mCherry-tag; Kan^R	This work
hLIMP-2.cmr.GFP	human LIMP-2.WT/CD36 chimera; GFP-tag	Prof. D. Neculai
hLIMP-2.cmr.mCherry	human LIMP-2.WT/CD36 chimera; mCherry-tag	Prof. D. Neculai

hLIMP-2.cmr.A379W/V415W.mCherry	human LIMP-2 tunnel mutant/CD36 chimera; mCherry-tag	Prof. D. Neculai
PB-T-PAF.protein A.His_6.hLIMP-2.aa35–430	plasmid for generating the recombinant LIMP-2 luminal domain	Prof. D. Neculai
pCEpuro-his-myc-hDHHC6	human DHHC6;his- and myc-tag Amp^R	Prof. van der Goot
pEF-Bos-DHHC20.HA	human DHHC20;HA-tag Amp^R	

3.1.7. Oligonucleotides

Table 3-7: List of utilized oligonucleotides

#*	Name	Sequence 5'→3'
22	SCARB2_intr3-4_rev_2	actaaacagaaaatccaaccagtgac
24	SCARB2_intr3-4_for_4	cacacacacacagagtaataggagaaag
26	SCARB2_EcoRI_for	actGAATTCCatgggcagatg
27	SCARB2_BamHI_rev	agtGGATCCGAGGTTCGTATGAG
28	pmCherry2N1_end_rev	AAAACCTCTACAAATGTGGTATGGCTG
29	mCherry_middle_rev	ACCCTTGGTCACCTTCAGCTTG
33	pFROG_for	gagaacccactgcttactgg
34	pFROG_rev	agaacacccgaatggagtctc
40	mSCARB2_C4S_for	gtgtagaagcaggatctgcccatggtggc
41	mSCARB2_C4S_rev	gccaccatgggcagatcctgcttctacac
42	mSCARB2_C5S_for	CGCCGTGTAGAAGGAGCATCGGCCCAT
43	mSCARB2_C5S_rev	ATGGGCCGATGCTCCTTCTACACGGCG
44	mSCARB2_C458S_for	cctgtcctcgagacgccagccacgtg
45	mSCARB2_C458S_rev	cacgtggctggcgtctcgaggacagg
46	mSCARB2_C4SC5S_for	ccgccgtgtagaaggaggatctgcccatggtg
47	mSCARB2_C4SC5S_rev	caccatgggcagatcctccttctacacggcgg
48	seq_mSCARB2pFROG_rev	TCACCAGCAGCAGCAGAGACAGC
49	seq_hSCARB2pFROG_rev	CCAGCAGGAGCAGGGA
96	GenoLi2Cris_for	CCGGCCCCTTTACAAATA
97	GenoLi2Cris_rev	TGAGACTTGGCCCAGTCTAC

*: number referring to the lab's primer list

3.1.8. siRNA

Table 3-8: List of utilized siRNAs.

Target	Name of siRNA	Manufacturer
hLIMP-2	Silencer™ Select, #s2526	Thermo Fisher Scientific
hNPC1	Silencer™ Select, #9669	Thermo Fisher Scientific
Negative control	Silencer™ Select Negative control 1, #4390843	Thermo Fisher Scientific

3.1.9. Enzymes

Table 3-9: List of utilized enzymes

Description	Manufacturer
DNA-polymerases	
Phusion DNA polymerase	Thermo Fisher Scientific
DreamTag™ polymerase	Thermo Fisher Scientific
Restriction endonucleases & other enzymes	
DpnI (10 U/µl)	Thermo Fisher Scientific
EcoRI	Thermo Fisher Scientific
HindIII	Thermo Fisher Scientific
T4 DNA ligase	Thermo Fisher Scientific
Proteinase K	Roche

3.1.10. Antibodies

Table 3-10: List of primary antibodies utilized for immunofluorescence (IF) and Western blot (WB).

Name	Host	Dilutions		Source
		IF	WB	
α-β-Actin (#A2066)	rabbit	-	1:8000	Sigma Aldrich
α-GFP (#29565)	rabbit	-	1:1000	Cell Signaling
α-mGC (#4171)	mouse	-	1:500	Sigma Aldrich
α-hGC (8E4)	rabbit	-	1:500	Prof. Dr. Johannes M.F.G. Aerts, NL

α-HA (3F10)	rat	-	1:1000	Sigma Aldrich
α-mLAMP-1 (1D4B)	rat	1:500	1:1000	DSHB
α-hLAMP-2 (H4B4)	mouse	1:500	1:1000	DSHB
α-LIMP-2 (Tier 2; L2T2)	mouse	1:250	1:2000	Pineda Antibody Service
α-myc (9B11)	mouse	1:250	1:2000	Cell Signaling
α-myc (71D10)	rabbit	1:100	1:1000	Cell Signaling
α-TMEM55B	rabbit	-	1:2000	Proteintech
α-GAPDH (#sc-25778)	rabbit	-	1:2000	Santa Cruz Biotechnology
α-NPC1 (#ab134113)	rabbit	-	1:2000	Abcam
α-NPC2	rabbit	-	-	
α-SREBP2	mouse	-	1:250	
α-LDLR	rabbit	-	1:1000	
α-HMGCR	rabbit	-	1:1999	

Table 3-11: Secondary antibodies utilized for immunofluorescence (IF) and Western blot (WB).

Name	Host	Dilutions		Source
		IF	WB	
α-Mouse-HRP (#515-035-062)	sheep	-	1:10,000	Dianova GmbH
α-Rabbit-HRP (#111-035-144)	sheep	-	1:10,000	Dianova GmbH
α-Rat-HRP (#112-035-143)	rabbit	-	1:10,000	Dianova GmbH
α-Mouse-Alexa Fluor 488/594/647 (A21202, A21203, A31571)	goat or donkey	1:500	-	Thermo Fisher Scientific
α-Rabbit-Alexa Fluor 488/594/647 (A21206, A21207, A31573)	goat or donkey	1:500	-	Thermo Fisher Scientific
α-Rat-Alexa Fluor 488/594/647 (A21208, A21209, A21447)	goat or donkey	1:500	-	Thermo Fisher Scientific

3.2. Molecular biological methods

3.2.1. Generation of expression constructs by site-directed mutagenesis PCR

LIMP-2 mutants used for assessing LIMP-2 palmitoylation were generated using specifically designed primers (#40-47, see 3.1.7) that harbored the desired base pair change and the plasmid encoding the DNA for the wild type protein (pFROG-LIMP-2.WT.myc) as template DNA in a mutagenesis PCR. Amplification of the template DNA with these primers led to the exchange of amino acids at the desired position in the LIMP-2 sequence.

Mutagenesis PCR mix	**PCR-program**			
	Reaction	**Duration**	**Temperature**	
10 ng template DNA	Denaturation	5 min	98 °C	
1 µl of 500 ng/µl				
10 µl 5x HF buffer	Denaturation	30 s	98 °C	34x
1 µl 10 µM primer forward	Annealing	30 s	x °C	
1 µl 10 µM primer reverse	Elongation	3.5 min	72 °C	
6.25 µl 2 mM dNTPs	final Elongation	10 min	72 °C	
0.75 µl Phusion Polymerase	Storage	∞	10 °C	
ad 50 µl ddH_2O				

The Annealing temperature was chosen according to the melting temperature of the primers used for the reaction and was usually between 55 °C and 65 °C. 1 µl of the enzyme DpnI was added to the PCR products and samples were incubated at 37 °C for 1 h. DpnI is a methylation-sensitive restriction enzyme. Only the plasmid template which had been propagated in bacteria contains methylated DNA and is therefore digested by DpnI. Thus, only the PCR product containing the mutated sequence was retained. The PCR products were subsequently transformed into bacteria (3.2.4) and clones were analyzed.

3.2.2. Agarose gel electrophoresis

For genotyping and cloning, samples of a PCR reaction were subsequently separated via DNA agarose gel electrophoresis. For genotyping, a 2 % (w/v) agarose (in 1x TAE buffer) gels were used and for cloning purposes, a 1 % (w/v) agarose gel was used. The specific pore size of the agarose matrix and the application of an electric field (130 V for 20-40 min) allow the samples to migrate into the gel matrix. Due to the negative charge of their backbone, DNA fragments have distinct migration velocities and thus are separated according to their size.

Prior to separation, 6x DNA loading dye was added to the samples (Thermo Fisher Scientific). For visualization of the bands in the gel, 500 ng/ml ethidium bromide, which intercalates into the DNA and can be visualized under UV light (λ = 312 nm), was added to the gel before polymerization. The size of the separated DNA fragments was assessed using Gene Ruler 1 kb DNA Ladder (Thermo Fisher Scientific).

3.2.3. Generation of chemically competent *Escherichia coli*

An aliquot of *E.coli* XL1-blue cells was added to 5 ml LB medium (3.1.4) supplemented with 5 µl tetracycline stock solution and cultured over night at 37 °C, 200 rpm. On the next day, 40 ml LB medium was inoculated with the overnight culture and incubated at 37 °C for 2-3 h, until an OD_{600} of 0.4-0.6 was reached. The culture was stored on ice in 50 ml sterile plastic tubes for 20 min and subsequently pelleted for 15 min at 5,000 g and 4 °C. The supernatant was discarded and the pellets resuspended in 20 ml ice-cold TBS. Cells were pelleted again (10 min, 5,000 g and 4 °C), the supernatant discarded and the pellet resuspended in 20 ml of ice-cold $CaCl_2$ after which the bacteria were incubated on ice for 20-60 min. Centrifugation (10 min, 5,000 g and 4 °C) was followed by discarding of the supernatant and next, the cell pellet was resuspended in 2 ml ice-cold $CaCl_2$ and incubated on ice for 1 h. Finally, 500 µl of 86 % glycerol solution were added to the bacteria, the mixture was vortexed and placed on ice. The cell suspension was divided into 50 µl aliquots and frozen in liquid nitrogen. Chemically competent cells were stored at -80 °C.

Solution	**Composition**
TBS (200 ml)	0.1M NaCl
	5mM Tris
	5mM MgCl2 x 6H2O
	Adjust to pH 7.0 with 1M HCl
	autoclave
$CaCl_2$ (200 ml)	0.1M CaCl2 x 6H2O
	5mM Tris
	5mM MgCl2 x 6H2O
	Adjust to pH 7.0 with 1M HCl
	autoclave

3.2.4. Transformation of chemically competent *Escherichia coli*

PCR products and plasmid cDNA were transformed into chemically competent *E. coli* cells (strains XL1-blue) via heat-shock transformation. A 50 µl aliquot frozen at -80°°C was thawed

on ice for 10 min. 4 µl of PCR product or 1 µl of plasmid DNA, respectively, was added to the cells followed by incubation for 30 min on ice. The bacteria were subjected to a 45s heat-shock at 42 °C. Cells were immediately incubated on ice for 3 min before 300 µl of pre-warmed LB medium (w/o antibiotics) were added for the cell's recovery. Then the cells were incubated for 45 min at 37° C and 750 rpm. Then, the cells were pelleted (30 s, 13,000 rpm), the supernatant was discarded except for the last 100 µl in which the cells were resuspended and subsequently plated onto LB agar plates containing antibiotics according to the resistances encoded on the generated plasmid. For amplification of plasmids via midi prep (3.2.5), the cell suspension was not pelled, but added directly to 150-200 ml of LB medium supplemented with the respective antibiotic. Cells were grown overnight at 37 °C. LB agar plates were subsequently stored at 4 ° C.

3.2.5. Expression and purification of plasmid DNA

To verify successful mutagenesis of an expression plasmid (3.2.1), the plasmid was transformed into chemically competent cells as describe above and single clones were picked from the LB agar plate. They were grown over night in 3 ml LB + antibiotics (usually 100 µg/ml ampicillin or kanamycin) at 37 ° and 200 rpm. The plasmid DNA was isolated using the GeneJET™ Plasmid-Miniprep-Kit (Thermo Fisher Scientific) according to the manufacturer's protocol. Subsequently, an aliquot of the DNA was sequenced with appropriate primers (3.1.7) at Eurofins Genomic GmbH.

For the amplification of expression plasmids, an 150-200 ml overnight culture was prepared as described in 3.2.4 and subsequently, cells were pelleted and the plasmid DNA was isolated using the PureYield™ Plasmid Midiprep System (Promega) according to the manufacturer's protocol.

3.3. Cell biological methods

3.3.1. Cultivation of mammalian cell lines

The mammalian cell lines were grown in HeraCell240 cell culture incubator at 37 °C and 5 % CO_2. For maintenance, cells were grown to 100 % confluency and subsequently passaged into a new cell culture dish. To this end, old media was removed, cells were gently washed with sterile PBS and 1 ml of Trypsin/EDTA was added to a 10 cm dish (0.5 ml for a 6 cm dish) until the cells detached. They were then gently resuspended in fresh medium and transferred to the new dish at a median dilution of 1:10 (when passaging twice a week).

Material	Ingredients
Medium HeLa A431 MEFs	Dulbecco´s Modified Eagle Medium (DMEM) 4.5 g/ml D-Glucose, L-Glutamine (Gibco, Thermo Fisher Scientific) + additives: 10 % FCS 1 % Penicillin/Streptomycin
CHO M12 (NPC1-deficient)	Dulbecco's Modified Eagle Medium/Nutrient Mixture F-12 (DMEM/F-12) (Gibco, Thermo Fisher Scientific) + additives: 10 % FCS 1 % Penicillin/Streptomycin 2 mM L-glutamine
CHO K1 WT	Ham's F12 medium (Shanghai Basalmedia Technologies Co., Ltd., L410) + additives: 10 % FCS 1 % Penicillin/Streptomycin
Trypsin/EDTA	0.5 mg/ml Trypsin 0.22 mg/ml EDTA, in PBS

3.3.2. Cryopreservation and thawing of mammalian cell lines

Aliquots of each cell line were frozen for long-term storage in liquid nitrogen. For this purpose, cells were grown to 100 % confluency on 10 cm plates and subsequently detached with trypsin/EDTA. Cells were resuspended in 6 ml of culture medium and pelleted for 5 min at 800 rpm and room temperature. The pellet was then resuspended in 1 ml of ice-cold freezing medium and the cell suspension was immediately transferred to a cryotube and stored on ice. Cells were subsequently frozen at 80 °C for 24-48 h and next transferred to a liquid nitrogen tank.

In order to thaw aliquots of cells, cryotubes were carefully removed from liquid nitrogen storage and warmed till cells began to thaw. The content of the cryotube was transferred to a tube containing 9 ml of pre-warmed culture medium. Cells were pelleted (5 min at 800 rpm, room temperature) and the pellet resuspended in 10 ml of fresh pre-warmed culture medium and

transferred to a cell culture dish (10 or 6 cm, depending on the cell pellet size). The dishes were transferred to the cell culture incubator. After 4 hours, attachment of the cells to the bottom of the dish was monitored. Cells were passaged for one week after thawing before utilization for an experiment.

Material	**Ingredients**
Medium HeLa A431 MEFs	Dulbecco´s Modified Eagle Medium (DMEM) 4.5 g/ml D-Glucose, L-Glutamine (Gibco, Thermo Fisher Scientific) + additives: 10 % FCS 1 % Penicillin/Streptomycin
Medium for freezing	Dulbecco´s Modified Eagle Medium (DMEM) 4.5 g/ml D-Glucose, L-Glutamine (Gibco, Thermo Fisher Scientific) + additives: 20 % FCS 10 % DMSO 1 % Penicillin/Streptomycin
Trypsin/EDTA	0.5 mg/ml Trypsin 0.22 mg/ml EDTA, in PBS

3.3.3. Transient transfection of mammalian cell lines

Cells were seeded in DMEM + 10% FCS + 1% P/S (or the cell-specific medium) in 6 cm or 10 cell culture dishes such that they were ~70 % confluent the next day. For indirect immunofluorescence experiments (3.3.6), cells were seeded onto glass coverslips (cs, 13 mm diameter) which were placed in wells of 6-well plates (4 cs per well). Cells were transfected the next day following the pipetting scheme in Table 3-12. The mixture was gently mixed and briefly spun down and incubated for 20 min at room temperature. The transfection mix was added to the cells (dropwise). After 4-6 h, the medium was replaced with fresh medium. After 48 h, cells were either fixed with 4 % PFA (for IF) or harvested in PBS + cOmplete^{TM} protease inhibitor cocktail. Fixed cells were stored in PBS at 4 °C and cell pellets were stored at -20 °C.

Table 3-12: Pipetting scheme for transient transfection of mammalian cell lines.

Reagent	6-well-plate	6 cm dish	10 cm dish
DMEM only (µl)	100	150	200
Plasmid DNA (µg)	1	2	3
Turbofect (Thermo Fisher Scientific) (µl)	2	4	6
Total medium	2 ml	3 ml	6 ml

3.3.4. siRNA transfection

In order to transiently deplete a protein from cells, the expression of the respective gene was down-regulated with the use of silencing RNAs (siRNAs, 3.1.8). To accomplish this, cells were seeded in the desired dish and immediately transfected with the reaction mixture as indicated in Table 3-13. The mix was prepared in the order indicated in the table and vortexed immediately for 10 s. The mixture was spun down and incubated at RT for 15 min. In the meantime, the cells were seeded into the cell culture dishes and then the transfection mixture was added to the cells (dropwise) and distributed by gentle shaking of the dish. The cells were cultured at 37 °C and 5 % CO_2 for 48 h. The medium was replaced with fresh medium and the siRNA transfection was repeated (w/o detaching the cells first). After another 24 h, the transfection was repeated again and after an additional 6 h, the cells were harvested in PBS + cOmplete™ protease inhibitors.

Table 3-13: Pipetting scheme for siRNA-mediated knockdown

Reagent	6-well plate	6 cm dish	10 cm dish
DMEM only	200	400	666
siRNA (stock 20 µM), diluted 1:10 in ddH_2O	5 nM (5,5 µl)	5 nM (11 µl)	5 nM (18 µl)
Interferin (PolyScience)	5 µl	10 µl	16 µl
Medium total	2 ml	4 ml	6 ml

3.3.5. Generation of CRISPR/Cas9 knockout cell lines

The CRISPR-Cas9 system utilizes the bacterial endonuclease Cas9 to introduce double-stranded DNA (dsDNA) breaks at a specific DNA locus. It is directed there by a guide RNA (gRNA) consisting of a crispr RNA (crRNA) complementary to the targeting sequence and a trans-activating crRNA (tracrRNA) serving as a binding scaffold for the Cas9 enzyme. The two

RNA molecules can also be fused together to form a single guide RNA (sgRNA), thus simplifying the experimental procedure (Jinek *et al.* 2012). The cellular DNA repair machinery in cells uses nonhomologous end joining (NHEJ) to restore the strands and in the course of this process may insert or delete a few base pairs leading to frame shift mutations. Alternatively, homology-directed repair (HDR) can incorporate a donor sequence during the repair of the dsDNA break (Knott and Doudna 2018).

To generate HeLa LIMP-2 and HeLa NPC1/LIMP-2 KO cell lines, single guide RNA (sgRNA # 76195843) and Cas9 enzyme from Synthego were used. Electroporation was carried out with the Neon Transfection System from Thermo Fisher Scientific. The procedure was carried out as described in the protocol provided by Synthego (CRISPR Editing of Immortalized Cell Lines with RNPs using Neon Electroporation).

In order to assess the targeting efficacy of the transfection, genomic DNA was isolated from each single clone. An aliquot of the transfected cells was harvested and lysed in 100 µl DirectPCR® Lysis Reagent Tail (Peqlab) and + 1 µl proteinase K (no mixing) while incubating at 55 °C and 800 rpm (thermocycler) for 2-4 h. In the following, the samples were incubated at 85 °C for 45 min and briefly spun down to pellet cell debris. 1 µl of the supernatant was used for genotyping PCR. An aliquot of the PCR reaction was subsequently sequenced and analyzed with the Interference of CRISPR edits (ICE) tool from Synthego to confirm the presence of frame-shifting insert/ deletions (indels). Furthermore, the expression of the targeted protein was analyzed via Western blot. Finally, single clones were isolated and grown to be used in future experiments.

Table 3-14: Components and program of CRISPR genotyping PCR.

Genotyping PCR mix	**PCR-program**			
	Reaction	**Duration**	**Temperature**	
1 µl genomic DNA	Denaturation	2 min	94 °C	
5 µl 10x DreamTag buffer	Denaturation	30 s	94 °C	35x
0.5 µl 20 µM primer forward (#96)	Annealing	30 s	56.8 °C	
0.5 µl 20 µM primer reverse (#97)	Elongation	1 min	72 °C	
1 µl 10 mM dNTPs	final Elongation	2 min	72 °C	
0.5 µl DreamTag polymerase	Storage	∞	10 °C	
ad 50 µl ddH_2O				

3.3.6. Indirect immunofluorescence (IF) staining

To visualize proteins in fixed cells, they were seeded in 6-well-dishes containing class coverslips and, if desired, transiently transfected with plasmid DNA as described in 3.3.3. Prior to fixation, cells were washed three times with PBS. They were then incubated with 4 % paraformaldehyde (PFA) in PBS for 20 min, protected from light. Afterwards, the cells were washed again three times with PBS. To quench unreacted PFA, the coverslips were next incubated with 50 mM NH_4Cl in PBS for 15 min at RT and afterwards rinsed again with PBS. For the immunofluorescence staining, the coverslips were washed in PBS-saponin for 5 min at RT with gentle shaking. In the following, the samples were incubated with 0.12 % glycine/PBS-saponin for 10 min at RT with gentle shaking. Next, the coverslips were washed twice with PBS-saponin and incubated with 10 % FCS in PBS-saponin for 15 min at RT with gentle shaking. The primary antibodies were diluted in 10 % FCS in PBS-saponin at appropriate concentrations (3.1.10). In a wet chamber, each coverslip was placed on top of a 50 µl-droplet of primary antibody solution with the cell-coated side of the coverslip facing downwards. Incubation ensued for 1 h at RT (or 37 °C). The coverslips were washed in PBS-saponin and incubated in a 50 µl-droplet of secondary antibody solution which was previously prepared in 10 % FCS in PBS-saponin at a 1:500 dilution. The samples were incubated for 30 min at RT (or 37 °C). Samples were washed again with PBS-saponin (2-3x) and afterwards with distilled water. Excess liquid was drained on a paper towel. Finally, each coverslip was mounted on a microscopic glass slides in 10 µl pre-warmed Mowiol-DABCO-DAPI mixture. Until microscopic analysis, the samples were stored at 4 °C in the dark.

Material	**Composition**
Washing buffer	0.2 % saponin in PBS
Permeabilization buffer	0.12 % glycine 0.2 % saponin in PBS
Blocking buffer	10 % FCS 0.2 % saponin in PBS
Mounting Medium	1x PBS, pH 7.4 17 % (w/v) Mowiol 4-88 33 % (v/v) Glycerol 20 mg/ml 1,4-diaza-bicyclo-[2,2,2]-octane (DABCO)

3.3.7. Filipin staining

The polyene antibiotic filipin (F9765 (Sigma-Aldrich) derived from the bacterium *Streptomyces filipinensis*) can be used as a fluorescent probe to detect unesterified cholesterol in fixed cells. The antibiotic is extremely sensitive to light and dissolved aliquots (50 mg/ml in DMSO) are prone to oxidation, which is why they are store in liquid nitrogen. Cells were seeded and fixed

as described (3.3.6). The next steps were carried out in a dark environment. The protocol was adapted from (Linder *et al.* 2007).

Filipin was diluted 1:100 in 10 % FCS in PBS and coverslips were placed of 50 µl-droplets of filipin-solution in a wet chamber. The wet chamber was incubated at 37 °C for 30 min. Next, coverslips were washed in PBS 2-3x. Since filipin permeabilizes cell membranes, it is usually not necessary to add detergent, but if needed, 0.1 % saponin can be added. A higher concentration of detergent is not advisable, since PFA does not fix lipids as it fixes proteins and lipids may be washed out if permeabilization is too drastic. Primary antibodies were diluted as indicated in 3.1.10 in 5 % FCS in PBS and the coverslips in the wet chamber were incubated at 37 °C for 1 h. Afterwards, the coverslips were washed again 2-3x in PBS. The secondary antibodies were diluted 1:500 in 5 % FCS and incubated with the coverslips for 30 min at 37 °C. Finally, each coverslip was washed 2-3x in PBS and subsequently in distilled water. The excess liquid was drained onto a paper towel and coverslips were mounted on microscopic glass slides in Mowiol-DABCO. No DAPI (visualization of nuclei) was added, since filipin and DAPI have an overlapping excitation/emission spectrum. Filipin exhibits an extinction spectrum of 240 nm – 380 nm and an emission spectrum of 385 nm – 470 nm.

3.3.8. DiI-LDL binding assay

CHO cells were seeded onto 15 mm coverslips in wells of a 12-well-plate and transfected with hLIMP-2.cmr.WT.mCherry or hLIMP-2.cmr.A379W/V415W.mCherry, respectively, 10 h later. 24 h post transfection, the cells were washed 2x with cold HBSS (Shanghai Basalmedia Technologies Co. Ltd., B410KJ) and incubated with acidic buffer (0.3M $NaCH_3COO$ pH 4.8, 150mM NaCl, 1mM $MgCl_2$, 1mM $CaCl_2$) for 2 min. Next, 20 µg/ml DiI-LDL (20614ES76, YEASEN) which was resuspended in acidic buffer was added to cells and incubated for 20 min on ice. Subsequently, the cells were washed 3x with either acidic buffer or HBSS and lastly fixed with 4 % paraformaldehyde in PBS (15 min, RT).

3.3.9. Labelling of LDL and loading with BODIPY-cholesterol

LDL particles were labelled with Alexa Fluor 647 succinimidyl ester (Thermo Fisher Scientific, A20106) according to the manufacturer's protocol. Next, the labelled LDL was dialyzed for 2 days at 4 °C against PBS using a micro-dialysis apparatus for small volumes. Alexa Fluor 647 labelled LDL (AF647-LDL). To incorporate BODIPY-cholesterol (Avanti, 810255 P) into AF647-LDL (or HDL) particles, the lipid was first dissolved in chloroform, dried under a stream of argon and subsequently dissolved in DMSO and added to the lipoproteins at a concentration of 20 nmol BODIPY-cholesterol for 1 mg lipoprotein with a final DMSO concentration of 10 %. The mixture was incubated at 40 °C for 2 h and afterwards dialyzed for 24 h against PBS +

1 mM EDTA using a MWCO 3,000 dialysis membrane. The PBS/EDTA was exchanged the next day and dialysis repeated three more times. This procedure was adapted from (Blom *et al.* 2012).

3.3.10. Saposin A picodiscs

The preparation of the BODIPY-cholesterol containing saposin A picodiscs was based on the methods described in (Popovic *et al.* 2012, Leney *et al.* 2015) and was modified as described in (Heybrock *et al.* 2019).

3.3.11. Live-cell cholesterol transport assay

Human epithelial A431 cells were seeded onto glass bottom dishes (Nunc LabTek 4-well chambered cover glass) and immediately transfected with siRNAs (3.1.8), before the cells were attached to the dish bottom. After 48 h, the medium was changed to DMEM + 200 µM oleic acid/BSA in 5% LPDS + 50 µg/ml Alexa Fluor 647-dextran (10,000 MW; Thermo Scientific) to induce formation of lipid droplets and label late endosomes/ lysosomes, respectively. After 24 h, the cells were pulse-labelled for 2 h with 50 µg/ml BODIPY-cholesterol-linoleate-LDL in serum-free DMEM. For the last 30 min of pulse-labeling, HCS LipidTox Red or HCS LipidTox Deep Red (1:1000; Thermo Scientific) was added to the medium to visualize lipid droplets. The cells were then washed and chased in serum-free CO_2-independent medium (Gibco) for the 0-4 h and imaged at the indicated time points by live-cell confocal microscopy. Imaging was performed on a Leica TCS SP8 X attached to a motorized DMi8 inverted microscope with ×63 HC PL APO CS2 water objective (1.20 NA). The pulse-chase experiments were performed at 37 °C in CO_2-independent medium (Gibco) which was supplemented with HCS LipidTox Red/Deep Red (1:1000) in a temperature-controlled environmental chamber. The fraction of BODIPY-cholesterol co-localizing with dextran-positive organelles and LipidTox-positive organelles was quantified from background-subtracted images with ImageJ by using Mander's overlap coefficient.

3.3.12. Cholesterol uptake assays

CHO or HeLa cells were seeded onto 15 mm coverslips in wells of a 12-well-plate and transfected with hLIMP-2.cmr.WT.mCherry or hLIMP-2.cmr.A379W/V415W.mCherry, respectively, 10 h later. 24 h post transfection, the cells were washed 2x with pre-warmed HBSS (Shanghai Basalmedia Technologies Co. Ltd., B410KJ) and incubated with acidic buffer (0.3M $NaCH_3COO$ pH 4.8, 150mM NaCl, 1mM $MgCl_2$, 1mM $CaCl_2$) for 2 min. Next, 20 µg/ml LDL that had previously been labelled with AlexaFluor647 dye and loaded with BODIPY-cholesterol (3.3.9), or 10 µl of BODIPY-cholesterol-containing saposin A picodiscs (3.3.10)

were added to cells in acidic buffer and incubated for 15 min at 37 °C. Subsequently, the cells were washed 3x with either acidic buffer or HBSS and lastly fixed with 4 % paraformaldehyde (15 min, RT).

3.4. Protein biochemical methods

3.4.1. Preparation of cell lysates and protein extraction

Cells were washed two times with cold PBS. For a 10 cm dish, 1 ml of PBS + complete protease inhibitors were added (0-5 ml for a 6 cm dish) and the cells were scraped off the dish with a cell scraper and transferred to a 1.5 ml reaction tube. The cells were pelleted (10 min, 10,000 rpm, 4 °C) and the supernatant discarded. The pellet was frozen until further processing. To generate cell lysates, the pellet was solubilized in PBS + Complete protease inhibitor cocktail + 0.5 % Triton by gentle pipetting. The amount of buffer depended on the size of the pellet. The lysate was sonicated 2x 20 s, followed by incubation on ice (30 min). A second sonication step (2x 20 s) was performed and next, the lysate was centrifuged (10 min, 13,000 rpm, 4 °C) and the supernatant transferred to a new tube. The protein concentration was measured via BCA assay (3.4.4) and samples prepared for several downstream applications.

3.4.2. Preparation of murine tissue homogenates

For the preparation of tissue lysates from mouse organs, approximately 100-150 mg tissue was utilized. For brain (or half of a brain), heart, kidney and spleen the whole organ was used. To each sample, 9-fold amount of tissue lysate buffer was added, e.g. to 100 mg tissue 900 µl buffer. Approximately 10 small ceramic beads were added to each sample and the tissues were homogenized with a Precellys® homogenizer (Peqlab) at 5,500 rpm for 2x 20 seconds with 20 s break. The samples were sonicated (2x 20 s) and incubated on ice for 30-60 min after which they were sonicated again (2x 20 s). Cellular debris was pelleted by centrifugation for 15 min at 12,000 rpm and 4 °C. The supernatant was transferred to a fresh tube and protein concentration was determined via BCA (3.4.4). For prolonged storage, tissue lysates were kept at -80 °C.

Chemical	**Amount**
10 mM Tris/HCl pH 7.4	1 ml 1 M Tris/HCl pH 7,4
150 mM NaCl	15 ml 1 M NaCl
1x Complete protease inhibitors	2 pellets
1x PEFA (toxic!)	95.8 mg
5 mM EDTA	1 ml 0.5 M EDTA

+ 0.5% Triton	5 ml Triton (10%)
	78 ml A. dest.
100 ml lysis buffer, check pH (7.4), aliquot buffer and store at -20 °C	

3.4.3. Membrane fractionation of tissue samples

Tissue samples were homogenized with a glass douncer in homogenization buffer (250 mM sucrose, 10 mM Tris-HCl pH 7.2, complete protease inhibitors; 1 ml buffer/ 100 mg tissue) and centrifuged 10 min at 1,000 g and 4 °C. The perinuclear supernatant (PNS) was transferred to a new plastic tube. The pellet was resuspended with buffer (500 µl/ 100 mg tissue) and centrifuged again 10 min at 1,000 g and 4 °C. The PNS was pooled and sonicated 3x 30 s followed by cycles of freeze-thaw (3x). The samples were then centrifuged in an ultracentrifuge at 186,000 g (55,000 rpm with TLA-55) for 1 h at 4°C to separate soluble proteins from membrane proteins and membrane-associated proteins. The supernatant containing soluble proteins was kept for later analysis. The pellet was washed with 1 ml of buffer and centrifuged again at 186,000 g (55,000 rpm with TLA-55) for 1 h at 4°C. The washing step was repeated. Finally, the supernatant was discarded. The pellet was divided in half and one half was resuspended in 2% SDS (1/5th of the volume from the first step, e.g. 200 µl for a half-pellet derived from 200 mg tissue which was resuspended in 2 ml buffer) while the other half was used for the APEGS assay (3.4.18).

3.4.4. Determination of protein concentration

The concentration of the cell and tissue protein extracts was assessed using a colorimetric protein assay, the Bicinchoninic acid (BCA) assay (Pierce™ BCA Protein Assay Kit, Thermo Fisher Scientific). For each BCA assay, a calibration curve with 0 µg/µl - 2 µg/µl BSA was established. By referring the measured absorbance of the sample to the calibration curve, the amount of protein in the measured sample and thus the protein concentration in the initial sample can be calculated as the absorbance of the sample at 562 nm is proportional to amount of protein in that sample. Lysates were diluted 1:10- 1:50. 10 µl of each dilution and the standard curve were pipetted in wells of 96-well-plates. The BCA reagent was diluted according to the manufacturers manual and 200 µl were added to each well. All measurements were carried out in duplicate. The 96-well-plate was incubated for 30 min at 37 °C, protected from light. The absorbance of the samples was measured with a Synergy HT (BioTek) microplate reader.

3.4.5. Co-immunoprecipitation (coIP) studies

To study the interaction between two proteins, co-immunoprecipitation was utilized. This technique employs magnetic beads (Dynabeads™, see Table 3-15) with recombinant protein G covalently bound coupled to the bead surface. Protein G has a high affinity for the Fc region of immunoglobulins from various species (including mouse, rat and rabbit). Antibodies directed against a protein of interest are added to the beads and the bead-antibody complexes are incubated with cell lysates. The target protein will be bound by the antibody. Subsequent washing steps remove any unbound material. Proteins that are interacting with the captured protein of interest will thus be co-purified. For analysis, the protein complexes are detached from the beads/antibody and subsequently analyzed via SDS-PAGE and Western blot (3.4.6, 3.4.8).

The coIP experiments described in this thesis were performed according to the following protocol. Cells were seeded and transfected as described in 3.3.3. After 48 h, cells harvested and lysed as described in 3.4.1, but using 500 µl of EBC buffer as lysis buffer. After determination of protein concentration (3.4.4), 80 µg of lysate was mixed with 5x Laemmli buffer (lysate control). For the IP, 1000 µg of protein lysate was transferred to a new tube and filled up to 400 µl with EBC. 1.5 µl of antibody directed against the protein of interest or protein tag was added to the IP sample. Another tube with 1000 µg of lysate filled up to 400 µl of EBC was prepared, but no antibody was added (beads control sample). In another tube. 400 µl EBC buffer + 1.5 µl antibody was prepared. In parallel, Dynabeads™ were prepared: 50 µl beads-slurry per sample was added to a reaction tube and placed in a magnetic tube holder. The supernatant was removed and an equal amount of blocking buffer (SEA buffer, diluted 1:1 with EBC buffer) was added to the beads. All samples were incubated over night at 4 °C on a rotation wheel. Next, the blocking buffer was removed from the beads and an equal volume of EBC buffer was added. To each IP, beads control and antibody control sample 45 µl of beads slurry was added. All samples were incubated for 1-2 h at 4 °C on a rotation wheel. After the incubation period, samples were briefly spun down, placed in a magnetic tuber holder and the supernatant was removed. The beads (with bound proteins) were washed 4 x 10 min 300 µl EBC per sample (rotating rack at RT). Between washes and after the final wash the supernatant was removed. To detach the bound proteins (and antibody) from the beads, 45 µl of 1x Laemmli buffer was added to each sample and all samples (including lysate control) were heated at 60 °C for 30 min. The beads were briefly pelleted and the supernatant (containing the eluted proteins) transferred to a new tube. For analysis, 30 µg of lysate control and 20 µl of IP, beads control and antibody control samples were loaded onto a polyacrylamide gel for SDS-PAGE and Western blotting. If the same antibody or an antibody raised in the same species was used for IP and detection via Western blot, the Clean-Blot™ IP Detection Reagent

(HRP) was used instead of a secondary antibody. The reagent detects only non-denatured antibodies (whole IgG), thus avoiding unspecific signals derived from the IP antibody fragments. 40 µl reagent was added to 2 ml of 5 % skim milk in TBS-T and the nitrocellulose membrane was incubated for 1 h at RT.

Table 3-15: Materials and buffers used for coIP studies

Material	Composition/Manufacturer
EBC buffer	50mM Tris 120mM NaCl 0.5% NP40 pH 7.4 (HCl) Complete ® protease inhibitors (1 tablet per 50 ml)
SEA BLOCK Blocking Buffer	Thermo Fisher Scientific (#37527)
Dynabeads™ Protein G for Immunoprecipitation	Invitrogen (Thermo Fisher Scientific, #10004D)
Clean-Blot™ IP Detection Reagent (HRP)	Thermo Fisher Scientific (#21230)

3.4.6. SDS polyacrylamide electrophoresis (SDS-PAGE)

Sodium dodecylsulfate polyacrylamide gel electrophoresis (SDS-PAGE) is a method to analyze proteins by separating them according to their molecular weight. Because the binding of negatively charged SDS molecules to the hydrophobic regions of proteins (in a ratio roughly corresponding to the protein's size), the protein's own charge is superimposed and thus the migration speed is related solely to the protein's size. To allow an even start for all samples on a gel, the discontinuous SDS-PAGE system is usually employed consisting of a stacking gel and a separating gel. The large pore size of the stacking gel allows accumulation of the proteins at the border to the separating gel. Thus, the proteins migrate into the separating gel simultaneously and migration speed and migration distance can be correlated to the protein's molecular weight. For this purpose, a molecular weight standard is loaded on each gel (PageRuler™Plus Prestained Protein Ladder, Thermo Fisher Scientific).

Following protein extraction (3.4.1 and 3.4.2), lysates were adjusted to the desired protein concentration and Laemmli buffer (3.1.1) was added to 1x final concentration. Samples were heated for 10 min at 55 °C and 1000 rpm in a thermocycler. Afterwards smaples were briefly spun down. Directly before loading on the gel, the samples were gently mixed.

Proteins were separated either on self-cast gels (composition see 3.4.6) or on NuPAGE™ Novex™ 4-12 % Bis-Tris-protein gels (Thermo Fisher Scientific). Electrophoresis conditions consisted of 80 V for 10 min followed by 120 V for 1.5 h at room temperature.

Table 3-16: Buffer composition for self-cast gels and electrophoresis

Buffer	Composition
Separating gel buffer	1.5 M Tris/HCl pH 8.8 0.4 % (w/v) SDS
Stacking gel buffer	0.5 M Tris/HCl pH 6.8 0.4 % (w/v) SDS
SDS gel electrophoresis running buffer (10x):	0.25 M Tris 0.2 M Glycine 1 % (w/v) SDS
20 x MOPS buffer	Thermo Fisher Scientific

Table 3-17: Pipetting scheme for self-cast polyacrylamide gels

		Separating gel			Stacking gel
		8 %	12.5 %	15 %	4.5 %
Separating/ stacking gel buffer	[ml]		2.6		1.35
30 % (w/v) Acrylamide/ bisacrylamide Rotiphorese® Gel 30 (37.5:1)	[ml]	2.7	4.2	5	1.75
Water	[ml]	4.6	3.1	2.3	3.1
10 % (w/v) ammonium persulfate (APS)	[µl]		60		60
TEMED	[µ]		30		30

For analysis of separated proteins, the gels were subjected to Western blotting (3.4.8).

3.4.7. NativePAGE

In order to analyze proteins and protein complexes according to their net charge, size and native structure, protein lysates can be separated via native polyacrylamide gel electrophoresis (NativePAGE). Coomassie G-250 is used to confer a net negative charge to the proteins without denaturing (opposite to SDS used for SDS-PAGE, 3.4.6). The original blue native PAGE was developed by (Schagger and von Jagow 1991). In this thesis, the NativePAGE™ Bis-Tris-system from Thermo Fisher Scientific was employed. The samples are prepared in NativePAGE™ Sample Buffer containing 1 % Digitonin, a non-ionic detergent. Prior to loading, NativePAGE™ 5 % G-250 Sample Additive was added to the samples (G-250 concentration was 1/4th the detergent concentration). G-250 was furthermore present in the cathode buffer,

but not in the gels. Electrophoresis and subsequent western blotting were conducted according to the manufacturer's manual at 4 °C. For Western blot transfer, a polyvinylidene fluoride (PVDF) membrane was used, since the nitrocellulose membrane utilized for other Western blot transfers (3.4.8) is not compatible with the Coomassie staining the gel (Figure 3-1).

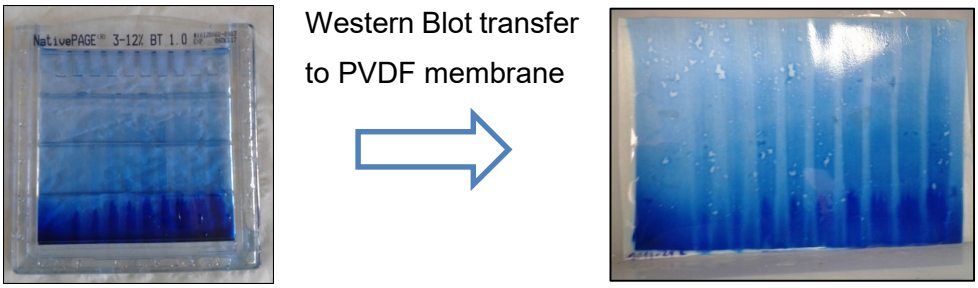

Figure 3-1: Coomassie-stained BN gel/ membrane. A PVDF membrane needs to be used for transfer of proteins by WB after BN-PAGE since the Coomassie dye from the running buffer is incompatible with nitrocellulose membranes.

Native proteins and protein complexes bound on the PVDF membrane were detected with specific antibodies as described below (3.4.8).

3.4.8. Western blot, immunodetection and re-probing of membranes

Following SDS-PAGE, the separated proteins were transferred from the polyacrylamide gels to nitrocellulose membranes (GE Healthcare). The gel was placed on the nitrocellulose membrane and both were placed between a layer of Whatman paper on each side. The layers were placed into a blotting cassette and put into the blotting chamber of the TANK-blot system containing the pre-cooled transfer buffer, fully immersing the blotting cassette in transfer buffer. A current of 800 - 850 mA, perpendicular to the blotting cassette, was applied and the blot was run for 120 minutes at 4 °C. In order to avoid any unspecific binding of the antibody, the nitrocellulose membrane was then incubated in blocking buffer for at least one hour at room temperature before incubating the membrane with primary antibody (in blocking buffer) at 4 °C over night on a rotating device. The next day, membranes were washed 3x 10 min with TBS-T and subsequently incubated with the respective horseradish peroxidase-coupled secondary antibody (in blocking buffer) for 1 h at room temperature. For employed primary and secondary antibodies, see 3.1.10. Prior to detection, the membranes were again washed 3x with TBS-T (10 min each). Chemiluminescence from horseradish peroxidase activity was monitored using the Amersham™ Imager 680. To this end, the membrane was placed on the detection plate, residual TBST was removed and 300 µl ECL (enhanced chemiluminescence) mix was added to the membrane. Immediately afterwards, the detection plate was placed inside the imager and detection was started. Obtained signals were quantified with ImageJ. The band intensity was normalized to the respective loading control.

In order to incubate the membrane with additional primary and secondary antibodies, the initially bound antibodies were removed from the membrane by incubating them with either acidic stripping buffer (mostly removes secondary antibody) or β-mercaptoethanol-containing stripping buffer for 30 min at 80 °C. Afterwards the membrane was washed (3x for acidic buffer, 3-4 h for stripping buffer w/ β-mercaptoethanol) with TBS-T and subsequently incubated with blocking buffer and in the following with primary antibody as described above.

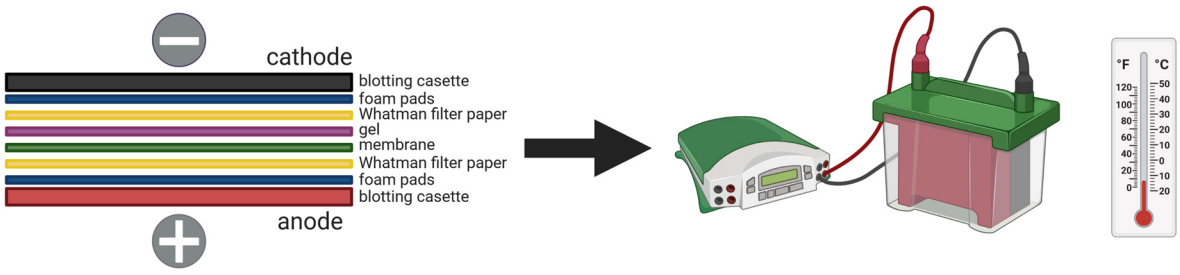

Figure 3-2: Arrangement of gel and membrane in the blotting cassette. The negatively charged proteins migrate towards the positively charged anode. In the TANK blot system, the blotting cassette is fully immersed in transfer buffer. The blotting procedure is carried out at 4 °C.

Table 3-18: Buffers and solutions needed for Western blotting and immunodetection

Buffer	Composition
Transfer buffer	20% (v/v) Methanol
	25 mM Tris
	200 mM Glycin
	ddH2O
TBS-T	20 mM Tris/HCl pH 7,0
	150 mM NaCl
	0.1% (v/v) Tween20
	ddH2O
Blocking buffer	5 % (w/v) skim milk powder (Roth) in TBS-T
Detection solution A	0.1 M TrisHCl pH 8,6
	0.025% (w/v) Luminol
Detection solution B	0.11% (w/v) p-coumaric acid in DMSO
ECL mix	1 ml detection solution A
	100 µl detection solution B
	50 µl ECL Ultra Solution A, LUMIGEN
	50 µl ECL Ultra Solution B, LUMIGEN
	3 µl 30% H2O2
Acidic stripping buffer	100 mM glycine
	20 mM Mg-Acetate x 4 H2O
	50 mM KCl

Stripping buffer w/ β-mercaptoethanol	In ddH2O, pH 2.2 2 % SDS 62.5 mM Tris/HCl 0.83 % β-mercaptoethanol

3.4.9. Measurement of lysosomal GCase activity in cell and tissue lysates

The assay for measurement of lysosomal GCase activity was based on the assay described by Aerts and colleagues (Aerts *et al.* 1985). Lysates were diluted to a concentration of 1 µg/µl to maintain an equal concentration of detergent (from the lysis buffer) in each sample. For each sample, 6 individual measurements were done (2x 3 replicates). Each consisted of 24 µl lysate that were pipetted into a black 96-well plate. To three wells of one sample, 400 µM of conduritol-β-epoxide (CBE) and to the other three wells of the same sample 1 µl of PBS were added. The 96-well plate was sealed with parafilm and incubated at 37 °C for 30 min. Next, 100 µl of the artificial substrate 4-MU-Glc mix were added to each well. A standard (1 nmole free 4MU + 124 µl water) and a control (ctrl) without lysate (25 µl water, 100 µl 4-MU-Glc mix) were incubated in additional wells. The plate was sealed again and incubated at 37 °C for 30 min. The reaction was then quenched with 200 µl stopping buffer and the fluorescence (E) measured with a Synergy HT (BioTek) microplate reader at excitation / emission wavelengths of 365 nm and 460 nm, respectively. CBE is a specific inhibitor for GCase (GBA1), thus in these wells, the activity of the non-lysosomal GCase (GBA2) is measured, while in the wells containing PBS instead the activity of both GBA1 and GBA2 is measured. Thus, for calculating the lysosomal GCase (GBA1) activity, the values obtained from the samples including CBE were subtracted from the values of samples containing PBS instead. The mean fluorescence of 3 replicates was calculated and the fluorescence of the negative control (ctrl) was subtracted. In the following, the GCase activity in nmoles/ µg/ hour was calculated. The value was multiplied with 1000 to yield nmoles/mg/h.

$$Activity\ [nmoles/\mu g/h] = ((\Delta E^{*}(\frac{60}{t[min]})/[Arbs]1\ \text{nmole}/\ V\ [\mu l]\ )/c\ \left[\frac{\mu g}{\mu l}\right])$$

$$\Delta E = \overline{E} - ctrl$$

Chemical	Composition/Manufacturer
CBE	FOCUS Biomolecules (Philadelphia, USA)
4-Mu-Glc mix	150 mM citrate-Na_2HPO_4, pH 5.2 0.2 % (w/v) taurocholate 0.1 % (v/v) Triton X-100 0.1 % (w/v) BSA 1.25 mg/mL 4-Methylumbelliferyl-β-D-glucopyranoside
Free 4-MU	0.5 mM 4-MU in 100 % ethanol
Stopping buffer	0.3 NaOH-glycine (pH 10.6)

3.4.10. Endoglycosidase H and Peptide:N-glycosidase F digest

For the analysis of the glycosylation status of proteins two enzymes can be employed. The glycosidase endoglycosidase H (endo H) cleaves high mannose type sugars within their chitobiose core as well as some hybrid *N*-linked oligosaccharides. The amidase Peptide:N-glycosidase F (PNGase F) cleaving between the innermost *N*-acetylglucosamine (GlcNAc) and asparagine residues of high mannose, hybrid, and complex oligosaccharides, therefore almost all *N*-linked oligosaccharides. Fo both enzymatic assays, 50 µg of protein lysate was used and filled up to 20 µl. For endo H digest, 23 µl endo H buffer were added and the sample incubated at 95 °C for 5 min. Upon cooling of the sample 2 µl endo H enzyme were added and the sample was incubated at 37 °C over night in a thermocycler. Next, 5x Laemmli buffer (Table 3-2) was added to a final concentration of 1x. As negative control, PBS instead of endoglycosidase H was added to the lysate. For PNGase F digestion, 11 µl of PNGase F buffer 1 was added to the prepared sample (see above). Incubation at 95 °C for 5 min was followed by addition of 2 µl of PNGase F enzyme and 12 µl of PNGase F buffer 2 and overnight incubation at 37 °C (thermocycler). As described above, 5x Laemmli buffer (Table 3-2) was added to a final concentration of 1x. For subsequent analysis, all samples were incubated at 55 °C for 30 min and separated on a SDS-PAGE followed by Western blotting (3.4.6, 3.4.8).

Table 3-19: Buffers needed for enzymatic digest with endo H and PNGase F, respectively.

Material	Composition/ Supplier
Endoglycosidase H buffer	100 mM sodium citrate 0.1 % β-mercaptoethanol 1 % SDS 1x cOmplete™ protease inhibitor pH 5.5
Peptide:N-glycosidase F-buffer 1	50 mM sodium phosphate 1 % SDS 1 % β-mercaptoethanol 1x cOmplete™ protease inhibitor pH 7.8
Peptide:N-glycosidase F-buffer 2	50 mM sodium phosphate 1 % NP-40 1x cOmplete™ protease inhibitor

	pH 7.5
Endoglycosidase H	Roche Diagnostic GmbH
Peptide:N-glycosidase F	Roche Diagnostic GmbH

3.4.11. SREBP2 cleavage assay

The assay was adapted from (Chu *et al.* 2015). HeLa WT and NPC1 KO cells were transfected with the indicated siRNAs (3.1.8) for 72 h, then incubated for 16 h in either standard medium (DMEM + 10 % FCS + 1 % Pen/-Strep) or cholesterol-depletion medium (DMEM + 5 % LPDS + 10 µM mevalonate + 1 µM atorvastatin (Sigma Aldrich)), respectively. Then, 50 µg/ml LDL was added to the respective samples for 2–24 h at 37 °C. 25 µg/ml calpain inhibitor I (Cayman via Biomol) was added for 1 h at 37 °C before harvesting the cells in PBS + cOmplete™ protease inhibitor cocktail (Roche). Cells were lysed in PBS + cOmplete™ protease inhibitor cocktail containing 0.5 % Triton-X 100. The lysates were analyzed via SDS-PAGE followed by Western blotting and subsequent immunodetection using anti-SREBP2, anti-LDLR, anti-HMGCR, anti-LIMP-2, anti-NPC1, anti-GAPDH and anti-Actin antibodies (for vendors and dilutions see 3.1.10).

3.4.12. Recombinant protein expression and purification

The recombinant His-tagged LIMP-2 ectodomain (His6.hLIMP-2(aa35-430) was transfected into HEK293T cells. 12 h after transfection, doxycycline and aprotinin were added (both at final of 1 µg/ml) to induce expression. Media was collected 24, 48 and 60 h after induction in 50 ml tubes which were stored at 4 °C till purification. Per purification, a total of 900 ml medium was collected in total (from 30 cell culture dishes with 10 ml medium each). The medium was concentrated to 50 ml. Next, any detached cells and debris present in the supernatant was pelleted by centrifugation (4,000 rpm, 10 min, 4 °C). After centrifugation, the media was filtrated with a 0.45 µm filter (1 ml flask, vacuum). The Protein A beads (50 % IgG beads 6FF, solarbio, 8600) were prepared: 800 µl beads slurry were added to a 15 ml tube with a cut-off pipet tip, along with 12 ml cold PBS. The beads were spun down (1,200 rpm, 5 min, 4 °C, accelerate and brake at 3 (every time with beads)), the supernatant removed and the beads were resuspended in cell culture media. The media containing the recombinant protein was distributed into 50 ml tubes and 0.5 ml of resuspended beads slurry was added to each 50 ml tube. The samples were incubated for 4 h at 4 °C on a rotation rack. Next, the tubes were centrifuged (1,200 rpm, 10 min 4 °C, accelerate and brake at 3), the supernatant removed (save for the last 5 ml) and the residual media with the beads combined into one tube. The

beads were pelleted again and the supernatant removed. The beads were subjected to multiple washing steps (5x) and finally transferred to a 1.5 ml reaction tube and again pelleted. The supernatant was carefully removed completely and the beads resuspended in 500 µl TEV buffer + 1 mM DTT + 20 µl TEV enzyme. The samples were rotated at 4 °C for approximately 12 h. The supernatant containing the recombinant His-tagged LIMP-2 ectodomain liberated from the beads was transferred to a new tube and the cleaving step was repeated two times. The tubes containing the eluted protein were centrifuged to pellet any contaminating beads (1,200 rpm, 4 °C, accelerate & brake 3) and the supernatant transferred to a new tube. The protein concentration was measured and samples of the elution fractions were applied to SDS-PAGE and Western blotting.

3.4.13. Microscale Thermophoresis (MST)

Purified His_6-tagged LIMP-2 (3.4.12) protein was labelled using the Monolith His-Tag Labelling Kit Red-tris-NTA (NanoTemper Technologies) and diluted in buffer (300 mM NaAc pH 6.0, 150mM NaCl, 0.05 % Tween 20) with 0.1 % Fos-Choline 13 to a concentration of 25 nM. The protein was subsequently mixed with cholesterol in binding buffer at indicated concentrations ranging from 0.1 nM to 6 µM at room temperature and aspirated into thin capillaries (Premium Coated Capillaries by NanoTemper Technologies) by capillary force. Fluorescence was determined with a Monolith NT.115 instrument (NanoTemper Technologies) using a thermal gradient at 60 % LED power and medium [low/high] MST. Data were analyzed by MO.Affinity Analysis v2.3.

3.4.14. Measurement of [^{3}H]oleic acid incorporation into cholesteryl esters

The ability of LIMP-2 WT and KO MEFs to form cholesterol esters containing radioactively labeled oleic acid was performed as described in (Heybrock *et al.* 2019).

3.4.15. Determination of [^{3}H]cholesterol esterification

The ability of LIMP-2 WT and KO MEFs to form cholesterol esters containing radioactively labeled cholesterol under basal conditions and under lipid loading conditions was performed as described in (Heybrock *et al.* 2019).

3.4.16. Click chemistry conjugation of LIMP-2 luminal domain

The his_6-tagged recombinant luminal domain of LIMP-2 was purified as described in 3.4.12. The click chemistry reactions with the luminal domain and photo-clickable lipids were performed as described in (Heybrock *et al.* 2019).

3.4.17. Determination of protein S-palmitoylation with AcylRAC assay

This protocol for the acyl-resin assisted capture assay (AcylRAC) is modified from the assay published by (Forrester *et al.* 2011).

Cells were seeded in 10 cm plates (1-2 plates per sample). For analysis of the LIMP-2 palmitoylation mutants, cells were transfected 24 h later, see 3.3.3. After 48 h cells were washed with ice-cold PBS, scraped off in 1 ml PBS- cOmplete™ into 2 ml tubes and pelleted (10 min, 10.000 rpm, 4 °C). To lyse the cell pellet, it was resuspended in 500 µl blocking buffer and sonicated twice for 20 s followed by the addition of 0.5 µl methylmethanethiosulfonate (MMTS). Samples were incubated at 40 °C with constant shaking (1,000 rpm) for 4 h. Next, 1.5 ml (three volumes of sample) of acetone were added, samples mixed thoroughly and proteins precipitated at -20 °C for 20 min. The precipitated proteins were centrifuged at 16,000 g for 5 min, the supernatant discarded, and the pellet washed five times with each 1 ml 70 % acetone. After the last washing step, the pellet was air dried completely. The pellet was subsequently dissolved in 300 µl binding buffer and incubated at 40 °C and constant shaking until the pellet was dissolved (30 min to 1.5 h). The samples were then centrifuged at 16,000 g for 1 min to remove insoluble material and divided into two 120 µl samples each. In the following, one of these two samples is referred to as the experimental sample and the other one as the negative control sample. 30 µl of each sample were kept as input fraction. Meanwhile, 2 ml binding buffer were added to thiopropyl sepharaose beads and rotated for 1 h at room temperature (120 µl which equals 24 mg of beads/sample). Next, the beads were pelleted at 13.000 rpm for 1 min, the supernatant removed, and the beads resuspended in 80 µl binding buffer per sample. 70 µl of the bead suspension were pipetted into b the experimental and the negative control sample using cut off pipette tip. Next, 19 µl of a freshly prepared 2 M NH2OH solution were added to the experimental samples and 19 µl 2 M NaCl were added to the negative control samples, respectively. All samples were subsequently incubated for 3 h at room temperature on a rotor wheel. Afterwards, the beads were recovered by centrifuging at 16,000 g for 1 min. 50 µl of each supernatant were kept as cleaved unbound fraction, cUB, (from experimental samples) and preserved unbound fraction, pUB, (from negative control samples). The remaining supernatant was discarded and the beads with bound proteins washed 5x with 1 ml binding buffer each, 5 min rotation and afterwards 1 min of centrifugation at 16,000 g for 1 min. Proteins were eluted with 30 µl of 2x Laemmli buffer from the beads. The experimental samples contained the cleaved bound fraction and the negative control samples contained the preserved bound fraction. The input fraction and the unbound fractions were also mixed with 2x Laemmli buffer and all samples were heated to 60 °C for 10 min. For analysis, the fractions which were separated on an SDS-PAGE (3.4.6) and

subsequently transferred to a nitrocellulose membrane via Western blot (3.4.8) and subsequently staining with respective antibodies.

Table 3-20: Buffers utilized for the AcylRAC assay.

Material	Composition/ Supplier
2x Laemmli-Buffer	Dilute 5x Laemmli (3.4.6) buffer with ddH2O
Blocking buffer	100 mM HEPES
	1 mM EDTA
	2.5 % SDS
	pH 7.5
Binding buffer	100 mM HEPES
	1 mM EDTA
	1 % SDS
	pH 7.5
2 M NH_2OH	NH_2OH HCl in 2 M NaOH, pH 7.5
	freshly prepared
2 M NaCl	Roth
Methylmethanethiosulfonate (MMTS)	Merck
Thiol Sepharose® 4B Beads	Merck

3.4.18. Acyl-PEG exchange gel shift (APEGS)

The APEGS assay is a modification of the AcylRAC assay and uses maleimide-functionalized polyethylene glycol regents that allow for site-specific alkylation of cysteine residues, thereby inducing a mobility shift of palmitoylated proteins when separated by SDS-PAGE (Howie et al. 2014; Percher et al. 2016; Yokoi et al. 2016). Thus, different levels of palmitoylation of a protein can be determined.

Cells were seeded in 10 cm plates (2-3 plates per sample). Upon reaching confluency, cells were washed with ice-cold PBS, scraped off in 1.5 ml PBS- cOmplete™ (for 3 dishes) and pelleted (10 min, 10.000 rpm, 4 °C). The pellet was resuspended in 125 µl buffer A by incubating for 10 min at 37 °C and subsequently 375 µl buffer B were added. Following sonication (3x 20 s), the protein concentration was determined via BCA (3.4.4) and adjusted to a concentration of 0.5 mg/µl with buffer D. In addition, a fraction of the lysate was kept as input control. Each sample was divided in two 500 µl fractions (one control and one experimental sample) and incubated for 30 min at room temperature after the addition of 10 µl 0.5 M Tris-(2-carboxyethyl)-phosphin (TCEP) (final concentration of TCEP: 10 mM) on a rotating rack. This served to reduce possible disulphide bridges. Next, 10 µl of 2 M *N*-

ethylmaleimide (NEM) dissolved in ethanol were added to the samples (final concentration of NEM: 40 mM) followed by rotation incubation at room temperature for 3 h in order to protect free thiol groups. Afterwards, samples were precipitated with acetone as described in 3.4.17The dried pellets were stored at -20 °C until further use.

In the next step, the pellets were dissolved in 125 µl buffer A by incubation in a thermocycler at 37 °C for 30-60 min. To the control sample, 375 µl buffer T were added, while the experimental sample was incubated with 375µl buffer H, which contained hydroxylamine to cleave thioester bonds. Both samples were incubated on a rotation rack for 1 h at 37 °C. Afterwards, samples were precipitated with acetone as described above. The dried pellets were stored at -20 °C until further use.

The frozen pellets were dissolved in 110 µl buffer C by incubating for up to 1 h at 37 °C. Then, samples were pelleted (5 min, 14.000 rpm, RT) to remove undissolved debris. The protein concentration was determined as described above. Both control and experimental sample were subdivided into 2x 100 µl each at a protein concentration of 0.5 µg/µl (adjusted with buffer C) all samples were supplied with 2 µl 0.5 M TCEP. To one of the subsamples 10 µl 200mM mPEG-5kDa (slightly heat mPEG and use cut off tip for pipetting, very viscous) was added and to the other subsample 10 µl 200 mM NEM was added. All samples were incubated for 1 h at RT while shaking in a thermocycler. In the following, the samples were subjected to action precipitation as before. Lastly, the pellets were resuspended in 50 µl 1x Laemmli buffer and boiled at 99 °C for 2 min before separation of samples via SDS-PAGE and subsequent Western blotting as described before.

Table 3-21: Buffers utilized for the APEGS assay.

Buffer	Composition
Buffer A	4 % (w/v) SDS, 5 mM EDTA in PBS -cOmplete™
Buffer B	5 mM EDTA in PBS -cOmplete™
Buffer C	2 % (w/v) SDS in PBS -cOmplete™
Puffer D	1 % (w/v) SDS in PBS-cOmplete™
Buffer H	1.33 M hydroxylamine, 5 mM EDTA, 13 mM TCEP, pH 7
Buffer T	1.33 M Tris-HCl, 5 mM EDTA, 13 mM TCEP pH 7

3.5. Histological methods

3.5.1. Toluidin blue staining of myelin sheaths

Mice were perfused with 3 % Glutaraldehyde in 0.1 M phosphate buffer. Semi-thin sections (0.5-1 µm) of peripheral nerves of LIMP-2 WT, LIMP-2 KO and LIMP-2.Y163D mice were prepared. Subsequently, tissue sections were subjected to toluidine blue staining. The preparation of the nerves, staining and imaging were carried out by Prof. Dr. R. Lüllmann-Rauch and Mrs. D. Niemeier from the Institute of Anatomy, CAU Kiel.

3.5.2. Electron microscopy of ultra-thin cryosections of murine peripheral nerves

The preparation of the nerves from LIMP-2 KO mice and electron microscopy imaging were carried out by Prof. Dr. R. Lüllmann-Rauch and Mrs. D. Niemeier from the Institute of Anatomy, CAU Kiel. WT and LIMP-2 KO mice were perfused with 6 % glutaraldehyde in 0.1 M PB. Blocks of tissue were rinsed in 0.1 M PB and post-fixed for 2 h in OsO_4. Embedding of tissue blocks in Araldite or Epon 812 using routine procedures. Ultrathin sections were collected on Ni-grids. As contrasting substance, uranyl acetate and lead citrate were used. Images were collected with a Zeiss EM 900 or EM 902 microscope.

3.5.3. Electron microscopy of fixed cells

Cells were seeded in 25 cm^2 cell culture flasks and transfected the next day with 3 µg of plasmid DNA (pFROG.LIMP-2.WT.myc). After 48 h, cells were fixed (directly after removal from incubator) with 4% freshly prepared PFA (from 16% stock) in 0.1 M phosphate buffer. The fixing buffer was added directly to the cell culture media in a 1:1 ratio. After 5 min, the fixative was removed and replaced with fresh fixative (4 % PFA). Cells were fixed overnight at 4 °C. The following processing of the samples and imaging was done in the laboratory of Prof. Dr. Judith Klumperman at UMC Utrecht, The Netherlands.

3.6. Animal experiments

3.6.1. Animal housing

The mice were housed in a pathogen-free environment in individually ventilated cages (IVC). Lighting conditions consisted of 12 hours light and subsequently 12 hours darkness. A humidity of 45- 60 % and room temperature of 19-22 °C were maintained. All animals had access to water and standard laboratory animal food (pellets provided by Ssniff Spezialdiäten) *ad libitum*. Animal handling and care were performed in agreement with the German animal welfare law

according to the guidelines of the Christian-Albrechts University of Kiel. Experiments involving animals were approved by the Ministry of Energy, Agriculture, the Environment and Rural Areas Schleswig-Holstein under the reference number V312-72241.121-3.

3.6.2. Generation of LIMP-2.Y163D knock-in mice

In order to assess functions of LIMP-2 independent of transport of GCase, a mouse strain expressing a mutated version of LIMP-2 incapable of binding GCase was generated. The conditional knock-in mice were generated by Ozgene Pty Ltd using homologous recombination in embryonic stem (ES) cells which were then injected into blastocysts of host animals, leading to the generation of chimeric animals which were then crossed with wild type mice (C57BL/6-N) to yield mice heterozygous for the mutation. Amino acid residue Tyrosine163 is located in exon 4. Thus, wild type exons 4-12 of the *SCARB2* gene were flanked (floxed) by recombinase recognition sites (loxP) as depicted in Figure 3-3. The presence of the neomycin phopshotransferase cassette (neo^r) was used as a positive selection marker. Neo^r-positive mice were bred with a Cre recombinase-deleter mouse strain (line #0320, (Schwenk *et al.* 1995)), causing site-specific DNA recombination between the loxP sites which leads to the deletion of the WT cDNA and neomycin phosphotransferase cassette flanked by the loxP sites (Figure 3-4). As a consequence, these mice expressed the mutated version of LIMP-2, LIMP-2.Y163D. Mice heterozygous for the mutated allele (YD/+) were mated with each other to generate homozygous (YD/YD) mice. For experimental analysis, homozygous mice were compared to heterozygous and wild type litter mates.

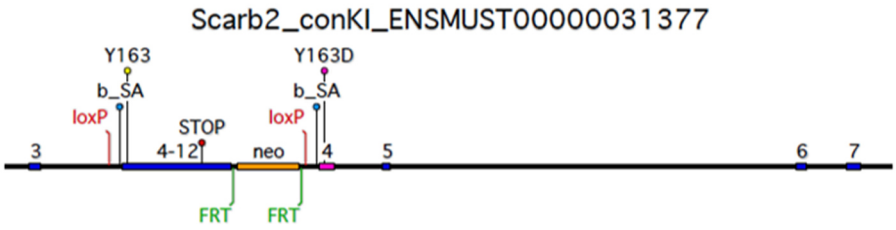

Figure 3-3: Scheme for generation of LIMP-2.Y163D inducible knock-in mice. Blue boxes: exons; b_SA: branch site and splice acceptor; neo: neomycin cassette for selection in embryonic stem cells; FRT: recognition sequence for flp recombinase-mediated neo removal; loxP: recognition sequence for cre recombinase-mediated WT cDNA deletion. STOP: stop codon.

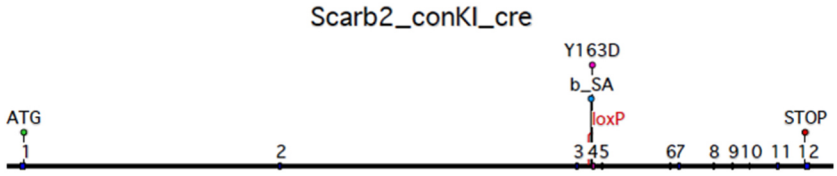

Figure 3-4: Gene targeted locus after Cre-mediated deletion of the WT cDNA. Mice harboring this allele will express LIMP-2.Y163D. b_SA: branch site and splice acceptor; loxP: recognition sequence for cre recombinase-mediated WT cDNA deletion. STOP: stop codon.

3.6.3. Tail biopsy and isolation of genomic DNA

To isolate genomic DNA needed to genotype of mice, tail biopsies from 3-5 week old animals were digested with DirectPCR® Lysis Reagent Tail (Peqlab) and 0.3 mg/ml proteinase K at 55 °C and shaking (1000 rpm, thermocycler) over night. Next, proteinase K was inactivated by incubation of the samples at 85 °C for 45 min followed by pelleting undigested debris at 13,000 rpm and room temperature for 1 min. The lysate contained isolated genomic DNA which was used in a PCR reaction for genotyping (3.6.4).

3.6.4. Genotyping of mice

The genotype of mice was determined via polymerase chain reaction (PCR). Previously isolated genmic DNA (3.6.3) was used as template DNA for the reaction. Primers (3.1.7) were designed to amplify approximately 150 base pairs (bp) flanking the loxP site, as depicted in Figure 3-5 A. The pipetting scheme used to determine the genotype of offspring from heterozygous LIMP-2-Y163D mice is listed in Table 3-22:

Table 3-22: Pipetting scheme for genotyping LIMP-2.Y163D mice.

Premix	**1x**
Primer # 24 for (100 µM stock)	1 µl
Primer # 22 rev (100 µM stock)	1 µl
10x DreamTaq Puffer (w MgCl2)	5 µl
dNTP, stock 10 mM	1 µl
DreamTaq polymerase™ (5 U/µl)	0.5 µl
H_2O	40.5 µl
DNA template	1 µl
Total volume	50 µl

Table 3-23: PCR program for genotyping of LIMP-2.Y163D mice

Step	Temperature	Duration	
Initial denaturation	95 °C	3 min	
Denaturation	95 °C	30 s	30x
Annealing	59 °C	30 s	
Elongation	72 °C	1 min	
Final elongation	72 °C	5 min	
Hold	4 °C	∞	

The obtained PCR products were separated via agarose gel electrophoresis (3.2.2) and the size of the bands was analyzed as depicted in Figure 3-5 B.

Figure 3-5: Genotyping strategy for LIMP-2.Y163D mice. A Primers were designed to amplify approximately 150 base pairs (bp) flanking the loxP site. The difference of PCR product size between WT alleles and mutated ones was 34 bp, which is the size of the loxP site. **B** PCR products were analyzed via agarose gel electrophoresis. The targeting vector (TV) was used as a control for the Y163D allele and genomic DNA from a WT mouse was used as a control for the WT allele. This allowed differentiation between mice homozygous (YD/YD) or heterozygous (+/YD) for the mutated allele or WT mice (+/+).

3.6.5. Perfusion of mice

Mice were anaesthetized by intraperitoneal injection of 10 µl/ g body weight narcotic agent consisting of 10 mg/ml Ketamin and 6 mg/ml Rompun® in 0.9 % NaCL solution. The pinch-withdrawal reflex of narcotized animals was monitored to ensure feasible narcotic depth before proceeding with perfusion. A butterfly needle was inserted into the left ventricle and the right ventricle was cut to start perfusion with 30 ml of 0.1 M phosphate buffer (PB) at a flow rate of 1.5 ml/min. The organs were collected and either directly frozen in liquid nitrogen followed by storage at -80°C until further processing or post-fixed in 4 % PFA in PB for 4 hours for immunohistochemistry analysis.

3.7. Computer software

The web-based software Biorender was used for the creation of schematic figures. The following figures were created with Biorender.com: Figure 1-1, Figure 1-2, Figure 1-3, Figure

1-4, Figure 1-5, Figure 1-6, Figure 1-7, Figure 1-9, Figure 1-10, Figure 1-11, Figure 3-2, Figure 5-2, Figure 5-5, Figure 5-3.

Lysosomal filipin fluorescence in HeLa WT, LIMP-2 KO, NPC1 KO and NPC1/LIMP-2 KO cells was quantified by ImageJ (Fiji). The outlines of cells were traced manually. After subtracting background fluorescence, the mean filipin intensity within each cell was measure and related to the cell size.

To evaluate signals derived from Western blot analyses by densitometry, the integrated density of the individual signals was calculated with ImageJ. Raw values were used for the quantification. The average of the wild type (or untreated) cells was set as 100% and represented as 1. The ratio of the KO (or treated) cells is depicted relative to the WT/untreated cells.

Additional software employed for data analysis and generation and edition of figures is listed in Table 3-24.

Table 3-24: Computer software used for data analysis and figure editing.

Software	Company
Photoshop	Adobe Systems Inc.
Adobe Illustrator	Adobe Systems Inc.
GraphPad Prism 8	GraphPad Software Inc.
EndNote X9	Thomson Reuters/ Clarivate Analytics
Leica LAS X	Leica Microsystems
FluoView-10 ASW 4.2	Olympus
ZEN Blue Software	Zeiss

3.8. Statistical analysis

Experiments to which statistical analysis was applied were repeated at least three times. Statistical analysis was performed with unpaired, two-tailed t-test using the GraphPad Prism 8 software. Significant values were measured at $p < 0.05$. Unless indicated otherwise, values are expressed as mean ± SEM, and significance is denoted as $*p < 0.05$, $**p < 0.005$, and $***p < 0.0001$.

4. Results

4.1. Role of LIMP-2 in the lysosome beyond transport of beta-glucocerebrosidase

The trafficking of the acid hydrolase beta-glucocerebrosidase (GCase) from the ER to lysosomes depends on its receptor LIMP-2 (Reczek *et al.* 2007). Hence, generating a knockout mouse model of LIMP-2 simultaneously depletes the lysosomes of GCase, adding an additional layer of complexity to the analysis of occurring phenotypes. In order to differentiate between functional impairments caused solely by absence of LIMP-2 and abnormalities related to decreased GCase protein levels and activity, mutants of LIMP-2 were generated that contained modifications in the previously characterized binding region of GCase in the alpha-helices 5 and 7 of LIMP-2 (Neculai *et al.* 2013). Replacing the amino acid tyrosine at position 163 in exon 4 with an aspartate residue did not impair the trafficking of the LIMP-2 mutant to lysosomes in cell culture models ((Zunke 2015) and Figure 4-1 A), however, it completely abolished binding of GCase to LIMP-2 as evidenced by co-immunoprecipitation studies (Zunke 2015), Figure 4-1 B.

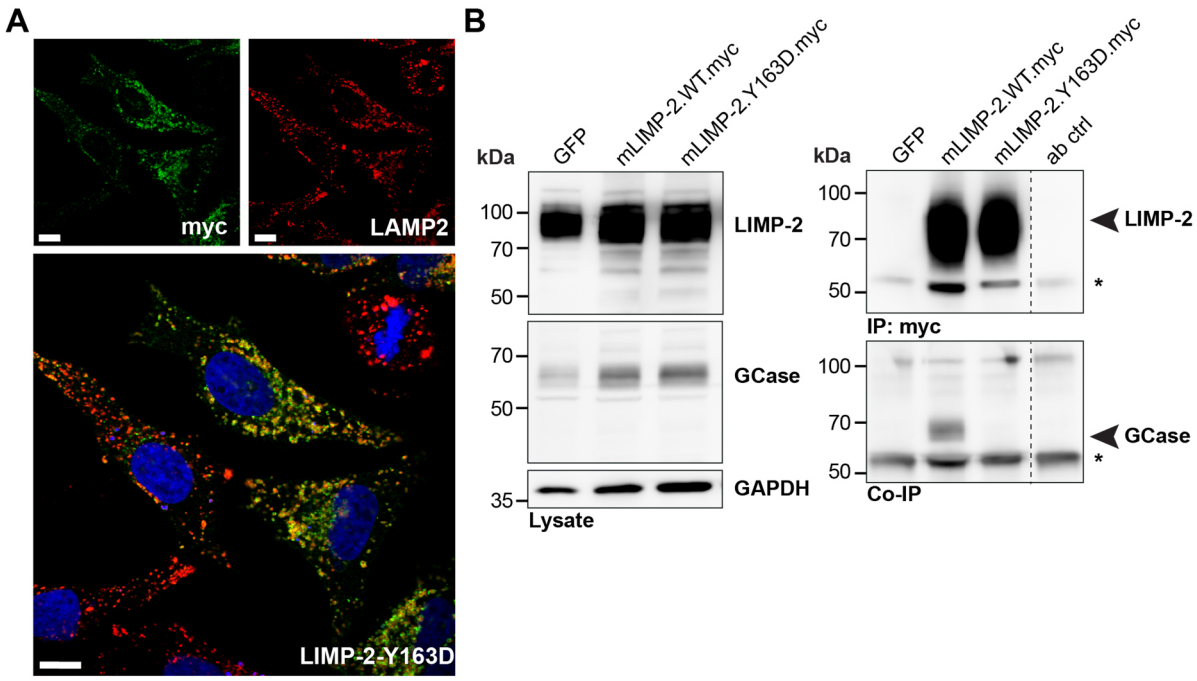

Figure 4-1: Cellular characterization of the LIMP-2.Y163D mutant. A In transiently transfected HeLa cells, mLIMP-2-Y163D localizes to lysosomes where it co-localizes with LAMP-2 as demonstrated by overlapping immunofluorescence staining. Scale bars: 10 µm **B** mLIMP-2 WT, but not mLIMP-2-Y163D is able to co-precipitate GCase. HeLa cells were transfected with either WT or mutant LIMP-2 and precipitated using an antibody directed against the myc-tag. To analyze co-immunoprecipitation, an antibody raised against endogenous GCase was used. Glyceraldehyde 3-phosphate dehydrogenase (GAPDH) was used as loading control. Arrows refer to specific antibody signals in the IP an coIP fractions; asterisks denote unspecific signals caused by fragments of the IP antibody.

Prompted by these experiments, a conditional knock-in mouse model was generated that harbored the GCase-binding deficient mutant LIMP-2-Y163D using the *Cre/loxP* recombination system (3.6.2). The targeting vector contained the LIMP-2 wild type (WT) gene with exons 4 to 12 being flanked by *loxP* sites as well as the mutated exon. Mating of the mice with a Cre recombinase-deleter mouse strain (Schwenk et al. 1995) led to the expression of the Cre recombinase and subsequent removal of the floxed wild type exons, thus enabling the expression of LIMP-2-Y163D (3.6.2).

LIMP-2-Y163D was expressed to the same extent as LIMP-2 wild type as demonstrated by analysis of brain, liver and spleen tissue lysates from 6 week and 4 months old mice, respectively (data not shown).

LIMP-2 is being modified with multiple *N*-linked carbohydrates in the ER and Golgi before reaching the lysosome (Lewis *et al.* 1985). Since the type of glycans differ between organelles - high mannose in ER and complex type in Golgi- analysis of the glycosylation pattern can be employed to determine if a protein is being retained in the ER, indicating instability or improper folding. Using endoglycosidases that are either unable to cleave most complex type glycans (Endoglycosidase H, Endo H) or cleave all *N*-linked glycans (Peptide-N-Glycosidase F, PNGase F), liver lysates of 4 months WT and KI litter mates as well as of 7.5 months old WT and LIMP-2 KO litter mates were digested with the respective enzyme and the samples subsequently separated by SDS-PAGE followed by immunoblot transfer. As depicted in Figure 2, Endo H-treated LIMP-2 WT and KI samples were largely resistant to cleavage. The small molecular weight shift observed indicates that LIMP-2 harbors at least one glycosylation site that is comprised of only high-mannose type glycans and thus susceptible to Endo H cleavage.

As a lysosomal-resident hydrolase, GCase is also heavily glycosylated possibly to withstand the acidic environment and lysosomal hydrolases. While the overall protein levels of GCase were reduced in KI mouse samples, upon Endo H/ PNGase F digest GCase was resistant to Endo H in samples derived from WT and KI mice (Figure 4-2). This indicates that the majority of GCase that can be detected in liver lysates from KI mice is exported from the ER. This does not exclude the existence of a pool of GCase that is retained in the ER and quickly degraded to protect the ER from toxicity or secreted (Reczek *et al.* 2007) as it is likely the case in LIMP-2 KO samples, where no GCase could be detected in this assay.

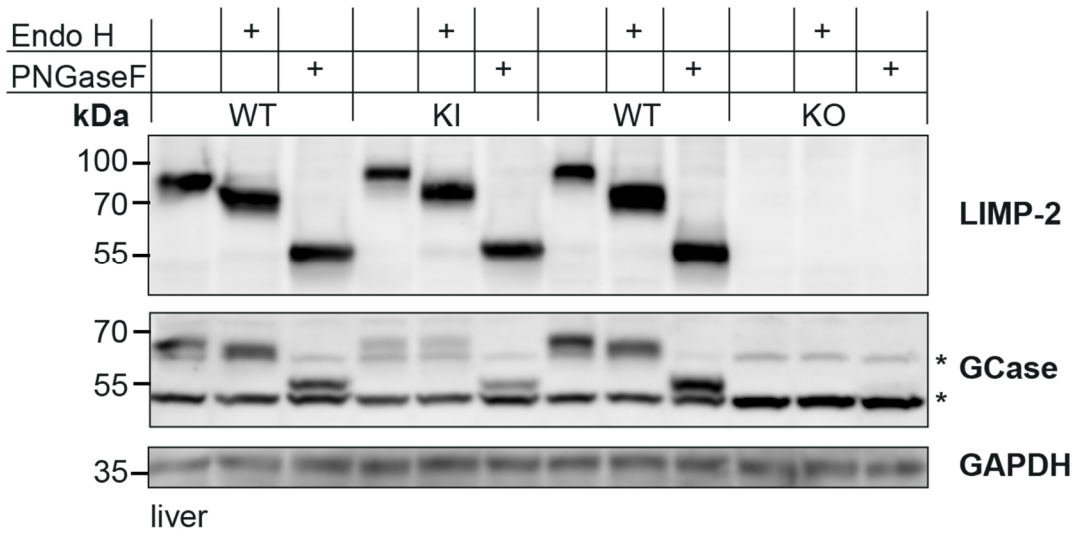

Figure 4-2: Analysis of glycosylation pattern of LIMP-2 WT/Y163D and GCase by means of Endo H/ PNGase F digestion. Liver lysates were incubated with either the enzyme Endo H or PNGase F, respectively, and the cleavage pattern was compared to control groups. Sensitivity to Endo H indicates the absence of complex type glycans as typically found in ER-resident proteins.

Since many of the phenotypic alterations of LIMP-2 knockout mice like the development of uni- or bilateral hydronephrosis (Gamp *et al.* 2003) are most prominent in older mice (six to eight months of age), the detailed analysis of multiple tissues was carried out with 4 WT versus 4 KI mice, all 8 months old. Upon visual inspection, the LIMP-2-Y163D did not develop any alterations in tissues like the kidney or the peripheral nerves (*Nervus phrenicus*, *Nervus ischiadicus*). Protein lysates from brain regions (cortex depicted as an example), liver, kidney and spleen were prepared and analyzed in regard to LIMP-2 and (total) GCase levels. The percentage of the protein levels as quantified from immunoblot images and normalized to wild type levels are summarized in Table 4-1:

Table 4-1: Protein levels of LIMP-2 and GCase quantified from immunoblot data (M. Schwake, not shown) . The protein levels were normalized to WT levels (%), n= 7 (WT), 4 (LIMP-2-Y163D and LIMP-2 KO, respectively). The data for protein levels of GCase in the brain of LIMP-2 KO were not evaluable, but have been described before (Rothaug *et al.* 2014).

Tissue	LIMP-2-Y163D		LIMP-2 KO
	LIMP-2	GCase	GCase
Cortex	61	65	n/a
Liver	73	32	13
Kidney	65	44	30
Spleen	107	71	50

Except for spleen, protein levels for LIMP-2-Y163D were reduced by 30-40 % in the analyzed tissues. While cell-based studies demonstrated correct targeting of mLIMP-Y163D to lysosomes, it is not possible to deduct from these immunoblot data whether the decrease of LIMP-2-Y163D is due to a defect in lysosomal transport and thus accumulation in the ER,

possibly leading to degradation to avoid ER stress or instability of the protein in lysosomes and consequently a higher turnover. Additionally, expression of the mutated *SCARB2* gene may be down-regulated in these tissues. GCase protein levels in cortex and liver were reduced by approximately one-third (35-29 % decrease), whereas in the other tissues they were more drastically reduced. In LIMP-2 knockout tissues, GCase levels were reduced as has been described before (Reczek *et al.* 2007), with the mildest effect observed in the cortex (35 % reduction) and the most severe lack of GCase observed in the liver (nearly 90 % reduction).

Next, enzyme activity of GCase in these samples was investigated (Table 4-2). Even in complete absence of LIMP-2, tissues display different levels of residual GCase activity. While in MEFs, liver and spleen the reduction is 84-88 % in comparison to wild type, in the brain more than half of the activity of the wild type situation was still reached. If the introduction of the Y163D mutation in LIMP-2 in mice had led to complete abolishment of GCase transport as observed in the cell culture studies (Figure 4-1), the expected residual GCase activity would have been similar to the LIMP-2 KO situation. However, as already indicated by the increased GCase protein levels in KI vs KO mice (Table 4-1), the measured GCase activity was markedly higher in KI lysates than in KO lysates, reaching up to 82 % of wild type activity in the cortex (versus 54 % in KO) and a nearly 4-fold increase in MEFs (63% versus 16 %). These data indicate that despite the introduced mutation a portion of GCase still reaches lysosomes in various tissues of 8-month old LIMP-2-Y163D mice and is able to exert its enzymatic functions.

Table 4-2: Residual GCase activity in different tissues normalized to WT (%). Data provided by M. Schwake.

Tissue	LIMP-2.Y163D	LIMP-2 KO
Cortex	82	54
Liver	40	22
Kidney	37	25
Spleen	30	22
MEFs	63	16

Besides uni- or bilateral hydronephrosis, loss of LIMP-2 is characteristically leading to defects in the Schwann cells of the peripheral nerves, causing the myelin layer around the axons to degenerate which in most likely causes axonal loss. To clarify if the correct function of the Schwann cells is solely relaying on the presence of LIMP-2 or necessitates both LIMP-2 and GCase, tissue sections of *Nervus phrenicus* were subjected to Toluidine blue staining and subsequently light-microscopically examined as depicted in Figure 4-3:

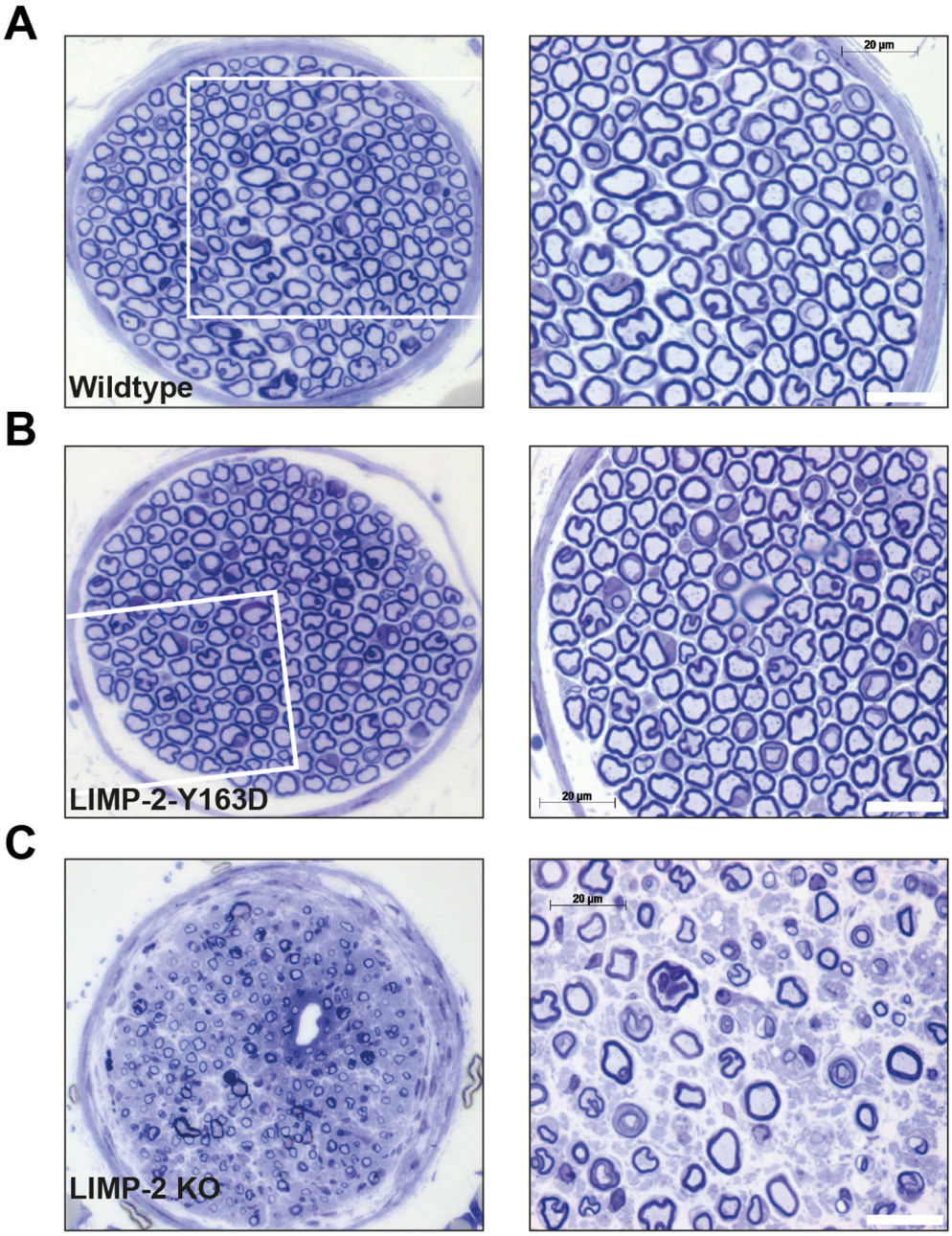

Figure 4-3: **Toluidine blue staining of tissue sections of *Nervus phrenicus* from 7 month old WT (A), LIMP-2-Y163D (B) and LIMP-2 KO (C) mice, respectively.** Dark blue staining indicates the insulating myelin sheath that surrounds healthy axons as observed in WT. In LIMP-2 KO mice, this layer is heavily disrupted and degenerating, as also previously describe (Gamp *et al.* 2003). The myelin layer of axons in LIMP-2-Y163D mice do not exhibit any of the defects observed in the KO situation. Scale bars: 20 µm.

While the deterioration of the myelin sheath and axonal loss are obvious in the nerve tissue of LIMP-2 KO mice (C), no difference in the number of axons and myelin sheath could be observed when comparing tissue sections from LIMP-2-Y163D mice (B) and wild type mice (A).

4.2. LIMP-2: A lipid transporter?

The LIMP-2-Y163D knock-in mouse model demonstrates that LIMP-2 fulfills important functions in cells and mammalian tissues. Even though one of its main known functions, the lysosomal transport of GCase, was reduced, LIMP-2.Y163D mice did not significantly differ from wild type mice on a phenotypic level. While it cannot be ruled out that the residual lysosomal amounts of GCase present in these mice contributed to phenotypic correction, it seems likely that functions of LIMP-2 separate from GCase-transport are essential for maintaining normal cellular function and prevent the development of e.g. hydronephrosis, deafness and peripheral neuropathy as observed in LIMP-2 KO mice (Gamp *et al.* 2003).

The detection of a hydrophobic cavity inside the luminal domain of LIMP-2 (Neculai *et al.* 2013) offered intriguing possibilities as to what these functions may comprise of. In their study, Neculai et al described that based on the resolved structure of LIMP-2's luminal domain, a similar tunnel for the scavenger receptor protein family member SR-BI could be modelled (Neculai *et al.* 2013). As mentioned in 1.4.3, the plasma membrane-localized SR-BI is an important receptor for binding HDL-derived cholesterol at the cell surface. It also functions in the transport of cholesterol and other lipids (Rigotti *et al.* 1995, Acton *et al.* 1996). Another scavenger protein family member, CD36, shares the same topology as SR-BI and LIMP-2 (see 1.4.2). Thus, it likely also contains a similar hydrophobic cavity as for example indicated by homology modelling of the ectodomain of the *Drosophila* CD36 homologue sensory neuron membrane protein (SNMP) on the basis of the mammalian LIMP-2 crystal structure (Gomez-Diaz *et al.* 2016). CD36 participates in the uptake or translocation of lipid molecules such as fatty acids and oxidized LDL at the plasma membrane (Nozaki *et al.* 1995, Coburn *et al.* 2000, Drover *et al.* 2008).

4.2.1. Implications for a function of LIMP-2 in cholesterol metabolism

A function of the LIMP-2 luminal domain in a similar transport process of lipid molecules at the lysosome can be envisaged. Given LIMP-2's apparent role in the maintenance of Schwann cells and the lipid-rich myelin sheath (Gamp *et al.* 2003), Schwann cells from peripheral nerves were analyzed in more detail by electron microscopy. As illustrated in Figure 4-4 A, Schwann cells (SCs) are highly specialized cells that form a multi-layer myelin sheath around axons of peripheral nerves to enable rapid electrical signal conduction. Major components of myelin are phospholipids (50-58 % of total lipids) and cholesterol (20-30 % of total lipids) (Garbay *et al.* 2000). Electron microscopy of peripheral nerve tissue from LIMP-2 KO mice revealed membrane surrounded needle-like crystalline structures of variable size in the cell bodies of Schwann cells. These structures were electron lucent in appearance and were not present in

wild type mice (not shown). These inclusions are reminiscent of cholesterol crystals which can typically be found in foam cells of atherosclerotic lesions (Bocan *et al.* 1986, Tangirala *et al.* 1994, Klinkner *et al.* 1995)

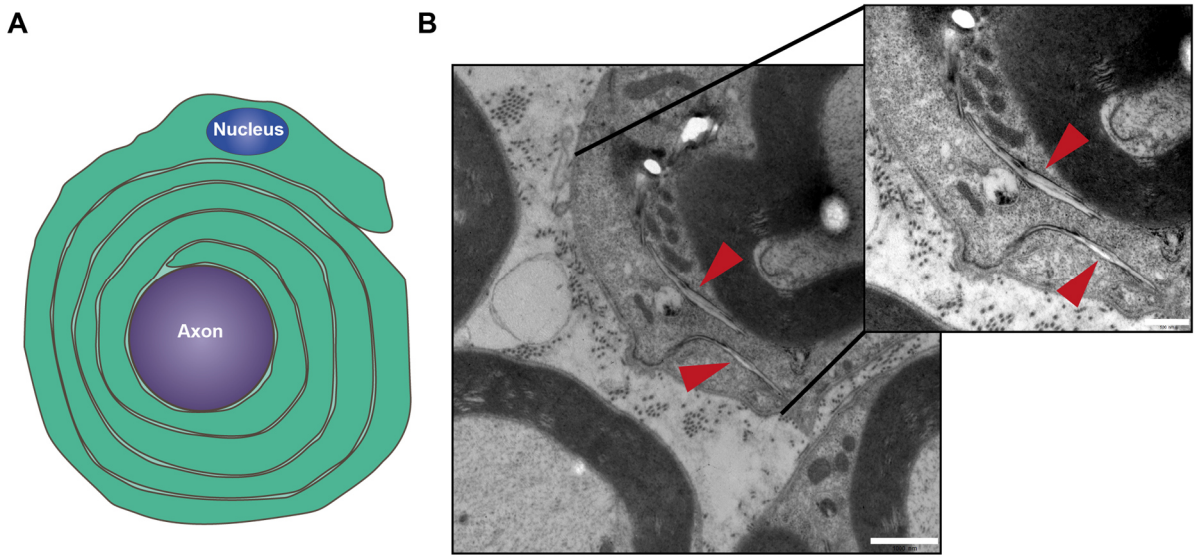

Figure 4-4: A Schematic depiction of an axon being surrounded by a layer of myelin produced by a myelinating Schwann cell. In the peripheral nervous system, Schwann cells wrap around one axon multiple times, thereby forming a densely packed myelin sheath. The myelin layer insulates the axon, allowing for rapid salutatory impulse conduction along the nodes of Ranvier. **B** Electron micrographs of Schwann cells from nerve tissue of *Nervus ischiadicus* from 12 weeks old LIMP-2 KO mice. Red arrows point towards electron lucent, needle-like inclusions. Scale bars: main panel, 1000 nm; inset, 500 nm. The images in B were acquired by Professor R. Lüllmann-Rauch from the Department of Anatomy, CAU Kiel.

Prompted by the observation of a potentially lipid-related phenotype caused by loss of LIMP-2 it was investigated whether LIMP-2 can associate with lipids. To this end, the luminal domain of human LIMP-2 consisting of amino acid residues 35 - 430 and fused with a His_6 tag was recombinantly expressed in HEK293T cells and the secreted protein was purified from the cell culture supernatant. Binding of the recombinant LIMP-2 luminal domain to different lipid species was assessed using UV-crosslinkable lipid probes (Figure 4-5 A) that are visualized with rhodamine-azide staining (see section 3.4.16). While weak signals could be observed for fatty acids, ceramide and sphingosine, the strongest crosslink could be observed between LIMP-2's luminal domain and trans-sterol, indicating that sterols like cholesterol could bind to the luminal part of LIMP-2, suggesting that they could be a potential substrate for LIMP-2 (Figure 4-5 A).

To obtain a more quantitative measure for the binding of cholesterol and the LIMP-2 luminal domain microscale thermophoresis was employed which measures the binding-induced changes in thermophoretic mobility of a fluorescently labelled target as a function of the concentration of a non-fluorescent ligand, thus allowing to determine binding affinities between two molecules of interest (Jerabek-Willemsen *et al.* 2011, Seidel *et al.* 2013). Indeed, monitoring of the binding affinities between the recombinant luminal domain of LIMP-2 and

varying concentrations of free cholesterol by microscale thermophoresis (Figure 4-5 B) resulted in an EC_{50} of 112 ± 32 nM. This is comparable to the affinities described for other cholesterol binding proteins like the ER-localized transcription factor nuclear factor erythroid 2 related factor-1 (Nrf1) that is involved in protection of the cell against excess cholesterol levels by sensing and binding cholesterol. Under excess cholesterol levels in the ER, Nrf1 primes inflammatory signaling and promotes cholesterol excretion in the liver (Widenmaier *et al.* 2017).

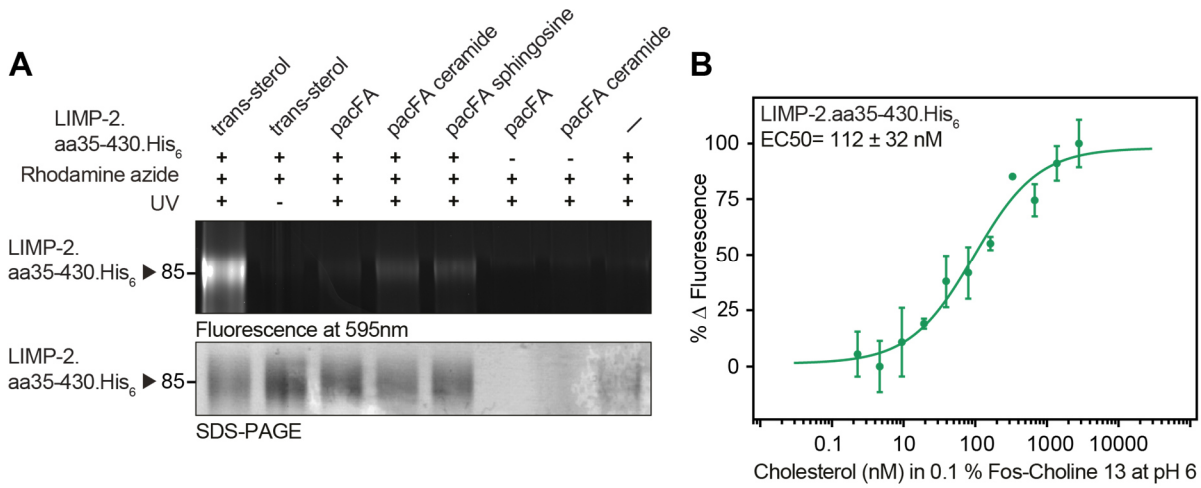

Figure 4-5: The recombinant luminal domain of LIMP-2 (amino acids 35-430) binds cholesterol (and other lipids). A Lipid binding assay using the purified recombinant LIMP-2 luminal domain and cross-linkable lipid probes (sterol, fatty acid (FA), ceramide and sphingosine, respectively). Images were acquired by fluorescence gel scanning at 595 nm and Coomassie staining to visualize the LIMP-2 luminal domain, respectively. **B** Microscale thermophoresis assay as described in 3.4.13 monitoring the affinity between the recombinant LIMP-2 luminal domain and cholesterol. 25 nM of fluorescently labelled LIMP-2 luminal domain (Monolith His-Tag Labeling Kit Red-tris-NTA, NanoTemper Technologies) was incubated with a concentration gradient of cholesterol. The data was generated in collaboration with Ying Meng and Prof. Dante Neculai, Zhejiang University, Hangzhou, China.

Based on these results, it was further investigated whether (free) cholesterol could be a substrate for the LIMP-2 luminal domain. A typical readout to assess intralysosomal accumulation of free cholesterol is staining fixed cells with the fluorescent antibiotic filipin III complex, hereafter denoted filipin. It binds to the 3'-hydroxygroup of cholesterol and is excited at 320 – 380 nm (Norman *et al.* 1972). Cells lacking the known lysosomal cholesterol exporter NPC1 or its partner in cholesterol handling, NPC2, exhibit strong filipin staining and this method has been used for a long time to identify NPC patients (Pentchev *et al.* 1985, Vanier *et al.* 2016, Patterson *et al.* 2017). While no difference in filipin staining intensity could be observed when LIMP-2 WT vs KO MEFs were compared under basal conditions, free cholesterol did accumulate in LIMP-2 KO cells in contrast to WT cells when challenged with 50 µg/ml LDL for 6 hours as indicated by microscopy analysis of filipin-positive lysosomes (Figure 4-6). Quantification of > 20 WT and LIMP-2 KO cells, respectively, revealed a significant increase of filipin intensity in LIMP-2 KO cells compared to WT cells as depicted in Figure 4-6 B:

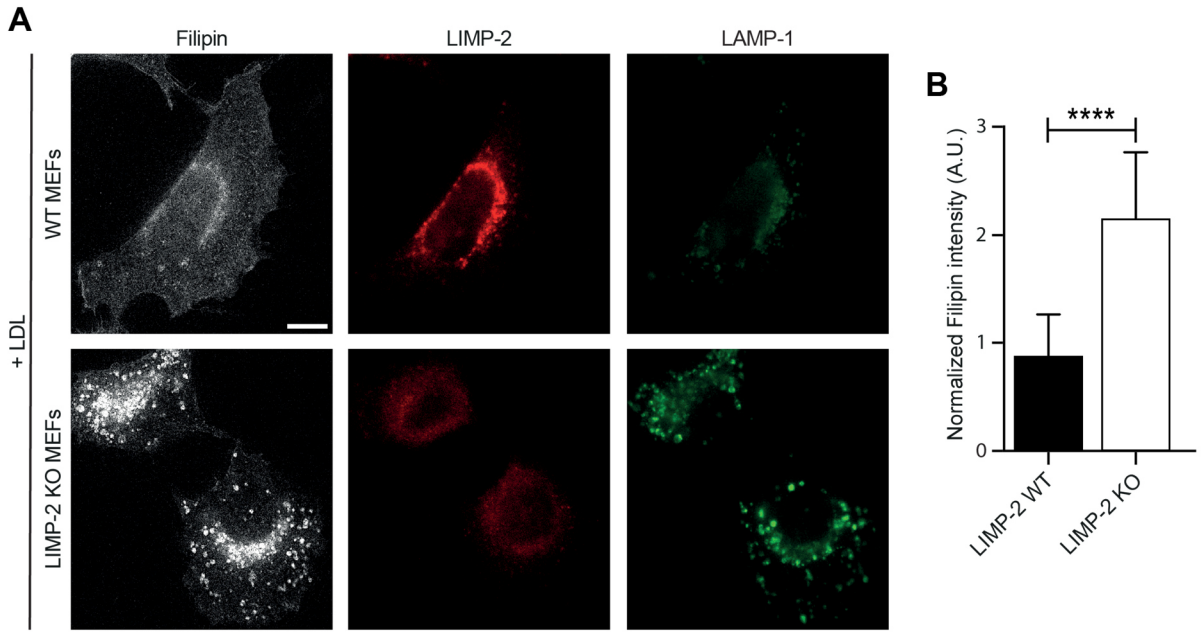

Figure 4-6: LIMP-2 KO MEFs are susceptible to cholesterol storage when challenged with LDL. A Cells were incubated with 50 µg/ml LDL for 6 h, subsequently fixed and stained with filipin and antibodies directed against LIMP-2 and LAMP1. While in WT MEFs, no storage of cholesterol (filipin-positive vesicles) could be observed, lysosomes of LIMP-2 KO cells were positive for filipin staining, indicating increased amounts of cholesterol. Scale bar: 10 µm. **B** Quantification of filipin intensity (mean ± SD) and normalized to WT; n = 25 (WT), n =22 KO) cells.

Cells lacking NPC1 are characterized by substantial accumulation of free cholesterol inside lysosomes. To investigate if a surplus of LIMP-2 could alleviate this, HeLa NPC1 KO cells were transiently transfected with myc-tagged LIMP-2 and filipin signal normalized to cell area was compared between transfected and non-transfected cells. While the signal intensity was found to be quite variable in both NPC1 KO cells and NPC1 KO cells overexpressing LIMP-2.myc, a slight reduction in filipin signal was observed in the transfected cells (Figure 4-7 C). Strikingly, a closer look at the overlay of filipin and LIMP-2.myc staining revealed that the filipin signal intensity in the LIMP-2.myc-positive vesicles was decreased in comparison to the LIMP-2.myc-negative vesicles within the same cell (Figure 4-7 A inset, white arrow heads). This phenomenon was further investigated using Chinese Hamster Ovary (CHO)-M12 cells, that are lacking NPC1. Overexpression of murine LIMP-2.mCherry significantly reduced the filipin-stained free cholesterols in LIMP-2.mCherry-positive vesicles (Figure 4-7 C and D). Importantly, this was not the case when overexpressing the LIMP-2.G379W/V415W.mCherry tunnel mutant, indicating the necessity of a functional LIMP-2 tunnel for reduction of cholesterol load.

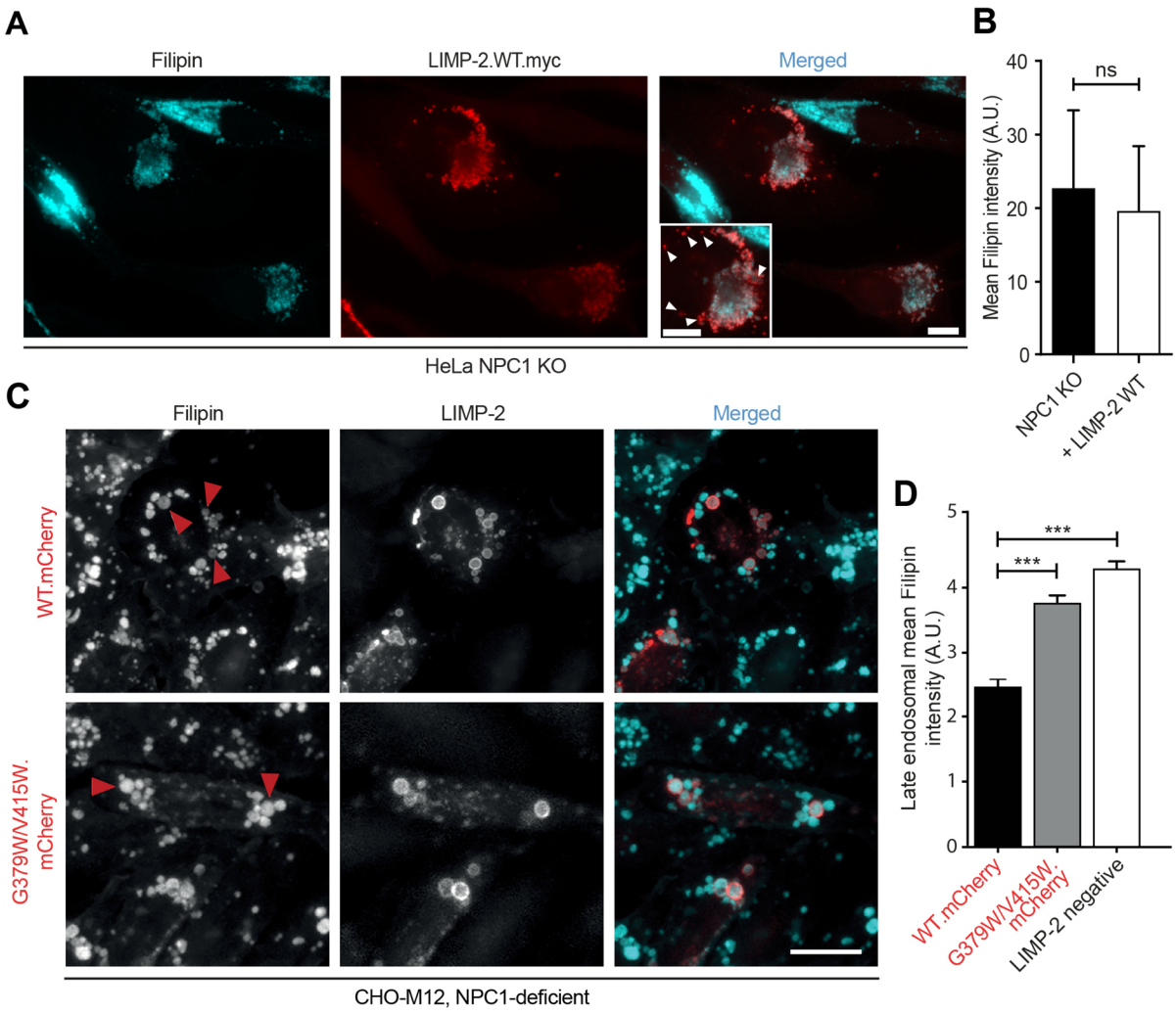

Figure 4-7: Overexpression of LIMP-2 in NPC1-deficient cells reduces lysosomal cholesterol load. A HeLa NPC1 KO cells were transfected with murine LIMP-2.WT.myc for 48 h. Cells were fixed with 4 % PFA and stained with filipin and anti-myc antibodies to visualize free cholesterol and transfected cells, respectively. White arrowheads indicate LIMP-2-positive vesicles. Scale bars: 10 µm. **B** Quantification of mean filipin intensity (Arbitrary units, A.U.) in relation to cell size. The integrated density of the cells was measured with ImageJ and divided by the cell area. Data ± SD. A two-tailed unpaired Student's t-test was utilized to compare mean filipin intensities between transfected and non-transfected NPC1 KO cells. ns = not significant; NPC1 KO n = 43 cells, NPC1 KO + LIMP-2.WT.myc n = 37 cells. **C** Immunofluorescence pictures of CHO-M12 cells lacking NPC1 that were transfected with LIMP-2.mCherry or LIMP-2.G379W/V415W.mCherry, respectively, and after fixation were stained with filipin. Red arrowheads indicate LIMP-2-positive vesicles. Scale bars: 10 µm. **D** Quantification of late endosomal mean filipin intensity in organelles expressing WT LIMP-2 (WT.mCherry) or mutated LIMP-2 (G379W/V415W.mCherrry) as well as non-expressing (LIMP-2 neg.) n = 75, 77, 152 organelles, respectively, from 15 cells. Data (mean ± SEM) from two independent experiments, unpaired two-tailed Student's t-test (**** $p < 0.0001$). Data in C and D generated in the framework of a collaboration by Kristiina Kanerva and Elina Ikonen, University of Helsinki, Finland.

4.2.2. Cholesterol delivery through the LIMP-2 luminal domain

To better observe and understand cholesterol association and possibly transport by LIMP-2, a construct was engineered that contained the C-terminal sequence of family member CD36 responsible for the plasmalemmal localization of CD36, therefore leading to plasma membrane targeting of the LIMP-2 chimera. Additionally, the protein was fused to GFP (or mCherry, see

Figure 4-9) to enable tracking via live-cell imaging (LIMP-2.cmr.GFP, Figure 4-8 A). After confirming the plasma membrane localization of LIMP-2.cmr.GFP (Figure 4-8 A and cell surface protein biotinylation experiments, data not shown), CHO cells that had been transfected with the construct were incubated with 20 µg/ml 1,1′-Dioctadecyl-3,3,3′,3′-tetramethylindocarbocyanine perchlorate (DiI)-labelled LDL particles at pH 5 and pH 7, respectively, and after a washing step, binding of LDL to cells expressing the chimera was monitored via live-cell imaging. As depicted in Figure 4-8 B and C, LDL binding to the LIMP-2 ectodomain was pH-dependent and only visible at acidic pH which mimics the physiological pH of lysosomes.

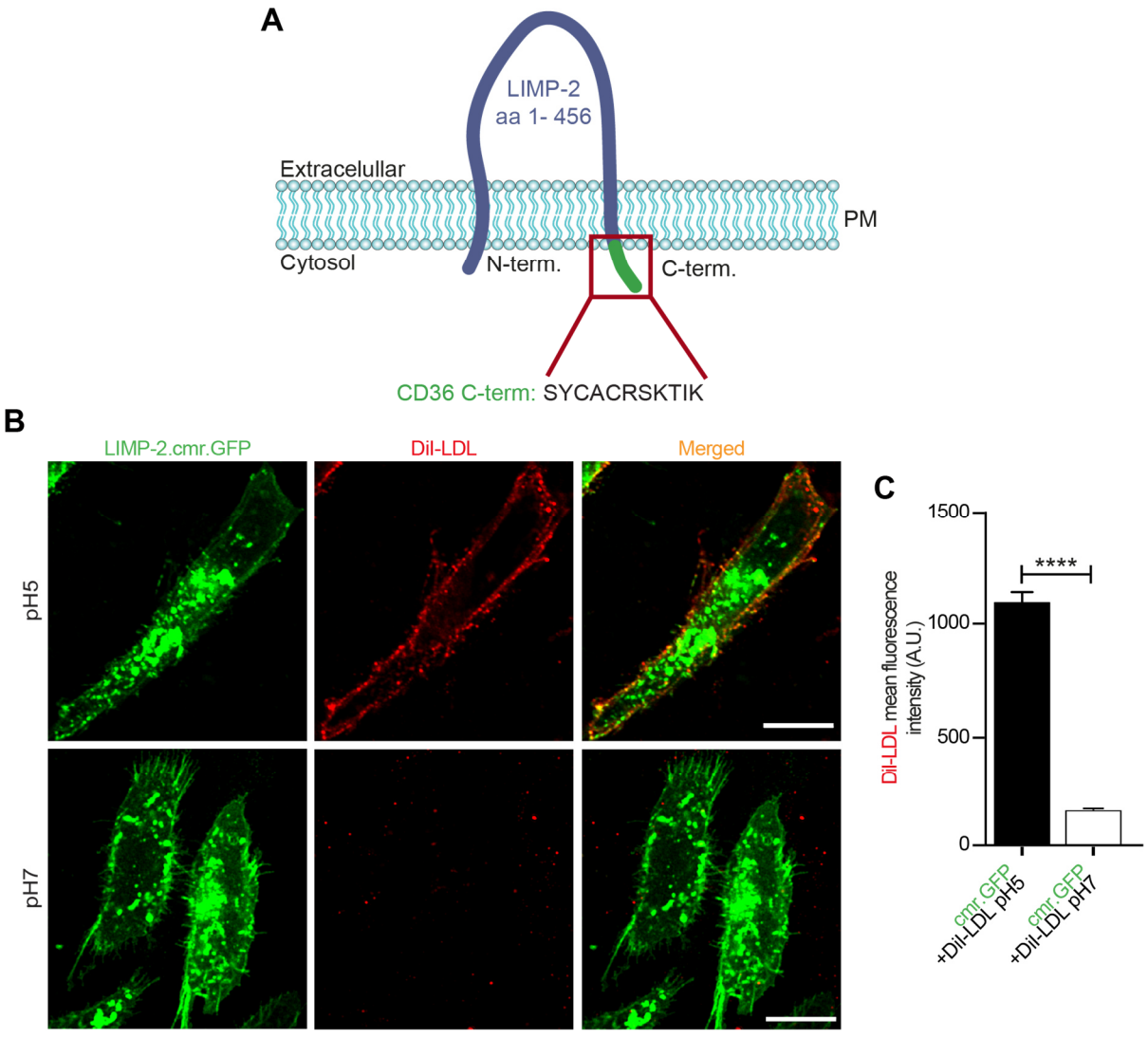

Figure 4-8: Generation of a LIMP-2 chimera and pH-dependent binding to DiI-LDL particles. A The chimera contained amino acids (aa) 1-456 of LIMP-2, while the C-terminus of LIMP-2 was replaced with the C-terminus of CD36 (highlighted in green) causing it to re-locate to the plasma membrane (PM) instead of lysosomes. **B** CHO cells expressing the LIMP-2.cmr.GFP construct were incubated with fluorescently labelled LDL at pH 5 or pH 7. Binding of LDL to cells was only observed at pH 5. Scale bars: 10 µm. **C** Quantification of confocal images from B: pH 5: n =78, pH 7: n = 9 cells from two experiments, mean ± SEM (**** P < 0.0001, unpaired two-tailed Student's t-test). Data in B and C generated in the framework of a collaboration by Ying Meng and Prof. Dante Neculai, Zhejiang University, Hangzhou, China.

Having established cell surface expression of the LIMP2 chimera and its ability to bind LDL, it was next investigated if the luminal domain of LIMP-2 is indeed capable of mediating lipid transport. To this end, a tunnel mutant was generated by exchanging two amino acids lining the inner face of the tunnel, alanine at position 379 and valine at position 415, with bulky tryptophan residues, thereby causing a steric block inside the tunnel. Cells were subsequently transiently transfected with a chimeric version of this tunnel mutant (LIMP-2.cmr. A379W/V415W.mCherry) and uptake of BODIPY-cholesterol that had previously been incorporated into LDL-particles was compared to cells expressing the mCherry-tagged WT chimera (Figure 4-9 A). While in cells expressing the LIMP-2 wild type chimera integration of BODIPY-cholesterol into the plasma membrane was evident, about 44 % lower levels of cholesterol uptake were measured in cells expressing the tunnel mutant chimera as evident from the quantification depicted in Figure 4-9 B. This argues for an uptake mechanism that involves transport specifically through LIMP-2's luminal domain. To elucidate whether LIMP-2 is specifically accepting cholesterol from lipoproteins like LDL (and HDL), cholesterol was next incorporated in Saposin A picodiscs and offered to CHO cells transiently transfected with LIMP-2.cmr. WT.mCherry or LIMP-2.cmr. A379W/V415W.mCherry. Saposin A belongs to the lysosomal saposin family whose members are required for degradation of sphingolipids by lysosomal hydrolases and recent research demonstrated Saposin A's ability to form picodiscs with lipids thus forming a lipoprotein particle similar to HDL (Popovic *et al.* 2012). The data presented in Figure 4-9 C and D shows that the LIMP-2 luminal domain is indeed able to bind Saposin A-containing picodiscs and deliver cholesterol to the plasma membrane. Consistent with the observations made for LDL-derived cholesterol, the delivery of cholesterol from the picodiscs depended on the integrity of the LIMP-2 tunnel. Hence, LIMP-2 can apparently accept cholesterol from multiple proteolipid complexes and -given their lysosomal location and lipid-solubilizing capability- saposins may play a role in presenting cholesterol to LIMP-2.

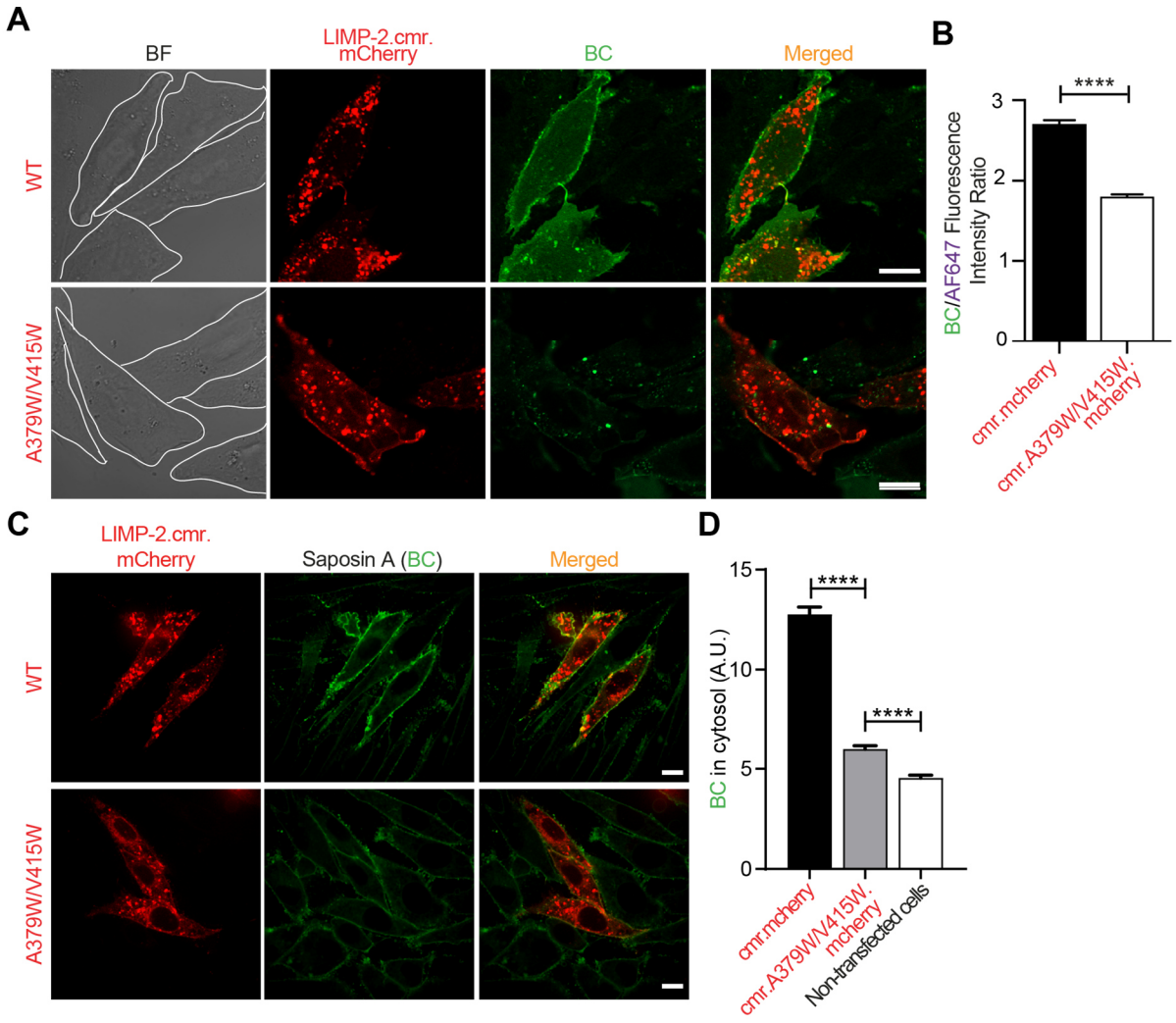

Figure 4-9: Plasma membrane integration of BODIPY-cholesterol by LIMP-2.cmr.WT and tunnel mutant A CHO cells expressing either the WT or A379W/V415W chimera were incubated with BODIPY-cholesterol (BC) that had been incorporated into AlexaFluor 647 (AF647)-labelled LDL particles. While BODIPY-cholesterol was readily integrated into the plasma membrane in cells expressing the WT chimera, a much lower extent of uptake was observed in cells expressing the mutant. Of note, the experiment was carried out in an acidic buffer to mimic the environment of the lysosome. Scale bars: 10 µm. **B** The ratio of green (BC) over far-red (AF647-labeled LDL) fluorescence measured in A was quantified for LIMP-2.cmr.mCherry n = 59, LIMP-2.cmr.A379W/V415W.mCherrry n = 50 cells from 3 experiments. Data are mean ± SEM of triplicate samples (**** $P < 0.0001$, unpaired two-tailed Student's t-test). **C** LIMP-2-mediated BC uptake from BC-loaded Saposin A picodiscs in CHO cells transiently expressing mCherry-tagged-wild type (LIMP-2.cmr.mCherry) or tunnel-blocking mutant LIMP-2 chimera (LIMP-2.cmr.A379W/V415W.mCherrry). After transfection with the respective LIMP-2 construct, cells were incubated with SapA(BC) picodiscs at acidic pH followed by washing with PBS. **D** Quantification of BC uptake from Saposin A (BC) picodisks described in C. The fluorescence intensities of cells transfected with LIMP-2.cmr.mCherry or LIMP-2.cmr.A379W/V415W.mCherrry were compared to the total fluorescence intensity of non-transfected cells. The total cellular fluorescence intensity of BC was measured using Volocity (LIMP-2.cmr.mCherry n = 67, LIMP-2.cmr.A379W/V415W.mCherrry n = 90, non-transfected cells n = 152 cells from 3 experiments). Data are the mean ± SEM of triplicate samples (**** $P < 0.0001$, unpaired two-tailed Student's t-test). A.U., arbitrary units. Scale bars: 10 µm. Data generated in the framework of a collaboration by Ying Meng and Prof. Dante Neculai, Zhejiang University, Hangzhou, China.

4.2.3. Live-cell tracking of cholesterol distribution in absence of LIMP-2

While providing some valuable mechanistic insight, the experiments described above do not reflect the physiological situation because the majority of LIMP-2 is found in lysosomes (Barriocanal *et al.* 1986, Fujita *et al.* 1991). Based on the low pH preference (Figure 4-8) this is likely the relevant organelle for a cholesterol transport function of LIMP-2.

Therefore, live-cell imaging was utilized to follow the fate of LDL-derived BODIPY-cholesterol from late endosomes/lysosomes to lipid droplets, the storage site for excess lipids within the cell in presence or absence of LIMP-2. Since a disturbed export of cholesterol from lysosomes is well described (Pentchev *et al.* 1985), NPC1-silenced cells were used as a positive control and as a basis of comparison for potential defects in transport caused by loss of LIMP-2. Briefly, human epidermoid carcinoma cells (A431) were first treated with siRNA directed against LIMP-2 or NPC1, siLIMP-2 and siNPC1, respectively, or with scrambled siRNA as control (siCtrl) for 72 h. To induce the formation of lipid droplets, cells were treated with 200 µM oleic acid/BSA in 5 % lipoprotein-depleted serum (LPDS) for 24 h followed by a 2-h pulse with BODIPY cholesteryl linoleate-labeled LDL particles (BC LN-LDL, Figure 4-10 A) . Cells were also labelled with 50 µg/ml Alexa Fluor 647-dextran (10,000 MW; Thermo Scientific) simultaneous to oleic acid incubation to visualize late endosomes/ lysosomes. The trafficking of the liberated BODIPY-cholesterol was followed for a chase period of 0 - 4 h and the incorporation of the lipid into lipid droplets was analyzed (Figure 4-10 B, C). In order to verify the effects observed by knock-down of LIMP-2, rescue experiments were conducted where the LIMP-2 siRNA treated cells were transfected with mCherry-tagged mLIMP-2 WT or mLIMP-2 tunnel mutant (G379W/V415W), respectively. At the start of the chase period (0 h chase), BODIPY-cholesterol was largely co-localizing with dextran-labelled compartments in all genetic conditions (Figure 4-10 B upper panels). After 4 h chase approximately half of the measured BODIPY-cholesterol was instead co-localizing with lipid droplets (that were visualized with the neutral lipid stain LipidTox™) in cells treated with siCtrl, indicating its export from late endosomes/lysosomes (Figure 4-10 B lower panel). Contrarily, in NPC1-silenced cells, only a small fraction of BODIPY-cholesterol was found to co-localize with lipid droplets after 4 h chase, while the majority of the lipid was still retained in dextran-labelled late endosomes/lysosomes. In cells treated with LIMP-2-silencing siRNA an intermediate phenotype was observed: While the portion of BODIPY-cholesterol arriving to lipid droplets was higher than in NPC1-depleted cells, a statistically significant amount was retained in late endosomes/lysosomes when compared to siCtrl treated cells (Figure 4-10 C). These data, acquired using physiological conditions, demonstrate that lipid transport through the tunnel domain present in LIMP-2 is indeed taking place in lysosomes and loss of LIMP-2 alters this lipid flux.

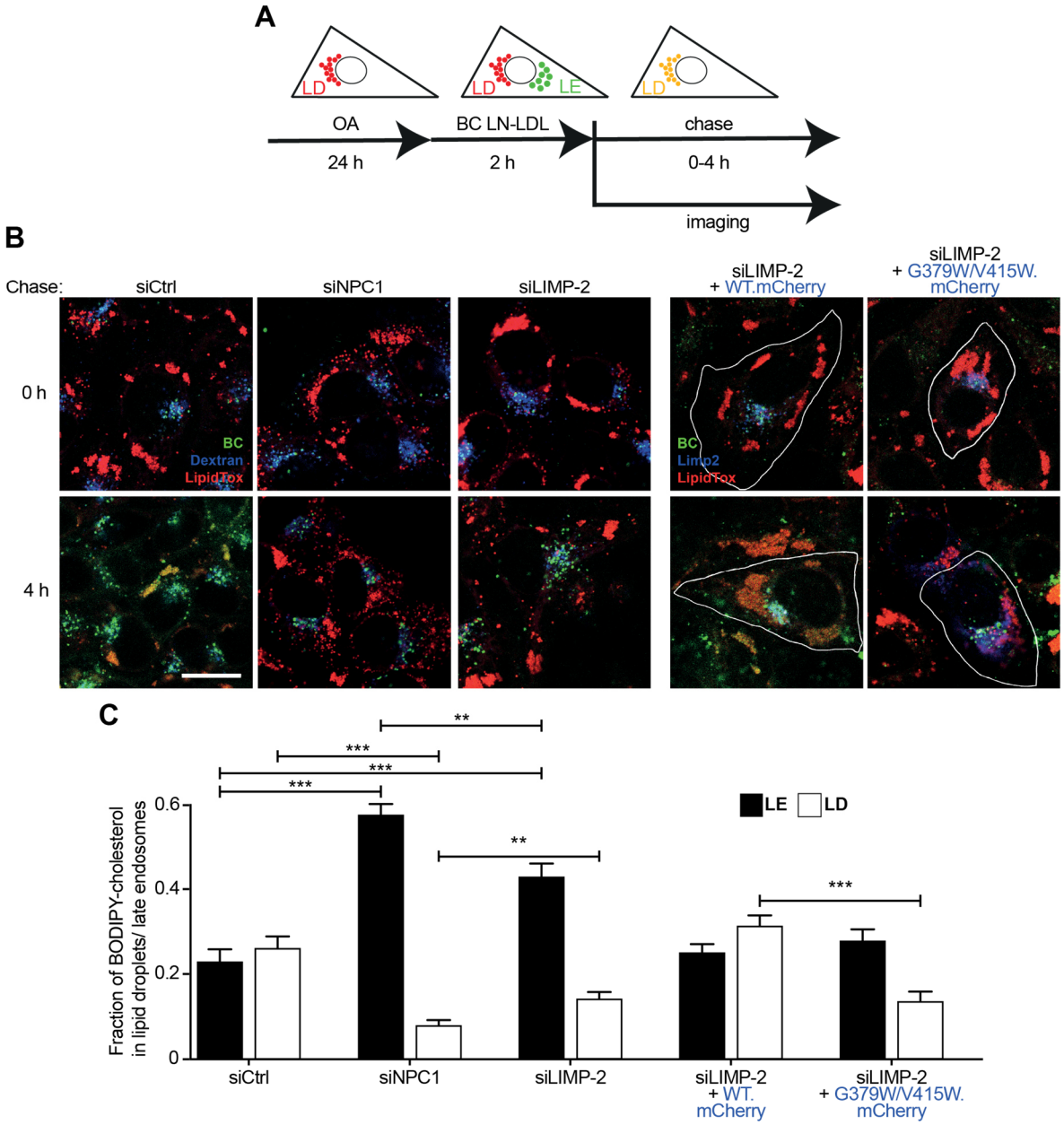

Figure 4-10: Live-cell monitoring of distribution of BODIPY-cholesterol in A431 cells. A Schematic description of BODIPY-cholesterol efflux assay. A431 cells were incubated with oleic acid (OA) for 24 h, to induce formation of lipid droplets. They were then subjected to a 2 h pulse with BODIPY-cholesterol incorporated into LDL particles. For the chase, the medium was changed to serum-free CO_2 –independent medium suitable for live cell imaging and the trafficking of BODIPY-cholesterol from late endosomes and lysosomes (LE) to lipid droplets (LD) was followed for 0 - 4 h. **B** Representative images of cells that were previously depleted of NPC1 or LIMP-2 (siNPC1, siLIMP-2), respectively, and compared to control-treated cells (siCtrl) as well as cells depleted of LIMP-2 and re-transfected with mLIMP-2.WT.mCherry or mLIMP-2.G379W/V415W.mCherry, respectively. Scale bar: 10 µm. **C** Quantification of the fraction of LDL-derived BODIPY-cholesterol present in LE or LD, respectively. n = 21 (siLIMP-2, siCtrl), 22 (siLIMP2 + WT.mCherry) or 23 (siNPC1, siLIMP-2 + G379W/V415W.mCherry) cells. Data (mean ± SEM) from 3 experiments. Data generated in the framework of a collaboration by Kristiina Kanerva and Elina Ikonen, University of Helsinki, Finland.

Lipid droplets are the storage site for excess sterols and triglycerides within the cell. Once the threshold concentration of these lipids are reached in the ER, they form an oil lens and upon exceeding the maximum capacity begin to bulge out to form a nascent lipid droplet which eventually buds off from the ER (Jacquier *et al.* 2011, Wang 2016). Cholesterol is being esterified by the ER-resident enzyme sterol O-acyltransferase 1 (SOAT1 or ACAT1) prior to its incorporation into lipid droplets (Devries-Seimon *et al.* 2005, Kedi *et al.* 2009, Walther *et al.* 2017). A lack of free cholesterol as a consequence of diminished export from lysosomes would therefore cause a drop in esterified cholesterol stores. Having observed a hampered transport of BODIPY-cholesterol from late endosomes/ lysosomes to lipid droplets (Figure 4-10) in cells lacking LIMP-2, it was next investigated whether the hampered lysosomal export of cholesterol is also reflected in the lipid stores present in the cell.

LIMP-2 WT and KO MEFs were pulsed with tritium-labelled oleic acid:BSA complex additionally to being challenged (or not) with LDL for 6 h. High concentrations of fatty acids lead to lipotoxicity in cells which is why they are coupled to free cholesterol to form cholesterol esters or incorporated into triglycerides and stored in non-toxic lipid droplets (Listenberger *et al.* 2003). After the labelling period, cells were scraped and lipids extracted using the Bligh/Dyer method (Bligh and Dyer 1959). Lipids were separated on a thin layer chromatography plate. Cholesterol esters were isolated and subjected to scintillation counting (Figure 4-11 A).

While there was no difference in uptake of oleic acid (Figure 4-11 B) between LIMP-2 WT and KO cells, the amount of ^{3}H-oleic-acid containing cholesterol esters was significantly reduced in cells lacking LIMP-2 (Figure 4-11 C). This was the case independent of additional supplementation with LDL, indicating that exogenous lipid supplies like LDL are not the only source of cholesterol utilizing this pathway. As expected, the addition of U18666A, a drug that inhibits lysosomal cholesterol export (Lu *et al.* 2015), or Sandoz 58-035, an inhibitor of A:cholesterol acyltransferase-1 (ACAT1) (Kedi *et al.* 2009), led to hardly or no measurable levels of ^{3}H-oleate containing cholesterol esters in WT cells challenged with LDL. The same results were obtained when using ^{3}H-cholesterol instead of ^{3}H-oleic acid, confirming that lack of sterol in the ER is indeed causative for the decreased cholesterol ester formation (Figure 4-11 D). Taken together, these data demonstrate impairments in the trafficking of LDL-derived cholesterol from lysosomes to the ER in absence of LIMP-2 under physiological conditions.

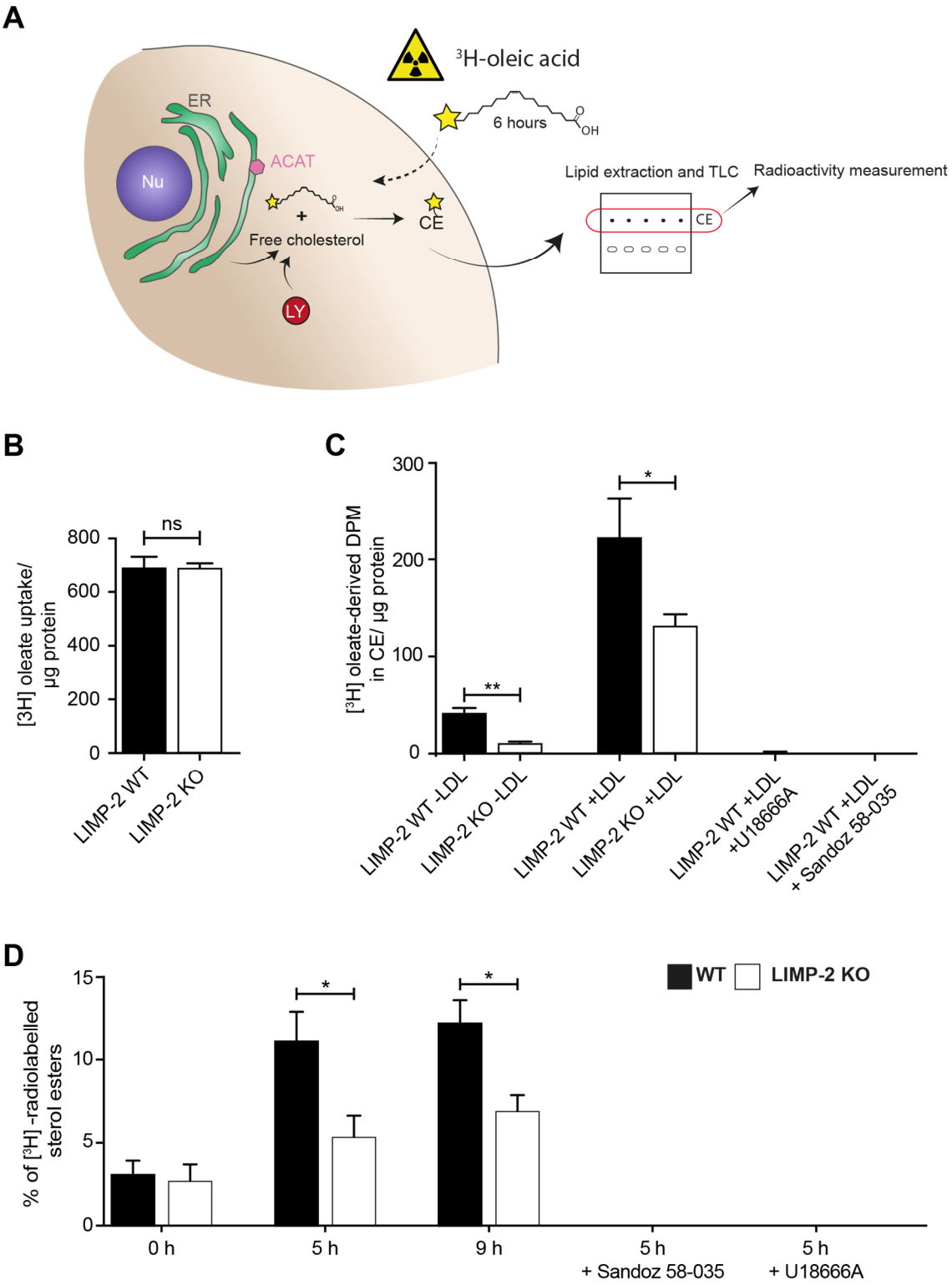

Figure 4-11: Incorporation of ^{3}H-labelled fatty acid or ^{3}H-labelled cholesterol into cholesterol esters in LIMP-2 WT and KO MEFs. A Schematic depiction of labelling and extraction procedure (for details, see text). **B** Comparison of cellular uptake of ^{3}H-oleic acid in LIMP-2 WT and KO MEFs. n = 18 (WT), 30 (KO). **C** Incorporation of [^{3}H]-oleic acid into cholesteryl esters ± LDL in LIMP-2 WT and KO MEFs, respectively, and in WT cells + LDL in presence of U18666A or Sandoz 58-035, respectively, as negative controls. Data (mean ± SEM) from two (for U18666A and Sandoz 58-035) to three (for LIMP-2 WT and KO +/- LDL) independent experiments. **D** Incorporation of [^{3}H]-cholesterol into cholesteryl esters in LIMP-2-WT and LIMP-2-KO MEFs in the presence and absence of U18666A or Sandoz 58-035 (n =7 (0 h/5 h), n = 3 (9 h), n = 4 (Sandoz 58-035/U18666A) samples), respectively. Data (mean ± SEM) from two (9 h chase) to 3 experiments (5 h chase), unpaired two-tailed Student's t-test (*P ≤ 0.05). Data in B, C and D generated in the framework of a collaboration by Kristiina Kanerva and Elina Ikonen, University of Helsinki, Finland

4.2.4. The regulation of the cellular cholesterol homeostasis is influenced by LIMP-2

Within a cell, various types of membranes with unique properties, such as thickness, and lipid compositions exist, determining e.g. rigidity of a membrane (van Meer *et al.* 2008). Cholesterol distribution in different cellular compartments is heterogeneous and strict regulation of cholesterol homeostasis is necessary to maintain physiological levels of cholesterol within the cell. The sophisticated ER-resident protein machinery involved in these maintenance processes has been introduced in 1.1and is also briefly summarized in Figure 4-12 A. A central factor is the transcription factor sterol-regulatory element binding protein 2 (SREBP2) which, upon cholesterol depletion in the ER, activates the transcription of genes involved in LDL uptake and endogenous cholesterol synthesis, i.e. LDLR and 3-hydroxy-methyl-glutaryl-COA reductase (HMGCR), respectively, in the nucleus.

Consequently, impairment of the cholesterol flux from lysosomes to the ER should be reflected in an altered response of the cholesterol regulatory machinery. Using a modified version of a SREBP2 cleavage assay that was first published by Chu and co-workers (Chu *et al.* 2015), the processing of the transcription factor in response to either sterol depletion or re-addition of LDL in HeLa cells previously treated with siCtrl, siNPC1 or siLIMP-2 was assessed (Figure 4-12 B). Since in the control cells LDL-derived cholesterol should be able to reach the ER and replenish the cholesterol stores, the formation of nSREBP2 should be decreasing once the threshold limit is reached. A block of lysosomal cholesterol export as observed for NPC1 deficient cells on the other hand is expected to prevent the replenishment of the ER cholesterol levels, thus enforcing SREBP2 translocation and processing. Thus, siCtrl- and siNPC1- treated cells serve as positive and negative controls, respectively, and allow classification of the impact of LIMP-2 silencing on lysosomal cholesterol export and subsequent regulation of the ER cholesterol regulatory machinery.

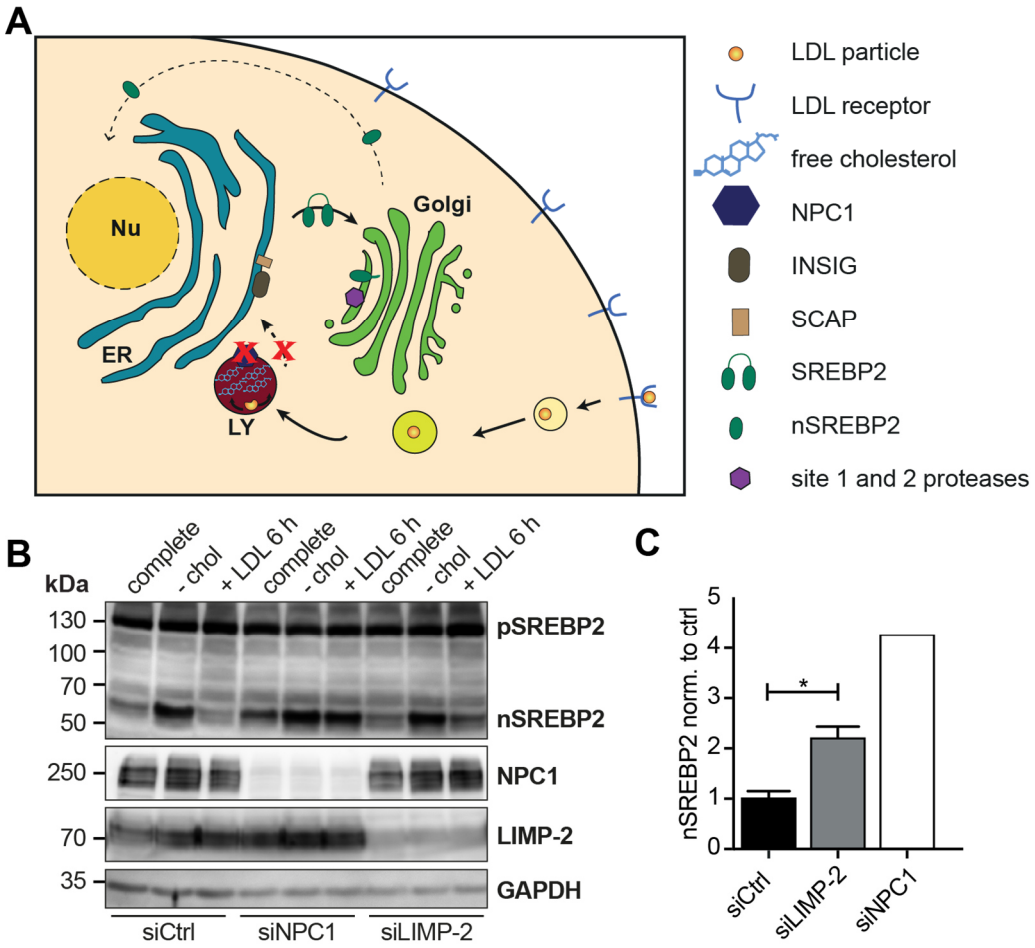

Figure 4-12: SREBP2 cleavage assay. A Schematic description of the reaction of the cholesterol regulatory machinery in the ER in response to a lack of lysosome-derived cholesterol as e.g. in the case of NPC1 deficiency. Due to the lack of lysosomal cholesterol in the ER caused by absence of NPC1 the transcription factor sterol-regulatory element binding protein 2 (SREBP2) is no longer being retained in the ER by insulin-induced gene 1 (INSIG) and sterol regulatory element-binding protein cleavage-activating protein (SCAP) and therefore translocates to the Golgi in COPII-coated vesicles. There, it is cleaved by site 1 and site 2 proteases, releasing a small fragment, nuclear SREBP2 (nSREBP2), that traffics to the nucleus to activate the transcription of genes needed to enhance uptake of exogenous cholesterol like the LDL receptor and genes that lead to an elevation of endogenous cholesterol synthesis, like 3-hydroxy-methyl-glutaryl-COA reductase (HMGCR). **B** HeLa cells were first treated with the indicated siRNAs for 60 h. For cholesterol depletion, cells were then incubated in lipoprotein-free medium for 12 h. Finally, 50 µg/ml LDL was added to the starved cells where indicated for 6 h. Cells were pelleted and protein lysates prepared and analyzed for processing of precursor SRBEP2 (pSREBP2) in response to the sterol status. **C** Quantification of nSREBP2 levels after LDL loading in cells treated with scrambled (ctrl), NPC1 or LIMP-2 siRNA, respectively n = 3; data (mean ± SEM) from two independent experiments; * P ≤ 0.05, t-test.

Under conditions of cholesterol depletion (- chol) SREBP2 is cleaved to generate nSREBP2. The cleavage is terminated once sterol stores in the ER are resupplied, e.g. by re-addition of LDL (+ LDL). As demonstrated in Figure 4-12 B, after 6 h of LDL re-addition, nSREBP2 levels reach basal levels in HeLa cells treated with control siRNA. In the case of a loss of NPC1, levels of nSREBP2 do not change when cells are fed with LDL, indicating that the LDL-derived cholesterol does not reach the ER to terminate SREBP2 processing. In cells treated with siRNA down-regulating LIMP-2 nSREBP2 levels were decreasing after 6 h of LDL re-addition, but remained higher than in control treated cells or cells that had not been subjected to cholesterol

depletion (Figure 4-12 B and C), suggesting that while LDL-derived cholesterol is reaching the ER, the amount is either too little to fully restore balance or delayed in comparison to WT cells.

LDL arrives in lysosomes via the endocytic pathway approximately 45-60 min after uptake (Castellano *et al.* 2017) and two major constituents of LDL particles, triglycerides and cholesterol esters, subsequently undergo hydrolysis by lysosomal acid lipase (Dubland and Francis 2015). In order to further characterize the kinetics of the impaired cholesterol export in LIMP-2 deficiency, short LDL incubation times (Figure 4-13) as well as long incubation times (Figure 4-14) were analyzed.

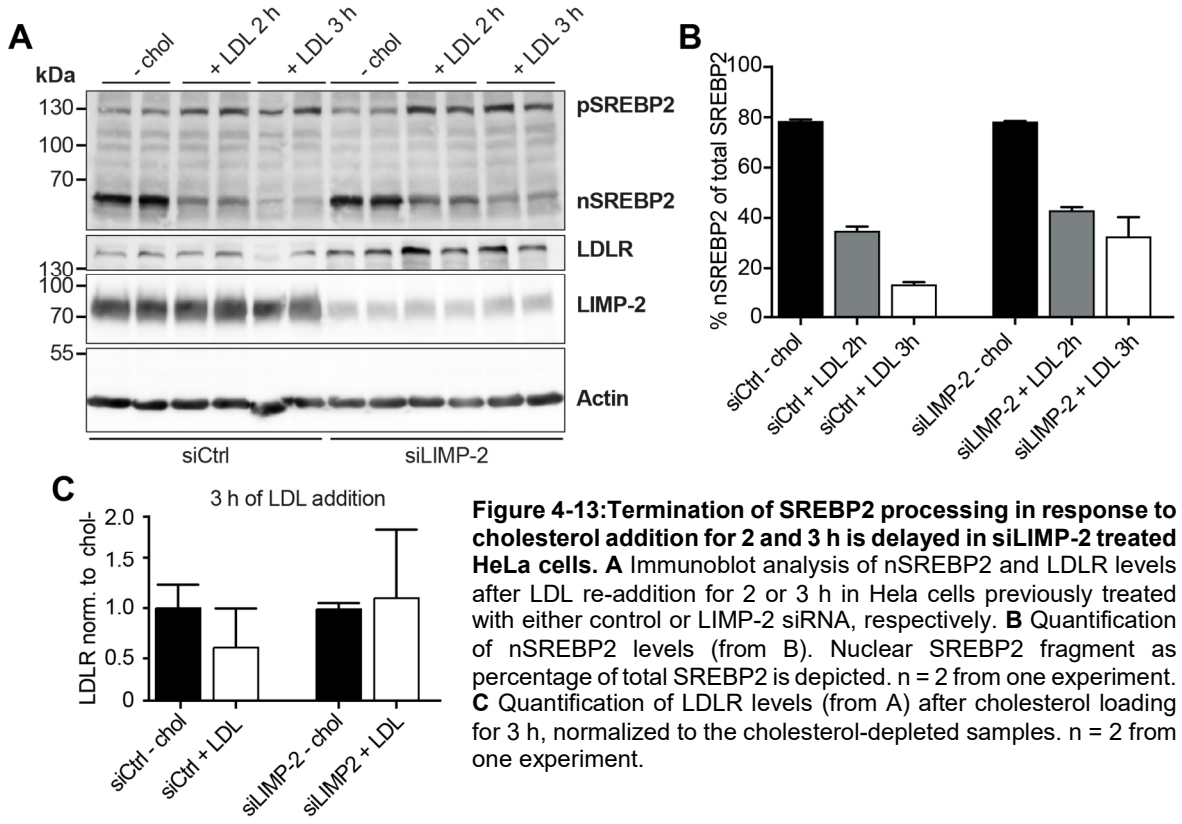

Figure 4-13:Termination of SREBP2 processing in response to cholesterol addition for 2 and 3 h is delayed in siLIMP-2 treated HeLa cells. A Immunoblot analysis of nSREBP2 and LDLR levels after LDL re-addition for 2 or 3 h in Hela cells previously treated with either control or LIMP-2 siRNA, respectively. **B** Quantification of nSREBP2 levels (from B). Nuclear SREBP2 fragment as percentage of total SREBP2 is depicted. n = 2 from one experiment. **C** Quantification of LDLR levels (from A) after cholesterol loading for 3 h, normalized to the cholesterol-depleted samples. n = 2 from one experiment.

While siCtrl- and siLIMP-2- treated cells were expressing equal amounts of nSREBP2 and LDLR in cholesterol depleted cells (-chol) as evident from the quantification of protein levels depicted in Figure 4-13 B and C, respectively, re-supplying the siCtrl- and siLIMP-2- treated cells with LDL for 2 h or 3 h had different effects on nSREBP2 levels. In both cell types, a decrease in nSREBP2 protein levels could be observed. While after 2 h of LDL addition, the drop of nSREBP2 was in a similar range between control and LIMP-2-silenced cells, after 3 h of supplementation with LDL nSREBP2 levels dropped below 15 % of the levels of total SREBP2 in control cells as an indication that cholesterol levels were increasing in the ER while nSREBP2 levels in siLIMP-2-treated cells were still 2.5-fold higher (Figure 4-13 B), indicating an impairment or delay in arrival of LDL-derived cholesterol in the ER in cells with diminished levels of LIMP-2. This was also evident in the levels of LDLR the expression of which is

regulated by nSREBP2. While in control cells, 3 h of cholesterol loading with LDL led to a decrease in LDLR protein levels, this decrease did not occur in siLIMP-2-treated cells (Figure 4-13 C).

As described above, loss of NPC1 prevents the termination of nSREBP2 formation even after 6 h of LDL re-addition and this is still the case after 10 h of LDL supply. However, after 24 h of LDL re-addition, there is a decrease in nSREBP2 as well as LDLR, indicating that by an alternative mechanism enough cholesterol is reaching the ER to restore supplies and terminate the signaling cascade (Figure 4-14 A, B).

To investigate if LIMP-2 could be involved in such an alternative mechanism for cholesterol export, HeLa NPC1 KO cells were treated with LIMP-2 siRNA and starved as described above. After 24 h of LDL re-addition, nSREBP2 was still being formed and LDLR levels were still upregulated, in contrast to NPC1 KO treated with control siRNA (Figure 4-14 A-D). The same effect was observed with 3-hydroxy-3-methyl-glutaryl-coenzyme A reductase (HMGCR), the rate-limiting enzyme of endogenous cholesterol synthesis and the second gene regulated by nSREBP2 besides LDLR (Figure 4-14 E), demonstrating that double deficiency of NPC1 and LIMP-2 had additive effects on cholesterol levels and that even though depletion of NPC1 already drastically restricts lysosomal cholesterol export, a portion of cholesterol can still reach the ER, albeit at a slower rate, through the LIMP-2 transport mechanism and this additional route of export is lost in absence of LIMP-2 leading to a more severe disturbance in lysosomal cholesterol export in NPC1/LIMP-2-double deficient cells as compared to cells only lacking NPC1.

Taken together, these findings demonstrate a role for LIMP-2 in cholesterol transport from lysosomes to the ER in vivo.

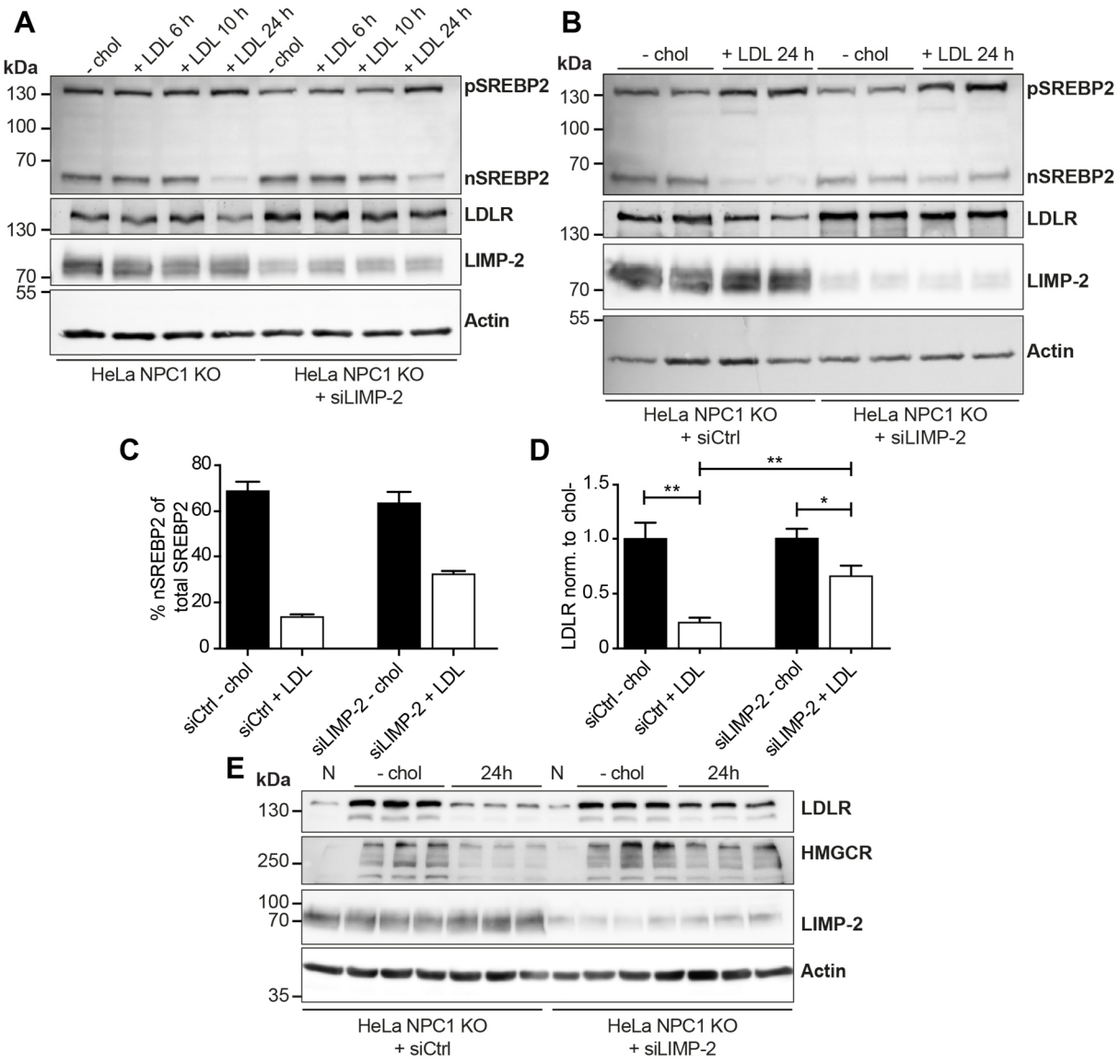

Figure 4-14: Additive effects of NPC1/LIMP-2 double deficiency on transcriptional response to cholesterol levels. A and **B** Immunoblot analysis of nSREBP2 and LDLR levels in response to cholesterol loading for indicated times in HeLa NPC1 KO cells and HeLa NPC1 KO additionally treated with LIMP-2 siRNA, respectively. **C** Quantification of nSREBP2 levels. Nuclear SREBP2 fragment as percentage of total SREBP2 is depicted. (n = 2; data (mean ± SD) from one experiment). **D** Quantification of LDLR levels after cholesterol loading, normalized to the cholesterol-depleted samples (n = 5; data (mean ± SEM) from two experiments. **E** Independent repeat of experiment shown in B demonstrating the response of the cholesterol-regulatory machine to LDL re-addition for 24 h after cholesterol depletion in NPC1- deficient and NPC1/LIMP-2 double-depleted HeLa cells. In addition to LDLR levels, the protein levels of HMGCR was monitored by immunoblot analysis.

4.2.5. LIMP-2 does not associate with NPC1

While LIMP-2 can to some extent compensate for loss of NPC1 (Figure 4-14, (Heybrock *et al.* 2019)), the mode of transport appears to be slower than that of NPC1 and deficiency of NPC1 leads to drastic accumulation of cholesterol and sphingolipids in spite of the presence of LIMP-2. Recently, several research groups have demonstrated the existence of unique populations of lysosomes within the same cell that do not always harbor the same set of proteins or differ in pH and other characteristics and therefore have different functions (Johnson *et al.* 2016, Jongsma *et al.* 2016, Pu *et al.* 2016, Ballabio and Bonifacino 2020). In order to better understand the relevance of lipid transport by LIMP-2 in vivo, it was investigated whether LIMP-2 and NPC1 are both present in the same (sub)populations of lysosomes and if protein levels of LIMP-2 might modulate those of NPC1. As depicted in Figure 4-15 A, the fluorescent signals observed for LIMP-2.mCherry and NPC1.GFP overlap. Additionally, both signals also overlap with antibody-stained endogenous LAMP2. Thus, in HeLa cells all three proteins can be found in the same organelle. While loss of NPC1 leads to an increase in several lysosomal membrane proteins such as LAMP1, LAMP2 and LIMP-2 (which can likely be attributed to the increase in lysosome size and number caused by lipid accumulation), absence of LIMP-2 did not affect NPC1 protein levels significantly as demonstrated by Western blot analysis of protein lysates of WT and LIMP-2 KO MEFs (Figure 4-15 B). Overexpression of a LIMP-2 WT or tunnel mutant construct did not alter NPC1 levels either (Figure 4-15 C), disfavoring the idea of a tightly controlled transcriptional regulation of NPC1 and LIMP-2 as part of e.g. a negative feedback loop.

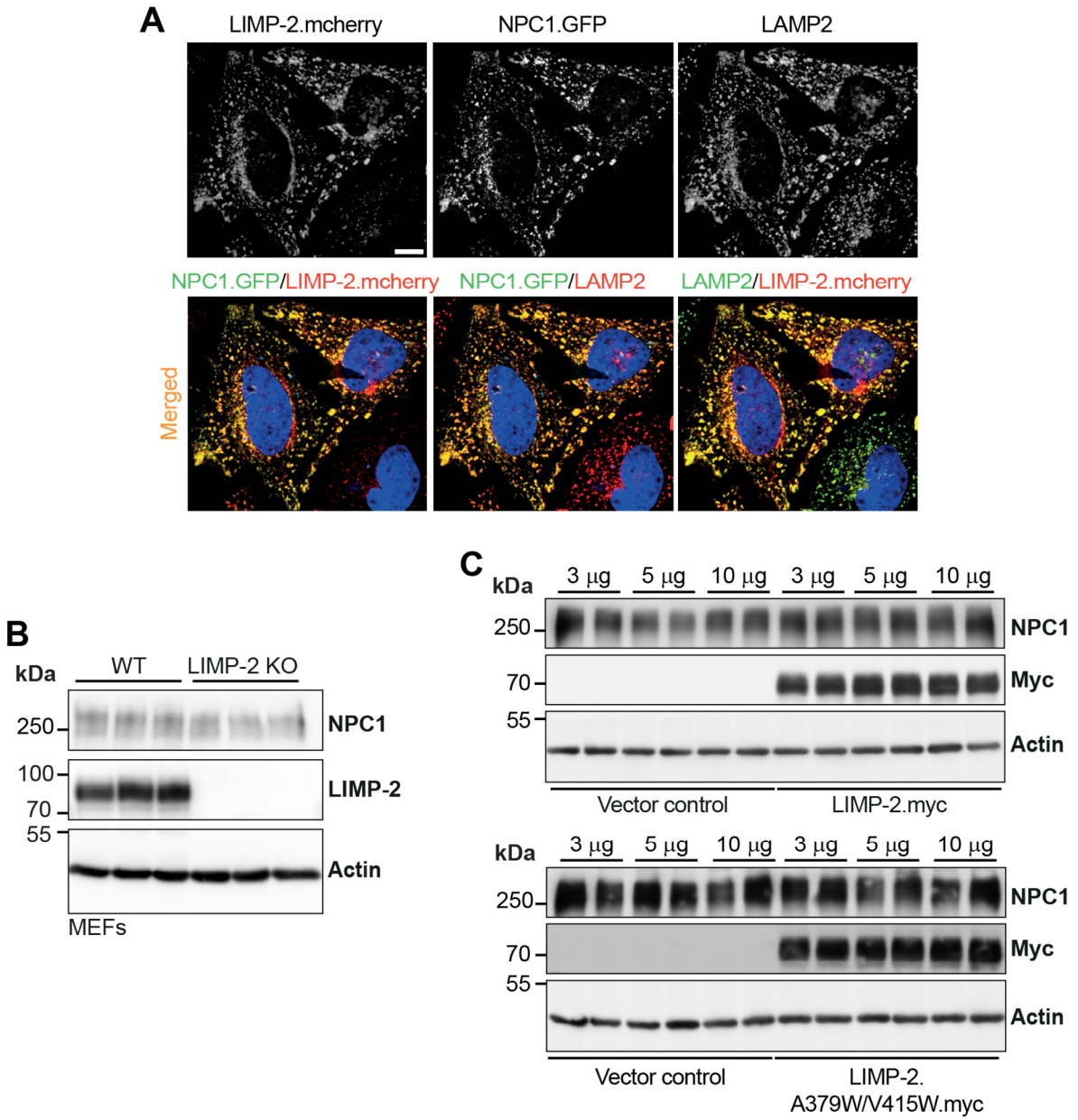

Figure 4-15: While LIMP-2 and NPC1 reside in the same vesicles, they don't influence each other's stability. **A** Confocal microscopy of HeLa cells transfected with LIMP-2.WT.mCherry and NPC1.GFP were co-stained with endogenous LAMP2 demonstrating that all three proteins reside in the same organelles. Scale bar 10 µm. **B** Protein levels of NPC1 were analyzed in MEFs deficient for LIMP-2. **C** HeLa cells were transfected with increasing amounts of LIMP-2.WT.myc or LIMP-2.A379W/V415W.myc, respectively, and protein levels of NPC1 were analyzed by immunoblot.

The previous experiments do not exclude the possibility that LIMP-2 and NPC1 might act in concert in lipid export and directly interact with each other. Moreover, it is feasible to hypothesize that the soluble cholesterol-binding protein NPC2 is delivering the hydrophobic lipid not only to NPC1, but also to LIMP-2. Therefore, co-immunoprecipitation studies were conducted where LIMP-2 was precipitated either via its myc-tag when overexpressed or using an antibody directed against the C-terminus of LIMP-2 for precipitation of the endogenous protein. While a strong co-immunoprecipitation (co-IP) of NPC2 and a weaker of NPC1 could indeed be observed under overexpression conditions (Figure 4-16 A), in follow-up studies

focusing on the endogenous proteins, no association of LIMP-2 with either NPC1 or NPC2 could be overserved (Figure 4-16 B). While the results are contrary, the co-IPs of NPC1 and NPC2, respectively, under overexpression conditions likely results from an overload of the proteins during synthesis in the ER and therefore 'unnatural' association. On the other hand, this implies that LIMP-2 might in principle be capable of interacting with both proteins, but does not do so under physiological conditions or in the cell type chosen for the co-IP experiment.

Further evidence that negate a complex consisting of NPC1 and LIMP-2 stems from blue native polyacrylamide gel electrophoresis (BN PAGE) studies (Figure 4-16 C) where cell or tissue is lysed under non-denaturing conditions, thus allowing protein complexes to stay intact (Schagger and von Jagow 1991, Wittig *et al.* 2006). Instead of SDS that is the negative charge-conferring molecule in a standard SDS-PAGE, the NativePAGE™ bis-tris gel system (Thermo Fisher Scientific) that was used in this study utilizes Coomassie G-250 in the sample buffer as well as in the cathode running buffer to convert the proteins to a net negative charge and allow them to migrate towards the anode. Separation of these complexes under non-denaturing conditions occurs according to the molecular weight and gives an estimate about stoichiometry and composition of such complexes. Separation of lysates from WT MEFs by Blue Native PAGE revealed that LIMP-2 and NPC1 do not have the same migration pattern. The respective protein bands were detected at different molecular weights, with natively folded NPC1 migrating at 480 kDa, whereas LIMP-2 was migrating between 146 kDa and 242 kDa. If both proteins would form a complex, they would have to be migrating at the same speed in this non-denaturing gel. The fact that they migrate differently indicates that they exists separately (Figure 4-16 C).

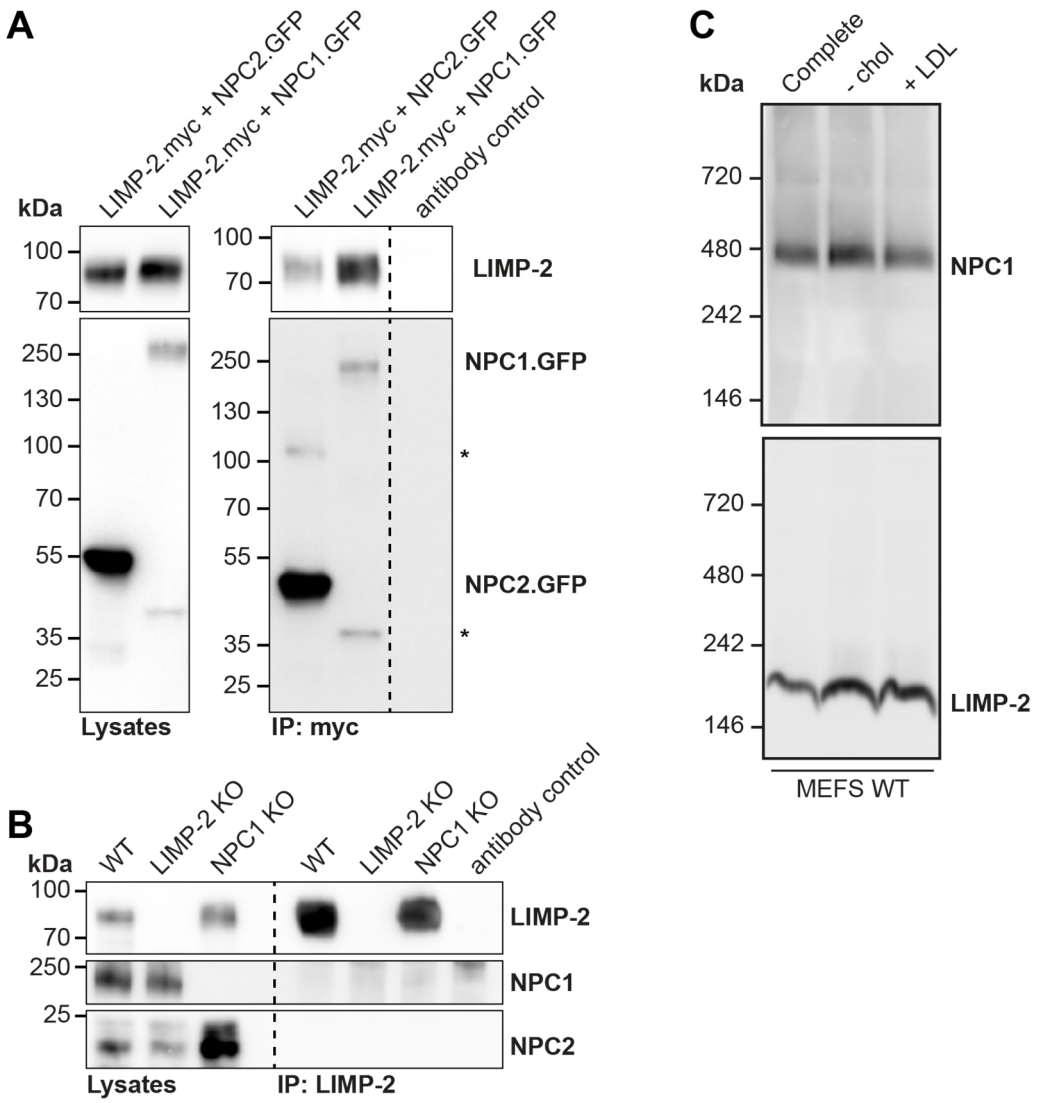

Figure 4-16 LIMP-2 does not interact with either NPC1 or NPC2 endogenously. A Immunoprecipitation (IP) experiment using HeLa WT cells that were co-transfected with LIMP-2.myc and NPC2.GFP or NPC1.GFP, respectively. LIMP-2 was precipitated via its myc-tag. 1 mg of total cell lysate was used for precipitation. Both NPC2 and NPC1 were detected in the co-immunoprecipitation (co-IP) fractions via their respective GFP-tags. The dashed line indicates that part of the blot containing non-relevant samples has been cut. **B** Immunoprecipitation experiment using HeLa WT, LIMP-2 KO (described in 4.3) and NPC1 KO cells. 2 mg of cell lysate was used for IP of LIMP-2. No co-precipitation of LIMP-2 with NPC1 or NPC2 could be detected. The dashed line indicates that part of the blot containing non-relevant samples has been cut. **C** Native PAGE of protein lysates from WT MEFs that were previously kept in either complete medium containing 10 % FCS and 1 % antibiotics (complete) or depleted of sterols over night by incubation in DMEM supplemented with 5 % LPDS as well as 10 µM Mevalonate and 1 µM Atorvastatin (- chol). For the third condition, starved cells were re-fed with 50 µg/ml LDL for 6 h. Samples were prepared and separated under non-denaturing conditions using NativePAGE™ Bis-tris gels (Thermo Fisher Scientific) allowing protein complexes to stay intact. No complex consisting of NPC1 and LIMP-2 was observed.

Of note, this migration pattern was not influenced by availability of sterols as demonstrated by incubation of cells in low versus high cholesterol media, respectively, which excludes that an association of NPC1 and LIMP-2 only occurs in situations of e.g. sterol overload induced by LDL loading. Therefore, the cholesterol export routes of LIMP-2 and NPC1 appear to exists and operate separately from each other.

4.3. Generation and analysis of HeLa LIMP-2 KO and NPC1/LIMP-2 KO cells

Studying cell lines deficient for the protein under investigation has been pivotal in uncovering functions of proteins and understand associated disease phenotypes. The protein of interest (POI) can be depleted from cells by many different ways, both temporarily by RNA interference (RNAi) mediated by silencing RNAs (siRNA) or short hairpin RNAs (shRNA) as well as permanently by disrupting the gene coding for the protein. While for a long time, methods based on engineered nucleic acid binding proteins such as TALENs, zinc fingers and meganucleases were the gold standard for targeted gene editing (Urnov 2018), the Clustered regularly interspaced short palindromic repeats (CRISPR)/CRISPR-associated (CRISPR/Cas) toolkit is now a widely used method for genetic manipulation and can be used to disrupt genes as well as to modify genes to express a mutated version of the POI, a process that is referred to as knock-in (KI) (Knott and Doudna 2018).

An advantage of a transient depletion of a POI is that cells are acutely affected and are likely not able to create mechanism to compensate for the loss of function of the protein, thereby allowing unfiltered observation of the consequences caused by loss of the POI. On the other hand, knockdown efficiency achieved with siRNA or shRNA varies and residual protein may hamper the evaluation of the observed effects.

Overall, a combination of utilizing cells transiently or permanently lacking the POI ensures the validity of the experimental outcome and complements each other.

As described above, LIMP-2 KO MEF cells as well as HeLa and A431 cells treated with LIMP-2-silencing siRNA were employed to study LIMP-2 function in lipid transport. In order to extend the pool of existing LIMP-2-deficient cells lines, the CRISPR-Cas9 system was used to create HeLa LIMP-2 KO cell lines (for methodical details, see 3.3.5).

4.3.1. Experimental procedure and selection of single clones

In addition to treatment of HeLa WT cells with sgRNA and Cas9 to create LIMP-2-deficient cells, a HeLa NPC1 KO cell line (Tharkeshwar *et al.* 2017) was also transfected with sgRNA/Cas9 targeting the SCARB2 gene to create a HeLa cell line deficient for both NPC1 and LIMP-2 (HeLa NPC1/LIMP-2 KO cells). The sgRNA targets the second exon of LIMP-2 as depicted in Figure 4-17.

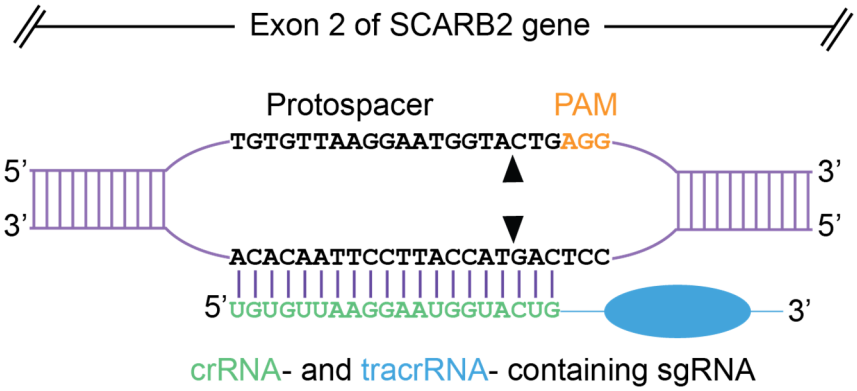

Figure 4-17: Schematic depiction of the targeting strategy used to introduce dsDNA breaks on the gene coding for LIMP-2. A single guide RNA (sgRNA) consisting of crispr RNA (crRNA) and trans-activating crRNA (tracrRNA) was engineered to bind to a complementary sequence in exon 2 of the SCARB2 gene and thus mediate assembly of the endonuclease Cas9 (not shown) which, upon recognition of the protospacer adjacent motif (PAM, NGG for *Streptococcus pyogenes* Cas9), cuts both DNA strands (indicated by black arrowheads). HeLa LIMP-2 KO and NPC1/LIMP-2 KO cells were generated using a sgRNA with the crRNA sequence indicated in green (#76195843, Synthego). The scheme was generated based on the description by Jinek and colleagues (Jinek *et al.* 2012).

The sgRNA and Cas9 were introduced into HeLa cells as described in 3.3.5 and cells were grown to confluency. In order to assess the targeting efficacy of the sgRNAs, genomic DNA was isolated from each single clone and a DNA fragment containing the region of exon 2 of SCARB2 targeted by the sgRNA was amplified by PCR. According to sequencing analysis using the Interference of CRISPR edits (ICE) tool from Synthego, several clones had frame-shifting insert/ deletion (indel) (data not shown). To test whether the indel also led to the desired loss of protein, an aliquot of these cells was lysed and analyzed via immunoblot. Using antibodies directed against LIMP-2 and comparing HeLa WT cells with the treated cells a drastic decrease of LIMP-2 protein levels could be observed indicating that the disruption of the SCARB2 gene was successful in most cells (data not shown). Next, single clones were isolated and propagated and analyzed by immunoblot. As shown in Figure 4-18 A expression of the SCARB2 gene was not abolished in all cells. To proceed, single cell clones that were devoid of LIMP-2 were chosen. The same was done with the NPC1/LIMP-2-deficient cells (Figure 4-18 B). Two clones for each cell line were chosen for the subsequent analysis: Clone 4 and 5 for the HeLa LIMP-2 KO cell lines and clone 2 and 4 for HeLa NPC1/LIMP-2 KO cell lines.

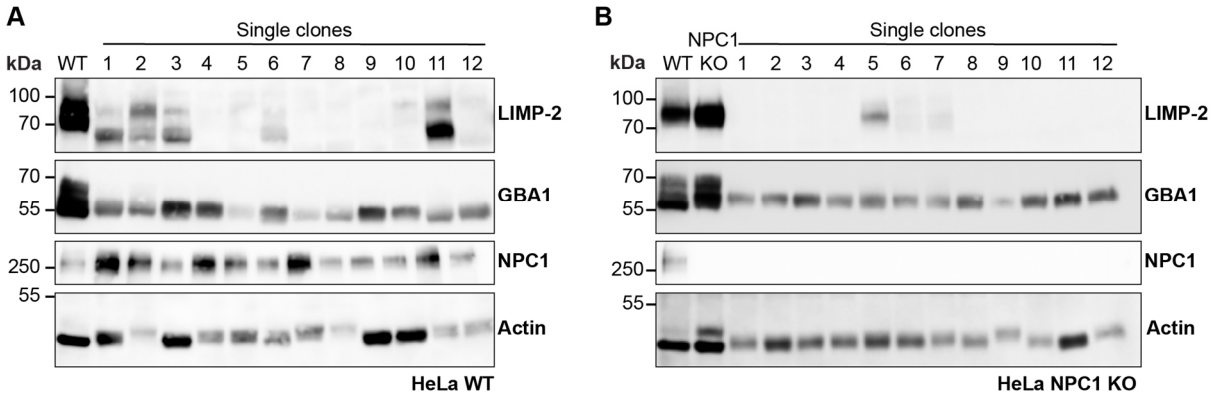

Figure 4-18: Generation of HeLa LIMP-2 KO and HeLa NPC1/LIMP-2 KO cells. A Western blot analysis of single clones with a successful deletion of LIMP-2 in HeLa WT cells. **B** Western blot analysis of single clones with a successful deletion of LIMP-2 in HeLa NPC1 KO cells.

4.3.2. Evaluation of cholesterol storage in HeLa LIMP-2 and NPC1/LIMP-2 KO cells

In order to investigate if the newly generated HeLa LIMP-2 KO cells are prone to cholesterol accumulation after LDL overload, as was the case with the LIMP-2 KO MEFs (Figure 4-6), HeLa WT cells as well as LIMP-2 KO clones 4 and 5 were starved overnight as previously described and subsequently challenged with 50 µg/ml LDL for 6 hours. Cells were fixed and stained with filipin to visualize free cholesterol and with anti-LAMP2 antibody to assess lysosomal morphology and distribution. As depicted in Figure 4-19 A, the shape of the lysosomes appears to be similar between WT and LIMP-2 KO cells and lysosomes are similarly dispersed throughout the cell in all three cell lines. The filipin staining reveals a stronger accumulation of lysosomal cholesterol in both LIMP-2 KO lines as compared to the control cells, which is also evident from the quantification depicted in Figure 4-19 B.

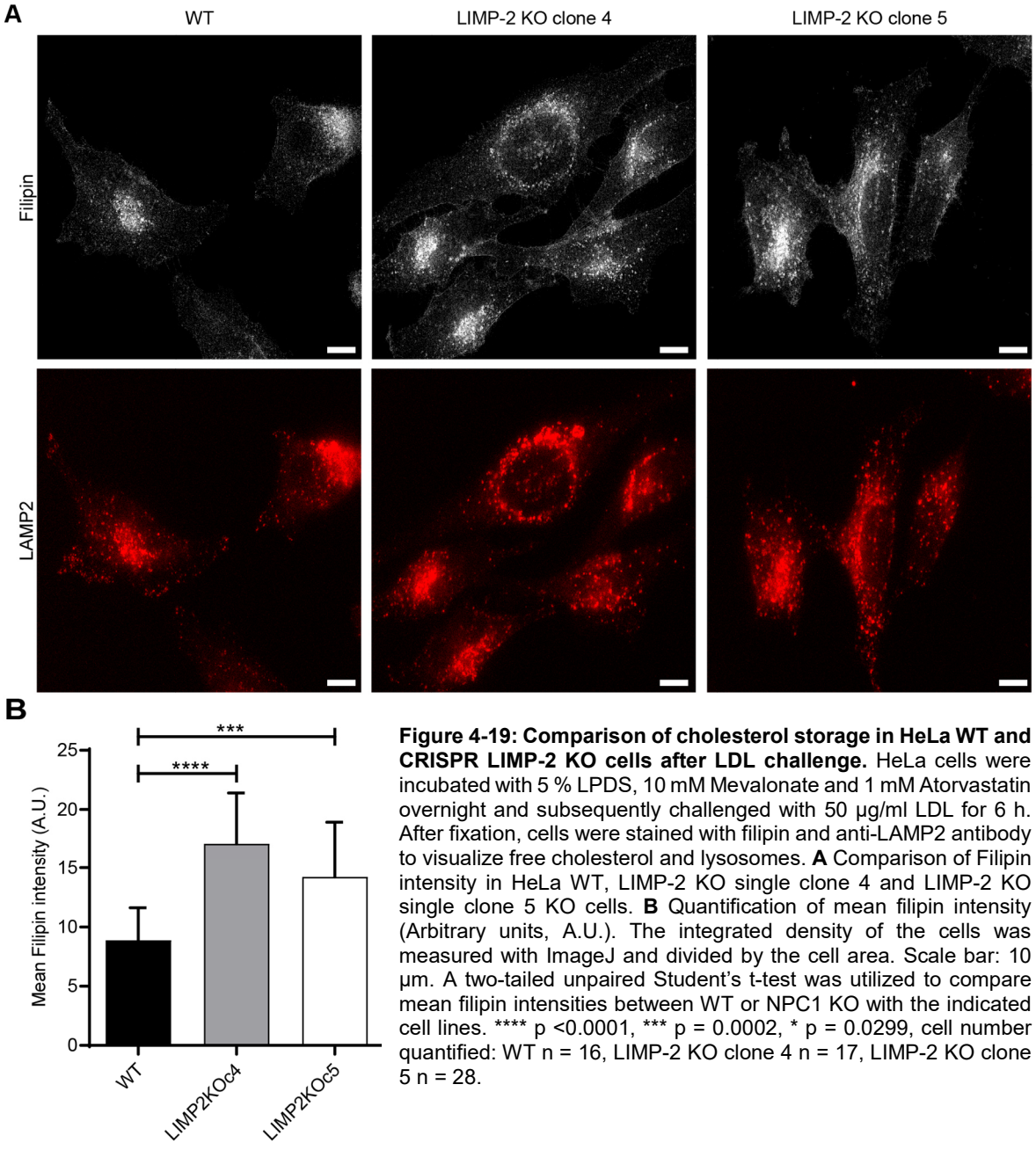

Figure 4-19: Comparison of cholesterol storage in HeLa WT and CRISPR LIMP-2 KO cells after LDL challenge. HeLa cells were incubated with 5 % LPDS, 10 mM Mevalonate and 1 mM Atorvastatin overnight and subsequently challenged with 50 µg/ml LDL for 6 h. After fixation, cells were stained with filipin and anti-LAMP2 antibody to visualize free cholesterol and lysosomes. **A** Comparison of Filipin intensity in HeLa WT, LIMP-2 KO single clone 4 and LIMP-2 KO single clone 5 KO cells. **B** Quantification of mean filipin intensity (Arbitrary units, A.U.). The integrated density of the cells was measured with ImageJ and divided by the cell area. Scale bar: 10 µm. A two-tailed unpaired Student's t-test was utilized to compare mean filipin intensities between WT or NPC1 KO with the indicated cell lines. **** p <0.0001, *** p = 0.0002, * p = 0.0299, cell number quantified: WT n = 16, LIMP-2 KO clone 4 n = 17, LIMP-2 KO clone 5 n = 28.

The same experimental procedure was carried out using HeLa NPC1 KO cells and the newly generated HeLa NPC1/LIMP-2 KO cell lines (clones 2 and 4) analyzing whether the double deficiency has any additives effects on cholesterol accumulation after LDL challenge as implied by the SREBP2 assays using HeLa NPC1 KO cells treated with siRNA silencing LIMP-2 (Figure 4-14). Indeed, both the LAMP2 and filipin staining in double KO cells were increased (Figure 4-20 A). While it cannot be excluded that there is an increase in lysosome number, the size of lysosomes seems to be enlarged in comparison to NPC1 KO cells (which already have enlarged lysosomes in relation to WT cells), likely to due to the massive cholesterol accumulation. However, the filipin staining intensity related to cells area was quite variable in

this experimental set up, both in NPC1 KO as well as in double KO cells, as depicted in Figure 4-20 B.

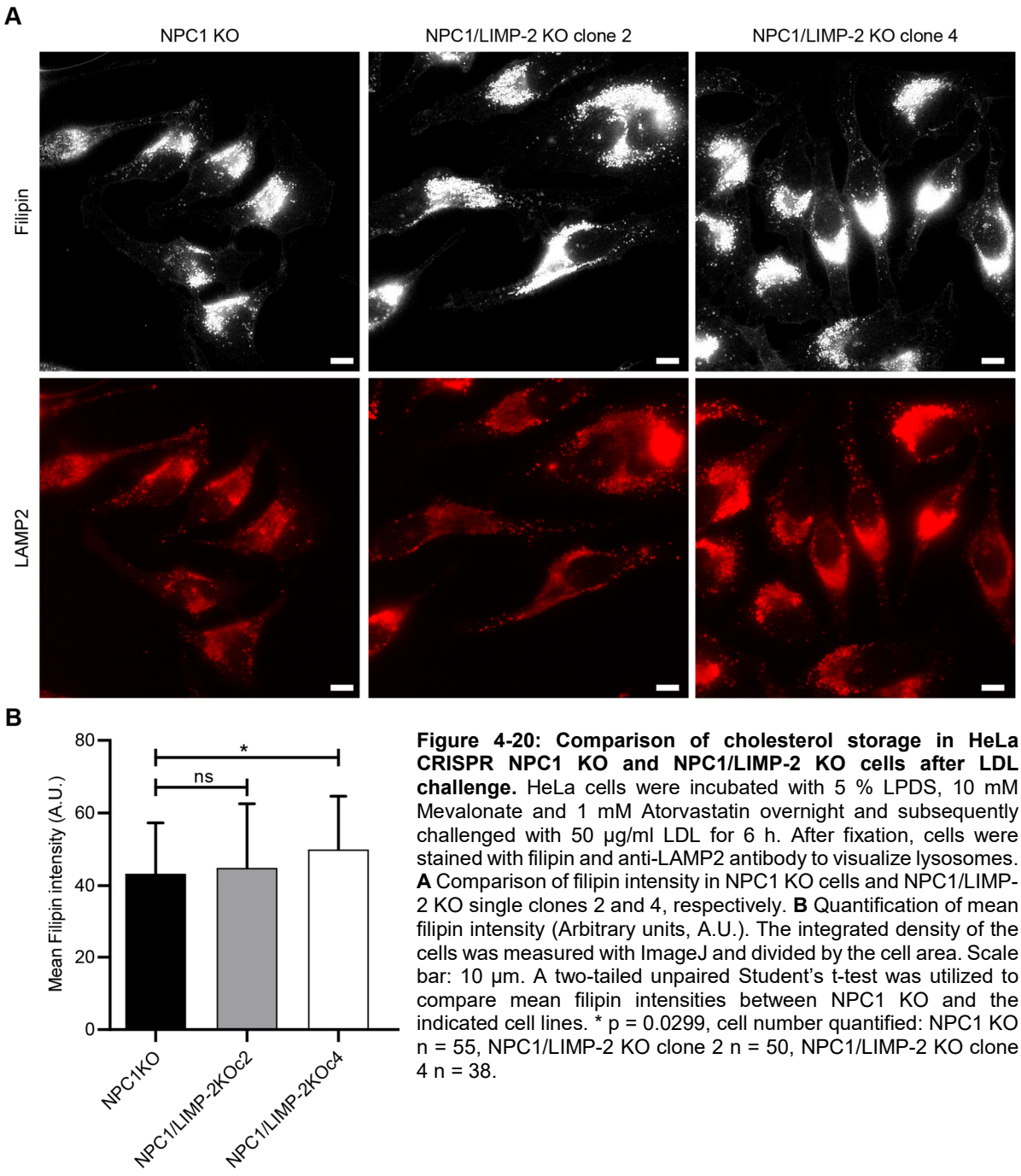

Figure 4-20: Comparison of cholesterol storage in HeLa CRISPR NPC1 KO and NPC1/LIMP-2 KO cells after LDL challenge. HeLa cells were incubated with 5 % LPDS, 10 mM Mevalonate and 1 mM Atorvastatin overnight and subsequently challenged with 50 µg/ml LDL for 6 h. After fixation, cells were stained with filipin and anti-LAMP2 antibody to visualize lysosomes. **A** Comparison of filipin intensity in NPC1 KO cells and NPC1/LIMP-2 KO single clones 2 and 4, respectively. **B** Quantification of mean filipin intensity (Arbitrary units, A.U.). The integrated density of the cells was measured with ImageJ and divided by the cell area. Scale bar: 10 µm. A two-tailed unpaired Student's t-test was utilized to compare mean filipin intensities between NPC1 KO and the indicated cell lines. * p = 0.0299, cell number quantified: NPC1 KO n = 55, NPC1/LIMP-2 KO clone 2 n = 50, NPC1/LIMP-2 KO clone 4 n = 38.

The properties of HeLa cells, namely their tendency to grow quickly and in a flat, spread-out shape and the fact that they are readily transfectable makes it possible to employ them in multifarious experimental settings. The LIMP-2- and NPC1/LIMP-2-double deficient cell lines of this cell type are a useful tool to study not only the consequences of the loss of these proteins, but also enable the characterization of mutated versions of these proteins by re-

introducing WT and mutated cDNAs into these cells and comparing the effects they have on e.g. susceptibility to cholesterol storage. Furthermore, they serve as important negative controls as e.g. depicted in Figure 4-16 B. The HeLa WT and LIMP-2 KO cells are the main cell lines used in the following chapters investigating LIMP-2's role at ER-contact sites (4.4) and palmitoylation of LIMP-2 (4.5).

4.4. LIMP-2 and ER contact sites

Once lipids such as free cholesterol have reached the outer leaflet of the limiting membrane of lysosomes by transport through LIMP-2 or NPC1, respectively, they need to be distributed to other membranes and compartments within the cells, like the ER or the plasma membrane (Neufeld *et al.* 1996, Underwood *et al.* 1998). Over recent years the notion emerged that membrane contact sites (MCSs) between membrane of different organelles play a major role in exchanging lipids and other nutrients. Especially the ER forms contacts with almost all other organelles (Vance 1990, Helle *et al.* 2013, Eisenberg-Bord *et al.* 2016, Huang *et al.* 2020). The nature of these contacts appears transient and dynamic, allowing the cell to react and adapt to any changes in nutrient homeostasis, although some proteins also seem to form stable membrane contact sites (Helle *et al.* 2013). Given LIMP-2's function in transport of lipids to the lysosomal limiting membrane one is prompted to speculate that LIMP-2 is involved in the formation of such contact sites, either passively by being present or by actively being involved in the formation of contact sites through interaction with ER-resident proteins.

4.4.1. LIMP-2 localizes to ER-lysosome membrane contact sites

In order to clarify whether LIMP-2 plays a role at MCSs, immunoelectron microscopy (IEM) was conducted in LIMP-2 KO MEFs that had been transfected with myc- tagged LIMP-2 and endogenous ER marker proteins carrying the amino acid sequence KDEL were labelled with antibodies containing gold particles (PAG) in two different sizes, respectively therefore enabling the analysis of the distribution of these proteins electron-microscopically (Figure 4-21).

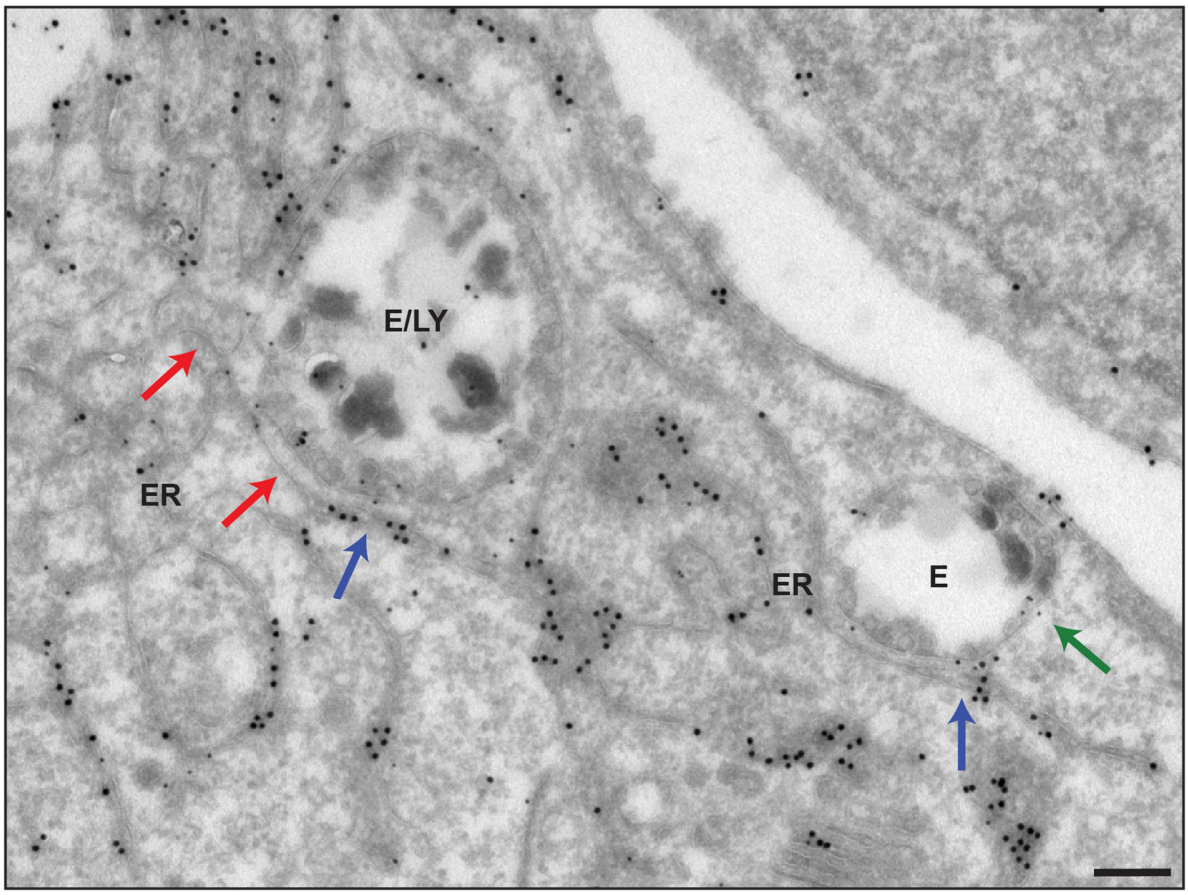

Figure 4-21: Immunoelectron microscopy (IEM) images of LIMP-2 KO MEF cells transfected with either mLIMP-2.myc and labelled with Protein A Gold (PAG) 10 after fixation. KDEL-containing ER proteins were labelled with PAG 15. Both sizes of gold particles were observed in close proximity in areas where late endosomes/lysosomes and part of the ER came in contact (blue arrows), indicating that LIMP-2 is present at ER contact sites. However, LIMP-2 is not exclusively found at ER/endosome contact sites (green arrow). Of note, the ER appears to be more narrow in some areas of contact with endosomes/lysosomes and devoid of KDEL-containing proteins (red arrows). Scale bar: 200 nm. Images acquired in the framework of a collaboration by Judith Klumperman, University Medical Center (UMC) Utrecht, the Netherlands.

As depicted in Figure 4-21, in some areas of close contact between membranes of ER and endosomes/lysosomes the ER tubules appeared more narrow than in other areas. Interestingly, the narrowed ER stretches were devoid of KDEL-containing proteins (red arrows). The blue arrows highlight membrane contact sites where small and large gold particles could be detected, indicating the presence of LIMP-2 and KDEL-containing proteins at these contact sites. The staining of LIMP-2 in other areas of lysosomes (green arrow) also confirmed that the protein had been properly delivered to lysosomes and was not retained in the ER (which would also have caused a co-localization with KDEL-containing proteins).

While this experiment indicates a possible role for LIMP-2 at ER-endosome/lysosome contact sites, it does not offer insight to the question if LIMP-2 is actively involved in the formation of these contact sites by interacting with ER-resident proteins.

4.4.2. LIMP-2 interacts with proteins involved in ER-lysosome MCS formation

A mass spectrometry screen (BioID) utilizing a proximity-based biotin ligase and the C-terminal cytosolic domain of LIMP-2 as bait to identify potential interaction partners of LIMP-2 yielded several hits, among them ER proteins known to play a vital role in the establishment of contact sites between the ER and other organelles (Table 4-3, highlighted in green).

Table 4-3: Selected hits from proximity-dependent biotin identification (BioID) screen. Hits are shown in alphabetical order. Proteins known to form ER contacts sites are highlighted in green. The screen was performed by Prof. Dante Neculai, Hangzhou, China.

Gene	Full Name
AP1B1	Adaptor-related protein complex 1, beta 1 subunit
AP3B1	Adaptor-related protein complex 3, beta 1 subunit
BLOC1S1	Biogenesis of lysosomal organelles complex-1, subunit 1
CLCN7	Chloride channel 7
ESYT1	**Extended synaptotagmin-1**
KIF1A	Kinesin family member 1A
LAMTOR1	Ragulator complex protein LAMTOR1
MFSD8	Major facilitator superfamily domain containing 8
OSBPL11	**Oxysterol binding protein-like 11, also known as ORP11**
OSBPL9	**Oxysterol binding protein-like 9, also known as ORP9**
RAB7A	RAB7A, member RAS oncogene family
RAB9A	RAB9A, member RAS oncogene family
SOAT1	Sterol O-acyltransferase 1
STARD3	**StAR-related lipid transfer (START) domain containing 3**
STX8	Syntaxin 8
VAMP3	vesicle-associated membrane protein 3 (cellubrevin)
VAMP7	Vesicle-associated membrane protein 7
VAMP8	Vesicle-associated membrane protein 8 (endobrevin)
VAPB	**VAMP (vesicle-associated membrane protein)-associated protein B**
DHHC20	Palmitoyltransferase 20

Of note, the enzyme responsible for esterification of free cholesterol in the ER, sterol O-acyltransferase, SOAT1, also known as acyl-coenzyme A:cholesterol acyltransferase-1, ACAT1, was among the proteins identified to be in close proximity to LIMP-2.

While the BioID screen provided some first hints as to which proteins could potentially interact with LIMP-2 due to their close proximity to its the cytosolic tail, each hit needs to be validated

in a separate experiment. Co-immunoprecipitation studies were carried out with the most promising and interesting candidates from the screen. STARD3 is a membrane protein of the endolysosomal system and it is known to transfer cholesterol from as well as to the ER via its large C-terminal hydrophobic pocket, called START domain and its interaction with ER-contact site protein VAPB (Alpy *et al.* 2013, Wilhelm *et al.* 2017). Therefore, it could be imagined that cholesterol released from LIMP-2 is shuffled to STARD3 which in turn mediates the transfer of the lipid to the ER, meaning that LIMP-2 would not actively be involved in the formation of membrane contact sites, but be present there nonetheless.

On the other hand, a direct interaction of LIMP-2 and VAPB could also be envisaged. VAPB interacts with a number of proteins in different organelles to mediate MCS formation (Lev *et al.* 2008, Peretti *et al.* 2008, Alpy *et al.* 2013, Murphy and Levine 2016, Phillips and Voeltz 2016). While most of the so far identified VAPB interactors harbor a distinct FFAT (two phenylalanines in an acidic tract)-like motif, some interaction partners use other binding sites as well (Murphy and Levine 2016). The closely related protein VAPA was also thought to be a potential interactor for LIMP-2 despite its absence from the BioID screen since it also mediates the formation of inter-organelle contact sites (Mesmin *et al.* 2013). Another promising candidate is ESYT1, which has been implicated in sterol transfer from the plasma membrane to the ER involving the sterol transporter and scavenger receptor family member SR-BI (unpublished observations Prof. Dr. D. Neculai).

Recently, the protein ASTERB or Gramd1b was described as an important player in sterol transfer at ER-LY MCS (Sandhu *et al.* 2018) and e.g. shown to form MCS with NPC1 (Hoglinger *et al.* 2019). Therefore, it was included in the analysis as well.

HeLa WT cells were transfected with the respective putative interaction partner and endogenous LIMP-2 was precipitated using an anti-LIMP-2 antibody. Upon interaction, the partner proteins could be detected in the IP fractions. For ESYT1 and LIMP-2 no interaction could be detected (data not shown). However, both STARD3-HA and VAPB-Flag as well as VAPA-GFP and Gramd1b-GFP could be co-immunoprecipitated, suggesting physical interaction with LIMP-2 (Figure 4-22). Cells transfected with GFP were used as a negative control.

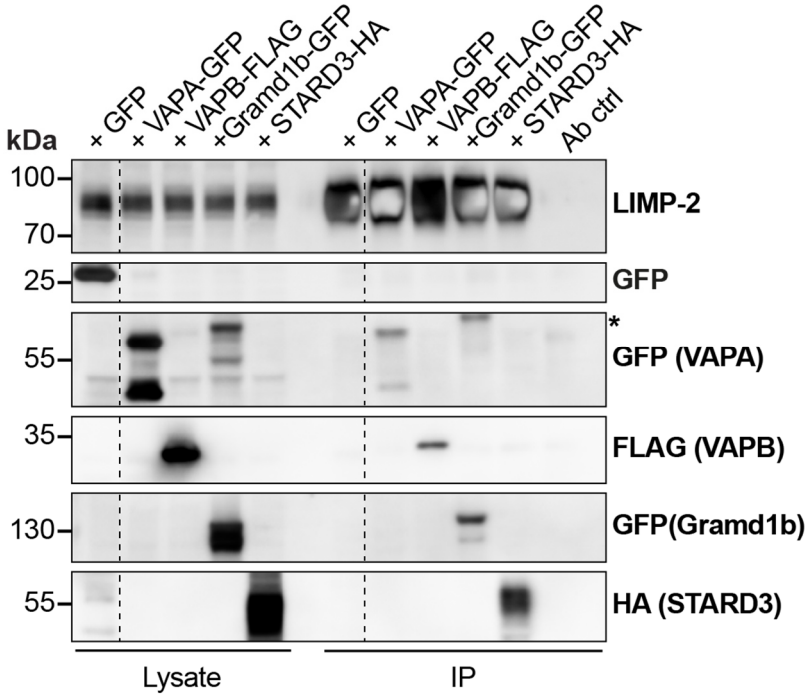

Figure 4-22: Co-immunoprecipitation studies following up selected hits from a proximity-dependent biotin identification (BioID) screen and other putative LIMP-2 interactors. HeLa WT cells were transfected with the respective potential interaction partners and LIMP-2 was precipitated using an antibody directed against the C-terminus of LIMP-2. 30 µg of lysate and 20 µl of IP fractions were separated via SDS-PAGE and analyzed by Western blotting. The LIMP-2 signals in the IP lanes are more intense in comparison to the other signals on the blot that they are overexposed in these settings and appear washed out. Asterisks denote remaining signal from probing the membrane with a different antibody previously as well as unspecific signal, likely representing the light chain of the IP antibody, respectively. Dashed lines indicated that the image was sliced at this position, but all samples shown belong to the same blot.

4.4.3. Lipid homeostasis may influence LIMP-2's function at membrane contact sites

Since membrane contact sites between different organelles are often transient and exert a regulatory function in nutrient distribution throughout the cell, interaction of contact site-located proteins such as e.g. LIMP-2 and VAPB might be fluctuating accordingly. Based on LIMP-2's role in delivering cholesterol to the lysosomal membrane, the influence of sterol depletion on the interaction of LIMP-2 with the proteins depicted in Figure 4-22 was investigated.

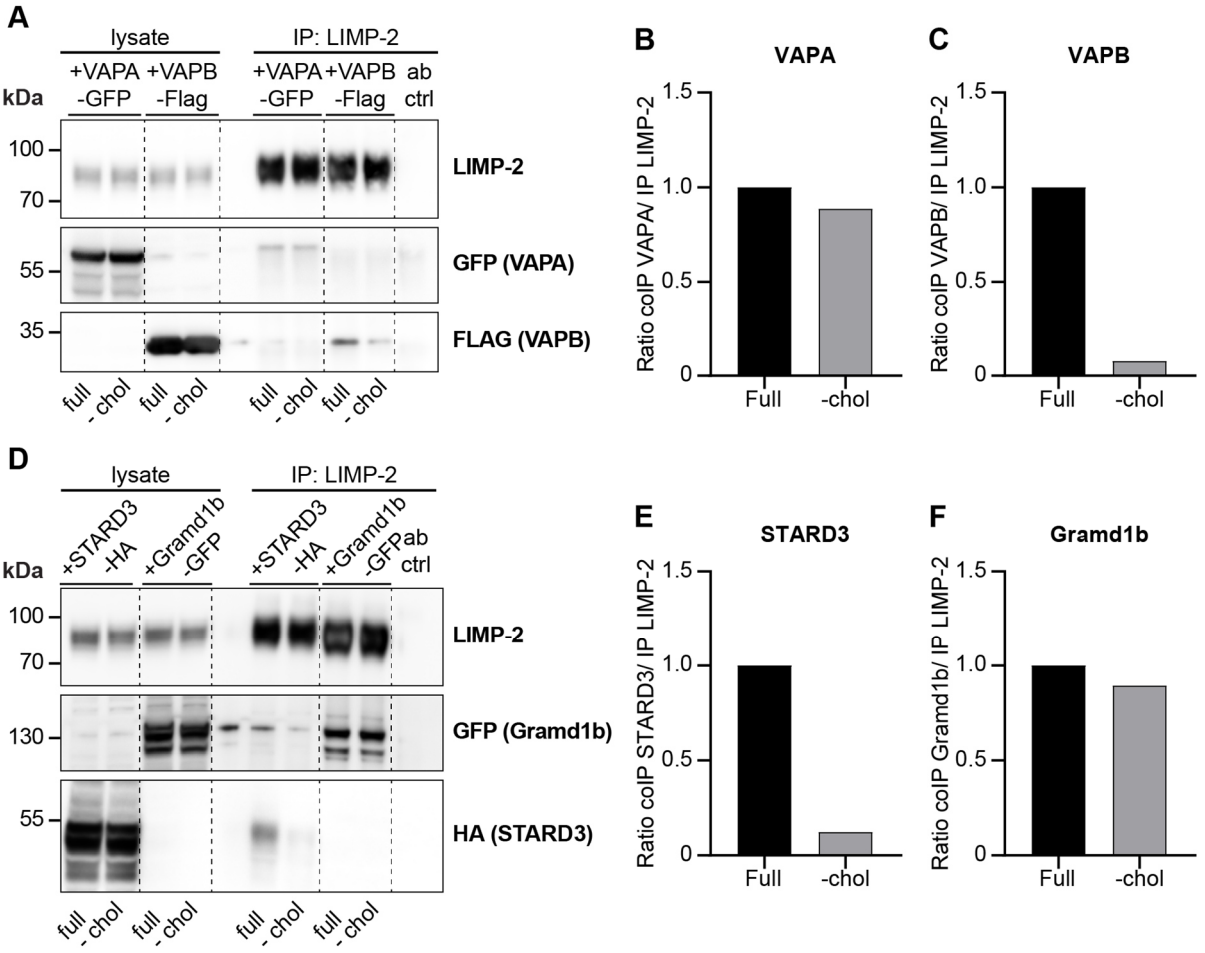

Figure 4-23: Influence of lipoprotein depletion on the interaction of LIMP-2 with ER contact site proteins. A (Co)-immunoprecipitation experiment using lysates from HeLa WT cells previously transfected with VAPA-GFP or VAPB-Flag, respectively, and kept in DMEM + 10 % FCS (Full) or DMEM + 5 % LPDS + 1 µM Atorvastatin and 10 µM Mevalonate (-chol). Endogenous LIMP-2 was precipitated with an antibody directed against LIMP-2's C-terminus. Dashed lines indicated that the image was sliced at this position, but all samples shown belong to the same blot. **B, C** Quantifications indicate the amount of co-precipitation of VAPA and VAPB, respectively, divided by the amount of precipitated LIMP-2 in each sample. The result obtained for interaction between VAPA and VAPB and LIMP-2 in full medium was set as baseline and compared to that obtained for interaction in cholesterol-depleted medium. **D** (Co)-immunoprecipitation experiment using lysates from HeLa WT cells previously transfected with STARD3-HA or Gramd1b-GFP, respectively, and kept in DMEM + 10 % FCS (Full) or DMEM + 5 % LPDS + 1 µM Atorvastatin and 10 µM Mevalonate (-chol). Endogenous LIMP-2 was precipitated with an antibody directed against LIMP-2's C-terminus. Dashed lines indicated that the image was sliced at this position, but all samples shown belong to the same blot. **E, F** Quantifications indicate the amount of co-precipitation of STARD3 and Gramd1b, respectively, divided by the amount of precipitated LIMP-2 in each sample. The result obtained for interaction between STARD3 and Gramd1b and LIMP-2 in full medium was set as baseline and compared to that obtained for interaction in cholesterol-depleted medium.

While sterol depletion does not seem to influence the interaction between LIMP-2 and VAPA, the co-IP of VAPB with LIMP-2 under sterol depletion was markedly decreased to about 8 % to that observed in full media, even though the same amount of LIMP-2 was precipitated (Figure 4-23 A-C). The same observation was made for the co-IP of STARD3 with LIMP-2 under sterol depletion (12 % in comparison to full media) while the co-IP of Gramd1b with LIMP-2 was only slightly decreased under these conditions (Figure 4-23 D-F).

Taken together, these experiments suggest a role for LIMP-2 at membrane contact sites between the ER and endosomes/lysosomes. Not only can LIMP-2 be found at these contacts, but it was also demonstrated to interact with various ER proteins like VAPA, VAPB and Gramd1b as well as with other proteins involved in mediating transport of molecules across membrane contact sites such as STARD3. Interestingly, some of these interactions appear to be regulated by the lipid status of the cell, as depletion of lipoproteins diminished the interaction of LIMP-2 with VAPB and STARD3. A similar dependence on lipid supply has been observed for the interaction of Gramd1b with NPC1 (Hoglinger *et al.* 2019). The interaction between LIMP-2 and Gramd1b, on the other hand, was not decreased in response to LPDS treatment-contrarily, it appeared to be slightly increased.

While several proteins have been implicated in playing a vital part in the establishment of ER-lysosome contact sites and some may be redundant, it is feasible to assume that the deletion of LIMP-2 in cells might lead to a decrease in the number or speed of contact site formation between ER and lysosome as has been observed for other contact site pairs (Hoglinger *et al.* 2019). Hence, WT and LIMP-2 KO MEF cells were subjected to indirect immunofluorescence staining and microscopic analysis with the aim to quantify the number of ER-lysosome contact sites in each cell line. For this purpose, the ER was visualized with anti-KDEL antibody, which targets the KDEL-motif in ER-resident proteins, and lysosomes were visualized with anti-LAMP1 staining. Representative images of WT and LIMP-2 KO MEFs are depicted in Figure 4-24 A and B, respectively. While the ER tubules and LAMP-1-positive lysosomes appear to be in close proximity, only very few areas of co-localization between the two organelles, as indicated by orange color in the pictures and highlighted by white arrowheads, were observed in these samples. Because of the small number and lack of unequivocal identification of MCS it was not possible to determine whether the number of ER-lysosome contact sites in WT and LIMP-2-deficient cells are different in this experimental setting.

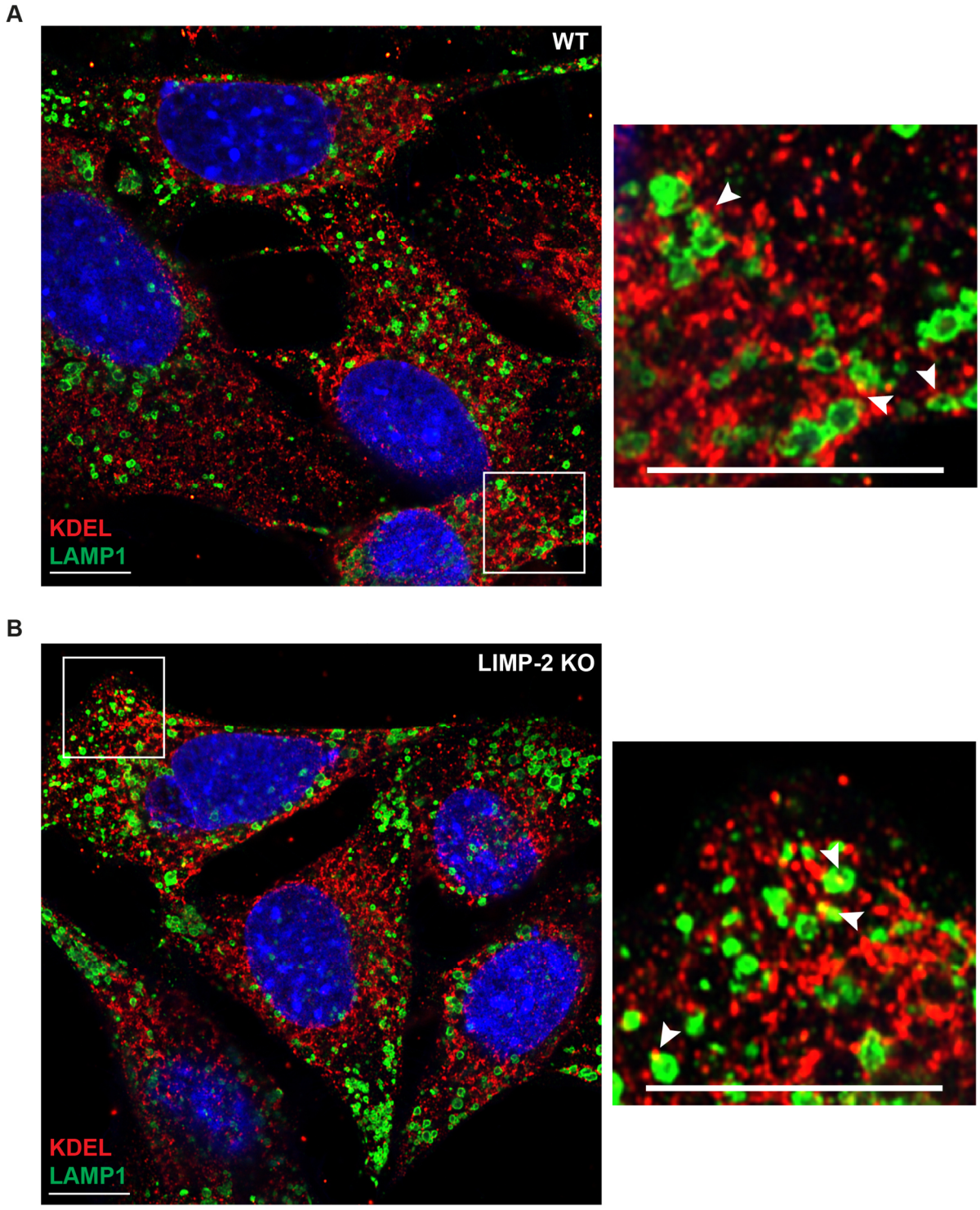

Figure 4-24: Observation of potential ER-lysosome contact sites in MEF cells. WT **(A)** and LIMP-2-deficient MEF cells **(B)** were grown in DMEM supplemented with 10 % FCS and 1 % antibiotics**.** After 48 h, cells were fixed with 4 % PFA and stained with anti-KDEL+ Alexafluor anti-mouse 594nm as well as anti-LAMP1 + Alexafluor anti-rat 488 nm antibodies to visualize ER tubules and lysosomes, respectively**.** Scale bars 10 µm. White arrowheads highlight potential ER-lysosome contact sites. Images were acquired with a Zeiss 880 microscope and processed with Airyscan using the ZEN blue software (Zeiss).

Overall, there are some indications that LIMP-2 exerts functions that are not solely restricted to lysosomes, but might involve other organelles as well. While in previous studies the interaction of LIMP-2's luminal domain with other lysosomal proteins was in the focus (Rothaug *et al.* 2014, Zunke *et al.* 2016), the identification of several new potential LIMP-2-interactors at the ER-lysosome interface suggests an important role for the transmembrane regions and especially for the cytosolic N- and C-terminal regions of LIMP-2. Although the precise nature and function of these interactions remain yet to be elucidated, the observation that the availability of lipids appears to modulate some of these interactions (Figure 4-23) is intriguing, especially considering LIMP-2's role in lysosomal cholesterol export.

4.5. Palmitoylation of LIMP-2

In addition to their complex secondary and tertiary structure, proteins can be modified during translation or post-translationally to regulate their potentially diverse functions, e.g. by lipidation of one or several amino acids. S-palmitoylation is one of the most common type of lipidations (Resh 2016, Lanyon-Hogg *et al.* 2017) and it targets cysteine residues that are present in the cytoplasmic or adjacent transmembrane regions of a protein. Advances in proteomic analyses have made it possible to conduct whole-cells screenings for these modifications and revealed that at least 10 % of the human proteome is being modified by S-palmitoylation (Sanders *et al.* 2015).

4.5.1. Prediction and experimental confirmation of LIMP-2's palmitoylation

Both human as well as rat and murine LIMP-2 (https://swisspalm.org/proteins/O35114, https://swisspalm.org/proteins/P27615, https://swisspalm.org/proteins/Q14108) were identified as a potentially palmitoylated proteins in several palmitoyl-proteomics studies as summarized in the palmitoylation database SwissPalm (Blanc *et al.* 2015). LIMP-2 harbors two cysteine residues in its N-terminal and one cysteine residue in its C-terminal domain, respectively. All three cysteines were predicted to be subject to palmitoylation (Figure 4-25 A). While being located in different parts of the cell, CD36 scavenger receptor family members CD36 and SR-BI share the same topology and 33 % (with CD36) or 34 % (with SR-BI) amino acid identity as well as 54 % (CD36) and 56 % (SR-BI) amino acid similarity (Neculai *et al.* 2013). Both proteins also harbor cysteines in their cytoplasmic N- and C-terminal regions. In fact, for CD36 palmitoylation at residues 3, 7, 464 and 468, respectively, has been demonstrated (Jochen and Hays 1993, Tao *et al.* 1996), whereas palmitoylation of SR-BI has not been experimentally validated yet. However, it was identified as a potentially palmitoylated protein in 9 out of 17 palmitoyl-proteomic studies and predicted to be modified at amino acid residue three according to SwissPalm (https://www.swisspalm.org/proteins/Q8WTV0). Figure 4-25 B depicts a sequence alignment of the N- and C-terminal regions of SR-BI, CD36 and SCARB2, highlighting experimentally confirmed (green) and predicted (blue) palmitoylation sites.

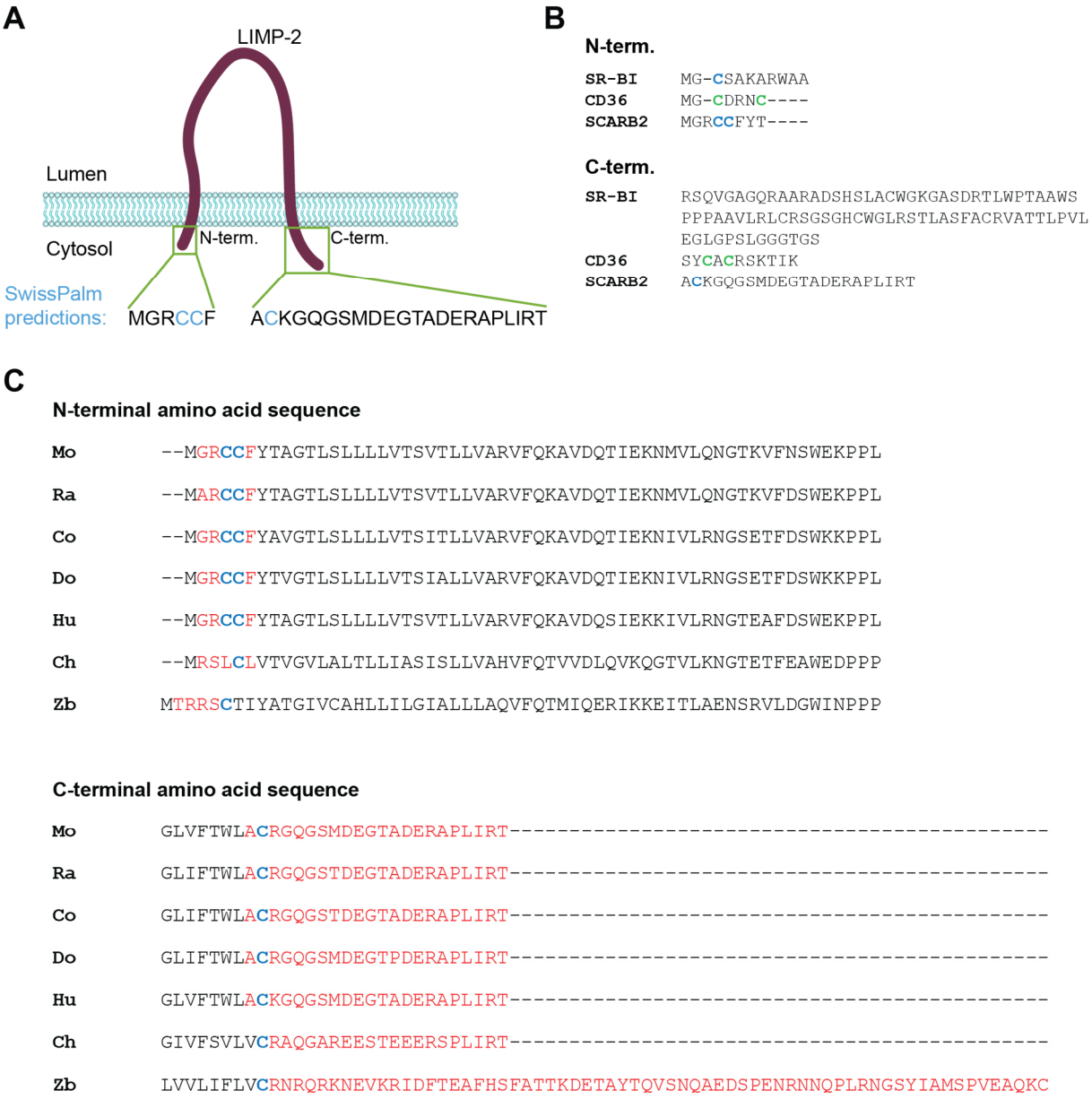

Figure 4-25: Prediction of palmitoylation sites in SCARB2/LIMP-2 and sequence comparison with family members and homologs. A Diagram of the LIMP-2 structure and its orientation in the membrane. The full amino acid sequence for the amino (N)- and carboxy (C)-terminal regions are shown with the putative palmitoylation sites highlighted in blue. **B** Sequence alignment of N- and C-terminal termini acids from SR-BI, CD36 and SCARB2, respectively, based on Uniprot entries O35114 (SCRB2_MOUSE), P27615 (SCRB2_RAT), A0A3S5ZPN6_BOVIN, F1PGJ5_CANLF, Q14108 (SCRB2_HUMAN), E1BRR6_CHICK, Q8JGR8_DANRE. Cysteines predicted to be palmitoylated are highlighted in blue. Experimentally validated palmitoylation sites are highlighted in green. **C** SCARB2 N- and C-terminal amino acid sequence alignments for mouse (Mo), rat (Ra), cow (Co), dog (Do), human (Hu), chicken (Ch) and zebrafish (Zb), respectively, based on Uniprot entries listed in the appendix. Amino acids included in cytosolic C- and N-terminus are highlighted in red, cysteines present in cytoplasmic sections of SCARB2 are highlighted in blue.

While the amino acids of the amino- and carboxy-terminal regions of LIMP-2 are not completely conserved between different vertebrate species, many members do share a high similarity and contain at least one cysteine in the N-terminus and C-terminus, respectively (Figure 4-25 C), indicating that these residues could play an important role. Furthermore, LIMP-2 is located, even though not exclusively, in detergent-resistant membranes (data not shown), which is a typical feature for many palmitoylated proteins (Melkonian *et al.* 1999, Chakrabandhu *et al.*

2007, Levental *et al.* 2010, Xiong *et al.* 2019). A standard assay to confirm/disprove the palmitoylation of proteins is the acyl-resin capture (acyl-RAC) assay, which is based on conjugating palmitoylated proteins to thiopyridinyl groups containing resin that is reactive towards thiol groups (Forrester *et al.* 2011). In this work, a slightly modified version was used as indicated in the material and methods section (3.4.17). Palmitoylation of murine and human LIMP-2 was investigated using mouse embryonic fibroblast (MEF) as well as HeLa cell lysates (Figure 4-26).

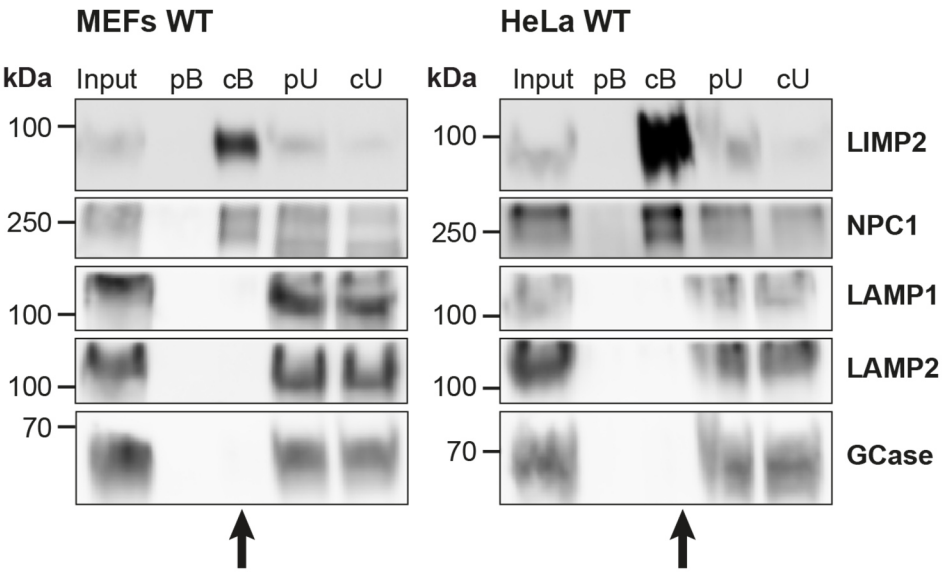

Figure 4-26: Acyl-RAC assay confirms palmitoylation of LIMP-2 in mouse embryonic fibroblast (MEF) and HeLa cell lysates. Lysates were prepared as described in 3.4.17and following hydroxylamine or PBS addition, thiopropyl-sepharose beads were added to the samples. Only proteins with an attached palmitoyl-moiety should be susceptible to hydroxylamine cleavage and subsequently be able to bind to the beads. After elution from the beads, palmitoylated proteins were recovered in a separate fraction (cleaved bound, cB, highlighted with black arrows) from the non-palmitoylated proteins that did not bind to the beads (cU, cleaved unbound). Two negative controls lacking hydroxylamine treatment are included in this experiment: 'preserved unbound' (pU) and 'preserved bound' (pB), the latter of which indicates non-specific binding of proteins to the beads.

Proteins containing palmitoylated cysteine residues are pulled down by binding to thiopropyl-sepharose beads and therefore recovered in the cleaved bound fraction (cB), while non-palmitoylated fractions do not bind the beads and can therefore be found in the cleaved supernatant fraction (cU). This was the case for proteins like LAMP1 and LAMP2 which were predicted to not be palmitoylated whereas NPC1 was identified as a potentially palmitoylated protein in several palmitoyl- proteomic screens according to the SwissPalm data bank (https://www.swisspalm.org/proteins/O15118) and could indeed be recovered in the cleaved bound fraction (Figure 4-26). Likewise, an enrichment of LIMP-2 in the fraction bound to the beads was observed, establishing its palmitoylation (Figure 4-26).

Experiments using HeLa LIMP-2 KO cells that were transiently transfected with LIMP-2.WT and treated with DMSO or the palmitate analog 2-bromopalmitate (2BP), respectively, provided additional evidence for a palmitoylation of LIMP-2 (published in the framework of a Master's

thesis: (Haugwitz 2019)). 2BP permanently binds to the catalytic center of palmitoyltransferases (zDHHCs/PATs) and is therefore prevents activity of all zDHHCs (Webb *et al.* 2000, Jennings *et al.* 2009). When lysates of 2BP-treated cells expressing LIMP-2.WT were fractionated in the Acyl-RAC assay, LIMP-2 was not recovered in the cleaved bound fraction, in contrast to the sample treated with DMSO (Haugwitz 2019).

4.5.2. The more the merrier? Establishing the number of LIMP-2 palmitoylation sites

So far, it could not be elucidated which criteria make a cytoplasmic (and juxtaposed transmembrane) cysteine residue eligible for palmitoylation since no consensus sequence for recognition by palmitoyltransferases (DHHCs) has been identified yet (Lemonidis *et al.* 2014, Blanc *et al.* 2015, Zaballa and van der Goot 2018). While LIMP-2's cytoplasmic regions contain three cysteines using the Acyl-RAC assay it cannot be specified which of them are modified by addition of palmitate. However, a modification of this assay, called acyl-PEG exchange gel shift (APEGS), developed by Howie and colleagues and modified further adapted by other groups (Howie *et al.* 2014, Percher *et al.* 2016, Yokoi *et al.* 2016) makes use of maleimide-functionalized polyethylene glycol regents that allow for site-specific alkylation of cysteine residues, thereby inducing a mobility shift of palmitoylated proteins when separated by SDS-PAGE. Thus, different levels of palmitoylation of a protein can be determined. This is especially important due to the dynamic nature of this modification and could offer information on the most common palmitoylation state of the respective protein. Applying a variation of the APEGS assay published by the van der Goot lab (Abrami *et al.* 2017) to HeLa and HEK cell lysates and subsequent analysis of the samples by Western Blot revealed that at least one cytosolic cysteine residue of human LIMP-2 is constantly modified with palmitate as the incubation with 5k-mPEG resulted in two to three prominent bands migrating slower than the band observed in the non-PEGylated fractions and the disappearance of this signal in the PEG-treated fractions (Figure 4-27).

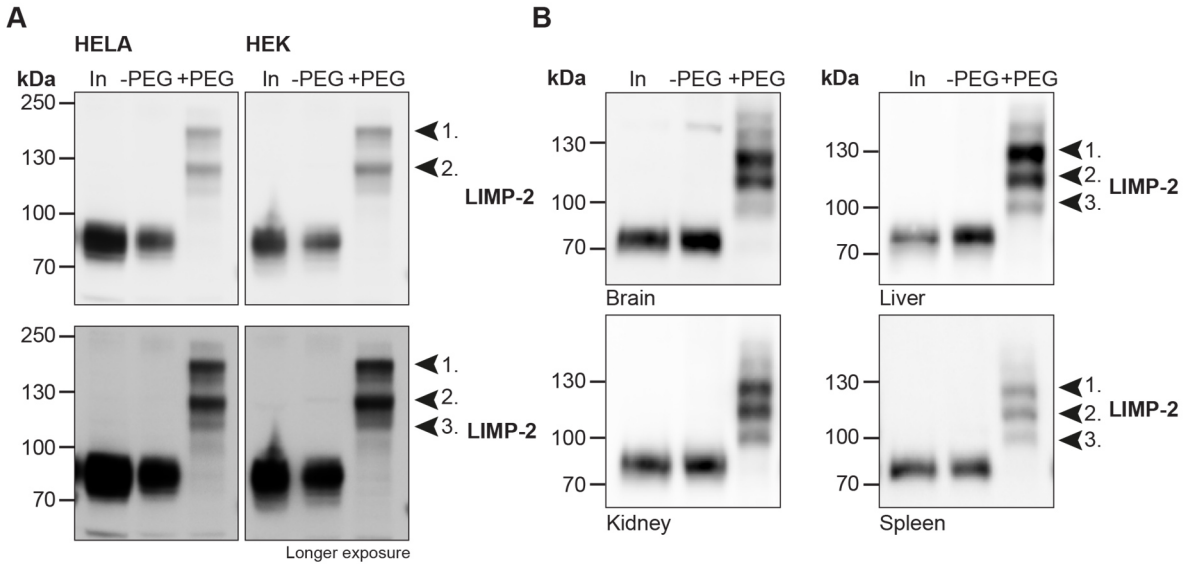

Figure 4-27: Acyl-PEG exchange gel shift (APEGS) assay reveals multiple palmitoylation sites in LIMP-2 in human cell lines as well as murine tissues. A Total cell lysates of HeLa and HEK cells, respectively, were subjected to APEGS assay as described in 3.4.18. Negative controls were incubated with NEM instead of 5k-mPEG. In, Input; -PEG, without addition of 5k-mPEG; +PEG, with addition of 5k-mPEG. Two to three different species of palmitoylated LIMP-2 were detected both in HeLa and HEK cells. **B** The same assay was conducted with murine brain, liver, kidney and spleen tissue after tissue homogenization and membrane fractionation as detailed in 3.4.2 and 3.4.3. Three distinct bands were observed in all investigated tissues, indicating the existence of three pools of palmitoylated LIMP-2.

The fragmentation of the LIMP-2 signal observed between 70 kDa and 100 kDa into two equally strong bands migrating slightly below and above 130 kDa, respectively, indicates that LIMP-2 exists in two major palmitoylation states. Since it harbors three putative palmitoylation sites, these two bands could correspond to single and double palmitoylation, single and triple palmitoylation or double and triple palmitoylation. Longer exposure of the blot manifested a third, albeit much weaker band (Figure 4-27 A), possibly representing single palmitoylation which in turn would indicate that the other two bands represent doubly and triply palmitoylated fractions of LIMP-2.

As demonstrated in Figure 4-26, mouse LIMP-2 is also subject to palmitoylation. To clarify whether the different species of palmitoylated LIMP-2 discovered by APEGS may vary in different tissues, total cell lysates from murine brain, liver, kidney and spleen tissue were subjected to membrane fractionation followed by APEGS assay and the samples analyzed by Western Blot (Figure 4-27 B). The overall palmitoylation pattern between the different tissues is similar with two prominent bands and a fainter third band below. While the two strongest bands are equally abundant in brain, kidney and spleen, in liver the signal of the third band is markedly stronger than that of the second band, possibly indicating that in this organ triple palmitoylation of LIMP-2 is favored.

In liver and brain, very faint bands at >130 kDa are additionally visible. Since LIMP-2 only harbors three cysteines in its cytosolic and adjacent transmembrane residues, it is not feasible to assume that these bands could represent additional palmitoylation sites. Rather they might reflect unspecific binding of PEG molecules which could stem from incomplete blockage of thiol groups or binding of PEG to non-palmitoylation-related thioester bonds (Zaballa and van der Goot 2018). It is also unclear why the overall migration pattern differs between the human cell lines analyzed in Figure 4-27 A and the murine tissues analyzed in Figure 4-27 B. The PEGylated LIMP-2 fractions in human cells appear to migrate more slowly than those in murine tissue and although the difference between the second and third band indicated in Figure 4-27 A should only be addition of one PEG molecule, the distance of these bands in relation to one another is much bigger than those observed in murine tissues. However, it has to be noted that these experiments and western blots were performed independently of each other and to fully assess differences in migration pattern these samples should be applied to the same SDS-PAGE gel.

Using site-directed mutagenesis, mutants of the three putative palmitoylation sites in LIMP-2's C- and N-terminus, respectively, were constructed. Cysteine residues at position 4, 5 and 458, respectively, were exchanged for serines and lysates of cells transfected with these mutated LIMP-2 constructs were subjected to the acyl-RAC assay, thus allowing further characterization of LIMP-2's palmitoylation.

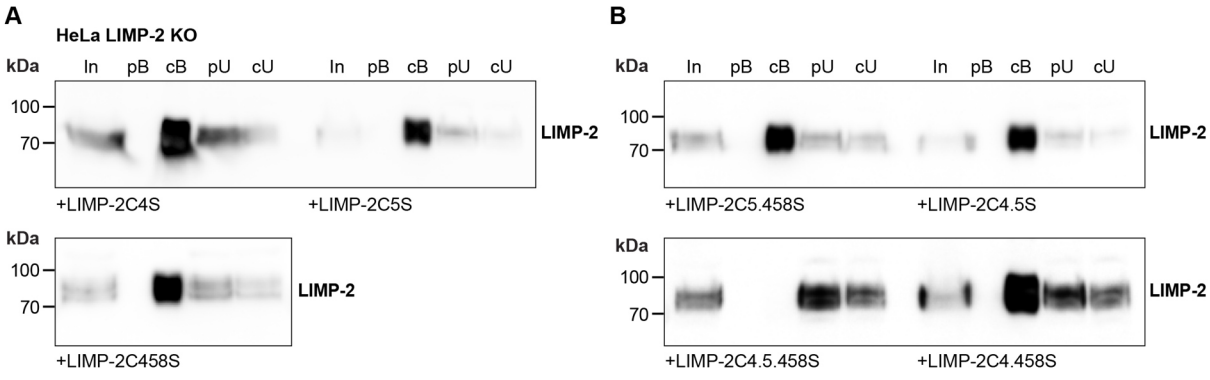

Figure 4-28: Determination of LIMP-2 palmitoylation sites using acyl-RAC assay. Single (**A**) as well as double and triple (**B**) mutants of the putative LIMP-2 palmitoylation sites were transfected in HeLa LIMP-2 KO cells and the lysates subjected analysis of the palmitoylation status using the acyl-RAC assay.

Replacing a single cysteine with serine did not abolish the palmitoylation as demonstrated in Figure 4-28 A and neither did the loss of two cysteines in the N-terminus or C- and N-terminus, respectively (Figure 4-28 B). Only the simultaneous lack of all three putatively palmitoylated cysteines (LIMP-2C4.5.458, henceforth LIMP-2-P3x) abolished palmitoylation of LIMP-2 as evidenced by absence of a signal in the cleaved bound fraction of the acyl-RAC assay. This

finding indicates that LIMP-2 is indeed subject to triple palmitoylation, or that the two neighboring cysteines C4 and C5 act as a dynamic switch in case one cysteine is lost. However, the data from the APEGS assay (Figure 4-27) favor the use of all three palmitoylation sites.

4.5.3. Physiological relevance of palmitoylation of LIMP-2

Based on these results, multiple palmitoylation appears to be an important feature of LIMP-2, however its physiological meaning remains to be elucidated. Experiments conducted in parallel to this study could show that absence of the palmitoylation did not alter the glycosylation pattern of LIMP-2, indicating that it is not retained in the ER due to misfolding, and palmitoylation-deficient LIMP-2 did still localize to lysosomes (Haugwitz 2019) (Master's thesis). However, in HeLa LIMP-2 KO cells transfected with LIMP-2-P3x drastically enlarged, swollen lysosomes were observed which were clustered around the nucleus or filling out the whole cell (Figure 4-29 A). While overexpression of LIMP-2.WT has also been associated with increased lysosomal size in certain cell types and conditions (Kuronita *et al.* 2002), in HeLa LIMP-2 KO cells the re-expression of LIMP-2.WT did not obviously change lysosome size, morphology and distribution to the same extent as the expression of LIMP-2.P3x did. Importantly, expressing the palmitoylation-deficient LIMP-2 mutant in HeLa WT cells had less pronounced effects on lysosomal morphology (Haugwitz 2019), arguing that endogenous (and palmitoylated) LIMP-2 present in HeLa WT cells can mitigate the disturbances caused by overexpression of LIMP-2.P3x. This points towards a vital role of palmitoylation of LIMP-2 for maintaining healthy lysosomes in HeLa cells. In the context of LIMP-2's potential role at ER contact sites, co-staining with KDEL-targeting antibodies was conducted in these cells to corroborate whether the loss of palmitoylation has an influence on the association of lysosomes with the ER (Figure 4-29 B). Similar to the analysis of lysosome-ER membrane contact sites in Figure 4-24, no quantifiable number of contact sites could be observed in HeLa LIMP-2 KO cells transfected with neither LIMP-2.WT or LIMP-2.P3x which may be due to experimental issues outlined in chapter 5.3.

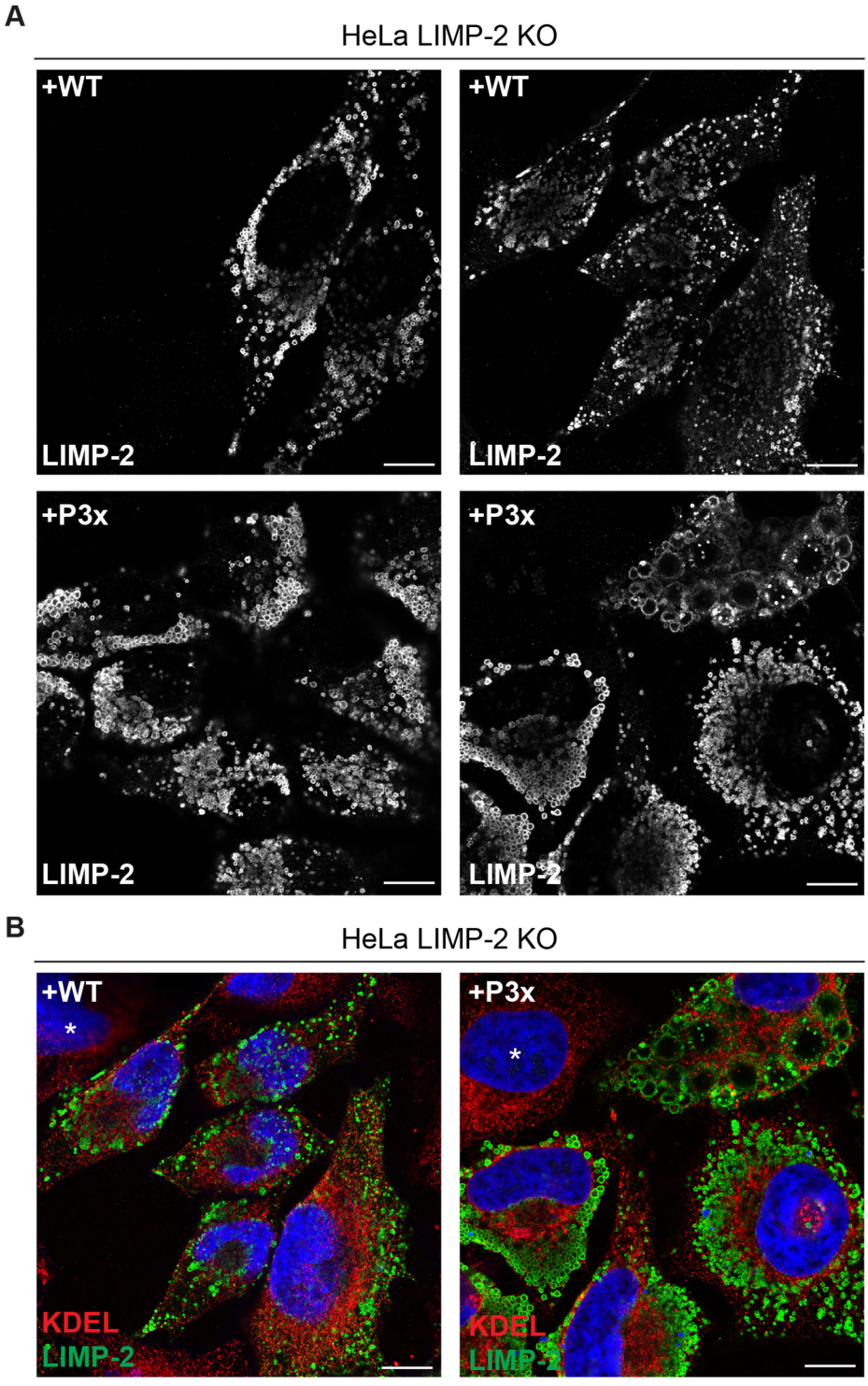

Figure 4-29: Immunofluorescence reveals change in lysosome morphology in cells expression a LIMP-2 palmitoylation mutant. HeLa LIMP-2 KO cells were transfected with mLIMP-2.WT.myc or mLIMP-2.P3x.myc, respectively, for 48 h and subsequently fixed with 4 % PFA. To visualize transfected cells, anti-LIMP-2-antibody staining was applied. Additionally, cells were stained with anti-KDEL antibody to visualize ER tubules. **A** The anti-LIMP-2 staining reveals drastic differences in size, amount and distribution of lysosomes in cells transfected with mLIMP-2.P3x.myc (lower panels) in comparison to those transfected with mLIMP-2.WT.myc (upper panels). Scale bars: 10. **B** Overlay of LIMP-2 with KDEL staining (same cells as shown in A top right and bottom right) was used to clarify if the enlarged lysosomes observed in cells transfected with mLIMP-2.P3x.myc exhibit an altered association with the ER. Scale bars: 10 µm. Asterisks denote untransfected cells. Images were acquired with a Zeiss 880 microscope and processed with Airyscan using the Zen software.

4.5.3.1. Expression pattern and stability of the LIMP-2 palmitoylation mutant

Palmitoylation is known to function as a regulatory mechanism for protein stability and can also influence protein-protein interaction (Zaballa and van der Goot 2018). Since the targeting of LIMP-2 to lysosomes was not affected, it was next investigated whether the absence of palmitoylation alters LIMP-2 protein levels and/or if it affects the ability of LIMP-2 to function as the chaperone and transporter of the acid hydrolase GCase from the ER to lysosomes. To this end, HeLa LIMP-2 KO cells were transiently transfected with plasmids harboring the cDNAs for murine LIMP-2.WT.myc or LIMP-2.P3x.myc, respectively (Figure 4-30). After 48 h of expression, cells were lysed and protein extracts were prepared, samples of which were separated via SDS-PAGE and subsequently analyzed by Western Blot and antibody staining (Figure 4-30 A-C). Normalizing the signal intensity measured for LIMP-2 to that of Actin revealed an increase of LIMP-2.Px3.myc protein levels by approximately 80 % in comparison to mLIMP-2.WT.myc and post-ER-GCase/ER-GCase levels were increased more than 2.5-fold (Figure 4-30 F and G).

To answer the question if non-palmitoylated LIMP-2 has an altered capability for GCase transport, the normalized post-ER GCase fraction was related to the respective normalized LIMP-2 fraction and the results obtained for cells expressing LIMP-2.WT were compared to those expressing LIMP-2.P3x (Figure 4-30 H). Importantly, while the total amount of post-ER GCase was higher in cells transfected with the LIMP-2 palmitoylation mutant, no significant difference in post-ER GCase fraction was measured when comparing the mutant and the WT control.

Cells were also transfected with human LIMP-2 constructs (hLIMP-2.WT.GFP or hLIMP-2.P3x.GFP), but both WT and P3x were poorly expressed and immunofluorescence staining revealed a considerable degree of mistargeting of both proteins, likely due to the large GFP-tag (data not shown).

The elevated protein levels of mLIMP-2.P3x.myc in comparison to mLIMP-2.WT.myc correspond to the observed increase in fluorescence intensity in HeLa LIMP-2 KO cells transfected with mLIMP-2.P3x.myc versus those transfected with mLIMP-2.WT.myc (Figure 4-29). Due to the increase in size, the total area of lysosomes in cells expressing mLIMP-2.P3x.myc is elevated which may explain the increase in protein levels of mLIMP-2.P3x.myc in the Western blot analysis (Figure 4-30 A). Since these cells were transiently transfected with a surplus of plasmid DNA it cannot be deduced whether mLIMP-2.P3x.myc is more stable than its WT counterpart, is influencing lysosome biogenesis or turnover or whether the transfection efficacy of this construct was simply higher (although the vector backbone for mLIMP-2.WT.myc and mLIMP-2.P3x.myc was identical). Of note, in HeLa LIMP-2 KO cells transiently

overexpressing mLIMP-2.WT treatment with 2-bromopalmitate (2-BP), a generic inhibitor of palmitoyltransferases, led to a decrease in mLIMP-2.WT abundance of 20 % in comparison to DMSO-treated cells (Haugwitz 2019), suggesting a scenario where palmitoylation enhances LIMP-2 protein stability rather than decreasing it. However, this inhibitor has considerable off-targets effects including influencing lipid synthesis, transport and metabolism (Lanyon-Hogg *et al.* 2017), which makes it difficult to interpret the observed variations in protein stability LIMP-2 in absence of palmitoylation. Overall, it can be concluded that the lack of palmitoylation does not render LIMP-2 acutely unstable, and prone to premature degradation and further does not interfere with the targeting of LIMP-2 to lysosomes. For extended analysis of the stability of murine (and human) LIMP-2.P3x techniques avoiding transient transfection and the associated drawbacks like variability in transfection efficacy should be employed.

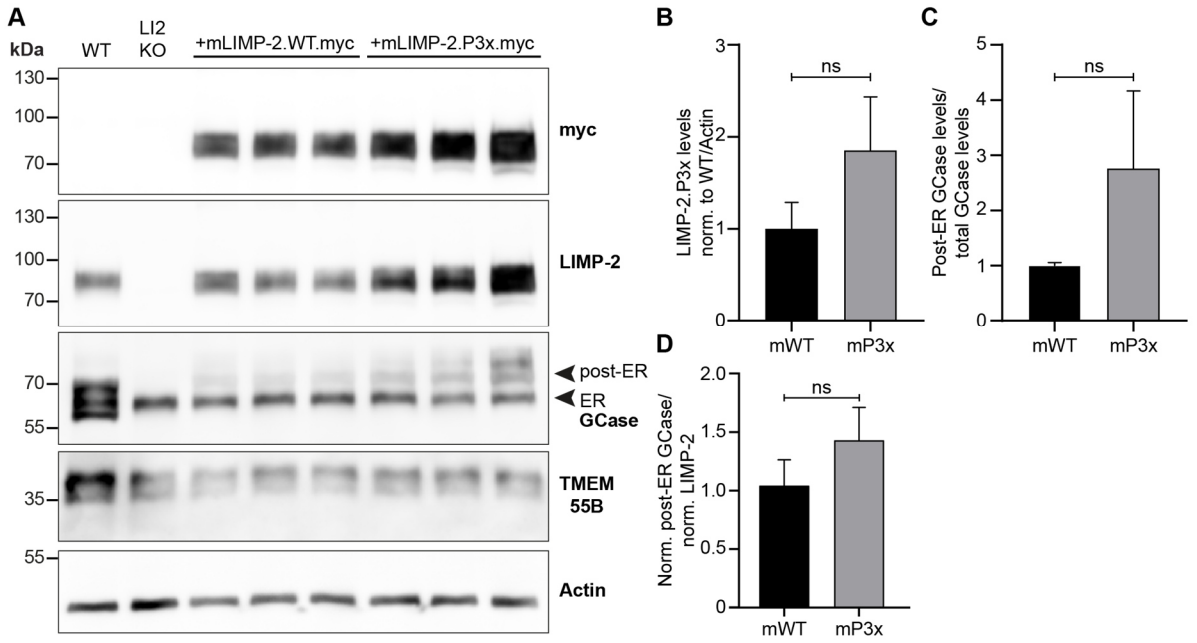

Figure 4-30: Expression patterns of human and murine LIMP-2 constructs and influence of depalmitoylated LIMP-2 on protein amount of post-ER GCase. A HeLa LIMP-2 KO cells were transfected for 48 h with either murine LIMP-2.WT-myc or LIMP-2.P3x.myc, respectively, and protein levels of LIMP-2 and GCase were analyzed via Western Blot. TMEM55 and Actin were utilized as lysosomal marker and loading control, respectively. WT, Hela WT cells; LI2 KO, Hela LIMP-2 KO cells. LIMP-2 protein levels of in relation to Actin were quantified (**B**) as well as the fraction of post-ER GCase in relation to total GCase protein levels (**C**) in cells transfected with either of the two different LIMP-2 constructs Additionally, normalized post ER GCase levels were normalized (norm.) to the normalized LIMP-2 levels (**D**). A two-tailed unpaired Student's t-test was utilized to compare protein levels. ns = non-significant; n = 3 independent samples from one experiment.

4.5.3.2. Influence of a lack of palmitoylation on LIMP-2-protein interaction

The human and murine LIMP-2 proteins share 85 % sequence identity on the amino acid level (Holmes 2012) and the N- and C-terminal regions share an even higher sequence identity with only one amino acid difference (Figure 4-31). Since the human LIMP-2 constructs were only weakly expressed (data not shown) and harbored a large C-terminal GFP tag which may prevent binding of interacting proteins (Weill *et al.* 2019), the murine LIMP-2.WT and –P3x

plasmids containing the small myc-tag were chosen to study if the loss of palmitoylation affects the interaction of LIMP-2 with the membrane contact site proteins described previously, VAPA, VAPB, STARD3 and Gramd1b.

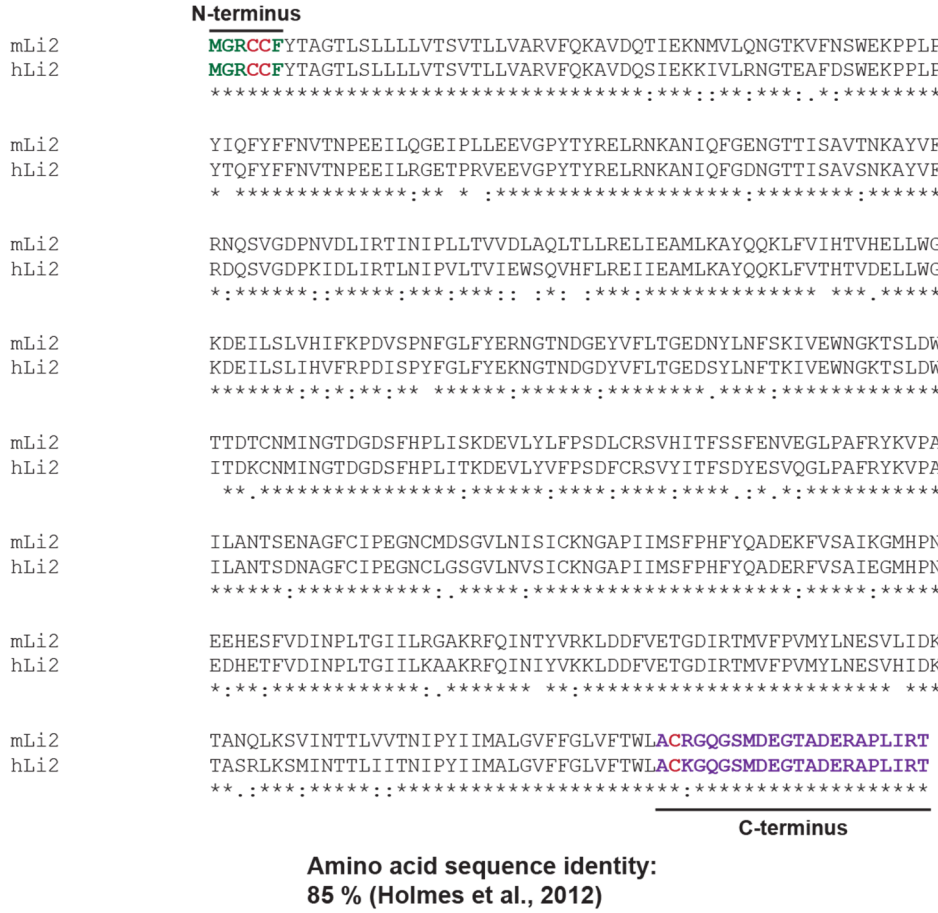

Figure 4-31: Alignment of amino acids sequences of human and murine LIMP-2 highlighting the amino- and carboxy-terminal domains (N- and C-terminus). The N-terminus is highlighted in green and the C-terminus is highlighted in purple. Palmitoylated cysteines in these domains are highlighted in red. Identical amino acids between human and mouse are underlined with an asterisk, while similar amino acids are underlined with a colon. Differing amino acids are underlined with a dot.

First, the interaction of LIMP-2.P3x with the ER MCS proteins VAPA and VAPB was assessed and compared to that of LIMP-2.WT. The signal obtained for the coIP of VAPA (Figure 4-32 A) and VAPB (Figure 4-32 C) was normalized to the amount of LIMP-2.WT or LIMP-2.P3x, respectively, that was immunoprecipitated. While no difference was observed for the interaction of VAPA with either LIMP-2.WT or the palmitoylation mutant (Figure 4-32 B), the amount of VAPB that was co-precipitated with LIMP-2.P3x was approximately 30 % less in comparison to coIP with LIMP-2.WT (Figure 4-32 D).

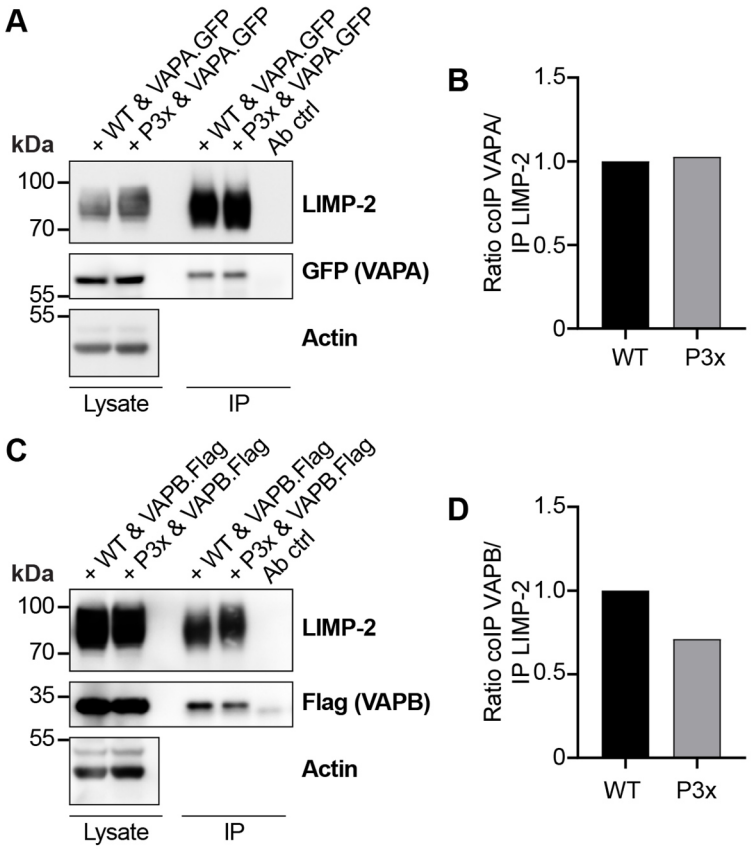

Figure 4-32: Co-immunoprecipitation studies indicate that LIMP-2's palmitoylation influences interaction with specific proteins. HeLa LIMP-2 KO cells were co-transfected with either mLIMP-2.WT or mLIMP-2.P3x, respectively, and VAPA (**A**) or VAPB (**C**), respectively, and LIMP-2 was precipitated using an antibody directed against the C-terminus of LIMP-2. 30 µg of lysate and 20 µl of IP fractions were separated via SDS-PAGE and analyzed by Western blotting. Dashed lines indicated that the image was sliced at this position, but all samples shown belong to the same blot. Ab ctrl, antibody control containing buffer instead of lysate. Quantifications depicted in **B** and **D** indicate the amount of co-precipitation of VAPA and VAPB, respectively, divided by the amount of precipitated LIMP-2 in each sample. The result obtained for interaction between VAPA and VAPB and LIMP-2.WT was set as baseline and compared to that obtained for interaction of VAPA and VAPB with LIMP-2.P3x.

The same experimental set-up was employed to characterize the interaction between LIMP-2.P3x and Gramd1b as well as STARD3 in comparison to the interaction of these proteins with LIMP-2.WT (Figure 4-33 A and C). In both cases, the absence of palmitoylation in LIMP-2 led to a decrease in co-precipitation of both Gramd1b and STARD3, respectively, with LIMP-2. In comparison to the coIP with LIMP-2 WT, the fraction of Gramd1b attached to LIMP-2.P3x was only 40 % (Figure 4-33 B). Similarly, STARD3 was recovered to 55 % (Figure 4-33 D), indicating that the palmitoylation of LIMP-2 could indeed be a factor to modulate LIMP-2's interaction with other proteins at the cytosolic side of the lysosomal membrane. It should be noted that in a control sample that contained lysate from cells transfected with LIMP-2.WT and Gramd1b and Dynabeads™ used for immunoprecipitation, but not the IP antibody (Figure 4-33, beads ctrl), a weak GFP-positive signal was also detected. This signal was of lower intensity than that detected in the IP sample and also migrating at a slightly higher molecular weight than the signal corresponding to Gramd1b.GFP. However, it cannot be excluded that the protein might partially attach to the beads irrespectively of the presence of LIMP-2 and this

needs to be further investigated in order to unequivocally determine the nature of LIMP-2's interaction with Gramd1b (and other proteins).

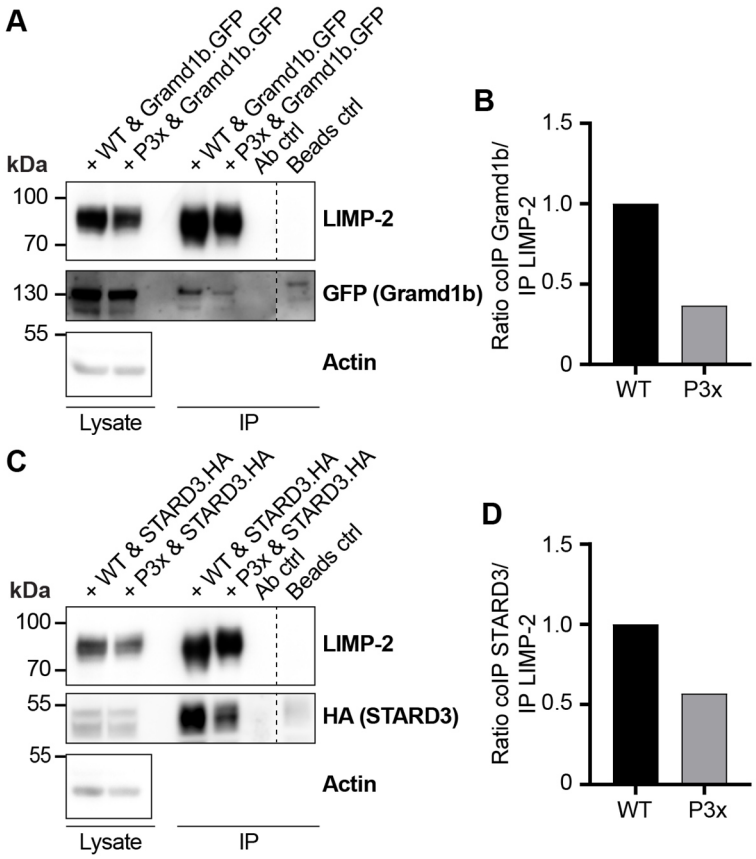

Figure 4-33: Co-immunoprecipitation (co-IP) studies indicate that LIMP-2's palmitoylation influences interaction with specific proteins. HeLa LIMP-2 KO cells were co-transfected with either mLIMP-2.WT.myc or mLIMP-2.P3x.myc, respectively, and Gramd1b (**A**) or STARD3 (**C**), respectively, and LIMP-2 was precipitated using an antibody directed against the C-terminus of LIMP-2. 30 µg of lysate and 20 µl of IP fractions were separated via SDS-PAGE and analyzed by Western blotting. Dashed lines indicate that the image was sliced at this position, but all samples shown belong to the same blot. Ab ctrl, antibody control containing buffer instead of lysate; beads ctrl, control containing lysate and beads without the IP antibody. Quantifications depicted in **B** and **D** indicate the amount of co-precipitation of Gramd1b and STARD3, respectively, divided by the amount of precipitated LIMP-2 in each sample. The result obtained for interaction between Gramd1b and STARD3 and LIMP-2.WT was set as baseline and compared to that obtained for interaction of Gramd1b and STARD3 with LIMP-2.P3x.

4.5.4. Which palmitoyltransferase(s) is/are modifying LIMP-2?

Palmitoylation is conveyed by palmitoyltransferases (DHHCs or PATs). In mammalians, 23 different versions of these enzymes have been described, with various membrane localization and/or different tissue expression (Jiang *et al.* 2018). LIMP-2 is synthesized in the ER, subsequently modified with complex glycans in the Golgi and then transported to late endosomes/ lysosomes by involvement of adaptor proteins 1 and 3 (Honing *et al.* 1998, Janvier *et al.* 2003). Therefore, there are multiple organelles where the palmitoylation of LIMP-2 could occur. Interestingly, the palmitoyltransferase DHHC20 was identified as a potential interactor

for LIMP-2 in the BioID screen described in Table 4-3. To verify whether LIMP-2 can indeed interact with DHHC20, endogenous LIMP-2 was immunoprecipitated in HeLa WT cells that had been transiently transfected with DHHC20.HA. Additionally, the possible interaction of LIMP-2 with another palmitoyltransferase, DHHC6.his.myc, was investigated. The rationale for this stems from unpublished observations from the van der Goot lab at École polytechnique fédérale de Lausanne, Switzerland, in the framework of a collaboration. As depicted in Figure 4-34, DHHC20 could indeed be identified in the IP fraction and a signal, albeit weaker than that for DHHC20, was detected for DHHC6 as well.

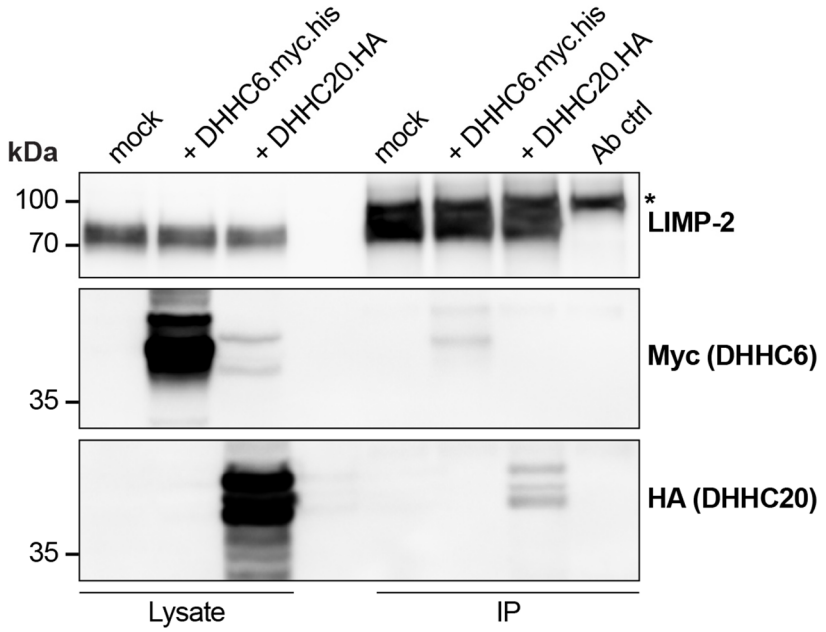

Figure 4-34: LIMP-2 interacts with palmitoyltransferases (DHHCs/PATs) DHHC6 and DHHC20. For the half-endogenous co-immunoprecipitation (coIP), HeLa WT cells were transfected with empty vector (mock), DHHC6.myc.his and DHHC20.HA, respectively, and LIMP-2 was precipitated. Both DHHCs were recovered in the coIP fractions. Ab ctrl, antibody control; asterisk denotes an unspecific antibody signal migrating directly above the LIMP-2 band.

While the exact mechanisms or amino acid motifs that underlie substrate recognition by DHHCs have yet to be fully elucidated, it is feasible to assume that time and/or strength of the binding between a DHHC and its target protein is altered if the cysteine residues subject to palmitoylation by the DHHC enzyme have been removed by mutagenesis. Therefore, association of LIMP-2.P3x and DHHC6 and DHHC20, respectively, was assessed by means of co-IP studies to gain more information about the relation between LIMP-2 and the palmitoyltransferases. As described in Figure 4-35, DHHC20 was recovered to a similar extent in IP fractions of LIMP-2.P3x and LIMP-2.WT as indicated by the ratio of IP of the respective LIMP-2 version an the co-IP of DHHC20 in these fractions (Figure 4-35 A, B). The amount of DHHC6 that was bound to LIMP-2.P3x, on the other hand, was only ~20 % in comparison to that bound to LIMP-2.WT (Figure 4-35 C).

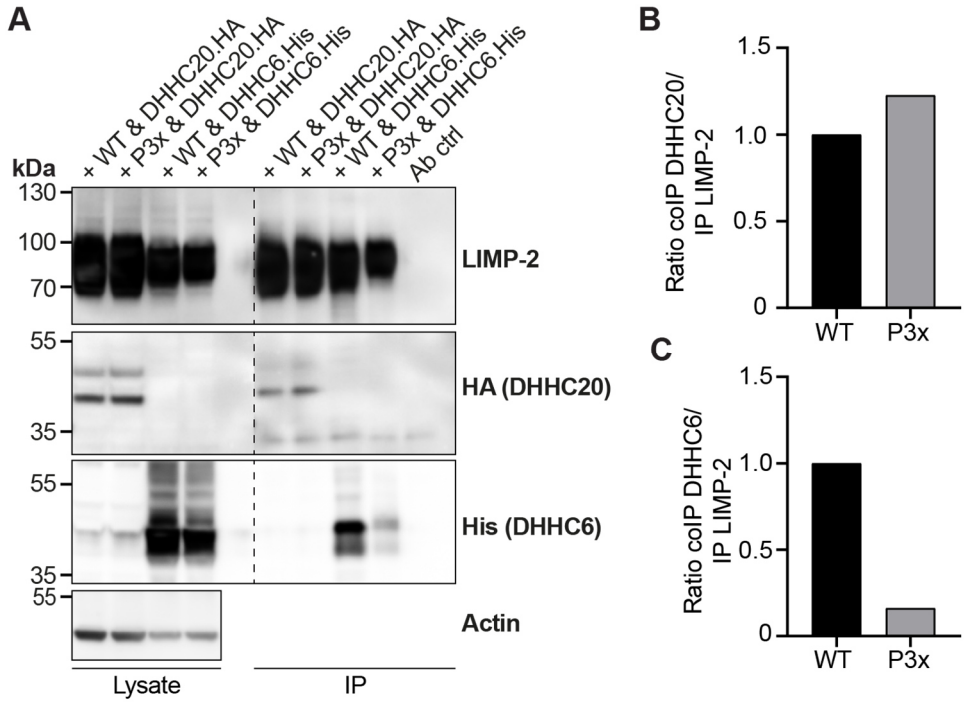

Figure 4-35: Depalmitoylation decreases co-immunoprecipitation of DHHC6 (but not of DHHC20) with LIMP-2. A HeLa LIMP-2 KO cells were co-transfected with mLIMP-2.WT.myc or mLIMP-2.P3x.myc and DHHC6.His or DHHC20.HA, respectively. While DHHC20 was co-precipitated to the same amount, the co-IP of DHHC6 with LIMP-2.P3x was reduced in comparison to that of LIMP-2.WT. Quantifications depicted in **B** and **C** indicate the amount of co-precipitation of DHHC20 and DHHC6, respectively, divided by the amount of precipitated LIMP-2 in each sample. The result obtained for interaction between DHHC6 and DHHC20 and LIMP-2.WT was set as baseline and compared to that obtained for interaction of DHHC6 and DHHC20 with LIMP-2.P3x.

While the results described in Figure 4-35 intriguingly suggest a role for DHHC6 in LIMP-2 palmitoylation, they do not prove that DHHC6 actually modifies LIMP-2 and further doesn't exclude that there could be several palmitoyltransferases that are involved in LIMP-2's palmitoylation. Palmitoylation has been described as a mechanism to regulate protein stability and half-life. Therefore, the deletion or down-regulation of the respective palmitoyltransferases and assessment of the effects on (endogenous) LIMP-2 abundance and stability might provide valuable information to determine which DHHC enzymes LIMP-2 is the substrate of and might also clarify the contrasting effects that mutagenesis-mediated removal of palmitoylation sites had on the protein abundance of human and murine LIMP-2 (Figure 4-30 D and E) under overexpression conditions. The CRISPR/Cas9 system and siRNA targeting either DHHC6 or DHHC20 would be suitable to create HeLa cell lines devoid of these palmitoyltransferases. However, it was not possible to unequivocally demonstrate the presence of the enzymes HeLa WT by immunoblot analysis using antibodies directed against DHHC6 or DHHC20, respectively (data not shown) and a second approach employing reverse transcriptase quantitative real time PCR (RT-qPCR) to measure mRNA transcript levels also failed to deliver robust results. The difficulties to detect the palmitoyltransferases likely stems from their low copy number in HeLa cells. In several studies, they were reported to range between 8,125 to 14,224 for DHHC20 and 1,500 to 11,250 for DHHC6 in HeLa cells (Nagaraj *et al.* 2011, Hein

et al. 2015, Itzhak *et al.* 2016, Zaballa and van der Goot 2018). In comparison the copy number per cell was 262,901 for LIMP-2 (Itzhak *et al.* 2016). Hence, more sensitive methods need to be employed to be able to address the issues described above.

In summary, the data presented in this chapter demonstrate that LIMP-2 is subject to palmitoylation at its three cytosolic cysteine residues. The trafficking of LIMP-2 to lysosomes is unaltered in absence of palmitoylation, however, overexpression of a palmitoylation-deficient LIMP-2 mutant induces morphological changes in lysosomes. While it could not be fully elucidated whether palmitoylation negatively or positively affects LIMP-2 stability, co-immunoprecipitation studies implicate that the attachment of palmitate to the N- and C-terminus of LIMP-2 is a regulatory factor influencing interaction between LIMP-2 and other proteins at the cytosolic face of lysosomes and the ER. Interestingly, this interaction is also modulated by the availability of lipids (as described in 4.4.3.) and it is intriguing to speculate about LIMP-2's role at these membrane contact sites in the context of its newly described lipid transport function (as discussed in chapter 5.4.3.).

5. Discussion

LIMP-2/SCARB2 is multifunctional lysosomal membrane protein. As several years of research have demonstrated, it plays critical roles in health and disease. One of the best-characterized functions to date is the transport of the lysosomal acid hydrolase β-glucocerebrosidase (GCase) from the ER to the lysosome, independently of the transport system utilized by the majority of soluble lysosomal proteins, the mannose-6-phosphate receptor pathway (Reczek *et al.* 2007, Schwake *et al.* 2013). The binding sites of GCase in LIMP-2 and the binding region of LIMP-2 in GCase were recently characterized in more detail (Zunke *et al.* 2016).

In the present work the functions of LIMP-2 beyond the transport of the acid hydrolase GCase were investigated. A mouse model harboring a point mutation in the binding motif for GCase was subjected to comparative analysis with a mouse model lacking LIMP-2 to differentiate between phenotypes caused solely by absence of LIMP-2 rather than concomitant depletion of LIMP-2 and GCase as is the case in the classical LIMP-2 KO mouse model.

Previous work indicated the existence of a hydrophobic cavity in all family members of the class B scavenger receptor family, namely SR-BI, CD36 and LIMP-2, which in the two latter cases could be validated by crystal structures (Neculai *et al.* 2013, Gomez-Diaz *et al.* 2016). Given the well-known involvement of SR-BI and CD36 in lipid translocation at the plasma membrane it was feasible to speculate that the cavity in the luminal domain of LIMP-2 might have a similar role in lipid transport, albeit at the lysosome, its primary residency. The data presented in this work uncover a function of the LIMP-2 luminal domain in lysosomal cholesterol export. Moreover, experiments presented in this thesis demonstrate that LIMP-2 is subject to palmitoylation, a wide-spread reversible posttranslational modification which likely impacts a novel role described for LIMP-2 at ER-lysosome contact sites.

5.1. Characterization of the LIMP-2.Y163D knock-in mouse

As described above, a knock-in mouse model expressing the LIMP-2 mutant LIMP-2.Y163D, which in cell-based assays failed to bind and transport GCase, was analyzed and compared to the previously described LIMP-2 KO mouse model (Gamp *et al.* 2003, Claussen 2005) in order to get a better understanding of LIMP-2 functions unrelated to the transport of GCase. While Gaucher disease and AMRF both share the lack of lysosomal GCase, pathology in these diseases is divergent (Chaves *et al.* 2011).

The fact that LIMP-2 deficiency and concomitant GCase deficiency do not result in a phenocopy of the pathological macrophages characteristic for Gaucher disease are attributed to the comparatively high residual amounts of GCase found in white blood cells of AMRF patients (Gaspar *et al.* 2014).

The complete correction of the usually observed defects in LIMP-2 KO mice in the LIMP-2.Y163D knock-in mice would point towards a pivotal role of LIMP-2 in these tissues and organs. However, as depicted in Table 4-1 and Table 4-2, in the knock-in mouse model a residual amount of GCase is able to reach lysosomes and function properly despite the lack of interaction between the mutant LIMP-2 and GCase in cell culture studies (Figure 4-1). Either GCase is able to reach the lysosome by an alternative route, as has previously been suggested (Gaspar *et al.* 2014) or the mutation Y163D in one of the binding domains for GCase in LIMP-2 is not sufficient in vivo to completely abolish GCase-LIMP-2 interaction. (Co)-immunoprecipitation of endogenous LIMP-2.Y163D and GCase from tissue lysate could clarify whether GCase still binds to the mutated LIMP-2 protein. If this is not the case, this mouse model might be useful to investigate alternative pathways by which GCase may reach lysosomes. Among the suggestions mentioned above are an alternative receptor for the hydrolase or re-uptake and endocytic delivery of GCase (in leucocytes) (Gaspar *et al.* 2014).

The observed residual GCase activity in tissue and MEF lysates is critical for the assessment of the observed phenotype correction in the LIMP-2-Y163D mice. While in one of the most drastically by loss of LIMP-2 affected tissues, the kidney, the residual GCase activity was measured to amount to only 37 % of wild type, the surplus of 12 % activity in comparison to the LIMP-2 KO situation (Table 4-2) could be sufficient to counter-balance any contribution that the low levels of GCase activity might be having to the development of hydronephrosis typically occurring in LIMP-2 KO mice. While complete loss of GCase results in perinatal lethality in mice and humans (Sidransky *et al.* 1992, Tybulewicz *et al.* 1992), it has been experimentally shown that even low levels of enzyme can significantly alleviate substrate accumulation. In a type 1 GD mouse model that is characterized by drastically reduced GCase activity in bone marrow, spleen and liver the transplantation of 10 % wild type-derive bone marrow cells with functional GCase was sufficient to correct pathology (Enquist *et al.* 2009). Another study reported that a residual GCase activity of 11 % - 15 % in relation to wild type prevents accumulation of the GCase substrate glucosylceramide in cells (Schueler *et al.* 2004). Similarly, in patient fibroblasts expressing either mutated arylsulfatase A or β-hexosaminidase A, respectively, 10 % - 15 % of residual enzyme activity yielded normal substrate turnover rate in fibroblasts (Leinekugel *et al.* 1992). These experimental observations are in agreement with a kinetic model put forth by Conzelmann and Sandhoff describing the ability of lysosomal enzymes to compensate reduction in enzyme amount or activity by increasing the steady-state concentration of their substrates (Conzelmann and Sandhoff 1983). This results in an unchanged substrate turnover rate until a critical threshold is reached where the influx rate of the substrate surpasses the remaining capacity of the residual enzyme, which leads to accumulation of non-degraded substrate and pathology (Conzelmann and Sandhoff 1983, Leinekugel *et al.* 1992).

Therefore, based on the conducted analysis of the LIMP-2.Y163D knock in mouse model, it is not possible to attribute the phenotypic correction observed in these mice solely to the presence of LIMP-2 in these mice since the fraction of GCase that is still able to reach lysosomes might be sufficient to avoid the accumulation of non-degraded substrate and thus prevent organelle and organ malfunction.

The introduction of a second mutation in the GCase binding site in LIMP-2 could increase the chances of generating a mouse model that is fully deficient of GCase-interacting LIMP-2.

As evident from the variability in severity of GD and LIMP-2 KO mouse tissue displaying different levels of residual enzyme, it is difficult to deduce the critical threshold concentration (as described above) of GCase needed to maintain substrate turnover and avoid substrate accumulation. In this regard, instead of analyzing a mouse model expressing a GCase-binding deficient LIMP-2 (or a mouse model for GD itself, since LIMP-2 function should not be affected), it might be more feasible to subject LIMP-2 KO mice to enzyme replacement therapy (ERT) to restore lysosomal GCase levels and analyze if any pathological changes still occur due to lack of LIMP-2. It has been demonstrated that intravenously administered recombinant GCase, which was modified to harbor terminal mannose residues, is taken up by the mannose receptor (and possibly other cell surface receptors) and therefore reaches lysosomes independently of LIMP-2 in tissue macrophages (Grabowski *et al.* 1995, Brady 2003, Haddley 2012). Limitations of this approach are the failure of ERT to overcome the blood brain barrier and deliver recombinant enzyme to the brain. Nevertheless, supplying LIMP-2 deficient tissues and cells with alternatively targeted GCase might provide valuable insight into LIMP-2-related pathology.

5.2. LIMP-2 is a lipid transporter

The most striking structural feature of LIMP-2 is its large intralysosomal domain which connects the two transmembrane domains of LIMP-2. With 10 to 11 potential glycosylation sites this domain contributes to the formation of the glycocalyx lining the inner face of the lysosomal limiting, thus protecting itself and other lysosomal membrane proteins from premature degradation by lysosomal proteases. The apical helices of the loop are of major importance for interaction with GCase as well as enterovirus 71 (EV71) as described in chapter 1.4.1. The discovery of a large hydrophobic tunnel inside this core domain (Neculai *et al.* 2013) prompted analysis of its function.

The thick glycocalyx that lines the inner face of the lysosomal limiting membrane serves as a protective layer for the membrane and its proteins thus avoiding premature degradation and lysosome rupture by limiting access of luminal enzymes to the lipid bilayer. Concomitantly, this

also prevents lysosomal degradation products such as the hydrophobic lipid cholesterol to easily partition into the membrane in order to be recycled. As mentioned earlier, the integral membrane protein NPC1 has a pivotal role in facilitating cholesterol export from lysosomes together with the luminal protein NPC2. Dysfunction or loss of either proteins results in Niemann-Pick disease which is characterized by severe intralysosomal cholesterol and sphingolipid storage. The experiments presented in this thesis provide evidence for a second lysosomal export route of cholesterol which mainly relies on the luminal domain of LIMP-2.

5.2.1. LIMP-2's luminal domain can bind and translocate cholesterol

A core question to assess LIMP-2's potential role in lipid and specifically cholesterol transport was whether direct association between the LIMP-2 tunnel domain and lipid substrate could be demonstrated. For this purpose, the recombinant luminal domain was subjected to lipid binding studies with UV-crosslinkable lipids. Indeed, crosslinks between LIMP-2 and several lipids such as ceramide and sphingosine were observed, however, the by far strongest association was detected between LIMP-2 and cholesterol. Determination of the effect of increasing concentrations of cholesterol on fluorescence decay of fluorescently labelled recombinant LIMP-2 luminal domain using microscale thermophoresis was employed as a measure of affinity between LIMP-2 and cholesterol and resulted in a high half-maximal effective concentration (EC_{50}), further supporting the notion that cholesterol could be a substrate of LIMP-2. Similar experiments had been conducted for other cholesterol binding proteins like the ER-localized transcription factor nuclear factor erythroid 2 related factor-1 (Nrf1) (Widenmaier *et al.* 2017). This protein protects the cell against excess cholesterol levels by sensing and binding cholesterol and promoting cholesterol excretion in the liver in the case of excess cholesterol levels in the ER. In their study, Widenmaier and colleagues compared the affinities between Nrf1 and cholesterol to those between Nrf1 and the cholesterol analogs campesterol, 27-hydroxycholesterol and epicholesterol. While Nrf1 had a comparable affinity for cholesterol, campesterol and 27-hydroxysterol, a much lower affinity between Nrf1 and epicholesterol was observed (Widenmaier *et al.* 2017). While the structural differences between cholesterol and campesterol and 27-hydroxysterol consist of modification of the iso-octyl lateral chain attached to C17 (additional methyl group at C24 and additional hydroxyl group at C27, respectively), in epicholesterol the C3- hydroxyl group is arranged in α-orientation instead of β-configuration as in cholesterol. The observation of decreased affinity between this cholesterol epimer and NRF1 indicates a pivotal role for the configuration of the C3-hydroxyl group for cholesterol-protein association and has in fact also been demonstrated for cholesterol-mediated inhibition of large-conductance voltage/Ca2+-gated K+ (BK) channels (Bukiya *et al.* 2011). It would therefore be of interest to investigate if LIMP-2 shows similar preferences or can bind various cholesterol analogs with similar affinities.

Intriguingly, this study also identified SCARB2/LIMP-2, but not NPC1, among 790 genes regulated by cholesterol in an NRF1-dependent manner which calls for further investigation (Widenmaier *et al.* 2017).

In 2017, a crystal structure of the LIMP-2 luminal domain was published that differed in several regards from previously published LIMP-2 crystal structures: While the previous structures were all monomers, Conrad et al were able to crystallize the LIMP-2 luminal domain as a dimer (Conrad *et al.* 2017). Moreover, they found several lipids, among them phosphatidylserine and phosphatidylcholine as well as cholesterol either attached to hydrophobic patches close to or inside the hydrophobic tunnel of each monomer, respectively. Not only does this verify the conclusions drawn from the data presented in this thesis regarding LIMP-2's ability to transport cholesterol through its tunnel, but also raises exciting possibilities for additional lipid substrates (discussed in more detail in section 5.2.5.). The newly reported crystal structure also sheds some light on the orientation of cholesterol inside the LIMP-2 tunnel: It appears to enter the tunnel with the hydroxyl group first which is the same orientation that cholesterol has when it is transferred from the hydrophobic pocket of NPC2 to the N-terminal domain (NTD) of NPC1 in the so-called hydrophobic hand-off (Kwon *et al.* 2009, Gong *et al.* 2016, Li *et al.* 2016). According to current data, the transfer of cholesterol from the NTD to the NPC1 tunnel causes cholesterol to enter the tunnel in opposite direction, with the iso-octyl chain first (Li *et al.* 2016, Trinh *et al.* 2018, Winkler *et al.* 2019). Careful analysis and comparison of the amino acid composition of the different cholesterol-transporting cavities in NPC1 and LIMP-2 might clarify the need for opposing orientation of cholesterol during transport.

Following the cholesterol-LIMP-2 binding studies, cell-based assays described in this work demonstrated LIMP-2's capability to transport fluorescently labelled LDL-derived cholesterol through the tunnel within its luminal domain. These experiments were carried out in several cell lines, such as CHO, HeLa and A431 cells, and included analysis of the transport capacity of a LIMP-2 tunnel mutant where amino acid exchanges within the tunnel led to blockage. While cells overexpressing WT LIMP-2 either as a lysosomal protein or in the form of a plasma membrane-targeted chimera were able to readily translocate cholesterol, the corresponding LIMP-2 tunnel mutant failed to do so.

As described in section 1.4, LIMP-2 has two structurally similar homologs, the plasma membrane proteins SR-BI and CD36. Both proteins bind a variety of lipids including oxidized LDL and fatty acids (CD36) (Endemann *et al.* 1993, Drover *et al.* 2008) as well as HDL (both) and anionic phospholipids and triglycerides (SR-BI) (Acton *et al.* 1996, Shen *et al.* 2018). The ability of SR-BI to selectively take up and transport cholesterol and cholesteryl esters from HDL into cells is well documented (Rigotti *et al.* 2003) and for CD36 translocation fatty acid-derived pheromones through its ectodomain was recently described (Gomez-Diaz *et al.* 2016),

underlining the importance of the tunnel-containing extracellular domain in these proteins. Hence, the demonstration of a lipid-transport function of the LIMP-2 luminal domain is not completely unexpected, even though its subcellular location is different from CD36 and SR-BI. Unlike these two plasma membrane proteins, LIMP-2 moreover displays a broad tissue expression pattern and given the diverse phenotypic manifestations caused by loss of LIMP-2 its function appears to be universally relevant. In this context, it will be of interest to elucidate if some of the diverse functions assigned to LIMP-2 like the newly discovered lipid transport are equally relevant in different tissues or if some cell type specificity can be expected similar to the lipid transport mediated by CD36 and SR-BI. Furthermore, the ability of both proteins to bind and transport different lipid species indicates that cholesterol might not be the sole lipid substrate for LIMP-2. These intriguing aspects are further discussed in sections 5.2.4 and 5.2.5.

5.2.2. The LIMP-2 cholesterol export pathway exists in parallel to the NPC1/2 route

The importance of the NPC2-NPC1 cholesterol export pathway (described in 1.3.2) for maintenance of lysosomal physiology is underlined by the severe alterations in lipid trafficking observed in humans and animal models lacking either NPC2 or NPC1 or harboring a mutated form of the protein. Cholesterol accumulation inside lysosomes has been a hallmark and visualization with the polyene macrolide filipin has been utilized for a long time for the identification of Niemann-Pick disease in patient fibroblasts (Pentchev *et al.* 1985, Vanier *et al.* 2016). The existence of a second lysosomal cholesterol export pathway is therefore somewhat unexpected and raised the question if both export routes operate in tandem or independently of each other. Data obtained from co-immunoprecipitation studies using overexpression conditions at first indicated that LIMP-2 could indeed associate with NPC2 as well as with NPC1. Contrarily, in a follow-up experiment where endogenous LIMP-2 was precipitated in lysates from HeLa cells, no association of NPC2 or NPC1 could be observed. The initially observed binding between LIMP-2 and NPC2 or NPC1, respectively, might therefore be an experimental artefact as a consequence of protein overload in the ER caused by co-overexpression of IP and bait protein and does not reflect a physiological process. This discrepancy underlines the need for careful validation of suspected interaction partners for a given protein of interest and argues for choosing, if possible, a natural, i.e. endogenous setting for protein-protein interaction studies. In this context, it would be advisable to repeat this experiment using an acidic buffer system to account for the possibility of a pH-dependent interaction as the association of LIMP-2 with GCase, for instance, is restricted to neutral pH which causes dissociation of the complex in lysosomes (Reczek *et al.* 2007, Zachos *et al.* 2012).

Overall, the current data negate a cooperative cholesterol transport between NPC1, NPC2 and LIMP-2. Rather, the LIMP-2 cholesterol recycling pathway seems to exists independently of the NPC1/NPC2 axis. Nevertheless, it seems likely that NPC1 is able to compensate for loss of LIMP-2 to some extent which is why mouse embryonic fibroblasts and HeLa cells lacking LIMP-2 do not accumulate lysosomal cholesterol under basal conditions and LIMP-2 KO mice kept on a standard Western diet do not develop a prominent cholesterol-related phenotype as mice lacking NPC1. Interestingly, Western blot analysis of cell lysates from LIMP-2 KO MEF cells did not reveal elevated levels of NPC1 as a response to a compensatory function, as one might expect. This is for example the case of the structurally related lysosomal membrane proteins LAMP1 and LAMP2, where deletion of LAMP-1 in mice was not associated with an overt phenotype, but LAMP-2 expression was upregulated, pointing towards a compensatory role for LAMP-2 (Andrejewski *et al.* 1999).

Of note, cholesterol levels were found to be elevated in purified liver lysosomes (tritosomes) from LIMP-2 KO mice (Prof. Dr. J.M.F.G. Aerts, unpublished observations) and storage of free cholesterol was apparent in LIMP-2 KO cells after challenge with LDL, indicating that NPC1 present in these cells was no longer able to fully compensate for lack of LIMP-2. In the reverse situation, overexpression of LIMP-2 WT reduced lysosomal cholesterol load as assessed by filipin staining intensity in comparison to untransfected cells and this was not the case in cells overexpression a mutated version of LIMP-2 where the hydrophobic tunnel was blocked by bulky amino acids. However, at endogenous level LIMP-2 does not seem to be able to provide enough cholesterol export capacity to counteract the lipid accumulation caused by loss or mutation of NPC1 as evidenced by patients suffering from NPC disease. Variations in lifespan of patients caused by variable age of onset (Yanjanin *et al.* 2010), on the other hand, suggests that alternative cholesterol recycling pathways might have a positive influence on disease progression. Based on the data presented in this study, the cholesterol recycling route provided by LIMP-2 seems to operate at different (slower) kinetics and efficiency. Possible reasons for this are evaluated in section 5.2.4.

In agreement with the notion of two cholesterol export pathways operating in parallel, an additive effect in terms of lysosomal cholesterol storage was observed in a newly generated HeLa CRISPR NPC1-LIMP-2 KO cell line and processing of the transcription factor SREBP2 was also altered in response to additional deletion of LIMP-2 in NPC1-deficient cells. To further characterize the effects of NPC1-LIMP-2 double deficiency, experiments analogous to those presented in this work, namely the evaluation of subcellular distribution of BODIPY-cholesterol in live cells and measurement of the cell's ability to form cholesteryl esters, would add valuable information.

The CRISPR technology can not only be employed to disrupt a gene, leading to depletion of the protein encoded by that gene, but can also be utilized to introduce mutations in endogenous proteins, thus creating stable knock- in cell lines that allow assessment of the potential effects of various mutations without the possible side effects of transient expression of a mutant protein, often including a large disruptive protein tag like GFP (Dave *et al.* 2016, Weill *et al.* 2019). In this regard, introducing the tunnel mutant of LIMP-2 into NPC1 KO cells and comparing phenotypes with the NPC1-LIMP-deficient cells would be of interest. Additionally, NPC1 KO cells stably overexpressing LIMP-2 might help to mitigate the variability observed in the rescue experiments discussed earlier, where NPC1 KO cells were transiently overexpressing either LIMP-2.WT or a LIMP-2 tunnel mutant.

A recent study by Li and Pfeffer described an unexpected involvement of the most abundant lysosomal membrane proteins, LAMP-1 and LAMP-2, in cholesterol handling (Li and Pfeffer 2016). Their data revealed that not only can both proteins bind cholesterol, but they also interact with NPC1 and NPC2 which led the authors to speculate that the LAMPs, and especially LAMP-2, might act as a reservoir for cholesterol sensing and transfer. Might LIMP-2 be able to accept cholesterol from LAMP-2 as well? Preliminary data from co-immunoprecipitation studies indicated a potential interaction of the two proteins under overexpression conditions, but as discussed above, follow-up studies on endogenous level need to be carried out to confirm this hypothesis (data not shown). Intriguingly, immunoblot analysis of protein lysates from tissues of LAMP-2 deficient mice revealed a significant decrease in protein levels of both LIMP-2 and NPC1, but not LAMP-1, in heart and muscle (data not shown). Future work is required to evaluate the potential relationship between LAMP-2 and LIMP-2/NPC1.

5.2.3. How is cholesterol delivered to LIMP-2?

Cholesterol is a highly hydrophobic molecule and therefore not soluble in aqueous environment. The current view is that free cholesterol, upon liberation from LDL, rapidly partitions into intralysosomal membranes from intraluminal vesicles (ILV) that also contain the unique phospholipid lysobisphosphatidic acid (LBPA, also denoted bismonoacylglycerophosphate, BMP) (Gruenberg 2020). The luminal protein NPC2 has a hydrophobic pocket able to accommodate cholesterol and extracts cholesterol from the ILV for which the presence of LBPA is required (McCauliff *et al.* 2019). Subsequently, NPC2 transfers cholesterol to the N-terminal domain of NPC1 and might also be able to mediate direct transfer of cholesterol to the lysosomal membrane (McCauliff *et al.* 2015). Since LIMP-2 is also residing in the lysosomal membrane it is feasible to assume that cholesterol reaches the LIMP-2 tunnel in a similar manner. Since no interaction between LIMP-2 and NPC2 could be detected,

however, it remains an open question how exactly cholesterol is delivered to LIMP-2. As discussed above, transfer of the lipid from LAMP-2 to LIMP-2 could be one possibility.

Class B scavenger receptor family member SR-BI directly binds HDL particles at the cell surface and accepts and translocates cholesterol. In a similar manner, incubation of HeLa and CHO cells expressing a LIMP-2 chimera together with cholesterol-loaded LDL was sufficient to mediate LIMP-2-dependent cholesterol uptake, indicating that LIMP-2 can also directly associate with lipoprotein particles. LDL enters the cell via binding to LDLR and subsequent endocytosis. Upon its arrival in lysosomes, the LDL particle is attacked by proteases and the lysosomal acid lipase (LAL or LIPA) which breaks down the protein and lipid components, respectively. Loss or malfunction of the serine hydrolase LAL is the cause for a rare fatal lysosomal storage disease, Wolman's disease (WD), as well as Cholesteryl ester storage disease (CESD), which in contrast to WD has a later onset of disease owing to 1-5 % residual LAL activity (Goldstein *et al.* 1975, Anderson *et al.* 1999).

The mechanistic details of how LAL hydrolyzes LDL-derived cholesteryl esters and triglycerides, respectively, have not been uncovered yet. Recently, Rajamohan and co-workers published the first crystal structure of recombinant human LAL (Rajamohan *et al.* 2020). This study revealed that substrate access to the catalytic pocket of LAL is likely regulated by a cap domain termed "lid" and two cavities close the active side which may function in providing solvent access to the catalytic center and/or serve to accommodate the substrate for hydrolysis (Rajamohan *et al.* 2020). No information has been provided so far about the spatial details of lysosomal LDL particle break down by LAL. It seems possible that the tunnel opening of LIMP-2's luminal loop and LAL are in close proximity and newly liberated cholesterol can therefore be directly transferred from LAL to LIMP-2. However, no data are currently available to support a direct (or indirect) association between LAL and LIMP-2.

The sphingolipid activator proteins (Saposins/ Saps) Saposin A, B, C and D are small lipid-binding proteins that reside in the lysosomal lumen and essential co-factors for the degradation of glycosphingolipids and sphingolipids by lysosomal hydrolases and defects in the precursor protein of all four saposins, prosaposin, triggers accumulation of these lipids as well as ILVs in lysosomes (Sandhoff and Sandhoff 2018). Most (glycol)sphingolipids destined for degradation reach the lysosome as part of ILVs and saposins mediate liberation of the substrate from these membranes thus making them accessible for lysosomal hydrolases (Wilkening *et al.* 2000). In the present study it was demonstrated that cholesterol packed into Sap A-containing picodiscs can be taken up by the LIMP-2 tunnel and thereby reaches the plasma membrane. While these data did not elucidate the mode of binding between the Sap A picodiscs and LIMP-2, they encourage follow-up studies that examine the potential relationship between these proteins in detail. Besides Sap A, interaction between Sap C and LIMP-2 could also be envisaged, since

Sap C is the activator protein for GCase in the degradation of glucosylceramide. In addition, GCase is able to transglucosylate cholesterol (Akiyama *et al.* 2013, Marques *et al.* 2016), a process which may also be aided by Sap C. As discussed below, glucosylated cholesterol could be a potential substrate for export facilitated by LIMP-2. Therefore, it would be interesting to investigate a possible role in saposins in general (and Sap A and C specifically) in facilitating the transfer of cholesterol and possibly other lipid degradation products to the tunnel opening of LIMP-2.

Recently, the crystal structure of a novel potential lipid transporter was reported (Wei *et al.* 2019) whose lysosomal localization had previously been demonstrated (Della Valle *et al.* 2006). The tertiary structure of ependymin-related protein 1 (EPDR1) comprises a distinct highly curved β-sheet fold and a hydrophobic groove that was previously only reported in bacterial proteins associated with lipoprotein transport (Takeda *et al.* 2003). Wei and colleagues further demonstrated that EPDR1 adopts a stable homodimer confirmation (Wei *et al.* 2019) and that at an acidic pH it can bind lipids present especially in membranes of ILVs, i.e. LBPA and monosialotetrahexosyl-ganglioside (GM1) (Schulze and Sandhoff 2014). Taken together, these characteristics of EPDR1 cause the authors to suggest a role for the dimer in binding and possibly extracting lipids as an activator protein similar to e.g. saposins A-D (Wei *et al.* 2019). If this assumption holds true it would be interesting to investigate whether LIMP-2 could be an acceptor of lipids extracted by EPDR1. While not much additional information regarding putative functions of EDPR1 are available at this point, it appears to be highly expressed in brain and is also present in heart, skeletal muscle, hematopoietic cells and was moreover found as a secreted protein in extracellular fluids (Apostolopoulos *et al.* 2001, Gregorio-King *et al.* 2002, Sleat *et al.* 2006, Sleat *et al.* 2007, Deshmukh *et al.* 2019). EPDR1 is associated with colorectal and prostate cancer as well as Dupuytren's disease (Riffo-Campos *et al.* 2016, Ng *et al.* 2017, Rosenberg *et al.* 2017). Recently, EPDR1 was identified as a novel batokine as part of the human brown adipocyte secretome (Deshmukh *et al.* 2019) and was proposed to fulfill functions critical for correct development of thermogenic adipocytes. Furthermore, EPDR1 deficiency in mice resulted in a pronounced accumulation of body fat, although the authors caution to over interpret these results due to the small number of mice analyzed. While the pathways in which EPDR1 may function remain to be elucidated, the data presented by Deshmukh et al indicate a role of EPDR1 as a metabolic regulator (Deshmukh *et al.* 2019). Overall, additional research is needed to elucidate the role of the putative lipid-binding protein in lysosomes.

5.2.4. Physiological relevance of LIMP-2-mediated cholesterol transport

LIMP-2 is broadly expressed in numerous cell types and tissues and appears to play an integral role in lysosome biogenesis. Yet, not all tissues lacking LIMP-2 are affected similarly, but on the contrary display a heterogeneous phenotype in mice and men (Gamp *et al.* 2003, Berkovic *et al.* 2008). This raises the question whether LIMP-2 function is more critical in some tissues than in others. Moreover, the existence of the LIMP-2 cholesterol export pathway despite the presence of the efficient NPC2-NPC1 lysosomal cholesterol export system is somewhat surprising and warrants further clarification as to what the physiological relevance of cholesterol transport by LIMP-2 is. A comparison of tissue expression patterns reveals that NPC1 and LIMP-2 are both abundant in liver, which is a key organ in the regulation of cholesterol metabolism (Figure 5-1). Expression of both proteins is moreover similar in several tissues, including kidney, pancreas, skin and bone. The most striking differences between expression of LIMP-2 and NPC1 are observed in heart, lung and fat tissues according to the bulk RNA sequencing data depicted in Figure 5-1. In all observed subtypes of fat tissue (brown, gonadal, mesenteric and subcutaneous fat) expression of LIMP-2 is strikingly higher than that of NPC1 and these expression patterns do not change significantly in younger or older mice according to the data available from the Tabula Muris Senis Consortium (https://twc-stanford.shinyapps.io/maca/) (Schaum *et al.* 2019). While the overall ubiquitous expression of NPC1 and LIMP-2 makes it unlikely that their respective cholesterol transport function is restricted to distinct tissues, the differences in expression described in fat tissue as well as heart and lung are worth further investigations.

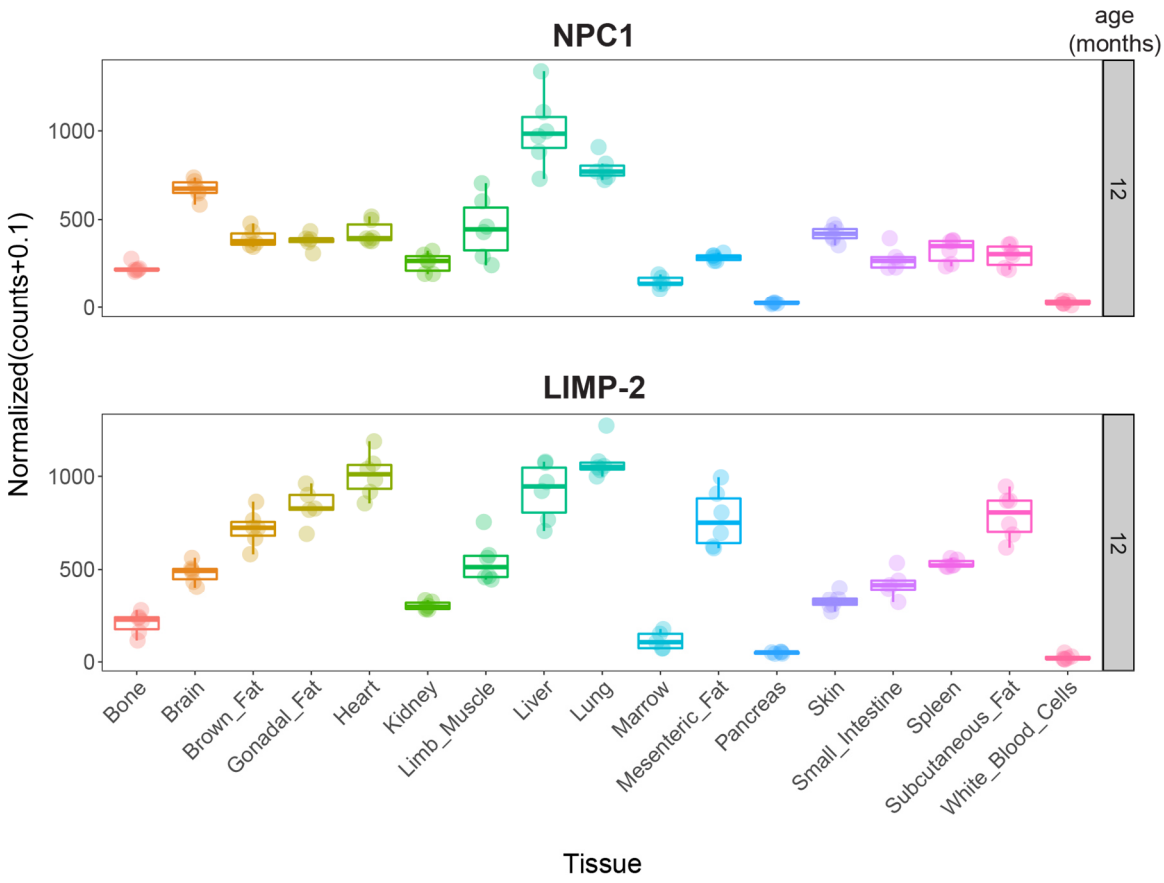

Figure 5-1: Tissue expression of NPC1 and LIMP-2 in mice 12 months of age. The data was derived from bulk RNA sequencing from various mouse tissues conducted by the Tabula Muris Senis Consortium (Schaum *et al.* 2019).

Based on the accumulation of putative cholesterol-like crystals in the cytoplasm of Schwann cells of LIMP-2 KO mice in the context of a demyelinating pathology and the importance of cholesterol for myelin, this cell type is further likely to specifically rely on the lipid transport function of LIMP-2 for correct cellular function. Cholesterol crystals are a hallmark in other pathologies as well: Such crystalline depositions of free cholesterol are characteristically observed in late stages of atherosclerotic plaque formation (Small 1988, Guyton and Klemp 1989). Accumulation of free cholesterol in lysosomes of macrophages/ foam cells during progression of plaque development has been documented as a consequence of increased lipoprotein-derived cholesteryl ester hydrolysis, ultimately leading to the formation of cholesterol crystals (Shio *et al.* 1979, Lewis *et al.* 1988, Tangirala *et al.* 1994). Tangirala and co-workers further observed that macrophage-derived cells had the capability to move cholesterol crystals within the cell (Tangirala *et al.* 1994) which encourages speculation that the cholesterol crystals observed in LIMP-2 KO Schwann cells may also be of lysosomal origin and result of intraluminal cholesterol accumulation due to defective cholesterol export in absence of LIMP-2. Of note, a role of LIMP-2 in the trafficking of myelin proteins, which are vital for maintaining structure and compactness of myelin, has been suggested since the protein levels of some of these proteins, i.e. protein zero (P0), peripheral myelin protein 22

kDa (PMP22) and myelin basic protein (MBP), are reduced in LIMP-2 KO mice (Gamp *et al.* 2003, Claussen 2005). To further study the role of LIMP-2 in the distribution of lipids and proteins in the highly specialized Schwann cells, the establishment of a cell culture model which can be utilized for some of the cell-based assays described in this study, e.g. filipin staining, would be useful. Furthermore, comparison of phenotypic traits of a mouse model harboring a LIMP-2 mutant with a blocked tunnel (LIMP-2.A379W/V415W) with those observed in the LIMP-2 KO should provide insight into the role the lipid transport function of LIMP-2 plays in the maintenance of Schwann cell physiology.

LIMP-2 is mainly targeted to lysosomes. However, a small pool of the protein can be found at the plasma membrane, possibly due to an independent trafficking mechanism (Blanz *et al.* 2015). The class B scavenger receptor protein family members CD36 and SR-BI are exclusively localized to the plasma membrane where they exert their lipid binding and transport function. A recent study established LIMP-2 as a phospholipid transporter at the plasma membrane (Conrad *et al.* 2017) which is a function that has also been proposed for CD36 and SR-BI (Rigotti *et al.* 1995). As mentioned earlier, Conrad et al published a crystal structure of a LIMP-2 dimer with two molecules of the phospholipid phosphatidylcholine attached to hydrophobic patches on the outside of the protein as well as cholesterol molecules inside the tunnel of the two monomers, respectively. They further sought to investigate LIMP-2's relationship to phospholipids and demonstrated that the protein can indeed transport phosphatidylcholine and, as a preferred substrate, phosphatidylserine (PS). Experiments involving PS-enriched liposomes and different endocytosis inhibitors demonstrated that in dimeric form, LIMP-2 mediates uptake of PS as a part of liposomes via dynamin-dependent endocytosis. The authors propose a role for LIMP-2 as a receptor for phospholipid-rich lipid vesicles at the cell surface (although the dimer is also present in lysosomes as indicated by bimolecular fluorescence complementation experiments) (Conrad *et al.* 2017). Could LIMP-2 also exert its lipid transport function at the plasma membrane similar to CD36 and SR-BI? While experiments reported in this thesis employ a chimeric mutant of LIMP-2 localizing to the plasma membrane, lipid binding and uptake was only observed at acidic pH and not at neutral pH, indicating that transport through the tunnel is restricted to the lysosomal environment. This view is further supported by a study published by Dang and colleagues (Dang *et al.* 2014). They report crystal structures of the LIMP-2 luminal domain both at neutral and acidic pH which demonstrate that at neutral pH the opening of the tunnel is obstructed by helices α5 and α7 and profound structural rearrangement of these helices that are observed at acidic pH is necessary to facilitate opening of the tunnel. These structural rearrangements are likely triggered by alteration of the protonation state of residue H150 (Dang *et al.* 2014). Taken together, the data reported by Dang et al and in this thesis favor a restriction of the lipid transfer function of LIMP-2 to late endosomes/ lysosomes. Of note, PS internalized as part of LIMP-2-

bound liposomes partially localized to lysosomes (Conrad *et al.* 2017). It is tempting to speculate that LIMP-2 may facilitate the re-distribution of phospholipids once the LIMP-2 tunnel opens in response to the acidic pH of lysosomes.

5.2.5. Potential additional substrates for the LIMP-2 tunnel

Similar to CD36 and SR-BI which can transport several ligands, including fatty acids, free cholesterol, cholesteryl esters, phospholipids and pheromones, the hydrophobic cavity of LIMP-2 is not exclusively occupied by free cholesterol. As mentioned above, phosphatidylcholine molecules were partially immersed in the tunnel of LIMP-2 (Conrad *et al.* 2017). Moreover, the first reported crystal structure contained a polyethylenglycol molecule, which was likely acquired from the crystallization buffer (Neculai *et al.* 2013) and indicates that small hydrophilic molecules may enter the tunnel. Furthermore, two molecules of the basic sphingolipid sphingosine can fit into the tunnel domain simultaneously as indicated by molecular docking simulations (Dang *et al.* 2014).

While experimental evidence for direct transport of lipids other than cholesterol through the LIMP-2 cavity are currently lacking, several scenarios can be imagined and are discussed in the following paragraphs.

Several groups described the ability of GCase (as well as GBA2, a non-lysosomal *β*-glucosidase) to transfer glucose groups between its substrate glucosylceramide (GlcCer) and cholesterol (Akiyama *et al.* 2013, Marques *et al.* 2016). This transglucosylation yields glucosyl-*β*-D-cholesterol or 1-*O*-cholesteryl- *β*-D-glucopyranoside (GlcChol). The study by Marques and colleagues revealed that GlcChol occurs naturally in many mammalian tissues and especially lung, brain, sciatic nerve and thymus contained high amounts of the lipid. Notably, the authors point out that in brain and sciatic nerve, the measured GlcChol may partly represent a different form of glycosylated cholesterol, e.g. galactosyl-*β*-D-cholesterol, as recombinant GCase was not able to hydrolyze the quantified structure to the same extent as in other tissues (Marques *et al.* 2016). Intriguingly, in most tissues of LIMP-2 KO mice, GlcChol is increased 1.5-fold in comparison to WT mice and in fat tissue and in highly purified lysosomes from hepatocytes the increase is even more pronounced (unpublished data, Prof. Dr. J.M.F.G. Aerts). A scenario seems possible where GCase generates GlcChol after hydrolysis of GlcCer and transfers the lipid to the LIMP-2 tunnel for export, possibly with the aid of saposins A/C. On the other hand, since GCase appears to predominantly catalyze the deglycosylation of GlcChol under basal conditions (Marques *et al.* 2016, Akiyama *et al.* 2020), cholesterol transported by LIMP-2 may be derived from a pool of lysosomal glucosylated cholesterol which is hydrolyzed by GCase and transferred to LIMP-2 as suggested above. Alternatively, transfer of the lipid to LIMP-2 may be accomplished by another lipid transfer protein (Figure 5-2).

Not much is known about the metabolic impact of GlcChol, except that induces expression of heat shock protein 70 (HSP70) following an increase in its biosynthesis as a consequence of heat shock. It therefore might play a role in the early stage of stress responsive signal transduction (Kunimoto *et al.* 2000, Kunimoto *et al.* 2002, Kunimoto *et al.* 2003). Since the addition of glucose increases the water solubility of the lipid, GlcChol may serve as a transport form of cholesterol (Marques *et al.* 2016). Besides utilizing biochemical assays described in this thesis and a traceable, i.e. fluorescently labelled GlcChol compound, to determine if LIMP-2 is capable of transporting GlcChol, molecular dynamic simulations would be a useful tool to investigate if the lipid would fit inside the LIMP-2 cavity similarly to free cholesterol (Heybrock *et al.* 2019).

In a recent study, Akiyama and colleagues confirmed the presence of and additional sterylglycosides, *β*-sitosterylglucoside (1-*O*-sitosteryl-*β*-D-glucopyranoside, *β*-GlcSito) and *β*-cholesterylgalactoside (1-*O*-cholesteryl-*β*-D-galactopyranoside, *β*-GalChol), in rodent and fish brain tissue (Akiyama *et al.* 2020). They further demonstrated the *in vitro* ability of lysosomal GCase (GBA1) as well as non-lysosomal GCase (GBA2) to perform transgalactosylation reactions by transferring a galactose residue from galactosylceramide (GalCer) to cholesterol. However, glucose derived from GlcCer seems to be the preferred substrate for transglycosylation reactions.

While the physiological relevance of these sterylglycosides and their function in lysosomes need to be investigated further, the addition of a sugar moiety likely adds to the already diverse functions of cholesterol. It should also be considered that additional glycosylated derivatives of cholesterol may exist in lysosomes.

Finally, cholesterol can be modified by oxidation which occurs preferentially at the carbon atoms at positions 4-7, but does also include side chain oxidation (Dias *et al.* 2019). Similar to unmodified cholesterol, oxysterols are incorporated into (ox)LDL particles and reach the lysosome via endocytosis. Since LIMP-2 can transport LDL-derived cholesterol, a similar function of LIMP-2 in the cellular re-distribution of oxysterols should be investigated.

The possibility of LIMP-2-mediated transport of phospholipids out of lysosomes following internalization of liposomes is discussed above (5.2.4). In their study, Dang et al clarify how enterovirus71 (EV71) binds to the apical domain of cell surface-located LIMP-2 which triggers internalization of the virus-receptor complex (Dang *et al.* 2014). The conformational changes in LIMP-2's luminal domain that are triggered by the acidification of late endosomes/ lysosomes open the tunnel and presumably enable the transfer of a so-called 'pocket-factor' from the capsid of the virus to the tunnel of LIMP-2. This in turn triggers the uncoating of the virus and release of its RNA into the cytosol. In the case of EV71, the pocket factor consists of

a sphingosine molecule. In their model, Dang and colleagues propose transfer of the sphingosine molecule through the LIMP-2 tunnel to the lysosomal membrane (Dang *et al.* 2014).

Sphingosine has also diverse function in the cell's metabolism, including regulation of membrane fluidity, cell growth arrest, apoptosis and lysosomal calcium release (Cuvillier 2002, Suzuki *et al.* 2004, Hoglinger *et al.* 2015). It is generated by hydrolysis of ceramide by ceramidases which reside in numerous cellular compartments like the plasma membrane, ER, Golgi and lysosomes (Bernardo *et al.* 1995, Hwang *et al.* 2005, Xu *et al.* 2006). Sphingosine is one among several lipids to accumulate in lysosomes as a consequence of loss of NPC1 (Lloyd-Evans *et al.* 2008, Hoglinger *et al.* 2015). However, a direct involvement of NPC1 in export of sphingosine has not been demonstrated. On the contrary, Blom and co-workers demonstrated that sphingosine efflux is not dependent on NPC1 function and they hypothesize that the increase in sphingosine that is characteristic for NPC1 deficiency is largely extralysosomal (Blom *et al.* 2012).

Interestingly, mouse embryonic fibroblasts deficient for LIMP-2 accumulate a catabolite of sphingosine, glucosylsphingosine (GlcSph) (data not shown) as do multiple tissues of LIMP-2 KO mice (unpublished data, Prof. Dr. J.M.F.G. Aerts). Moreover, high concentrations of the lipid were found in plasma of LIMP-deficient mice and Action Myoclonus Renal Failure Syndrome (AMRF) patients (Gaspar *et al.* 2014). The accumulation of GlcSph is much more prominent than that of the primary substrate of GCase, GlcCer, indicating that in absence of GCase (as a consequence of LIMP-2 deficiency) GlcCer is efficiently deacylated to GlcSph by acid ceramidase (Ferraz *et al.* 2016).

No lysosomal exporter for sphingosine and glucosylsphingosine has been described to date. Since the former was demonstrated to fit into the tunnel (Dang *et al.* 2014) and could also be cross-linked to the LIMP-2 luminal domain (this study) and the latter accumulates in absence of LIMP-2 as described in the previous paragraph, an involvement of LIMP-2 in the transport of these sphingolipids should be considered and experimentally addressed. A useful assay was introduced by Blom and colleagues where they complexed ^{3}H-labelled sphingosine or a fluorescent sphingosine analog, BODIPY-sphingosine, with LDL particles to ensure physiological targeting to lysosomes (Blom *et al.* 2012). Determination ^{3}H-labelled sphingosine in lysosomes isolated from WT and LIMP-2 deficient cells as well as microscopic analysis of the distribution of BODIPY-sphingosine in the aforementioned cells could be employed to elucidate whether LIMP-2 is able to transport these lipids. Of note, the observation that GlcSph levels are also elevated in Gaucher pathology despite the presence of LIMP-2 does not necessarily exclude LIMP-2-mediated GlcSph transport since the increase in GlcSph is most

prominent in plasma of patients and in the characteristic macrophage-derived Gaucher cells, in which GlcSph is likely secreted, thereby bypassing a putative lysosomal export route.

The GCase substrate itself, glucosylceramide, as well as the degradation product, ceramide, have been hypothesized to be substrates of the LIMP-2 tunnel as well (Zhao *et al.* 2014, Zunke *et al.* 2016), albeit substantial data for this has yet to be provided. In the lipid crosslinking experiment described in this study, the LIMP-2 luminal domain associated with ceramide to the same extent as sphingosine. Farber disease which stems from defects of the lysosomal enzyme acid ceramidase (ASAH1) is characterized by accumulation of ceramide (Yu *et al.* 2018). In light of a potential transport function by LIMP-2 it would be interesting to investigate if overexpression of LIMP-2 could alleviate the lipid accumulation in a cell model of the disease.

Microscopy analyses described in this thesis demonstrated the ability of LIMP-2 to bind to fluorescently labelled LDL particles and transport LDL-derived cholesterol. In lysosomes, lipids contained inside the core of LDL particles are released and hydrolyzed by action of lysosomal acid lipase as described in 1.1.1. While the experiments in this study focused on the fate of liberated free cholesterol, the other lipid species of LDL particles, triglycerides and fatty acids also need to be recycled from lysosomes. To date, no genuine lysosomal exporter for fatty acids has been described.

Thus, several lipids can and should be considered as potential substrates for the LIMP-2 tunnel and careful experimental analysis should help to clarify which lipids are indeed transported by LIMP-2 in a physiological setting.

All in all, the identification of LIMP-2 as a cholesterol transporter is an important milestone in unraveling the function of the intramolecular tunnel in LIMP-2. A summary of potential pathways and putative pools of lysosomal cholesterol designated for export through the LIMP-2 tunnel is depicted in Figure 5-2. Future research should focus on identifying the intralysosomal pathways by which cholesterol reaches the tunnel entrance of LIMP-2 and additional lipid substrates are likely to be identified.

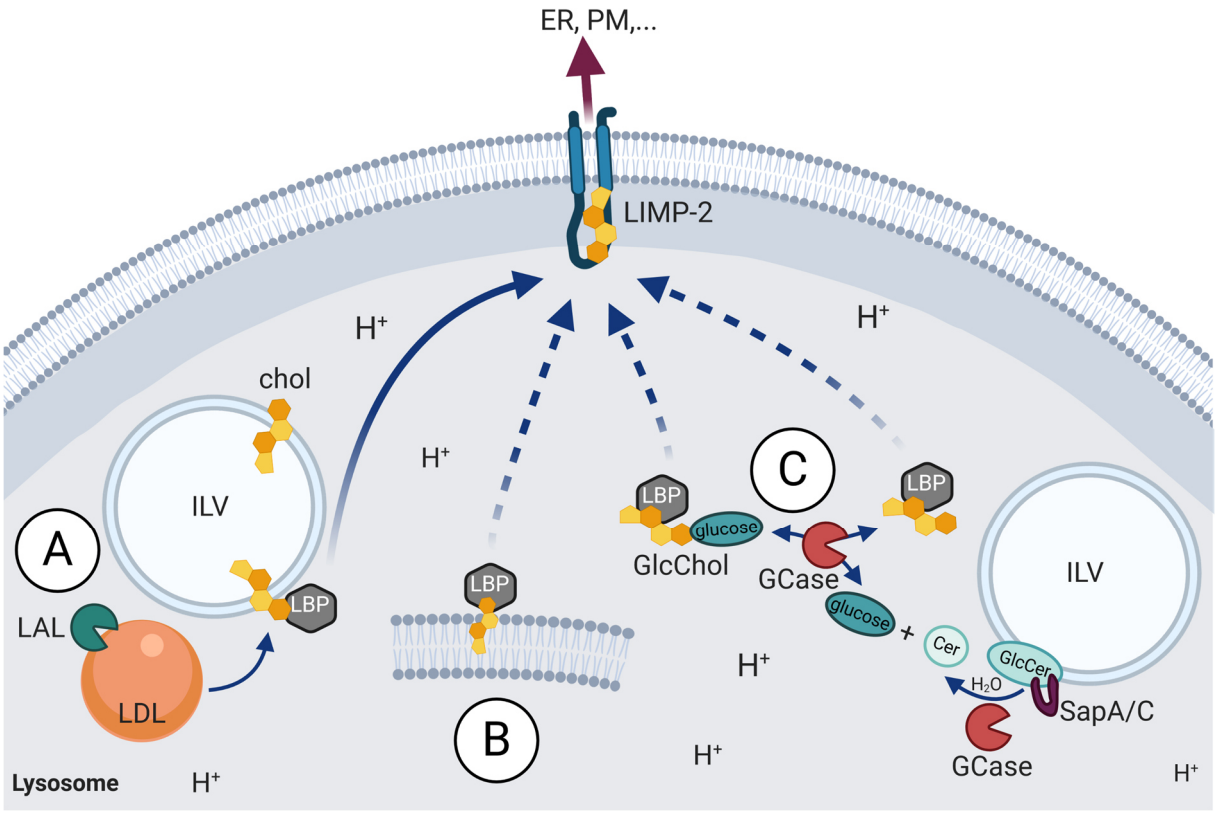

Figure 5-2: Pools of lysosomal cholesterol that may utilize LIMP-2 for export. A Cholesterol (chol) liberated from LDL particles by lysosomal acid lipase (LAL) rapidly integrates into membranes of intraluminal vesicles (ILV). From here, NPC2 transfers cholesterol to NPC1 (not pictured). In addition, another lipid binding protein (LBP), e.g. a saposin, binds and targets cholesterol to the tunnel entrance in the luminal domain of LIMP-2. **B** Intracellular membranes are degraded in lysosomes as a result of autophagy and therefore might provide a second pool of cholesterol that needs to be recycled. Again, the transfer of the lipid to LIMP-2 likely involves a lipid binding protein. **C** Degradation of glucosylceramide (GlcCer) by acid β-glucocerebrosidase (GCase) yields ceramide (Cer) and glucose. GCase likely also catalyzes the transfer of the glucose to cholesterol, thus forming glucosylated cholesterol (GlcChol). Furthermore, it catalyzes the reverse reaction, hydrolysis of GlcChol to cholesterol and glucose. GlcChol and newly deglucosylated cholesterol may also follow the LIMP-2 pathway for exit from lysosomes with the help of a lipid binding protein. Of note, a similar scenario might apply for other sterylglycosides, e.g. galactosylated cholesterol (GalChol). Since saposins A and especially C (SapA/C) are intimately involved in the processes catalyzed by GCase, they are likely candidates for the role of the so-far elusive lipid transfer protein for LIMP-2. Furthermore, LIMP-2 may be involved in transporting other lipids derived from LDL particles or products of sphingolipid degradation as well (see text).

5.3. A potential role for LIMP-2 at membrane contact sites

An increasing body of experimental evidence is forming that highlights the importance of nutrient exchange between cellular organelles mediated by membrane contact sites (MCS) (Di Mattia *et al.* 2020). Late endosomes and lysosomes form contact sites with ER, plasma membrane and peroxisomes to re-distribute sterols throughout the cell (Thelen and Zoncu 2017, Meng *et al.* 2020). Various proteins are involved in the establishment and maintenance of the contact sites. Interestingly, in this study electron microscopy analysis of mouse embryonic fibroblast (MEF) cells overexpressing LIMP-2 demonstrated that LIMP-2 localizes to areas of close contact between lysosomes and the ER. Morphological changes of stretches of the ER in close proximity to endosomes/ lysosomes were further observed in these cells.

Following the identification of putative interacting proteins for LIMP-2 in a proximity-dependent biotin identification (BioID) assay, co-immunoprecipitation studies indeed demonstrated that LIMP-2 can interact with the ER proteins VAPA, VAPB and Gramd1b as well as with the endolysosomal protein STARD3. All of these proteins are involved in forming contact sites between the organelle they are residing in and several others (Alpy *et al.* 2013, Gatta *et al.* 2015, Wilhelm *et al.* 2017, Sandhu *et al.* 2018). These observations intriguingly suggest an extension of the role of LIMP-2 in the re-distribution of sterols and potentially other lipids beyond simply facilitating the export from lysosomes.

5.3.1. Interaction of LIMP-2 with ER contact site proteins is regulated by lipids

The demonstration of an association of LIMP-2 with VAPA, VAPB, Gramd1b and STARD3 by co-immunoprecipitation was followed by the question of how these interactions might be regulated. Gramd1b also interacts with NPC1, presumably forming ER-lysosome contacts to transfer cholesterol following export by NPC1 (Hoglinger *et al.* 2019). Electron microscopy and co-immunoprecipitation experiments revealed that NPC1 only localizes to lysosome-ER contact sites under conditions of ample cholesterol. Consequently the interaction between Gramd1b and NPC1 was decreased upon induced lipoprotein starvation (Hoglinger *et al.* 2019).

The sterol environment of the cell proved to be a regulatory factor for the interaction of LIMP-2 and the aforementioned contact site proteins as well. Lipid starvation led to a decreased co-precipitation of VAPB and STARD3, respectively. Notably, this effect was not observed with Gramd1b. To further investigate how the availability of lipid influences LIMP-2 and its interaction partners, the co-localization of these proteins should be analyzed by indirect immunofluorescence and electron microscopy under conditions of ample lipids and lipoprotein starvation. The sub-membrane distribution of LIMP-2 and STARD3 are of special interest, since both proteins reside in the same membrane. To clarify whether LIMP-2 and STARD3 might localize to different domains in the lysosomal membrane upon lipid starvation, super-resolution techniques as mentioned earlier are required.

Finally, as a control for the validity and specificity of the observed effects caused by lipid depletion, a rescue experiment should be included where LDL is replenished after a period of starvation which should presumably restore the interaction between LIMP-2 and STARD3 and VAPB.

5.3.2. Possible mode of interaction between LIMP-2 and ER-contact site proteins

According to the protein interaction data base bioGRID, in humans over 300 and 200 physical interactor partners have been documented for the VAPA and VAPB, respectively (Chatr-Aryamontri *et al.* 2017). The binding of these interactors to VAP proteins is mediated by a small linear motif termed two phenylalanines (FF) in an acidic tract (AT) (FFAT) which interacts with the cytoplasmic major sperm protein (MSP) domain of the VAP proteins (Figure 5-3 B). The optimal core of the FFAT motif consists of the amino acids EFFDAxE, where x can be any amino acid. This motif is for instance present in members of the lipid binding and transfer proteins belonging to the oxysterol binding protein (OSBP)-relate proteins (ORPs) (Loewen *et al.* 2003). However, variations of this motif exist in proteins that still interact with VAPA/B. STARD3 (previously named metastatic lymph node 64, MLN64) and STARD3 N-terminal like (STARD3NL) interact with VAPs via a FFAT-like motif (QFYSPPE) (Alpy *et al.* 2013). A recent study by Slee and Levine screened eukaryotic proteomes for novel uncanonical FFAT motifs by using a position weight matrix (PWM) that predicted several new potential VAP-binding proteins with suboptimal FFAT motifs (Slee and Levine 2019).

The cytoplasmic domains of human and murine LIMP-2 are very short (6 residues in N-terminus, 22 residues in C-terminus (Holmes 2012)) and do not contain a FFAT-like motif Figure 5-3 A. It is therefore difficult to imagine a direct interaction between LIMP-2 and VAPs unless the mechanism deviates from the established MSP domain-FFAT motif binding. Alternatively, interaction between LIMP-2 and VAPs might be of indirect nature, i.e. as part of a bigger protein complex.

STARD3 (previously named metastatic lymph node 64, MLN64) is a ubiquitously expressed membrane protein residing in late endosomes (Alpy *et al.* 2001) and as described above forms tethers with the ER by interaction with VAP proteins. It is comprised of a conserved membrane-spanning metastatic lymph node 64 N-terminal (MENTAL) domain with four transmembrane helices (Alpy *et al.* 2005) and a large C-terminal cytosolic domain containing a conserved approximately 210 amino acid long StAR (steroidogenic acute regulatory protein) related lipid transfer (START) domain (Ponting and Aravind 1999), as schematically depicted in Figure 5-3 B. The START domain forms a hydrophobic lipid binding pocket which for STARD3 is specific for cholesterol (Alpy and Tomasetto 2005) and known to transfer cholesterol from as well as to the ER (Alpy *et al.* 2013, Wilhelm *et al.* 2017).

For the reasons outlined above instead of actively forming lysosome-ER contact sites, LIMP-2 possibly interacts with STARD3 and transfers lysosome-derived cholesterol to STARD3 which in turn interacts with VAPs and transfers the cholesterol molecules with its START domain. The MENTAL is involved in homo- and heteromeric interaction between STARD3 and

STARD3NL, respectively, and also contains the FFAT motif required for interaction with VAPB (Alpy *et al.* 2013) and therefore might also be involved in mediating interaction with LIMP-2. One way to test if the interaction is mediated by the MENTAL or the START domain of STARD3 would be to test whether LIMP-2 also associates with STARD3NL which also possesses the highly conserved MENTAL domain, but lacks the C-terminal START domain (Alpy *et al.* 2005).

In this scenario it is feasible to assume that the interaction between LIMP-2 and STARD3 and the subsequent tethering of VAPB is dependent on the lipid availability which corresponds to the observed decrease of interaction between LIMP-2 and STARD3 under lipoprotein starvation conditions. In addition, the interaction of the two proteins may be mediated or regulated by posttranslational modifications as outlined in 5.4.3. and in Figure 5-5.

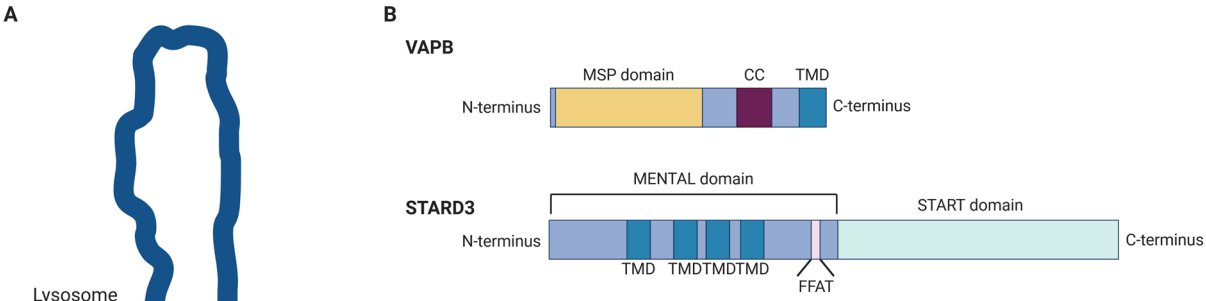

Figure 5-3: Schematic depiction of the domains of LIMP-2, VAPB and STARD3. A Domain structure of LIMP-2 with cytosolic amino acids depicted as small circles with single letter amino acid code. Cysteines subject to palmitoylation highlighted in purple. Di-leucine motif necessary for lysosomal targeting of LIMP-2 (Janvier *et al.* 2003) highlighted in green. **B** Depiction of distinct protein domains and binding motifs in VAPB and STARD3. MSP, major sperm protein domain; CC, coiled-coiled domain; TMD, transmembrane domain; MENTAL, metastatic lymph node 64 N-terminal; FFAT, two phenylalanines (FF) in an acidic tract (AT); START, StAR (steroidogenic acute regulatory protein) related lipid transfer.

Regarding Gramd1b (also called Aster B), it has been shown that the GRAM domain of the protein can directly bind phospholipids. When the cholesterol concentration in the plasma membrane reaches a critical threshold, the GRAM domain of Gramd1b is recruited to the phosphatidylserine (PS)-rich inner leaflet of the plasma membrane, thereby reducing the distance between ER and plasma membrane and enabling nonvesicular transfer of cholesterol from the plasma membrane to the ER (Sandhu *et al.* 2018). How Gramd1b binding to PS is facilitated in detail is currently unknown, but appears to be dependent on the amount of accessible cholesterol in the plasma membrane, possibly due to alterations in the presentation of PS in the inner leaflet of the plasma membrane due to cholesterol accumulation (Naito *et al.* 2019, Ferrari *et al.* 2020). Besides being involved in re-distribution of cholesterol at the plasma membrane, Gramd1b is also recruited to ER-lysosome MCS where it interacts with NPC1 and facilitate lysosome-to-ER cholesterol transfer (Hoglinger *et al.* 2019) in a sterol-dependent

manner. However, the interaction sites in either protein have not been characterized yet. While the co-immunoprecipitation experiments presented in this study indicate an interaction between Gramd1b and LIMP-2 as well, in contrast to the association between Gramd1b and NPC1 this was not found to be sensitive to the cellular sterol availability. The observation of unspecific binding of the GFP-tagged Gramd1b construct to the superparamagnetic beads used for the immunoprecipitation experiments described in this study warrants repetition of the described experiments, preferably with an untagged construct or endogenously, to evaluate the validity of the observed interaction between LIMP-2 and Gramd1b.

To understand more precisely the role of LIMP-2 at these contact sites, the total number of contact sites present in LIMP-2 WT and KO cells should be analyzed using electron microscopy or super-resolution microscopy techniques like structured illumination microscopy (SIM) or stimulation emission depletion (STED) microscopy. In the evaluation of these experiments has to be considered though that the VAP proteins, Gramd1b and STARD3 form contact sites with multiple proteins, so lack of LIMP-2 is unlikely to cause complete absence of contact sites between the ER and lysosomes.

Additionally, 3D live-cell imaging could be a useful approach to capture an informative number of the transient contact sites and avoid creation of artefacts that could stem from analyzing only a snap shot of contacts present in fixed cells and focusing the analysis only on one focal plane. This could clarify whether LIMP-2 is an integral part in forming these contacts or is rather utilizing areas of proximity between the ER and lysosomes to shuttle e.g. cholesterol from the limiting lysosomal membrane to the ER with the help of its interactors.

5.4. LIMP-2 is a multi-palmitoylated protein

The posttranslational modification palmitoylation, especially on cysteine residues (S-palmitoylation), has been gaining attention in recent years as a dynamic and widespread regulatory mechanism for protein stability, signaling, subcellular distribution, protein-protein interaction and more. Technical advances regarding the detection and identification of palmitoylated proteins allowed assessment of palmitoylated proteins on a proteome-wide scale. According to current knowledge, approximately 10 % of the proteins encoded in the genome are palmitoylated (Sanders *et al.* 2015). LIMP-2 was identified as a putatively palmitoylated protein in several proteomics studies (Blanc *et al.* 2015, Sanders *et al.* 2015), but experimental validation has been lacking so far. The data presented in this study confirms that LIMP-2 is indeed palmitoylated. In fact, an acyl-PEG exchange gel shift (APEGS) assay that allows semi-quantitative assessment of different palmitoylation states of a protein indicated that almost the complete pool of LIMP-2 present in HeLa cells is constitutively palmitoylated, indicating that this lipidation has a vital role for LIMP-2 function.

5.4.1. Characterization of the palmitoylation sites in LIMP-2

Palmitoylation primarily occurs on cytoplasmic domains of proteins where the amino acid residues are accessible to palmitoyltransferases (Zaballa and van der Goot 2018), but modification on residues within transmembrane domains has been reported as well (Rodenburg *et al.* 2017). The cytosolic N- and C-termini of LIMP-2 contain three cysteine residues in total and as analysis of palmitoylation site mutants of LIMP-2 could show, all three cysteines are subject to palmitoylation since only mutation of all cytosolic cysteine residues in LIMP-2 abolished palmitoylation. This observation is further supported by the data from the APEGS assay revealing 3 distinct bands migrating at different molecular weights on the SDS-PAGE indicating that LIMP-2 exists in different palmitoylation states within the cell. From this analysis it can however not be deduced which residues are favorably subjected to the lipidation. The occurrence of the two neighboring cysteines in LIMP-2's short N-terminus warrant special attention. Such double palmitoylation sites were proposed to trigger membrane embedding of the cysteine residues thus leading to inaccessibility to thioesterases which renders the palmitoylation irreversible (Dallavilla *et al.* 2016, Zaballa and van der Goot 2018). For the ER chaperone calnexin it was shown that palmitoylation at two adjacent cysteine residues occurs sequentially (Dallavilla *et al.* 2016): One cysteine is palmitoylated first which renders the second cysteine readily available for further palmitoylation. While the single palmitoylated calnexin pool can be rapidly de-palmitoylated by thioesterases, the palmitoylation of both sites drastically slowed down the removal which is reflected in the observation that in comparison to the non-palmitoylated or fully palmitoylated pools of calnexin, the pool of single palmitoylated species is very small (Dallavilla *et al.* 2016). Interestingly, the immunoblot signal intensity of the single palmitoylated species of LIMP-2 observed in the APEGS assay is also much weaker than the double and triple palmitoylated ones, suggesting that palmitoylation of the double cysteines in LIMP-2' N-terminus might be regulated in a similar way.

5.4.2. What role does palmitoylation play for LIMP-2 function?

As mentioned earlier, the effects palmitoylation can have on a protein are diverse and can even be opposite in different proteins (e.g. increasing or decreasing protein stability). A frequent function of palmitoylation is modulation of subcellular location. For instance, while absent palmitoylation does not abolish plasma membrane localization of CD36, it is required for efficient incorporation into detergent-resistant membrane rafts (Thorne *et al.* 2010). Moreover, palmitoylation is important for correct post-translational processing at the ER. Palmitoylation is also a prerequisite for ER export of amyloid precursor protein (APP) (Bhattacharyya *et al.* 2013) as well as for export of low-density lipoprotein receptor-related

protein 6 (LRP6), which is a co-receptor of Wnt. The latter protein has a transmembrane domain (TMD) that exceeds the thickness of the ER membrane and hence might trigger the unfolded protein response due to hydrophobic mismatch. Tilting of the membrane domain by palmitoylation of two juxtamembrane cysteine residues was suggested to avoid the mismatch, thus favoring ER export (Abrami *et al.* 2008). The transmembrane domain of LRP6 consists of 23 amino acids. The TMDs of LIMP-2 are similar in length (23 and 24 amino acids, respectively (Holmes 2012)) and therefore palmitoylation can be envisaged as a requirement for ER exit by LIMP-2. However, multiple lines of evidence suggest that this is indeed not the case. Overexpression of a palmitoylation-deficient LIMP-2 mutant (LIMP-2.P3x) yielded a comparable degree of co-localization with the lysosomal protein LAMP-2 as did overexpression of WT LIMP-2. In contrast to CD36, it was also found in detergent resistant membranes to a similar degree as WT LIMP-2 (data not shown). Moreover, LIMP-2.P3x did not exhibit sensitivity to digestion by endoglycosidase H (endo H) which indicates attachment of complex glycans acquired in the Golgi (data not shown). Overall, the posttranslational processing and lysosomal targeting of LIMP-2 was found to be normal in absence of palmitoylation. Western blot analysis of LIMP-2.P3x did further not indicate an overt reduced stability of the protein.

Strikingly, overexpression of LIMP-2.P3x in HeLa LIMP-2 KO cells led to an increase in size and potentially also number of lysosomes in comparison to overexpression of LIMP-2.WT. Previous studies uncovered a role for LIMP-2 in lysosomal biogenesis and morphology (Kuronita *et al.* 2002). The observations made in this study further indicate that palmitoylation of LIMP-2 could be involved in this function. It should be noted, however, that the studied HeLa LIMP-2 KO cells were transfected transiently with LIMP-2.WT and palmitoylation-deficient mutant and transfection efficiency and expression rate are difficult to compare under these conditions. To avoid variations and experimental artefacts caused by transient transfection of cells, a CRISPR knock-in cell line expressing either LIMP-2.WT or LIMP-2.Px (in HeLa LIMP-2 KO cells) would be useful for further analysis of the potential influence of LIMP-2 palmitoylation on lysosome morphology and biogenesis.

As mentioned earlier, LIMP-2 is able to form homodimers and dimer formation has recently been implicated in binding phosphatidylserine-rich liposomes (Conrad *et al.* 2017). While the denaturing conditions used to separate proteins via SDS-PAGE usually disrupt protein-protein interaction, a fraction of the LIMP-2 dimer pool could be detected in cell lysates separated via SDS-PAGE (Conrad *et al.* 2017). As Figure 5-4 depicts, the presumed dimer fraction was decreased in HeLa LIMP-2 KO cells transfected with LIMP-2.P3x. Follow-up experiments involving separation of protein lysates under non-denaturing conditions as well as co-immunoprecipitation studies using two differentially tagged LIMP-2.P3x constructs should be

employed to validate the hypothesis that palmitoylation is important for dimerization of LIMP-2. If that is indeed the case, it would furthermore be of interest to investigate if a palmitoylation deficient LIMP-2 mutant can still be found on the surface of some cell types as reported for LIMP-2 (Conrad *et al.* 2017).

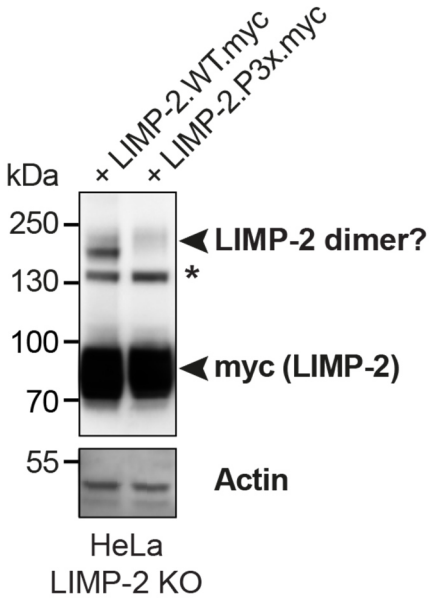

Figure 5-4: Palmitoylation of LIMP-2 potentially important for dimer formation. HeLa LIMP-2 KO cells were transiently expressing murine LIMP-2.WT.myc or LIMP-2.P3x.myc, respectively. Detection of transfected LIMP-2 was accomplished with an antibody recognizing the myc tag of either construct. A strong signal was detected between 70 kDa and 100 kDa corresponding to the molecular weight of glycosylated monomeric LIMP-2. In addition, a signal at > 130 kDa was detected for LIMP-2.WT while it was nearly absent for LIMP-2.P3x. The asterisk denotes an unspecific signal.

5.4.3. Palmitoylation influences the LIMP-2 interaction network at lysosome-ER contact sites

Another potential function for LIMP-2 palmitoylation is the regulation of its interaction with proteins at the cytosolic face of the lysosomal membrane. The interaction of LIMP-2 with STARD3 and VAPB, respectively, was decreased by absence of lipids (see 4.4.3) as well as by absence of palmitoylation of LIMP-2 (4.5.3.2). However, lipid depletion did not cause de-palmitoylation of LIMP-2 (data not shown). Therefore, the underlying causes for the observed decrease in interaction might be separate. It can be conceivable that STARD3 and LIMP-2 preferentially localize to ER-Lysosome contact sites under conditions of sufficient lipid supply. In order to transfer newly exported cholesterol to STARD3, LIMP-2 requires palmitoylation which possibly tilts the membrane domains or arranges the N- or C-terminus of LIMP-2 such that interaction with STARD3 is enabled. A schematic model for this hypothesis is depicted in Figure 5-5. The model further indicates that LIMP-2 is not directly interacting with VAPB, but the three proteins might also form a large oligomeric complex that acts as a cholesterol transfer network. Notably, both VAPB and STARD3 form homodimers and thus may contribute to the formation of large complexes (Alpy *et al.* 2013) that may include monomers or dimers of LIMP-2. Separation of the native protein complexes under non-denaturing electrophoresis conditions (Blue Native PAGE) followed by immunoblotting might clarify if all three proteins can indeed

be found in a protein complex. Furthermore, the co-immunoprecipitation studies described in this study need to be validated with experiments using endogenous proteins.

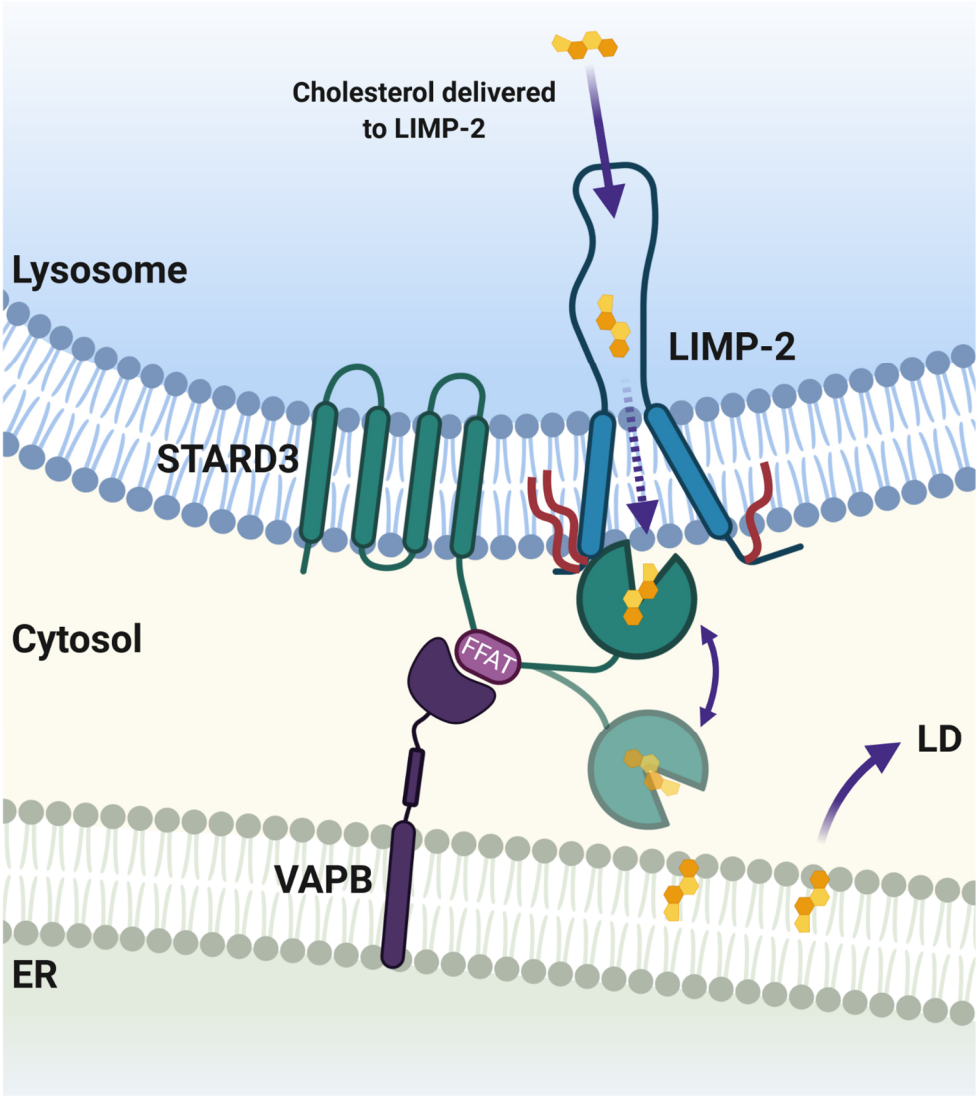

Figure 5-5: Proposal for a cholesterol transfer network formed by LIMP-2, STARD3 and VAPB under lipid-rich conditions. Binding of VAPB to the FFAT amino acid motif in the C-terminal domain of STARD3 tethers the ER and lysosomes, allowing sterol exchange across this membrane contact site. Lysosome-derived cholesterol is transferred through the hydrophobic cavity inside the LIMP-2 luminal domain and to the START domain of STARD3 which also has a lipid-binding pocket. The StAR (steroidogenic acute regulatory protein) related lipid transfer (START) domain then transfers cholesterol between the opposing membranes. Palmitoylation of LIMP-2 might be necessary to mediate access of the START domain to cholesterol transported by LIMP-2. Alternatively, LIMP-2 might interact with the metastatic lymph node 64 N-terminal (MENTA)L domain of STARD3 which comprises the four transmembrane domains of the protein (not pictured) and transfers cholesterol to STARD3 by an unknown mechanism. In the case of lipid depletion, contact site formation might be decreased and STARD3 and LIMP-2 might not localize to the same section of the lysosomal membrane (not pictured).

Further research should also focus on characterizing the interaction between LIMP-2 and STARD3 and assess the function of palmitoylation in this context. STARD3's most prominent feature is its large C-terminal START domain of approximately 210 amino acids. Since this domain has a hydrophobic pocket to transfer cholesterol, it is feasible to assume that interaction of LIMP-2 and STARD3 involves this domain. As mentioned earlier, this hypothesis could be investigated by conducting co-immunoprecipitation studies with LIMP-2 and

STARD3NL which is highly similar to STARD3 in its MENTAL domain, but lacks the START domain (Alpy *et al.* 2013). In terms of identifying the interaction site for STARD3 in LIMP-2, binding of the LIMP-2 single palmitoylation mutants that were described in this study to STARD3 should provide a better understanding of which palmitoylation site might be critical for interaction between LIMP-2 and STARD3. For instance, a reduced co-immunoprecipitation of STARD3 with LIMP-2.C458S would suggest that the C-terminus and its palmitoylation are important for the interaction.

5.4.4. Which palmitoyltransferase(s) palmitoylate(s) LIMP-2?

The 23 described mammalian palmitoyltransferases (DHHCs or PATs) responsible for enzyme-mediated protein palmitoylation localize to various subcellular membranes (Figure 1-11) and some are furthermore only expressed in specific tissues (Jiang *et al.* 2018). The reversibility of palmitoylation, the diverse impacts it can have on the modified protein and the absence of a designated recognition motif add a further layer of complexity in regards to identifying which DHHC mediates the palmitoylation of a given protein. If palmitoylation is needed to confer correct folding of a newly synthesized protein and avoid degradation by the ER quality control machinery, an ER-resident DHHC enzyme is likely involved. On the other hand, if palmitoylation of a protein is meant to adapt to cellular stimuli by e.g. re-locating a protein or activate/deactivate enzymatic activity, it may occur many hours after a protein is synthesized. For instance, palmitoylation of the ER chaperone calnexin serves as a mechanism to post-translationally regulate the amount of calnexin (Dallavilla *et al.* 2016). Phosphorylation prevents rapid palmitoylation of calnexin by zDHHC6 in resting cells, which leads to the degradation of the bulk of newly synthesized calnexin, thereby allowing cells to fine-tune the calnexin content in the ER (Dallavilla *et al.* 2016).

Western Blot analysis and indirect immunofluorescence studies presented in this study indicate that lack of palmitoylation of LIMP-2 is not decreasing the protein's stability which would have been an indicator of protein misfolding. On the contrary, it might lead to a slightly prolonged half-life, although it cannot be excluded that the increase in protein amount of LIMP-2.P3x observed in Western Blot images might be a consequence of overexpression artefacts. Nevertheless, palmitoylation of LIMP-2 might occur in the ER and in fact, LIMP-2 does associate with the ER-resident palmitoyltransferase zDHH6. An Acyl-RAC assay using cells overexpressing an ER-retention mutant of LIMP-2 could be utilized to clarify whether palmitoylation of LIMP-2 indeed takes place in the ER.

Expression of LIMP-2 is ubiquitous in murine tissues, however, protein amount varies among different tissues (Figure 5-1). Interestingly, both palmitoyltransferases that were analyzed in this study, DHHC6 and DHHC20, respectively, are of relative high abundance in brown and

white adipose tissue (BAT and WAT, respectively) (Wang *et al.* 2019) where LIMP-2 is abundant as well. According to other studies, DHHC20 levels are elevated in thyroid, liver, colon, prostate, placenta, testis, liver and lung (Fukata *et al.* 2004, Ohno *et al.* 2006, Draper and Smith 2010). Expression of DHHC20 was low in kidney, heart and brain, on the other hand (Fukata *et al.* 2004, Ohno *et al.* 2006). DHHC6, on the other hand, appears to be widely expressed in various tissues and DHHC6 mRNA is especially abundant in kidney. No mRNA could be detected in placenta and lung, respectively (Ohno *et al.* 2006). The two palmitoyltransferases also differ in subcellular localization, with DHHC6 residing in the ER (Ohno *et al.* 2006, Dallavilla *et al.* 2016) and DHHC20 in the plasma membrane (Ohno *et al.* 2006), although a Golgi localization for DHHC20 has also been suggested (Rana *et al.* 2019).

While LIMP-2 associates with both DHHC6 and DHHC20, respectively, as evidenced by coIP studies described in this thesis this does not necessarily mean that LIMP-2 is palmitoylated by these enzymes. Some DHHC PATs exert additional functions which are independent of their palmitoylation activity (Lemonidis *et al.* 2014, Zaballa and van der Goot 2018) and therefore it cannot be excluded that association between LIMP-2 and the two described DHHC PATs is unrelated to LIMP-2's palmitoylation. As discussed before, overexpression of proteins may also increase the chances of false-positive hits in co-immunoprecipitation studies, however, due to the low abundancy of most DHHC enzymes, studying the interaction of the enzymes with their substrate proteins is challenging.

Generating cell lines lacking a DHHC PAT suspected of palmitoylating a protein of interest and subjecting cell lysates from this cell line to the Acyl-RAC assay could be an alternative method to establish DHHC-substrate pairs. Since it is unclear whether some DHHC PATs are redundant and therefore might be able to compensate for the loss of each other, it would be advisable to target multiple DHHC PATs at once, creating cell lines depleted of for instance 5 DHHC PATs at the same time. Once the range of DHHCs putatively modifying a protein of interest is narrowed down, individual DHHC KO cell lines could be examined. Limitations of this approach include that due to the tissue specificity of some DHHC PATs, they might not be present in the chosen cell line and furthermore, some DHHC PATs need to be activated by at least one other DHHC PAT. Loss of DHHC16 for example leads to loss of activity of DHHC6 (Abrami *et al.* 2017), thus absent palmitoylation of a protein of interest in a DHHC16 KO cell line might be due to the lack of DHHC6 activity and not that of DHHC16.

The data presented in this study confirm that LIMP-2 is subject to the post-translational modification palmitoylation. At the lysosome, palmitoylation is involved in LIMP-2's newly described role as a part of a putative cholesterol transfer hub between the lysosome and ER that includes the membrane contact site proteins STARD3 and VAPB. Furthermore, initial experiments seeking to identify the palmitoyltransferase responsible for lipidating LIMP-2

suggest two DHHC PATs, DHHC6 and DHHC20, as valid starting points for extending the knowledge of LIMP-2 palmitoylation by (a) DHHC PAT(s). However, many questions in the field of DHHC-mediated protein palmitoylation need to be elucidated and the diversity and heterogeneity of the so-far described DHHC palmitoyltransferases pose experimental obstacles that future research needs to overcome.

5.5. Outlook

The data reported in the present thesis extend the understanding of LIMP-2 biology by revealing several novel functions for the protein. It also extends the current knowledge about intracellular lipid transport.

Having demonstrated the ability of the LIMP-2 luminal domain to transport cholesterol, it will be interesting to analyze additional potential substrates for the tunnel as well as their possible physiological relevance. Derivatives of cholesterol like GlcChol are likely candidates and in fact, an accumulation of GlcChol has been observed in tissues from LIMP-2 KO mice (Prof. Dr. J.M.F.G. Aerts, unpublished data). Furthermore, a potential cell type- or tissue-specificity for cholesterol transport by LIMP-2 should be investigated to elucidate the differences between cholesterol transport mediated by NPC1 and LIMP-2, respectively. In this regard, the generation and analysis of a knock-in mouse model harboring a tunnel mutant of LIMP-2 might provide further insight into the physiological relevance of LIMP-2-mediated lipid transport and could also serve to further characterize the GCase-unrelated functions of LIMP-2, since the tunnel mutant should still be able to transport GCase to lysosomes. Comparison of the phenotypes of the LIMP-2 KO mouse model with that observed in a LIMP-2 tunnel mutant mouse model should help to clarify which defects observed in the LIMP-2 KO mouse model are secondary to the lack of lysosomal GCase.

The presence of LIMP-2 at ER-lysosome membrane contact sites and its putative participation in a sterol transfer network together with STARD3 and VAPB are exciting new aspects of LIMP-2 biology and the further characterization of LIMP-2's role at these contact sites will be topic of future research. Specifically, it would be of interest to analyze whether LIMP-2 mutants either lacking palmitoylation or a functional tunnel still localize to membrane contact sites as observed for LIMP-2 WT. Further, the interaction between LIMP-2 and membrane contact site proteins observed in co-immunoprecipitation studies should be verified by an independent method, such as bimolecular fluorescence complementation (BiFC), which enables observation of protein-protein interactions in live cells (Kerppola 2006).

Special attention is warranted in evaluating which factors contribute to as well as modulate LIMP-2's role at membrane sites since the data described in this thesis suggest multiple regulatory mechanisms (i.e. lipid availability and palmitoylation) which may have distinct roles.

Again, a knock-in mouse model expressing a palmitoylation-deficient version of LIMP-2 is adequate to supplement cell-based assays to address the complex functions LIMP-2 exerts in various tissues as evident by the numerous phenotypic alterations observed in LIMP-2 KO mice.

Finally, it should be noted that besides S-palmitoylation at cysteine residues LIMP-2 might be additionally modified by further lipidations, e.g. N- or O-palmitoylation. Interestingly, LIMP-2 harbors an N-terminal glycine residue which is a prerequisite for co-translational myristoylation. Notably, LIMP-2 was identified as a potentially myristoylated protein in two independent myristoylome profiling screens (Thinon *et al.* 2014, Burnaevskiy *et al.* 2015). This modification often occurs in parallel to palmitoylation and myristoylation can be a prerequisite for subsequent palmitoylation on adjacent cysteine residues (Barylko *et al.* 2019). Fluorescence-based assays using Copper (Cu(I))-catalyzed Azide-Alkyne Click chemistry reactions (CuAAC)(Uttamapinant *et al.* 2012) could be used to establish whether LIMP-2 undergoes lipidation besides S-palmitoylation.

6. Summary

The lysosomal integral membrane protein type 2 (LIMP-2/SCARB2) is a multifunctional receptor and an essential component of lysosomal membranes. Previous studies focused on the elucidation of the transport of the acid hydrolase β-glucocerebrosidase (GCase) by LIMP-2 from the endoplasmic reticulum (ER) to lysosomes. The discovery of a hydrophobic cavity buried inside the large luminal domain of LIMP-2, however, indicated additional, GCase-independent, functions.

The fact that such a cavity is also present in the protein family members CD36 and SR-BI, both plasma membrane-resident proteins involved in binding and transport of lipoproteins and lipids, suggested a similar role for the intramolecular tunnel of LIMP-2. The purpose of the present study was to elucidate the function of this LIMP-2 tunnel and its potential role in lysosomal lipid transport.

Lipid binding studies using the recombinant luminal domain of LIMP-2 and cross-linkable lipids revealed that LIMP-2 can associate with lipids such as sphingosine and ceramide. Notably, the by far strongest crosslink was observed with a cholesterol-analog which is why the subsequent experiments focused on this lipid. Using an array of live-cell lipid transport assays, the ability of LIMP-2 to transport free cholesterol through its tunnel domain was demonstrated in CHO, HeLa and A431 cells.

Moreover, loss of LIMP-2 caused lysosomal accumulation of cholesterol and decrease in esterified cholesterol under conditions of LDL overload which resulted in aberrant signaling of the cholesterol regulatory machinery residing in the ER.

In addition, LIMP-2 was shown to reside at membrane contact sites between the ER and lysosomes and co-immunoprecipitation studies indicated that it interacts with contact site-mediating proteins such as STARD3 and VAPB in a lipid-dependent manner.

Finally, this study demonstrated that LIMP-2 is palmitoylated at multiple cysteine residues within its cytosolic amino- and carboxy-termini. While lack of palmitoylation did not interfere with correct lysosomal targeting of LIMP-2, microscopy analysis revealed drastically enlarged lysosomes, suggesting that palmitoylation of LIMP-2 is vital for correct lysosome physiology. Furthermore, absence of palmitoylation decreased the interaction with ER-contact site proteins VAPB, STARD3 and Gramd1b, emphasizing a role of LIMP-2 at lysosome-ER contact sites.

In summary, the data presented in this thesis reveal that LIMP-2 can bind and transport cholesterol and while the transport is not as efficient as the well-described NPC2-NPC1 route, it appears to be physiologically relevant in lysosomes and likely includes other lipids as well.

In addition to its transport function, LIMP-2 seems to participate in the re-distribution of these lipids to other organelles like the ER by interacting with membrane contact site proteins in dependency of the lipid status of the cell. While the mechanistic details remain to be elucidated, these interactions are modulated by palmitoylation of LIMP-2.

7. Zusammenfassung

Das Lysosomale Integrale Membranprotein Typ 2 (LIMP-2/SCARB2) ist ein multifunktioneller Rezeptor und ein wichtiger Bestandteil der Membran von Lysosomen. In bisherigen Studien stand die Rolle des durch LIMP-2 vermittelten Transportes der sauren Hydrolase β-Glukozerebrosidase (GCase) vom Endoplasmatischen Retikulum (ER) bis zu den Lysosomen im Vordergrund. Die strukturelle Entdeckung einer hydrophoben Höhle innerhalb der luminalen Domäne von LIMP-2 deutete hingegen auf weitere, GCase-unabhängige, Funktionen von LIMP-2 hin.

Die Tatsache, dass so eine Struktur auch in den Proteinfamilienmitgliedern CD36 und SR-BI, welches beide plasmamembranlokalisierte und im Lipidtransport involvierte Proteine sind, nachgewiesen wurde, deutete auf eine ähnliche Funktion für LIMP-2 hin. Das Ziel dieser Arbeit war es daher, die Funktion dieses intramolekularen Tunnels in LIMP-2 näher zu beschreiben, sowie die potentielle Rolle von LIMP-2 im Lipidtransport in Lysosomen zu untersuchen.

Studien zur Assoziation von Lipiden, die mit rekombinanter luminaler Domäne von LIMP-2 sowie quervernetzbaren Lipiden durchgeführt wurden, zeigten, dass LIMP-2 in der Tat Lipide wie Sphingosin und Ceramid binden kann. Die deutlichste Bindung wurde jedoch zwischen LIMP-2 und einem Cholesterinanalog beobachtet, weshalb Cholesterin in den nachfolgenden Experimenten im Fokus stand. Durch ein breites Spektrum an Analysen des Lipidtransportes in lebenden Zellen konnte in den Zelltypen CHO, HeLa und A431 gezeigt werden, dass LIMP-2 in der Lage ist, freies Cholesterin durch seine Tunneldomäne zu transportieren.

Darüber hinaus führte der Verlust von LIMP-2 in Kombination mit einem LDL-Überschuss zu einer Anreicherung von Cholesterin in Lysosomen sowie einer verminderten Bildung von Cholesterinestern, was sich auch in einer gestörten Funktion der ER-residenten Maschinerie zur Regulierung des Cholesterinhaushaltes auswirkte.

Zusätzlich konnte gezeigt werden, dass LIMP-2 an Membrankontaktstellen zwischen den Membranen des ERs und der Lysosomen zu finden ist und durch Ko-Immunopräzipitationsstudien wurde eine lipidabhängige Interaktion zwischen LIMP-2 und den Membrankontaktstellenproteinen STARD3 und VAPB nachgewiesen.

Schließlich wurde auch gezeigt, dass LIMP-2 an mehreren Cysteinen der zytoplasmatischen Amino- und Carboxy-termini palmitoyliert vorliegt. Die Abwesenheit der Palmitoylierung führte zwar nicht zu einem veränderten Transport von LIMP-2 zum Lysosom, jedoch demonstrierten mikroskopische Analysen stark vergrößerte Lysosomen, was darauf hindeutet, dass die Palmitoylierung von LIMP-2 wichtig für die korrekte Physiologie der Lysosomen ist. Des

Weiteren führte die Abwesenheit der Palmitoylierung zu einer verminderten Interaktion zwischen LIMP-2 und den ER-Kontaktstellenproteinen VAPB, STARD3 und Gramd1b, was eine Funktion von LIMP-2 an Kontaktstellen zwischen Lysosomen und dem ER unterstützt.

Zusammenfassend belegen die in dieser Arbeit präsentierten Daten, dass LIMP-2 Cholesterin binden und transportieren kann und obwohl dieser Transport nicht so effizient abläuft wie es bei dem bekannten NPC2-NPC1 Transportweg der Fall ist, so scheint dieser Weg in Lysosomen dennoch physiologisch relevant zu sein. Wahrscheinlich werden weitere Lipide durch LIMP-2 transportiert. Zusätzlich zu dieser Transportfunktion wirkt LIMP-2 an der Umverteilung der exportierten Lipide mit, indem es mit Membrankontaktstellenproteinen interagiert, was vom Lipidstatus der Zelle abhängt. Während die genauen Details dieser Interaktionen noch geklärt werden müssen, konnte bereits gezeigt werden, dass die Palmitoylierung von LIMP-2 hierbei eine modulierende Rolle spielt.

8. References

Abrami, L., T. Dallavilla, P. A. Sandoz, M. Demir, B. Kunz, G. Savoglidis, V. Hatzimanikatis and F. G. van der Goot (2017). "Identification and dynamics of the human ZDHHC16-ZDHHC6 palmitoylation cascade." Elife **6**.

Abrami, L., B. Kunz, I. Iacovache and F. G. van der Goot (2008). "Palmitoylation and ubiquitination regulate exit of the Wnt signaling protein LRP6 from the endoplasmic reticulum." Proc Natl Acad Sci U S A **105**(14): 5384-5389.

Abrami, L., S. H. Leppla and F. G. van der Goot (2006). "Receptor palmitoylation and ubiquitination regulate anthrax toxin endocytosis." J Cell Biol **172**(2): 309-320.

Acton, S., A. Rigotti, K. T. Landschulz, S. Xu, H. H. Hobbs and M. Krieger (1996). "Identification of scavenger receptor SR-BI as a high density lipoprotein receptor." Science **271**(5248): 518-520.

Aerts, J. M., C. Hollak, R. Boot and A. Groener (2003). "Biochemistry of glycosphingolipid storage disorders: implications for therapeutic intervention." Philos Trans R Soc Lond B Biol Sci **358**(1433): 905-914.

Aerts, J. M. F. G., W. E. Donkerkoopman, M. K. Vandervliet, L. M. V. Jonsson, E. I. Ginns, G. J. Murray, J. A. Barranger, J. M. Tager and A. W. Schram (1985). "The Occurrence of 2 Immunologically Distinguishable Beta-Glucocerebrosidases in Human Spleen." European Journal of Biochemistry **150**(3): 565-574.

Akiyama, H., M. Ide, Y. Nagatsuka, T. Sayano, E. Nakanishi, N. Uemura, K. Yuyama, Y. Yamaguchi, H. Kamiguchi, R. Takahashi, J. Aerts, P. Greimel and Y. Hirabayashi (2020). "Glucocerebrosidases catalyze a transgalactosylation reaction that yields a newly-identified brain sterol metabolite, galactosylated cholesterol." J Biol Chem **295**(16): 5257-5277.

Akiyama, H., S. Kobayashi, Y. Hirabayashi and K. Murakami-Murofushi (2013). "Cholesterol glucosylation is catalyzed by transglucosylation reaction of beta-glucosidase 1." Biochem Biophys Res Commun **441**(4): 838-843.

Akiyama, H., K. Nakajima, Y. Itoh, T. Sayano, Y. Ohashi, Y. Yamaguchi, P. Greimel and Y. Hirabayashi (2016). "Aglycon diversity of brain sterylglucosides: structure determination of cholesteryl- and sitosterylglucoside." J Lipid Res **57**(11): 2061-2072.

Alattia, J. R., J. E. Shaw, C. M. Yip and G. G. Prive (2007). "Molecular imaging of membrane interfaces reveals mode of beta-glucosidase activation by saposin C." Proc Natl Acad Sci U S A **104**(44): 17394-17399.

Allott, E. H., L. E. Howard, M. R. Cooperberg, C. J. Kane, W. J. Aronson, M. K. Terris, C. L. Amling and S. J. Freedland (2014). "Serum lipid profile and risk of prostate cancer recurrence: Results from the SEARCH database." Cancer Epidemiol Biomarkers Prev **23**(11): 2349-2356.

Alpy, F., V. K. Latchumanan, V. Kedinger, A. Janoshazi, C. Thiele, C. Wendling, M. C. Rio and C. Tomasetto (2005). "Functional characterization of the MENTAL domain." J Biol Chem **280**(18): 17945-17952.

Alpy, F., A. Rousseau, Y. Schwab, F. Legueux, I. Stoll, C. Wendling, C. Spiegelhalter, P. Kessler, C. Mathelin, M. C. Rio, T. P. Levine and C. Tomasetto (2013). "STARD3 or STARD3NL and VAP form a novel molecular tether between late endosomes and the ER." J Cell Sci **126**(Pt 23): 5500-5512.

Alpy, F., M. E. Stoeckel, A. Dierich, J. M. Escola, C. Wendling, M. P. Chenard, M. T. Vanier, J. Gruenberg, C. Tomasetto and M. C. Rio (2001). "The steroidogenic acute regulatory protein homolog MLN64, a late endosomal cholesterol-binding protein." J Biol Chem **276**(6): 4261-4269.

Alpy, F. and C. Tomasetto (2005). "Give lipids a START: the StAR-related lipid transfer (START) domain in mammals." J Cell Sci **118**(Pt 13): 2791-2801.

Anderson, R. A., G. M. Bryson and J. S. Parks (1999). "Lysosomal acid lipase mutations that determine phenotype in Wolman and cholesterol ester storage disease." Mol Genet Metab **68**(3): 333-345.

Andrejewski, N., E. L. Punnonen, G. Guhde, Y. Tanaka, R. Lullmann-Rauch, D. Hartmann, K. von Figura and P. Saftig (1999). "Normal lysosomal morphology and function in LAMP-1-deficient mice." J Biol Chem **274**(18): 12692-12701.

Apostolopoulos, J., R. L. Sparrow, J. L. McLeod, F. M. Collier, P. K. Darcy, H. R. Slater, C. Ngu, C. C. Gregorio-King and M. A. Kirkland (2001). "Identification and characterization of a novel family of mammalian ependymin-related proteins (MERPs) in hematopoietic, nonhematopoietic, and malignant tissues." DNA Cell Biol **20**(10): 625-635.

Asch, A. S., J. Barnwell, R. L. Silverstein and R. L. Nachman (1987). "Isolation of the thrombospondin membrane receptor." J Clin Invest **79**(4): 1054-1061.

Attie, A. D. (2007). "ABCA1: at the nexus of cholesterol, HDL and atherosclerosis." Trends Biochem Sci **32**(4): 172-179.

Ballabio, A. and J. S. Bonifacino (2020). "Lysosomes as dynamic regulators of cell and organismal homeostasis." Nat Rev Mol Cell Biol **21**(2): 101-118.

Balreira, A., P. Gaspar, D. Caiola, J. Chaves, I. Beirao, J. L. Lima, J. E. Azevedo and M. C. Miranda (2008). "A nonsense mutation in the LIMP-2 gene associated with progressive myoclonic epilepsy and nephrotic syndrome." Hum Mol Genet **17**(14): 2238-2243.

Bannan, B. A., J. Van Etten, J. A. Kohler, Y. Tsoi, N. M. Hansen, S. Sigmon, E. Fowler, H. Buff, T. S. Williams, J. G. Ault, R. L. Glaser and C. A. Korey (2008). "The Drosophila protein palmitoylome: characterizing palmitoyl-thioesterases and DHHC palmitoyl-transferases." Fly (Austin) **2**(4): 198-214.

Barriocanal, J. G., J. S. Bonifacino, L. Yuan and I. V. Sandoval (1986). "Biosynthesis, glycosylation, movement through the Golgi system, and transport to lysosomes by an N-linked carbohydrate-independent mechanism of three lysosomal integral membrane proteins." J Biol Chem **261**(35): 16755-16763.

Bartuzi, P., D. D. Billadeau, R. Favier, S. Rong, D. Dekker, A. Fedoseienko, H. Fieten, M. Wijers, J. H. Levels, N. Huijkman, N. Kloosterhuis, H. van der Molen, G. Brufau, A. K. Groen, A. M. Elliott, J. A. Kuivenhoven, B. Plecko, G. Grangl, J. McGaughran, J. D. Horton, E. Burstein, M. H. Hofker and B. van de Sluis (2016). "CCC- and WASH-mediated endosomal sorting of LDLR is required for normal clearance of circulating LDL." Nat Commun **7**: 10961.

Barylko, B., Y. J. Chen, J. Hennen, I. Angert, Y. Chen, J. D. Mueller, H. Q. Sun, C. A. t. Taylor, J. Liou, H. Yin and J. P. Albanesi (2019). "Myristoylation-Dependent Palmitoylation of the Receptor Tyrosine Kinase Adaptor FRS2alpha." Biochemistry **58**(25): 2809-2813.

Berg, J. M., J. L. Tymoczko, G. J. Gatto, L. Stryer, A. Held, M. Held, B. Jarosch, G. Maxam and L. Seidler (2018). Stryer Biochemie. Lehrbuch. Berlin, Springer Spektrum.

Berkovic, S. F., L. M. Dibbens, A. Oshlack, J. D. Silver, M. Katerelos, D. F. Vears, R. Lullmann-Rauch, J. Blanz, K. W. Zhang, J. Stankovich, R. M. Kalnins, J. P. Dowling, E. Andermann, F. Andermann, E. Faldini, R. D'Hooge, L. Vadlamudi, R. A. Macdonell, B. L. Hodgson, M. A. Bayly, J. Savige, J. C. Mulley, G. K. Smyth, D. A. Power, P. Saftig and M. Bahlo (2008). "Array-based gene discovery with three unrelated subjects shows SCARB2/LIMP-2 deficiency causes myoclonus epilepsy and glomerulosclerosis." Am J Hum Genet **82**(3): 673-684.

Bernardo, K., R. Hurwitz, T. Zenk, R. J. Desnick, K. Ferlinz, E. H. Schuchman and K. Sandhoff (1995). "Purification, characterization, and biosynthesis of human acid ceramidase." J Biol Chem **270**(19): 11098-11102.

Bhattacharyya, R., C. Barren and D. M. Kovacs (2013). "Palmitoylation of amyloid precursor protein regulates amyloidogenic processing in lipid rafts." J Neurosci **33**(27): 11169-11183.

Birkenkamp-Demtroder, K., L. L. Christensen, S. H. Olesen, C. M. Frederiksen, P. Laiho, L. A. Aaltonen, S. Laurberg, F. B. Sorensen, R. Hagemann and O. R. TF (2002). "Gene expression in colorectal cancer." Cancer Res **62**(15): 4352-4363.

Blanc, M., S. Blaskovic and F. G. van der Goot (2013). "Palmitoylation, pathogens and their host." Biochem Soc Trans **41**(1): 84-88.

Blanc, M., F. David, L. Abrami, D. Migliozzi, F. Armand, J. Burgi and F. G. van der Goot (2015). "SwissPalm: Protein Palmitoylation database." F1000Res **4**: 261.

Blanz, J., J. Groth, C. Zachos, C. Wehling, P. Saftig and M. Schwake (2010). "Disease-causing mutations within the lysosomal integral membrane protein type 2 (LIMP-2) reveal the nature of binding to its ligand beta-glucocerebrosidase." Hum Mol Genet **19**(4): 563-572.

Blanz, J., J. Groth, C. Zachos, C. Wehling, P. Saftig and M. Schwake (2010). "Disease-causing mutations within the lysosomal integral membrane protein type 2 (LIMP-2) reveal the nature of binding to its ligand beta-glucocerebrosidase." Hum.Mol.Genet. **19**(4): 563-572.

Blanz, J., F. Zunke, S. Markmann, M. Damme, T. Braulke, P. Saftig and M. Schwake (2015). "Mannose 6-phosphate-independent Lysosomal Sorting of LIMP-2." Traffic **16**(10): 1127-1136.

Bligh, E. G. and W. J. Dyer (1959). "A rapid method of total lipid extraction and purification." Can J Biochem Physiol **37**(8): 911-917.

Bloch, K. (1965). "The biological synthesis of cholesterol." Science **150**(3692): 19-28.

Blom, T., Z. Li, R. Bittman, P. Somerharju and E. Ikonen (2012). "Tracking sphingosine metabolism and transport in sphingolipidoses: NPC1 deficiency as a test case." Traffic **13**(9): 1234-1243.

Bocan, T. M., T. A. Schifani and J. R. Guyton (1986). "Ultrastructure of the human aortic fibrolipid lesion. Formation of the atherosclerotic lipid-rich core." Am J Pathol **123**(3): 413-424.

Boer, D. E. C., J. van Smeden, J. A. Bouwstra and J. Aerts (2020). "Glucocerebrosidase: Functions in and Beyond the Lysosome." J Clin Med **9**(3).

Boutin, J. A. (1997). "Myristoylation." Cell Signal **9**(1): 15-35.

Brady, R. O. (2003). "Enzyme replacement therapy: conception, chaos and culmination." Philos Trans R Soc Lond B Biol Sci **358**(1433): 915-919.

Brady, R. O., J. N. Kanfer, R. M. Bradley and D. Shapiro (1966). "Demonstration of a deficiency of glucocerebroside-cleaving enzyme in Gaucher's disease." J Clin Invest **45**(7): 1112-1115.

Brasaemle, D. L. and A. D. Attie (1990). "Rapid intracellular transport of LDL-derived cholesterol to the plasma membrane in cultured fibroblasts." J Lipid Res **31**(1): 103-112.

Braulke, T. and J. S. Bonifacino (2009). "Sorting of lysosomal proteins." Biochim Biophys Acta **1793**(4): 605-614.

Braun, A., B. L. Trigatti, M. J. Post, K. Sato, M. Simons, J. M. Edelberg, R. D. Rosenberg, M. Schrenzel and M. Krieger (2002). "Loss of SR-BI expression leads to the early onset of occlusive atherosclerotic coronary artery disease, spontaneous myocardial infarctions, severe cardiac dysfunction, and premature death in apolipoprotein E-deficient mice." Circ Res **90**(3): 270-276.

Brigidi, G. S., B. Santyr, J. Shimell, B. Jovellar and S. X. Bamji (2015). "Activity-regulated trafficking of the palmitoyl-acyl transferase DHHC5." Nat Commun **6**: 8200.

Brown, J. M., L. L. Rudel and L. Yu (2007). "NPC1L1 (Niemann-Pick C1-like 1) mediates sterol-specific unidirectional transport of non-esterified cholesterol in McArdle-RH7777 hepatoma cells." Biochem J **406**(2): 273-283.

Brown, M. S. and J. L. Goldstein (1986). "A receptor-mediated pathway for cholesterol homeostasis." Science **232**(4746): 34-47.

Brown, M. S. and J. L. Goldstein (1997). "The SREBP pathway: regulation of cholesterol metabolism by proteolysis of a membrane-bound transcription factor." Cell **89**(3): 331-340.

Buglino, J. A. and M. D. Resh (2012). "Palmitoylation of Hedgehog proteins." Vitam Horm **88**: 229-252.

Bukiya, A. N., J. D. Belani, S. Rychnovsky and A. M. Dopico (2011). "Specificity of cholesterol and analogs to modulate BK channels points to direct sterol-channel protein interactions." J Gen Physiol **137**(1): 93-110.

Burger, K., G. Gimpl and F. Fahrenholz (2000). "Regulation of receptor function by cholesterol." Cell Mol Life Sci **57**(11): 1577-1592.

Burnaevskiy, N., T. Peng, L. E. Reddick, H. C. Hang and N. M. Alto (2015). "Myristoylome profiling reveals a concerted mechanism of ARF GTPase deacylation by the bacterial protease IpaJ." Mol Cell **58**(1): 110-122.

Canton, J., D. Neculai and S. Grinstein (2013). "Scavenger receptors in homeostasis and immunity." Nat Rev Immunol **13**(9): 621-634.

Castellano, B. M., A. M. Thelen, O. Moldavski, M. Feltes, R. E. van der Welle, L. Mydock-McGrane, X. Jiang, R. J. van Eijkeren, O. B. Davis, S. M. Louie, R. M. Perera, D. F. Covey, D. K. Nomura, D. S. Ory and R. Zoncu (2017). "Lysosomal cholesterol activates mTORC1 via an SLC38A9-Niemann-Pick C1 signaling complex." Science **355**(6331): 1306-1311.

Chakrabandhu, K., Z. Herincs, S. Huault, B. Dost, L. Peng, F. Conchonaud, D. Marguet, H. T. He and A. O. Hueber (2007). "Palmitoylation is required for efficient Fas cell death signaling." EMBO J **26**(1): 209-220.

Chang, T. Y., C. C. Chang, S. Lin, C. Yu, B. L. Li and A. Miyazaki (2001). "Roles of acyl-coenzyme A:cholesterol acyltransferase-1 and -2." Curr Opin Lipidol **12**(3): 289-296.

Charollais, J. and F. G. Van Der Goot (2009). "Palmitoylation of membrane proteins (Review)." Mol Membr Biol **26**(1): 55-66.

Chatr-Aryamontri, A., R. Oughtred, L. Boucher, J. Rust, C. Chang, N. K. Kolas, L. O'Donnell, S. Oster, C. Theesfeld, A. Sellam, C. Stark, B. J. Breitkreutz, K. Dolinski and M. Tyers (2017). "The BioGRID interaction database: 2017 update." Nucleic Acids Res **45**(D1): D369-D379.

Chaves, J., I. Beirao, A. Balreira, P. Gaspar, D. Caiola, M. C. Sa-Miranda and J. L. Lima (2011). "Progressive myoclonus epilepsy with nephropathy C1q due to SCARB2/LIMP-2 deficiency: clinical report of two siblings." Seizure **20**(9): 738-740.

Chen, L., X. W. Chen, X. Huang, B. L. Song, Y. Wang and Y. Wang (2019). "Regulation of glucose and lipid metabolism in health and disease." Sci China Life Sci **62**(11): 1420-1458.

Chen, W. J., J. L. Goldstein and M. S. Brown (1990). "NPXY, a sequence often found in cytoplasmic tails, is required for coated pit-mediated internalization of the low density lipoprotein receptor." J Biol Chem **265**(6): 3116-3123.

Chesarino, N. M., T. M. McMichael and J. S. Yount (2014). "Regulation of the trafficking and antiviral activity of IFITM3 by post-translational modifications." Future Microbiol **9**(10): 1151-1163.

Chu, B. B., Y. C. Liao, W. Qi, C. Xie, X. Du, J. Wang, H. Yang, H. H. Miao, B. L. Li and B. L. Song (2015). "Cholesterol transport through lysosome-peroxisome membrane contacts." Cell **161**(2): 291-306.

Claussen, C.(2005). Analyse der LIMP-2 (Lysosomales Integrales Membranprotein-2) defizienten Maus, CAU Kiel.

Coburn, C. T., F. F. Knapp, Jr., M. Febbraio, A. L. Beets, R. L. Silverstein and N. A. Abumrad (2000). "Defective uptake and utilization of long chain fatty acids in muscle and adipose tissues of CD36 knockout mice." J Biol Chem **275**(42): 32523-32529.

Conrad, K. S., T. W. Cheng, D. Ysselstein, S. Heybrock, L. R. Hoth, B. A. Chrunyk, C. W. A. Ende, D. Krainc, M. Schwake, P. Saftig, S. P. Liu, X. Y. Qiu and M. D. Ehlers (2017). "Lysosomal integral membrane protein-2 as a phospholipid receptor revealed by biophysical and cellular studies." Nature Communications **8**.

Conzelmann, E. and K. Sandhoff (1983). "Partial enzyme deficiencies: residual activities and the development of neurological disorders." Dev Neurosci **6**(1): 58-71.

Crombie, R. and R. Silverstein (1998). "Lysosomal integral membrane protein II binds thrombospondin-1. Structure-function homology with the cell adhesion molecule CD36 defines a conserved recognition motif." J Biol Chem **273**(9): 4855-4863.

Cuvillier, O. (2002). "Sphingosine in apoptosis signaling." Biochim Biophys Acta **1585**(2-3): 153-162.

Dallavilla, T., L. Abrami, P. A. Sandoz, G. Savoglidis, V. Hatzimanikatis and F. G. van der Goot (2016). "Model-Driven Understanding of Palmitoylation Dynamics: Regulated Acylation of the Endoplasmic Reticulum Chaperone Calnexin." PLoS Comput Biol **12**(2): e1004774.

Dang, M., X. Wang, Q. Wang, Y. Wang, J. Lin, Y. Sun, X. Li, L. Zhang, Z. Lou, J. Wang and Z. Rao (2014). "Molecular mechanism of SCARB2-mediated attachment and uncoating of EV71." Protein Cell **5**(9): 692-703.

Dave, K., H. Gelman, C. T. Thu, D. Guin and M. Gruebele (2016). "The Effect of Fluorescent Protein Tags on Phosphoglycerate Kinase Stability Is Nonadditive." J Phys Chem B **120**(11): 2878-2885.

Davies, J. P. and Y. A. Ioannou (2000). "Topological analysis of Niemann-Pick C1 protein reveals that the membrane orientation of the putative sterol-sensing domain is identical to those of 3-hydroxy-3-methylglutaryl-CoA reductase and sterol regulatory element binding protein cleavage-activating protein." J Biol Chem **275**(32): 24367-24374.

De Duve, C., B. C. Pressman, R. Gianetto, R. Wattiaux and F. Appelmans (1955). "Tissue fractionation studies. 6. Intracellular distribution patterns of enzymes in rat-liver tissue." Biochem J **60**(4): 604-617.

Della Valle, M. C., D. E. Sleat, I. Sohar, T. Wen, J. E. Pintar, M. Jadot and P. Lobel (2006). "Demonstration of lysosomal localization for the mammalian ependymin-related protein using classical approaches combined with a novel density shift method." J Biol Chem **281**(46): 35436-35445.

Deshmukh, A. S., L. Peijs, J. L. Beaudry, N. Z. Jespersen, C. H. Nielsen, T. Ma, A. D. Brunner, T. J. Larsen, R. Bayarri-Olmos, B. S. Prabhakar, C. Helgstrand, M. C. K. Severinsen, B. Holst, A. Kjaer, M. Tang-Christensen, A. Sanfridson, P. Garred, G. G. Prive, B. K. Pedersen, Z. Gerhart-Hines, S. Nielsen, D. J. Drucker, M. Mann and C. Scheele (2019). "Proteomics-Based Comparative Mapping of the Secretomes of Human Brown and White Adipocytes Reveals EPDR1 as a Novel Batokine." Cell Metab **30**(5): 963-975 e967.

Devries-Seimon, T., Y. Li, P. M. Yao, E. Stone, Y. Wang, R. J. Davis, R. Flavell and I. Tabas (2005). "Cholesterol-induced macrophage apoptosis requires ER stress pathways and engagement of the type A scavenger receptor." J Cell Biol **171**(1): 61-73.

Di Mattia, T., C. Tomasetto and F. Alpy (2020). "Faraway, so close! Functions of Endoplasmic reticulum-Endosome contacts." Biochim Biophys Acta Mol Cell Biol Lipids **1865**(1): 158490.

Di Mattia, T., L. P. Wilhelm, S. Ikhlef, C. Wendling, D. Spehner, Y. Nomine, F. Giordano, C. Mathelin, G. Drin, C. Tomasetto and F. Alpy (2018). "Identification of MOSPD2, a novel scaffold for endoplasmic reticulum membrane contact sites." EMBO Rep **19**(7).

Dias, I. H., K. Borah, B. Amin, H. R. Griffiths, K. Sassi, G. Lizard, A. Iriondo and P. Martinez-Lage (2019). "Localisation of oxysterols at the sub-cellular level and in biological fluids." J Steroid Biochem Mol Biol **193**: 105426.

Dibbens, L., M. Schwake, P. Saftig and G. Rubboli (2016). "SCARB2/LIMP2 deficiency in action myoclonus-renal failure syndrome." Epileptic Disord **18**(S2): 63-72.

Dibbens, L. M., I. Karakis, M. A. Bayly, D. J. Costello, A. J. Cole and S. F. Berkovic (2011). "Mutation of SCARB2 in a patient with progressive myoclonus epilepsy and demyelinating peripheral neuropathy." Arch Neurol **68**(6): 812-813.

Dibbens, L. M., R. Michelucci, A. Gambardella, F. Andermann, G. Rubboli, M. A. Bayly, T. Joensuu, D. F. Vears, S. Franceschetti, L. Canafoglia, R. Wallace, A. G. Bassuk, D. A. Power, C. A. Tassinari, E. Andermann, A. E. Lehesjoki and S. F. Berkovic (2009). "SCARB2 mutations in progressive myoclonus epilepsy (PME) without renal failure." Ann Neurol **66**(4): 532-536.

Draper, J. M. and C. D. Smith (2010). "DHHC20: a human palmitoyl acyltransferase that causes cellular transformation." Mol Membr Biol **27**(2-3): 123-136.

Drover, V. A., D. V. Nguyen, C. C. Bastie, Y. F. Darlington, N. A. Abumrad, J. E. Pessin, E. London, D. Sahoo and M. C. Phillips (2008). "CD36 mediates both cellular uptake of very long chain fatty acids and their intestinal absorption in mice." J Biol Chem **283**(19): 13108-13115.

Du, K., S. Murakami, Y. Sun, C. L. Kilpatrick and B. Luscher (2017). "DHHC7 Palmitoylates Glucose Transporter 4 (Glut4) and Regulates Glut4 Membrane Translocation." J Biol Chem **292**(7): 2979-2991.

Duan, G. and D. Walther (2015). "The roles of post-translational modifications in the context of protein interaction networks." PLoS Comput Biol **11**(2): e1004049.

Dubland, J. A. and G. A. Francis (2015). "Lysosomal acid lipase: at the crossroads of normal and atherogenic cholesterol metabolism." Front Cell Dev Biol **3**: 3.

Duncan, J. A. and A. G. Gilman (1998). "A cytoplasmic acyl-protein thioesterase that removes palmitate from G protein alpha subunits and p21(RAS)." J Biol Chem **273**(25): 15830-15837.

Eblan, M. J., O. Goker-Alpan and E. Sidransky (2005). "Perinatal lethal Gaucher disease: a distinct phenotype along the neuronopathic continuum." Fetal Pediatr Pathol **24**(4-5): 205-222.

Edmonds, M. J. and A. Morgan (2014). "A systematic analysis of protein palmitoylation in Caenorhabditis elegans." BMC Genomics **15**: 841.

Eisenberg-Bord, M., N. Shai, M. Schuldiner and M. Bohnert (2016). "A Tether Is a Tether Is a Tether: Tethering at Membrane Contact Sites." Dev Cell **39**(4): 395-409.

Endemann, G., L. W. Stanton, K. S. Madden, C. M. Bryant, R. T. White and A. A. Protter (1993). "CD36 is a receptor for oxidized low density lipoprotein." J Biol Chem **268**(16): 11811-11816.

Enquist, I. B., E. Nilsson, J. E. Mansson, M. Ehinger, J. Richter and S. Karlsson (2009). "Successful low-risk hematopoietic cell therapy in a mouse model of type 1 Gaucher disease." Stem Cells **27**(3): 744-752.

Epstein, W. W., D. Lever, L. M. Leining, E. Bruenger and H. C. Rilling (1991). "Quantitation of prenylcysteines by a selective cleavage reaction." Proc Natl Acad Sci U S A **88**(21): 9668-9670.

Erickson, A. H., E. I. Ginns and J. A. Barranger (1985). "Biosynthesis of the lysosomal enzyme glucocerebrosidase." J Biol Chem **260**(26): 14319-14324.

Eskelinen, E.-L., Y. Tanaka and P. Saftig (2003). "At the acidic edge: emerging functions for lysosomal membrane proteins." Trends in Cell Biology **13**(3): 137-145.

Eskelinen, E. L., A. L. Illert, Y. Tanaka, G. Schwarzmann, J. Blanz, K. Von Figura and P. Saftig (2002). "Role of LAMP-2 in lysosome biogenesis and autophagy." Mol Biol Cell **13**(9): 3355-3368.

Fedoseienko, A., M. Wijers, J. C. Wolters, D. Dekker, M. Smit, N. Huijkman, N. Kloosterhuis, H. Klug, A. Schepers, K. Willems van Dijk, J. H. M. Levels, D. D. Billadeau, M. H. Hofker, J. van Deursen, M. Westerterp, E. Burstein, J. A. Kuivenhoven and B. van de Sluis (2018). "The COMMD Family Regulates Plasma LDL Levels and Attenuates Atherosclerosis Through Stabilizing the CCC Complex in Endosomal LDLR Trafficking." Circ Res **122**(12): 1648-1660.

Ferrari, A., C. He, J. P. Kennelly, J. Sandhu, X. Xiao, X. Chi, H. Jiang, S. G. Young and P. Tontonoz (2020). "Aster proteins regulate the accessible cholesterol pool in the plasma membrane." Mol Cell Biol.

Ferraz, M. J., A. R. Marques, M. D. Appelman, M. Verhoek, A. Strijland, M. Mirzaian, S. Scheij, C. M. Ouairy, D. Lahav, P. Wisse, H. S. Overkleeft, R. G. Boot and J. M. Aerts (2016). "Lysosomal glycosphingolipid catabolism by acid ceramidase: formation of glycosphingoid bases during deficiency of glycosidases." FEBS Lett **590**(6): 716-725.

Fitzgerald, M. L., Z. Mujawar and N. Tamehiro (2010). "ABC transporters, atherosclerosis and inflammation." Atherosclerosis **211**(2): 361-370.

Forgac, M. (1999). "Structure and properties of the vacuolar (H+)-ATPases." J Biol Chem **274**(19): 12951-12954.

Forrester, M. T., D. T. Hess, J. W. Thompson, R. Hultman, M. A. Moseley, J. S. Stamler and P. J. Casey (2011). "Site-specific analysis of protein S-acylation by resin-assisted capture." J Lipid Res **52**(2): 393-398.

Fox, E. M., J. Andrade and M. A. Shupnik (2009). "Novel actions of estrogen to promote proliferation: integration of cytoplasmic and nuclear pathways." Steroids **74**(7): 622-627.

Freed-Pastor, W. A., H. Mizuno, X. Zhao, A. Langerod, S. H. Moon, R. Rodriguez-Barrueco, A. Barsotti, A. Chicas, W. Li, A. Polotskaia, M. J. Bissell, T. F. Osborne, B. Tian, S. W. Lowe, J. M. Silva, A. L. Borresen-Dale, A. J. Levine, J. Bargonetti and C. Prives (2012). "Mutant p53 disrupts mammary tissue architecture via the mevalonate pathway." Cell **148**(1-2): 244-258.

Friedland, N., H. L. Liou, P. Lobel and A. M. Stock (2003). "Structure of a cholesterol-binding protein deficient in Niemann-Pick type C2 disease." Proc Natl Acad Sci U S A **100**(5): 2512-2517.

Friedman, J. R., J. R. Dibenedetto, M. West, A. A. Rowland and G. K. Voeltz (2013). "Endoplasmic reticulum-endosome contact increases as endosomes traffic and mature." Mol Biol Cell **24**(7): 1030-1040.

Fujita, H., J. Ezaki, Y. Noguchi, A. Kono, M. Himeno and K. Kato (1991). "Isolation and sequencing of a cDNA clone encoding 85kDa sialoglycoprotein in rat liver lysosomal membranes." Biochem Biophys Res Commun **178**(2): 444-452.

Fukata, M., Y. Fukata, H. Adesnik, R. A. Nicoll and D. S. Bredt (2004). "Identification of PSD-95 palmitoylating enzymes." Neuron **44**(6): 987-996.

Fukuda, M. (1991). "Lysosomal membrane glycoproteins. Structure, biosynthesis, and intracellular trafficking." J Biol Chem **266**(32): 21327-21330.

Gamp, A. C., Y. Tanaka, R. Lullmann-Rauch, D. Wittke, R. D'Hooge, P. P. De Deyn, T. Moser, H. Maier, D. Hartmann, K. Reiss, A. L. Illert, K. von Figura and P. Saftig (2003). "LIMP-2/LGP85 deficiency causes ureteric pelvic junction obstruction, deafness and peripheral neuropathy in mice." Human Molecular Genetics **12**(6): 631-646.

Garbay, B., A. M. Heape, F. Sargueil and C. Cassagne (2000). "Myelin synthesis in the peripheral nervous system." Prog Neurobiol **61**(3): 267-304.

Gaspar, P., W. W. Kallemeijn, A. Strijland, S. Scheij, M. Van Eijk, J. Aten, H. S. Overkleeft, A. Balreira, F. Zunke, M. Schwake, C. Sa Miranda and J. M. Aerts (2014). "Action myoclonus-renal failure syndrome: diagnostic applications of activity-based probes and lipid analysis." J Lipid Res **55**(1): 138-145.

Gatta, A. T. and T. P. Levine (2017). "Piecing Together the Patchwork of Contact Sites." Trends Cell Biol **27**(3): 214-229.

Gatta, A. T., L. H. Wong, Y. Y. Sere, D. M. Calderon-Norena, S. Cockcroft, A. K. Menon and T. P. Levine (2015). "A new family of StART domain proteins at membrane contact sites has a role in ER-PM sterol transport." Elife **4**.

Ge, L., J. Wang, W. Qi, H. H. Miao, J. Cao, Y. X. Qu, B. L. Li and B. L. Song (2008). "The cholesterol absorption inhibitor ezetimibe acts by blocking the sterol-induced internalization of NPC1L1." Cell Metab **7**(6): 508-519.

Gelissen, I. C., M. Harris, K. A. Rye, C. Quinn, A. J. Brown, M. Kockx, S. Cartland, M. Packianathan, L. Kritharides and W. Jessup (2006). "ABCA1 and ABCG1 synergize to mediate cholesterol export to apoA-I." Arterioscler Thromb Vasc Biol **26**(3): 534-540.

Giang, D. K. and B. F. Cravatt (1998). "A second mammalian N-myristoyltransferase." J Biol Chem **273**(12): 6595-6598.

Giglione, C., S. Fieulaine and T. Meinnel (2015). "N-terminal protein modifications: Bringing back into play the ribosome." Biochimie **114**: 134-146.

Goldstein, J. L., R. G. Anderson and M. S. Brown (1979). "Coated pits, coated vesicles, and receptor-mediated endocytosis." Nature **279**(5715): 679-685.

Goldstein, J. L. and M. S. Brown (1990). "Regulation of the mevalonate pathway." Nature **343**(6257): 425-430.

Goldstein, J. L., S. E. Dana, J. R. Faust, A. L. Beaudet and M. S. Brown (1975). "Role of lysosomal acid lipase in the metabolism of plasma low density lipoprotein. Observations in cultured fibroblasts from a patient with cholesteryl ester storage disease." J Biol Chem **250**(21): 8487-8495.

Goldstein, J. L., R. A. DeBose-Boyd and M. S. Brown (2006). "Protein sensors for membrane sterols." Cell **124**(1): 35-46.

Gomez-Diaz, C., B. Bargeton, L. Abuin, N. Bukar, J. H. Reina, T. Bartoi, M. Graf, H. Ong, M. H. Ulbrich, J. F. Masson and R. Benton (2016). "A CD36 ectodomain mediates insect pheromone detection via a putative tunnelling mechanism." Nat Commun **7**: 11866.

Gong, X., H. Qian, X. Zhou, J. Wu, T. Wan, P. Cao, W. Huang, X. Zhao, X. Wang, P. Wang, Y. Shi, G. F. Gao, Q. Zhou and N. Yan (2016). "Structural Insights into the Niemann-Pick C1 (NPC1)-Mediated Cholesterol Transfer and Ebola Infection." Cell **165**(6): 1467-1478.

Gonzalez Montoro, A., S. Chumpen Ramirez and J. Valdez Taubas (2015). "The canonical DHHC motif is not absolutely required for the activity of the yeast S-acyltransferases Swf1 and Pfa4." J Biol Chem **290**(37): 22448-22459.

Gonzalez Montoro, A., R. Quiroga, H. J. Maccioni and J. Valdez Taubas (2009). "A novel motif at the C-terminus of palmitoyltransferases is essential for Swf1 and Pfa3 function in vivo." Biochem J **419**(2): 301-308.

Gordon, J. I., R. J. Duronio, D. A. Rudnick, S. P. Adams and G. W. Gokel (1991). "Protein N-myristoylation." J Biol Chem **266**(14): 8647-8650.

Gorleku, O. A., A. M. Barns, G. R. Prescott, J. Greaves and L. H. Chamberlain (2011). "Endoplasmic reticulum localization of DHHC palmitoyltransferases mediated by lysine-based sorting signals." J Biol Chem **286**(45): 39573-39584.

Grabowski, G. A., N. W. Barton, G. Pastores, J. M. Dambrosia, T. K. Banerjee, M. A. McKee, C. Parker, R. Schiffmann, S. C. Hill and R. O. Brady (1995). "Enzyme therapy in type 1 Gaucher disease: comparative efficacy of mannose-terminated glucocerebrosidase from natural and recombinant sources." Ann Intern Med **122**(1): 33-39.

Grabowski, G. A., S. Gatt and M. Horowitz (1990). "Acid beta-glucosidase: enzymology and molecular biology of Gaucher disease." Crit Rev Biochem Mol Biol **25**(6): 385-414.

Greaves, J., J. A. Carmichael and L. H. Chamberlain (2011). "The palmitoyl transferase DHHC2 targets a dynamic membrane cycling pathway: regulation by a C-terminal domain." Mol Biol Cell **22**(11): 1887-1895.

Greaves, J. and L. H. Chamberlain (2014). "New links between S-acylation and cancer." J Pathol **233**(1): 4-6.

Gregorio-King, C. C., J. L. McLeod, F. M. Collier, G. R. Collier, K. A. Bolton, G. J. Van Der Meer, J. Apostolopoulos and M. A. Kirkland (2002). "MERP1: a mammalian ependymin-related protein gene differentially expressed in hematopoietic cells." Gene **286**(2): 249-257.

Gruenberg, J. (2020). "Life in the lumen: The multivesicular endosome." Traffic **21**(1): 76-93.

Guyton, J. R. and K. F. Klemp (1989). "The lipid-rich core region of human atherosclerotic fibrous plaques. Prevalence of small lipid droplets and vesicles by electron microscopy." Am J Pathol **134**(3): 705-717.

Haddley, K. (2012). "Taliglucerase alfa for the treatment of Gaucher's disease." Drugs Today (Barc) **48**(8): 525-532.

Harayama, T. and H. Riezman (2018). "Understanding the diversity of membrane lipid composition." Nat Rev Mol Cell Biol **19**(5): 281-296.

Haugwitz, G. v.(2019). Analysis of the role of lipidation of the Lysosomal Integral Membrane Protein Type 2 (LIMP2). Master of Science Master thesis, CAU Kiel.

Hein, M. Y., N. C. Hubner, I. Poser, J. Cox, N. Nagaraj, Y. Toyoda, I. A. Gak, I. Weisswange, J. Mansfeld, F. Buchholz, A. A. Hyman and M. Mann (2015). "A human interactome in three quantitative dimensions organized by stoichiometries and abundances." Cell **163**(3): 712-723.

Helle, S. C., G. Kanfer, K. Kolar, A. Lang, A. H. Michel and B. Kornmann (2013). "Organization and function of membrane contact sites." Biochim Biophys Acta **1833**(11): 2526-2541.

Heybrock, S., K. Kanerva, Y. Meng, C. Ing, A. Liang, Z. J. Xiong, X. Weng, Y. Ah Kim, R. Collins, W. Trimble, R. Pomes, G. G. Prive, W. Annaert, M. Schwake, J. Heeren, R. Lullmann-Rauch, S. Grinstein, E. Ikonen, P. Saftig and D. Neculai (2019). "Lysosomal integral membrane protein-2 (LIMP-2/SCARB2) is involved in lysosomal cholesterol export." Nat Commun **10**(1): 3521.

Hicks, S. W., G. Charron, H. C. Hang and J. E. Galan (2011). "Subcellular targeting of Salmonella virulence proteins by host-mediated S-palmitoylation." Cell Host Microbe **10**(1): 9-20.

Hoglinger, D., T. Burgoyne, E. Sanchez-Heras, P. Hartwig, A. Colaco, J. Newton, C. E. Futter, S. Spiegel, F. M. Platt and E. R. Eden (2019). "NPC1 regulates ER contacts with endocytic organelles to mediate cholesterol egress." Nat Commun **10**(1): 4276.

Hoglinger, D., P. Haberkant, A. Aguilera-Romero, H. Riezman, F. D. Porter, F. M. Platt, A. Galione and C. Schultz (2015). "Intracellular sphingosine releases calcium from lysosomes." Elife **4**.

Holmes, R. S. (2012). "Vertebrate scavenger receptor class B member 2 (SCARB2): comparative studies of a major lysosomal membrane glycoprotein." Journal of Molecular Biochemistry **1**: 99-115.

Honing, S., I. V. Sandoval and K. von Figura (1998). "A di-leucine-based motif in the cytoplasmic tail of LIMP-II and tyrosinase mediates selective binding of AP-3." EMBO J **17**(5): 1304-1314.

Hopfner, F., B. Schormair, F. Knauf, A. Berthele, T. R. Tolle, R. Baron, C. Maier, R. D. Treede, A. Binder, C. Sommer, C. Maihofner, W. Kunz, F. Zimprich, U. Heemann, A. Pfeufer, M. Nabauer, S. Kaab, B. Nowak, C. Gieger, P. Lichtner, C. Trenkwalder, K. Oexle and J. Winkelmann (2011). "Novel SCARB2 mutation in action myoclonus-renal failure syndrome and evaluation of SCARB2 mutations in isolated AMRF features." BMC Neurol **11**: 134.

Horenkamp, F. A., D. P. Valverde, J. Nunnari and K. M. Reinisch (2018). "Molecular basis for sterol transport by StART-like lipid transfer domains." EMBO J **37**(6).

Horowitz, M. and A. Zimran (1994). "Mutations causing Gaucher disease." Hum Mutat **3**(1): 1-11.

Howie, J., L. Reilly, N. J. Fraser, J. M. Vlachaki Walker, K. J. Wypijewski, M. L. Ashford, S. C. Calaghan, H. McClafferty, L. Tian, M. J. Shipston, A. Boguslavskyi, M. J. Shattock and W. Fuller (2014). "Substrate recognition by the cell surface palmitoyl transferase DHHC5." Proc Natl Acad Sci U S A **111**(49): 17534-17539.

Hu, J., Z. Zhang, W. J. Shen and S. Azhar (2010). "Cellular cholesterol delivery, intracellular processing and utilization for biosynthesis of steroid hormones." Nutr Metab (Lond) **7**: 47.

Huang, X., C. Jiang, L. Yu and A. Yang (2020). "Current and Emerging Approaches for Studying Inter-Organelle Membrane Contact Sites." Front Cell Dev Biol **8**: 195.

Huotari, J. and A. Helenius (2011). "Endosome maturation." EMBO J **30**(17): 3481-3500.

Hwang, Y. H., M. Tani, T. Nakagawa, N. Okino and M. Ito (2005). "Subcellular localization of human neutral ceramidase expressed in HEK293 cells." Biochem Biophys Res Commun **331**(1): 37-42.

Ikonen, E. (2008). "Cellular cholesterol trafficking and compartmentalization." Nat Rev Mol Cell Biol **9**(2): 125-138.

Ikonen, E. (2018). "Mechanisms of cellular cholesterol compartmentalization: recent insights." Curr Opin Cell Biol **53**: 77-83.

Itzhak, D. N., S. Tyanova, J. Cox and G. H. Borner (2016). "Global, quantitative and dynamic mapping of protein subcellular localization." Elife **5**.

Jacquier, N., V. Choudhary, M. Mari, A. Toulmay, F. Reggiori and R. Schneiter (2011). "Lipid droplets are functionally connected to the endoplasmic reticulum in Saccharomyces cerevisiae." J Cell Sci **124**(Pt 14): 2424-2437.

Jafurulla, M. and A. Chattopadhyay (2013). "Membrane lipids in the function of serotonin and adrenergic receptors." Curr Med Chem **20**(1): 47-55.

Janvier, K., Y. Kato, M. Boehm, J. R. Rose, J. A. Martina, B. Y. Kim, S. Venkatesan and J. S. Bonifacino (2003). "Recognition of dileucine-based sorting signals from HIV-1 Nef and LIMP-II by the AP-1 gamma-sigma1 and AP-3 delta-sigma3 hemicomplexes." J Cell Biol **163**(6): 1281-1290.

Jennings, B. C. and M. E. Linder (2012). "DHHC protein S-acyltransferases use similar ping-pong kinetic mechanisms but display different acyl-CoA specificities." J Biol Chem **287**(10): 7236-7245.

Jennings, B. C., M. J. Nadolski, Y. Ling, M. B. Baker, M. L. Harrison, R. J. Deschenes and M. E. Linder (2009). "2-Bromopalmitate and 2-(2-hydroxy-5-nitro-benzylidene)-benzo[b]thiophen-3-one inhibit DHHC-mediated palmitoylation in vitro." J Lipid Res **50**(2): 233-242.

Jerabek-Willemsen, M., C. J. Wienken, D. Braun, P. Baaske and S. Duhr (2011). "Molecular interaction studies using microscale thermophoresis." Assay Drug Dev Technol **9**(4): 342-353.

Jiang, H., X. Zhang, X. Chen, P. Aramsangtienchai, Z. Tong and H. Lin (2018). "Protein Lipidation: Occurrence, Mechanisms, Biological Functions, and Enabling Technologies." Chem Rev **118**(3): 919-988.

Jinek, M., K. Chylinski, I. Fonfara, M. Hauer, J. A. Doudna and E. Charpentier (2012). "A programmable dual-RNA-guided DNA endonuclease in adaptive bacterial immunity." Science **337**(6096): 816-821.

Jochen, A. and J. Hays (1993). "Purification of the major substrate for palmitoylation in rat adipocytes: N-terminal homology with CD36 and evidence for cell surface acylation." J Lipid Res **34**(10): 1783-1792.

Johansson, M., N. Rocha, W. Zwart, I. Jordens, L. Janssen, C. Kuijl, V. M. Olkkonen and J. Neefjes (2007). "Activation of endosomal dynein motors by stepwise assembly of Rab7-RILP-p150Glued, ORP1L, and the receptor betalll spectrin." J Cell Biol **176**(4): 459-471.

Johnson, D. E., P. Ostrowski, V. Jaumouille and S. Grinstein (2016). "The position of lysosomes within the cell determines their luminal pH." J Cell Biol **212**(6): 677-692.

Johnson, D. R., R. S. Bhatnagar, L. J. Knoll and J. I. Gordon (1994). "Genetic and biochemical studies of protein N-myristoylation." Annu Rev Biochem **63**: 869-914.

Johnson, W. J., G. K. Chacko, M. C. Phillips and G. H. Rothblat (1990). "The efflux of lysosomal cholesterol from cells." J Biol Chem **265**(10): 5546-5553.

Jongsma, M. L., I. Berlin, R. H. Wijdeven, L. Janssen, G. M. Janssen, M. A. Garstka, H. Janssen, M. Mensink, P. A. van Veelen, R. M. Spaapen and J. Neefjes (2016). "An ER-Associated Pathway Defines Endosomal Architecture for Controlled Cargo Transport." Cell **166**(1): 152-166.

Kandutsch, A. A. and A. E. Russell (1960). "Preputial gland tumor sterols. 2. The identification of 4 alpha-methyl-Delta 8-cholesten-3 beta-ol." J Biol Chem **235**: 2253-2255.

Kandutsch, A. A. and A. E. Russell (1960). "Preputial gland tumor sterols. 3. A metabolic pathway from lanosterol to cholesterol." J Biol Chem **235**: 2256-2261.

Kang, J. U., S. H. Koo, K. C. Kwon, J. W. Park and J. M. Kim (2008). "Gain at chromosomal region 5p15.33, containing TERT, is the most frequent genetic event in early stages of non-small cell lung cancer." Cancer Genet Cytogenet **182**(1): 1-11.

Kedi, X., Y. Ming, W. Yongping, Y. Yi and Z. Xiaoxiang (2009). "Free cholesterol overloading induced smooth muscle cells death and activated both ER- and mitochondrial-dependent death pathway." Atherosclerosis **207**(1): 123-130.

Kerppola, T. K. (2006). "Design and implementation of bimolecular fluorescence complementation (BiFC) assays for the visualization of protein interactions in living cells." Nat Protoc **1**(3): 1278-1286.

Kim, E., P. Goraksha-Hicks, L. Li, T. P. Neufeld and K. L. Guan (2008). "Regulation of TORC1 by Rag GTPases in nutrient response." Nat Cell Biol **10**(8): 935-945.

Kishimoto, Y., M. Hiraiwa and J. S. O'Brien (1992). "Saposins: structure, function, distribution, and molecular genetics." J Lipid Res **33**(9): 1255-1267.

Klinkner, A. M., C. R. Waites, W. D. Kerns and P. J. Bugelski (1995). "Evidence of foam cell and cholesterol crystal formation in macrophages incubated with oxidized LDL by fluorescence and electron microscopy." J Histochem Cytochem **43**(10): 1071-1078.

Knipper, M., C. Claussen, L. Ruttiger, U. Zimmermann, R. Lullmann-Rauch, E. L. Eskelinen, J. Schroder, M. Schwake and P. Saftig (2006). "Deafness in LIMP2-deficient mice due to early loss of the potassium channel KCNQ1/KCNE1 in marginal cells of the stria vascularis." J Physiol **576**(Pt 1): 73-86.

Knott, G. J. and J. A. Doudna (2018). "CRISPR-Cas guides the future of genetic engineering." Science **361**(6405): 866-869.

Ko, D. C., J. Binkley, A. Sidow and M. P. Scott (2003). "The integrity of a cholesterol-binding pocket in Niemann-Pick C2 protein is necessary to control lysosome cholesterol levels." Proc Natl Acad Sci U S A **100**(5): 2518-2525.

Kobayashi, K. and S. Koike (2020). "Cellular receptors for enterovirus A71." J Biomed Sci **27**(1): 23.

Kolter, T. and K. Sandhoff (2010). "Lysosomal degradation of membrane lipids." FEBS Lett **584**(9): 1700-1712.

Korber, M., I. Klein and G. Daum (2017). "Steryl ester synthesis, storage and hydrolysis: A contribution to sterol homeostasis." Biochim Biophys Acta Mol Cell Biol Lipids **1862**(12): 1534-1545.

Korolchuk, V. I., S. Saiki, M. Lichtenberg, F. H. Siddiqi, E. A. Roberts, S. Imarisio, L. Jahreiss, S. Sarkar, M. Futter, F. M. Menzies, C. J. O'Kane, V. Deretic and D. C. Rubinsztein (2011). "Lysosomal positioning coordinates cellular nutrient responses." Nat Cell Biol **13**(4): 453-460.

Korschen, H. G., Y. Yildiz, D. N. Raju, S. Schonauer, W. Bonigk, V. Jansen, E. Kremmer, U. B. Kaupp and D. Wachten (2013). "The non-lysosomal beta-glucosidase GBA2 is a non-integral membrane-associated protein at the endoplasmic reticulum (ER) and Golgi." J Biol Chem **288**(5): 3381-3393.

Kunimoto, S., T. Kobayashi, S. Kobayashi and K. Murakami-Murofushi (2000). "Expression of cholesteryl glucoside by heat shock in human fibroblasts." Cell Stress Chaperones **5**(1): 3-7.

Kunimoto, S., W. Murofushi, H. Kai, Y. Ishida, A. Uchiyama, T. Kobayashi, S. Kobayashi, H. Murofushi and K. Murakami-Murofushi (2002). "Steryl glucoside is a lipid mediator in stress-responsive signal transduction." Cell Struct Funct **27**(3): 157-162.

Kunimoto, S., W. Murofushi, I. Yamatsu, Y. Hasegawa, N. Sasaki, S. Kobayashi, T. Kobayashi, H. Murofushi and K. Murakami-Murofushi (2003). "Cholesteryl glucoside-induced protection against gastric ulcer." Cell Struct Funct **28**(3): 179-186.

Kuronita, T., E. L. Eskelinen, H. Fujita, P. Saftig, M. Himeno and Y. Tanaka (2002). "A role for the lysosomal membrane protein LGP85 in the biogenesis and maintenance of endosomal and lysosomal morphology." J Cell Sci **115**(Pt 21): 4117-4131.

Kuzu, O. F., M. A. Noory and G. P. Robertson (2016). "The Role of Cholesterol in Cancer." Cancer Res **76**(8): 2063-2070.

Kwon, H. J., L. Abi-Mosleh, M. L. Wang, J. Deisenhofer, J. L. Goldstein, M. S. Brown and R. E. Infante (2009). "Structure of N-Terminal Domain of NPC1 Reveals Distinct Subdomains for Binding and Transfer of Cholesterol." Cell **137**(7): 1213-1224.

Kwon, H. J., T. A. Lagace, M. C. McNutt, J. D. Horton and J. Deisenhofer (2008). "Molecular basis for LDL receptor recognition by PCSK9." Proc Natl Acad Sci U S A **105**(6): 1820-1825.

Laemmli, U. K. (1970). "Cleavage of structural proteins during the assembly of the head of bacteriophage T4." Nature **227**(5259): 680-685.

Lagace, T. A. (2014). "PCSK9 and LDLR degradation: regulatory mechanisms in circulation and in cells." Curr Opin Lipidol **25**(5): 387-393.

Lagace, T. A., D. E. Curtis, R. Garuti, M. C. McNutt, S. W. Park, H. B. Prather, N. N. Anderson, Y. K. Ho, R. E. Hammer and J. D. Horton (2006). "Secreted PCSK9 decreases the number of LDL receptors in hepatocytes and in livers of parabiotic mice." J Clin Invest **116**(11): 2995-3005.

Lange, Y. and T. L. Steck (1997). "Quantitation of the pool of cholesterol associated with acyl-CoA:cholesterol acyltransferase in human fibroblasts." J Biol Chem **272**(20): 13103-13108.

Lange, Y., J. Ye, M. Rigney and T. L. Steck (1999). "Regulation of endoplasmic reticulum cholesterol by plasma membrane cholesterol." J Lipid Res **40**(12): 2264-2270.

Lanyon-Hogg, T., M. Faronato, R. A. Serwa and E. W. Tate (2017). "Dynamic Protein Acylation: New Substrates, Mechanisms, and Drug Targets." Trends Biochem Sci **42**(7): 566-581.

Lawrence, R. E. and R. Zoncu (2019). "The lysosome as a cellular centre for signalling, metabolism and quality control." Nat Cell Biol **21**(2): 133-142.

Lee, R. E. (1968). "The fine structure of the cerebroside occurring in Gaucher's disease." Proc Natl Acad Sci U S A **61**(2): 484-489.

Leinekugel, P., S. Michel, E. Conzelmann and K. Sandhoff (1992). "Quantitative correlation between the residual activity of beta-hexosaminidase A and arylsulfatase A and the severity of the resulting lysosomal storage disease." Hum Genet **88**(5): 513-523.

Lemonidis, K., O. A. Gorleku, M. C. Sanchez-Perez, C. Grefen and L. H. Chamberlain (2014). "The Golgi S-acylation machinery comprises zDHHC enzymes with major differences in substrate affinity and S-acylation activity." Mol Biol Cell **25**(24): 3870-3883.

Leney, A. C., R. Rezaei Darestani, J. Li, S. Nikjah, E. N. Kitova, C. Zou, C. W. Cairo, Z. J. Xiong, G. G. Prive and J. S. Klassen (2015). "Picodiscs for facile protein-glycolipid interaction analysis." Anal Chem **87**(8): 4402-4408.

Lev, S. (2010). "Non-vesicular lipid transport by lipid-transfer proteins and beyond." Nat Rev Mol Cell Biol **11**(10): 739-750.

Lev, S., D. Ben Halevy, D. Peretti and N. Dahan (2008). "The VAP protein family: from cellular functions to motor neuron disease." Trends Cell Biol **18**(6): 282-290.

Levental, I., M. Grzybek and K. Simons (2010). "Greasing their way: lipid modifications determine protein association with membrane rafts." Biochemistry **49**(30): 6305-6316.

Levitan, I., D. K. Singh and A. Rosenhouse-Dantsker (2014). "Cholesterol binding to ion channels." Front Physiol **5**: 65.

Lewis, J. C., R. G. Taylor and K. Ohta (1988). "Lysosomal alterations during coronary atherosclerosis in the pigeon: correlative cytochemical and three-dimensional HVEM/IVEM observations." Exp Mol Pathol **48**(1): 103-115.

Lewis, V., S. A. Green, M. Marsh, P. Vihko, A. Helenius and I. Mellman (1985). "Glycoproteins of the lysosomal membrane." J Cell Biol **100**(6): 1839-1847.

Li, J. and S. R. Pfeffer (2016). "Lysosomal membrane glycoproteins bind cholesterol and contribute to lysosomal cholesterol export." Elife **5**.

Li, X., P. Saha, J. Li, G. Blobel and S. R. Pfeffer (2016). "Clues to the mechanism of cholesterol transfer from the structure of NPC1 middle lumenal domain bound to NPC2." Proc Natl Acad Sci U S A **113**(36): 10079-10084.

Li, X., J. Wang, E. Coutavas, H. Shi, Q. Hao and G. Blobel (2016). "Structure of human Niemann-Pick C1 protein." Proc Natl Acad Sci U S A **113**(29): 8212-8217.

Lin, Y. H., A. G. Doms, E. Cheng, B. Kim, T. R. Evans and M. P. Machner (2015). "Host Cell-catalyzed S-Palmitoylation Mediates Golgi Targeting of the Legionella Ubiquitin Ligase GobX." J Biol Chem **290**(42): 25766-25781.

Linder, M. D., R. L. Uronen, M. Holtta-Vuori, P. van der Sluijs, J. Peranen and E. Ikonen (2007). "Rab8-dependent recycling promotes endosomal cholesterol removal in normal and sphingolipidosis cells." Mol Biol Cell **18**(1): 47-56.

Listenberger, L. L., X. Han, S. E. Lewis, S. Cases, R. V. Farese, Jr., D. S. Ory and J. E. Schaffer (2003). "Triglyceride accumulation protects against fatty acid-induced lipotoxicity." Proc Natl Acad Sci U S A **100**(6): 3077-3082.

Lloyd-Evans, E., A. J. Morgan, X. He, D. A. Smith, E. Elliot-Smith, D. J. Sillence, G. C. Churchill, E. H. Schuchman, A. Galione and F. M. Platt (2008). "Niemann-Pick disease type C1 is a sphingosine storage disease that causes deregulation of lysosomal calcium." Nat Med **14**(11): 1247-1255.

Loewen, C. J., A. Roy and T. P. Levine (2003). "A conserved ER targeting motif in three families of lipid binding proteins and in Opi1p binds VAP." EMBO J **22**(9): 2025-2035.

Long, J. Z. and B. F. Cravatt (2011). "The metabolic serine hydrolases and their functions in mammalian physiology and disease." Chem Rev **111**(10): 6022-6063.

Lozach, P. Y., J. Huotari and A. Helenius (2011). "Late-penetrating viruses." Curr Opin Virol **1**(1): 35-43.

Lu, F., Q. Liang, L. Abi-Mosleh, A. Das, J. K. De Brabander, J. L. Goldstein and M. S. Brown (2015). "Identification of NPC1 as the target of U18666A, an inhibitor of lysosomal cholesterol export and Ebola infection." Elife **4**.

Luo, J., H. Yang and B. L. Song (2020). "Mechanisms and regulation of cholesterol homeostasis." Nat Rev Mol Cell Biol **21**(4): 225-245.

Marques, A. R., M. Mirzaian, H. Akiyama, P. Wisse, M. J. Ferraz, P. Gaspar, K. Ghauharali-van der Vlugt, R. Meijer, P. Giraldo, P. Alfonso, P. Irun, M. Dahl, S. Karlsson, E. V. Pavlova, T. M. Cox, S. Scheij, M. Verhoek, R. Ottenhoff, C. P. van Roomen, N. S. Pannu, M. van Eijk, N. Dekker, R. G. Boot, H. S. Overkleeft, E. Blommaart, Y. Hirabayashi and J. M. Aerts (2016). "Glucosylated cholesterol in mammalian cells and tissues: formation and degradation by multiple cellular beta-glucosidases." J Lipid Res **57**(3): 451-463.

Marques, A. R. A., A. Di Spiezio, N. Thiessen, L. Schmidt, J. Grotzinger, R. Lullmann-Rauch, M. Damme, S. E. Storck, C. U. Pietrzik, J. Fogh, J. Bar, M. Mikhaylova, M. Glatzel, M. Bassal, U. Bartsch and P. Saftig (2020). "Enzyme replacement therapy with recombinant pro-CTSD (cathepsin D) corrects defective proteolysis and autophagy in neuronal ceroid lipofuscinosis." Autophagy **16**(5): 811-825.

Marques, A. R. A. and P. Saftig (2019). "Lysosomal storage disorders - challenges, concepts and avenues for therapy: beyond rare diseases." J Cell Sci **132**(2).

Marques, P. E., S. Nyegaard, R. F. Collins, F. Troise, S. A. Freeman, W. S. Trimble and S. Grinstein (2019). "Multimerization and Retention of the Scavenger Receptor SR-B1 in the Plasma Membrane." Dev Cell **50**(3): 283-295 e285.

Marsh, M., S. Schmid, H. Kern, E. Harms, P. Male, I. Mellman and A. Helenius (1987). "Rapid analytical and preparative isolation of functional endosomes by free flow electrophoresis." J Cell Biol **104**(4): 875-886.

Massa Lopez, D., M. Thelen, F. Stahl, C. Thiel, A. Linhorst, M. Sylvester, I. Hermanns-Borgmeyer, R. Lullmann-Rauch, W. Eskild, P. Saftig and M. Damme (2019). "The lysosomal transporter MFSD1 is essential for liver homeostasis and critically depends on its accessory subunit GLMP." Elife **8**.

Maurer-Stroh, S., M. Gouda, M. Novatchkova, A. Schleiffer, G. Schneider, F. L. Sirota, M. Wildpaner, N. Hayashi and F. Eisenhaber (2004). "MYRbase: analysis of genome-wide glycine myristoylation enlarges the functional spectrum of eukaryotic myristoylated proteins." Genome Biol **5**(3): R21.

Maxfield, F. R., D. B. Iaea and N. H. Pipalia (2016). "Role of STARD4 and NPC1 in intracellular sterol transport." Biochem Cell Biol **94**(6): 499-506.

Maxfield, F. R. and I. Tabas (2005). "Role of cholesterol and lipid organization in disease." Nature **438**(7068): 612-621.

Maxfield, F. R. and G. van Meer (2010). "Cholesterol, the central lipid of mammalian cells." Curr Opin Cell Biol **22**(4): 422-429.

Mazzulli, J. R., Y. H. Xu, Y. Sun, A. L. Knight, P. J. McLean, G. A. Caldwell, E. Sidransky, G. A. Grabowski and D. Krainc (2011). "Gaucher disease glucocerebrosidase and alpha-synuclein form a bidirectional pathogenic loop in synucleinopathies." Cell **146**(1): 37-52.

Mazzulli, J. R., F. Zunke, T. Tsunemi, N. J. Toker, S. Jeon, L. F. Burbulla, S. Patnaik, E. Sidransky, J. J. Marugan, C. M. Sue and D. Krainc (2016). "Activation of beta-Glucocerebrosidase Reduces Pathological alpha-Synuclein and Restores Lysosomal Function in Parkinson's Patient Midbrain Neurons." J Neurosci **36**(29): 7693-7706.

McCauliff, L. A., A. Langan, R. Li, O. Ilnytska, D. Bose, M. Waghalter, K. Lai, P. C. Kahn and J. Storch (2019). "Intracellular cholesterol trafficking is dependent upon NPC2 interaction with lysobisphosphatidic acid." Elife **8**.

McCauliff, L. A., Z. Xu, R. Li, S. Kodukula, D. C. Ko, M. P. Scott, P. C. Kahn and J. Storch (2015). "Multiple Surface Regions on the Niemann-Pick C2 Protein Facilitate Intracellular Cholesterol Transport." J Biol Chem **290**(45): 27321-27331.

McEwan, D. G. and I. Dikic (2011). "The Three Musketeers of Autophagy: phosphorylation, ubiquitylation and acetylation." Trends Cell Biol **21**(4): 195-201.

McMichael, T. M., L. Zhang, M. Chemudupati, J. C. Hach, A. D. Kenney, H. C. Hang and J. S. Yount (2017). "The palmitoyltransferase ZDHHC20 enhances interferon-induced transmembrane protein 3 (IFITM3) palmitoylation and antiviral activity." J Biol Chem **292**(52): 21517-21526.

McMinn, P. C. (2002). "An overview of the evolution of enterovirus 71 and its clinical and public health significance." FEMS Microbiol Rev **26**(1): 91-107.

Mehta, A. (2006). "Epidemiology and natural history of Gaucher's disease." Eur J Intern Med **17 Suppl**: S2-5.

Melkonian, K. A., A. G. Ostermeyer, J. Z. Chen, M. G. Roth and D. A. Brown (1999). "Role of lipid modifications in targeting proteins to detergent-resistant membrane rafts. Many raft proteins are acylated, while few are prenylated." J Biol Chem **274**(6): 3910-3917.

Meng, Y., S. Heybrock, D. Neculai and P. Saftig (2020). "Cholesterol Handling in Lysosomes and Beyond." Trends Cell Biol **30**(6): 452-466.

Mesmin, B., J. Bigay, J. Moser von Filseck, S. Lacas-Gervais, G. Drin and B. Antonny (2013). "A four-step cycle driven by PI(4)P hydrolysis directs sterol/PI(4)P exchange by the ER-Golgi tether OSBP." Cell **155**(4): 830-843.

Millard, E. E., K. Srivastava, L. M. Traub, J. E. Schaffer and D. S. Ory (2000). "Niemann-pick type C1 (NPC1) overexpression alters cellular cholesterol homeostasis." J Biol Chem **275**(49): 38445-38451.

Mitchell, D. A., A. Vasudevan, M. E. Linder and R. J. Deschenes (2006). "Protein palmitoylation by a family of DHHC protein S-acyltransferases." J Lipid Res **47**(6): 1118-1127.

Mitsche, M. A., J. G. McDonald, H. H. Hobbs and J. C. Cohen (2015). "Flux analysis of cholesterol biosynthesis in vivo reveals multiple tissue and cell-type specific pathways." Elife **4**: e07999.

Moore, K. J., F. J. Sheedy and E. A. Fisher (2013). "Macrophages in atherosclerosis: a dynamic balance." Nat Rev Immunol **13**(10): 709-721.

Murphy, S. E. and T. P. Levine (2016). "VAP, a Versatile Access Point for the Endoplasmic Reticulum: Review and analysis of FFAT-like motifs in the VAPome." Biochim Biophys Acta **1861**(8 Pt B): 952-961.

Nagaraj, N., J. R. Wisniewski, T. Geiger, J. Cox, M. Kircher, J. Kelso, S. Paabo and M. Mann (2011). "Deep proteome and transcriptome mapping of a human cancer cell line." Mol Syst Biol **7**: 548.

Naito, T., B. Ercan, L. Krshnan, A. Triebl, D. H. Z. Koh, F. Y. Wei, K. Tomizawa, F. T. Torta, M. R. Wenk and Y. Saheki (2019). "Movement of accessible plasma membrane cholesterol by the GRAMD1 lipid transfer protein complex." Elife **8**.

Neculai, D., M. Schwake, M. Ravichandran, F. Zunke, R. F. Collins, J. Peters, M. Neculai, J. Plumb, P. Loppnau, J. C. Pizarro, A. Seitova, W. S. Trimble, P. Saftig, S. Grinstein and S. Dhe-Paganon (2013). "Structure of LIMP-2 provides functional insights with implications for SR-BI and CD36." Nature **504**(7478): 172-176.

Neufeld, E. B., A. M. Cooney, J. Pitha, E. A. Dawidowicz, N. K. Dwyer, P. G. Pentchev and E. J. Blanchette-Mackie (1996). "Intracellular trafficking of cholesterol monitored with a cyclodextrin." J Biol Chem **271**(35): 21604-21613.

Ng, M., D. Thakkar, L. Southam, P. Werker, R. Ophoff, K. Becker, M. Nothnagel, A. Franke, P. Nurnberg, A. I. Espirito-Santo, D. Izadi, H. C. Hennies, J. Nanchahal, E. Zeggini and D. Furniss (2017). "A Genome-wide Association Study of Dupuytren Disease Reveals 17 Additional Variants Implicated in Fibrosis." Am J Hum Genet **101**(3): 417-427.

Nielsen, S. F., B. G. Nordestgaard and S. E. Bojesen (2012). "Statin use and reduced cancer-related mortality." N Engl J Med **367**(19): 1792-1802.

Norman, A. W., R. A. Demel, B. de Kruyff, W. S. Geurts van Kessel and L. L. van Deenen (1972). "Studies on the biological properties of polyene antibiotics: comparison of other polyenes with filipin in their ability to interact specifically with sterol." Biochim Biophys Acta **290**(1): 1-14.

Nozaki, S., H. Kashiwagi, S. Yamashita, T. Nakagawa, B. Kostner, Y. Tomiyama, A. Nakata, M. Ishigami, J. Miyagawa, K. Kameda-Takemura and et al. (1995). "Reduced uptake of oxidized low density lipoproteins in monocyte-derived macrophages from CD36-deficient subjects." J Clin Invest **96**(4): 1859-1865.

Ockenhouse, C. F. and J. D. Chulay (1988). "Plasmodium falciparum sequestration: OKM5 antigen (CD36) mediates cytoadherence of parasitized erythrocytes to a myelomonocytic cell line." J Infect Dis **157**(3): 584-588.

Ogata, S. and M. Fukuda (1994). "Lysosomal targeting of Limp II membrane glycoprotein requires a novel Leu-Ile motif at a particular position in its cytoplasmic tail." J Biol Chem **269**(7): 5210-5217.

Ohkuma, S. and B. Poole (1978). "Fluorescence probe measurement of the intralysosomal pH in living cells and the perturbation of pH by various agents." Proc Natl Acad Sci U S A **75**(7): 3327-3331.

Ohno, Y., A. Kihara, T. Sano and Y. Igarashi (2006). "Intracellular localization and tissue-specific distribution of human and yeast DHHC cysteine-rich domain-containing proteins." Biochim Biophys Acta **1761**(4): 474-483.

Ohvo-Rekila, H., B. Ramstedt, P. Leppimaki and J. P. Slotte (2002). "Cholesterol interactions with phospholipids in membranes." Prog Lipid Res **41**(1): 66-97.

Pahwa, R. and I. Jialal (2020). Atherosclerosis. StatPearls. Treasure Island (FL).

Pan, X., P. Roberts, Y. Chen, E. Kvam, N. Shulga, K. Huang, S. Lemmon and D. S. Goldfarb (2000). "Nucleus-vacuole junctions in Saccharomyces cerevisiae are formed through the direct interaction of Vac8p with Nvj1p." Mol Biol Cell **11**(7): 2445-2457.

Patterson, M. C., P. Clayton, P. Gissen, M. Anheim, P. Bauer, O. Bonnot, A. Dardis, C. Dionisi-Vici, H. H. Klunemann, P. Latour, C. M. Lourenco, D. S. Ory, A. Parker, M. Pocovi, M. Strupp, M. T. Vanier, M. Walterfang and T. Marquardt (2017). "Recommendations for the detection and diagnosis of Niemann-Pick disease type C: An update." Neurol Clin Pract **7**(6): 499-511.

Patwardhan, P. and M. D. Resh (2010). "Myristoylation and membrane binding regulate c-Src stability and kinase activity." Mol Cell Biol **30**(17): 4094-4107.

Pentchev, P. G., M. E. Comly, H. S. Kruth, M. T. Vanier, D. A. Wenger, S. Patel and R. O. Brady (1985). "A defect in cholesterol esterification in Niemann-Pick disease (type C) patients." Proc Natl Acad Sci U S A **82**(23): 8247-8251.

Pepino, M. Y., O. Kuda, D. Samovski and N. A. Abumrad (2014). "Structure-function of CD36 and importance of fatty acid signal transduction in fat metabolism." Annu Rev Nutr **34**: 281-303.

Percher, A., S. Ramakrishnan, E. Thinon, X. Yuan, J. S. Yount and H. C. Hang (2016). "Mass-tag labeling reveals site-specific and endogenous levels of protein S-fatty acylation." Proc Natl Acad Sci U S A **113**(16): 4302-4307.

Peretti, D., N. Dahan, E. Shimoni, K. Hirschberg and S. Lev (2008). "Coordinated lipid transfer between the endoplasmic reticulum and the Golgi complex requires the VAP proteins and is essential for Golgi-mediated transport." Mol Biol Cell **19**(9): 3871-3884.

Peters, C. and K. von Figura (1994). "Biogenesis of lysosomal membranes." FEBS Lett **346**(1): 108-114.

Phillips, M. J. and G. K. Voeltz (2016). "Structure and function of ER membrane contact sites with other organelles." Nat Rev Mol Cell Biol **17**(2): 69-82.

Pike, L. J. (2004). "Lipid rafts: heterogeneity on the high seas." Biochem J **378**(Pt 2): 281-292.

Platt, F. M., A. d'Azzo, B. L. Davidson, E. F. Neufeld and C. J. Tifft (2018). "Lysosomal storage diseases." Nat Rev Dis Primers **4**(1): 27.

Ponting, C. P. and L. Aravind (1999). "START: a lipid-binding domain in StAR, HD-ZIP and signalling proteins." Trends Biochem Sci **24**(4): 130-132.

Popovic, K., J. Holyoake, R. Pomes and G. G. Prive (2012). "Structure of saposin A lipoprotein discs." Proc Natl Acad Sci U S A **109**(8): 2908-2912.

PrabhuDas, M. R., C. L. Baldwin, P. L. Bollyky, D. M. E. Bowdish, K. Drickamer, M. Febbraio, J. Herz, L. Kobzik, M. Krieger, J. Loike, B. McVicker, T. K. Means, S. K. Moestrup, S. R. Post, T. Sawamura, S. Silverstein, R. C. Speth, J. C. Telfer, G. M. Thiele, X. Y. Wang, S. D. Wright and J. El Khoury (2017). "A Consensus Definitive Classification of Scavenger Receptors and Their Roles in Health and Disease." J Immunol **198**(10): 3775-3789.

Prinz, W. A. (2007). "Non-vesicular sterol transport in cells." Prog Lipid Res **46**(6): 297-314.

Pu, J., C. M. Guardia, T. Keren-Kaplan and J. S. Bonifacino (2016). "Mechanisms and functions of lysosome positioning." J Cell Sci **129**(23): 4329-4339.

Radhakrishnan, A., J. L. Goldstein, J. G. McDonald and M. S. Brown (2008). "Switch-like control of SREBP-2 transport triggered by small changes in ER cholesterol: a delicate balance." Cell Metab **8**(6): 512-521.

Rajamohan, F., A. R. Reyes, M. Tu, N. L. Nedoma, L. R. Hoth, A. G. Schwaid, R. G. Kurumbail, J. Ward and S. Han (2020). "Crystal Structure of human Lysosomal Acid Lipase and its Implications in Cholesteryl Ester Storage Disease (CESD)." J Lipid Res.

Rana, M. S., C. J. Lee and A. Banerjee (2019). "The molecular mechanism of DHHC protein acyltransferases." Biochem Soc Trans **47**(1): 157-167.

Ravnskov, U., P. J. Rosch and K. S. McCully (2015). "Statins do not protect against cancer: quite the opposite." J Clin Oncol **33**(7): 810-811.

Reczek, D., M. Schwake, J. Schroder, H. Hughes, J. Blanz, X. Jin, W. Brondyk, S. Van Patten, T. Edmunds and P. Saftig (2007). "LIMP-2 is a receptor for lysosomal mannose-6-phosphate-independent targeting of beta-glucocerebrosidase." Cell **131**(4): 770-783.

Reczek, D., M. Schwake, J. Schroder, H. Hughes, J. Blanz, X. Jin, W. Brondyk, P. S. Van, T. Edmunds and P. Saftig (2007). "LIMP-2 is a receptor for lysosomal mannose-6-phosphate-independent targeting of beta-glucocerebrosidase." Cell **131**(4): 770-783.

Ren, W., Y. Sun and K. Du (2013). "DHHC17 palmitoylates ClipR-59 and modulates ClipR-59 association with the plasma membrane." Mol Cell Biol **33**(21): 4255-4265.

Ren, W., Y. Sun and K. Du (2015). "Glut4 palmitoylation at Cys223 plays a critical role in Glut4 membrane trafficking." Biochem Biophys Res Commun **460**(3): 709-714.

Resh, M. D. (2016). "Fatty acylation of proteins: The long and the short of it." Prog Lipid Res **63**: 120-131.

Riffo-Campos, A. L., J. Castillo, A. Vallet-Sanchez, G. Ayala, A. Cervantes, G. Lopez-Rodas and L. Franco (2016). "In silico RNA-seq and experimental analyses reveal the differential expression and splicing of EPDR1 and ZNF518B genes in relation to KRAS mutations in colorectal cancer cells." Oncol Rep **36**(6): 3627-3634.

Rigotti, A., S. L. Acton and M. Krieger (1995). "The class B scavenger receptors SR-BI and CD36 are receptors for anionic phospholipids." J Biol Chem **270**(27): 16221-16224.

Rigotti, A., H. E. Miettinen and M. Krieger (2003). "The role of the high-density lipoprotein receptor SR-BI in the lipid metabolism of endocrine and other tissues." Endocr Rev **24**(3): 357-387.

Rocha, E. M., G. A. Smith, E. Park, H. Cao, E. Brown, P. Hallett and O. Isacson (2015). "Progressive decline of glucocerebrosidase in aging and Parkinson's disease." Ann Clin Transl Neurol **2**(4): 433-438.

Rocha, N., C. Kuijl, R. van der Kant, L. Janssen, D. Houben, H. Janssen, W. Zwart and J. Neefjes (2009). "Cholesterol sensor ORP1L contacts the ER protein VAP to control Rab7-RILP-p150 Glued and late endosome positioning." J Cell Biol **185**(7): 1209-1225.

Rocks, O., A. Peyker, M. Kahms, P. J. Verveer, C. Koerner, M. Lumbierres, J. Kuhlmann, H. Waldmann, A. Wittinghofer and P. I. Bastiaens (2005). "An acylation cycle regulates localization and activity of palmitoylated Ras isoforms." Science **307**(5716): 1746-1752.

Rodenburg, R. N. P., J. Snijder, M. van de Waterbeemd, A. Schouten, J. Granneman, A. J. R. Heck and P. Gros (2017). "Stochastic palmitoylation of accessible cysteines in membrane proteins revealed by native mass spectrometry." Nat Commun **8**(1): 1280.

Rosenberg, E. E., G. V. Gerashchenko, N. V. Hryshchenko, L. V. Mevs, K. A. Nekrasov, R. A. Lytvynenko, Y. V. Vitruk, O. P. Gryzodub, E. A. Stakhovsky and V. I. Kashuba (2017). "Expression of cancer-associated genes in prostate tumors." Exp Oncol **39**(2): 131-137.

Rosenson, R. S., H. B. Brewer, Jr., W. S. Davidson, Z. A. Fayad, V. Fuster, J. Goldstein, M. Hellerstein, X. C. Jiang, M. C. Phillips, D. J. Rader, A. T. Remaley, G. H. Rothblat, A. R. Tall and L. Yvan-Charvet (2012). "Cholesterol efflux and atheroprotection: advancing the concept of reverse cholesterol transport." Circulation **125**(15): 1905-1919.

Rothaug, M., F. Zunke, J. R. Mazzulli, M. Schweizer, H. Altmeppen, R. Lullmann-Rauch, W. W. Kallemeijn, P. Gaspar, J. M. Aerts, M. Glatzel, P. Saftig, D. Krainc, M. Schwake and J. Blanz (2014). "LIMP-2 expression is critical for beta-glucocerebrosidase activity and alpha-synuclein clearance." Proc Natl Acad Sci U S A **111**(43): 15573-15578.

Rusch, M., T. J. Zimmermann, M. Burger, F. J. Dekker, K. Gormer, G. Triola, A. Brockmeyer, P. Janning, T. Bottcher, S. A. Sieber, I. R. Vetter, C. Hedberg and H. Waldmann (2011). "Identification of acyl protein thioesterases 1 and 2 as the cellular targets of the Ras-signaling modulators palmostatin B and M." Angew Chem Int Ed Engl **50**(42): 9838-9842.

Saftig, P. (2006). Physiology of the lysosome. Fabry Disease: Perspectives from 5 Years of FOS. A. Mehta, M. Beck and G. Sunder-Plassmann. Oxford.

Saftig, P. (2010). Lysosomes, Springer US.

Saftig, P., M. Hetman, W. Schmahl, K. Weber, L. Heine, H. Mossmann, A. Koster, B. Hess, M. Evers, K. von Figura and et al. (1995). "Mice deficient for the lysosomal proteinase cathepsin D exhibit progressive atrophy of the intestinal mucosa and profound destruction of lymphoid cells." EMBO J **14**(15): 3599-3608.

Saftig, P. and J. Klumperman (2009). "Lysosome biogenesis and lysosomal membrane proteins: trafficking meets function." Nat Rev Mol Cell Biol **10**(9): 623-635.

Sancak, Y., L. Bar-Peled, R. Zoncu, A. L. Markhard, S. Nada and D. M. Sabatini (2010). "Ragulator-Rag complex targets mTORC1 to the lysosomal surface and is necessary for its activation by amino acids." Cell **141**(2): 290-303.

Sanders, S. S., D. D. Martin, S. L. Butland, M. Lavallee-Adam, D. Calzolari, C. Kay, J. R. Yates, 3rd and M. R. Hayden (2015). "Curation of the Mammalian Palmitoylome Indicates a Pivotal Role for Palmitoylation in Diseases and Disorders of the Nervous System and Cancers." PLoS Comput Biol **11**(8): e1004405.

Sandhoff, R. and K. Sandhoff (2018). "Emerging concepts of ganglioside metabolism." FEBS Lett **592**(23): 3835-3864.

Sandhu, J., S. Li, L. Fairall, S. G. Pfisterer, J. E. Gurnett, X. Xiao, T. A. Weston, D. Vashi, A. Ferrari, J. L. Orozco, C. L. Hartman, D. Strugatsky, S. D. Lee, C. He, C. Hong, H. Jiang, L. A. Bentolila, A. T. Gatta, T. P. Levine, A. Ferng, R. Lee, D. A. Ford, S. G. Young, E. Ikonen, J. W. R. Schwabe and P. Tontonoz (2018). "Aster Proteins Facilitate Nonvesicular Plasma Membrane to ER Cholesterol Transport in Mammalian Cells." Cell **175**(2): 514-529 e520.

Sardi, S. P., J. Clarke, C. Kinnecom, T. J. Tamsett, L. Li, L. M. Stanek, M. A. Passini, G. A. Grabowski, M. G. Schlossmacher, R. L. Sidman, S. H. Cheng and L. S. Shihabuddin (2011). "CNS expression of glucocerebrosidase corrects alpha-synuclein pathology and memory in a mouse model of Gaucher-related synucleinopathy." Proc Natl Acad Sci U S A **108**(29): 12101-12106.

Schagger, H. and G. von Jagow (1991). "Blue native electrophoresis for isolation of membrane protein complexes in enzymatically active form." Anal Biochem **199**(2): 223-231.

Schaum, N., B. Lehallier, O. Hahn, S. Hosseinzadeh, S. E. Lee, R. Sit, D. P. Lee, P. M. Losada, M. E. Zardeneta, R. Pálovics, T. Fehlmann, J. Webber, A. McGeever, H. Zhang, D. Berdnik, W. Tan, A. Zee, M. Tan, A. Pisco, J. Karkanias, N. F. Neff, A. Keller, S. Darmanis, S. R. Quake and T. Wyss-Coray (2019). "The murine transcriptome reveals global aging nodes with organ-specific phase and amplitude." bioRxiv: 662254.

Schieweck, O., M. Damme, B. Schroder, A. Hasilik, B. Schmidt and T. Lubke (2009). "NCU-G1 is a highly glycosylated integral membrane protein of the lysosome." Biochem J **422**(1): 83-90.

Schueler, U. H., T. Kolter, C. R. Kaneski, G. C. Zirzow, K. Sandhoff and R. O. Brady (2004). "Correlation between enzyme activity and substrate storage in a cell culture model system for Gaucher disease." J Inherit Metab Dis **27**(5): 649-658.

Schulze, H. and K. Sandhoff (2014). "Sphingolipids and lysosomal pathologies." Biochim Biophys Acta **1841**(5): 799-810.

Schumaker, V. N. and G. H. Adams (1969). "Circulating lipoproteins." Annu Rev Biochem **38**: 113-136.

Schwake, M., B. Schroder and P. Saftig (2013). "Lysosomal membrane proteins and their central role in physiology." Traffic **14**(7): 739-748.

Schwenk, F., U. Baron and K. Rajewsky (1995). "A cre-transgenic mouse strain for the ubiquitous deletion of loxP-flanked gene segments including deletion in germ cells." Nucleic Acids Res **23**(24): 5080-5081.

Seidel, S. A., P. M. Dijkman, W. A. Lea, G. van den Bogaart, M. Jerabek-Willemsen, A. Lazic, J. S. Joseph, P. Srinivasan, P. Baaske, A. Simeonov, I. Katritch, F. A. Melo, J. E. Ladbury, G. Schreiber, A. Watts, D. Braun and S. Duhr (2013). "Microscale thermophoresis quantifies biomolecular interactions under previously challenging conditions." Methods **59**(3): 301-315.

Settembre, C., C. Di Malta, V. A. Polito, M. Garcia Arencibia, F. Vetrini, S. Erdin, S. U. Erdin, T. Huynh, D. Medina, P. Colella, M. Sardiello, D. C. Rubinsztein and A. Ballabio (2011). "TFEB links autophagy to lysosomal biogenesis." Science **332**(6036): 1429-1433.

Settembre, C., R. Zoncu, D. L. Medina, F. Vetrini, S. Erdin, S. Erdin, T. Huynh, M. Ferron, G. Karsenty, M. C. Vellard, V. Facchinetti, D. M. Sabatini and A. Ballabio (2012). "A lysosome-to-nucleus signalling mechanism senses and regulates the lysosome via mTOR and TFEB." EMBO J **31**(5): 1095-1108.

Shen, W. J., S. Azhar and F. B. Kraemer (2018). "SR-B1: A Unique Multifunctional Receptor for Cholesterol Influx and Efflux." Annu Rev Physiol **80**: 95-116.

Shio, H., N. J. Haley and S. Fowler (1979). "Characterization of lipid-laden aortic cells from cholesterol-fed rabbits. III. Intracellular localization of cholesterol and cholesteryl ester." Lab Invest **41**(2): 160-167.

Sidransky, E., M. A. Nalls, J. O. Aasly, J. Aharon-Peretz, G. Annesi, E. R. Barbosa, A. Bar-Shira, D. Berg, J. Bras, A. Brice, C. M. Chen, L. N. Clark, C. Condroyer, E. V. De Marco, A. Durr, M. J. Eblan, S. Fahn, M. J. Farrer, H. C. Fung, Z. Gan-Or, T. Gasser, R. Gershoni-Baruch, N. Giladi, A. Griffith, T. Gurevich, C. Januario, P. Kropp, A. E. Lang, G. J. Lee-Chen, S. Lesage, K. Marder, I. F. Mata, A. Mirelman, J. Mitsui, I. Mizuta, G. Nicoletti, C. Oliveira, R. Ottman, A. Orr-Urtreger, L. V. Pereira, A. Quattrone, E. Rogaeva, A. Rolfs, H. Rosenbaum, R. Rozenberg, A. Samii, T. Samaddar, C. Schulte, M. Sharma, A. Singleton, M. Spitz, E. K. Tan, N. Tayebi, T. Toda, A. R. Troiano, S. Tsuji, M. Wittstock, T. G. Wolfsberg, Y. R. Wu, C. P. Zabetian, Y. Zhao and S. G. Ziegler (2009). "Multicenter analysis of glucocerebrosidase mutations in Parkinson's disease." N Engl J Med **361**(17): 1651-1661.

Sidransky, E., D. M. Sherer and E. I. Ginns (1992). "Gaucher disease in the neonate: a distinct Gaucher phenotype is analogous to a mouse model created by targeted disruption of the glucocerebrosidase gene." Pediatr Res **32**(4): 494-498.

Silverstein, R. L. and M. Febbraio (2009). "CD36, a scavenger receptor involved in immunity, metabolism, angiogenesis, and behavior." Sci Signal **2**(72): re3.

Skowyra, M. L., P. H. Schlesinger, T. V. Naismith and P. I. Hanson (2018). "Triggered recruitment of ESCRT machinery promotes endolysosomal repair." Science **360**(6384).

Sleat, D. E., Y. Wang, I. Sohar, H. Lackland, Y. Li, H. Li, H. Zheng and P. Lobel (2006). "Identification and validation of mannose 6-phosphate glycoproteins in human plasma reveal a wide range of lysosomal and non-lysosomal proteins." Mol Cell Proteomics **5**(10): 1942-1956.

Sleat, D. E., H. Zheng and P. Lobel (2007). "The human urine mannose 6-phosphate glycoproteome." Biochim Biophys Acta **1774**(3): 368-372.

Slee, J. A. and T. P. Levine (2019). "Systematic prediction of FFAT motifs across eukaryote proteomes identifies nucleolar and eisosome proteins with the predicted capacity to form bridges to the endoplasmic reticulum." Contact (Thousand Oaks) **2**: 1-21.

Small, D. M. (1988). "George Lyman Duff memorial lecture. Progression and regression of atherosclerotic lesions. Insights from lipid physical biochemistry." Arteriosclerosis **8**(2): 103-129.

Smith, A. E. and A. Helenius (2004). "How viruses enter animal cells." Science **304**(5668): 237-242.

Sokol, J., J. Blanchette-Mackie, H. S. Kruth, N. K. Dwyer, L. M. Amende, J. D. Butler, E. Robinson, S. Patel, R. O. Brady, M. E. Comly and et al. (1988). "Type C Niemann-Pick disease. Lysosomal accumulation and defective intracellular mobilization of low density lipoprotein cholesterol." J Biol Chem **263**(7): 3411-3417.

Spann, N. J., L. X. Garmire, J. G. McDonald, D. S. Myers, S. B. Milne, N. Shibata, D. Reichart, J. N. Fox, I. Shaked, D. Heudobler, C. R. Raetz, E. W. Wang, S. L. Kelly, M. C. Sullards, R. C. Murphy, A. H. Merrill, Jr., H. A. Brown, E. A. Dennis, A. C. Li, K. Ley, S. Tsimikas, E. Fahy, S. Subramaniam, O. Quehenberger, D. W. Russell and C. K. Glass (2012). "Regulated accumulation of desmosterol integrates macrophage lipid metabolism and inflammatory responses." Cell **151**(1): 138-152.

Stancu, C. and A. Sima (2001). "Statins: mechanism of action and effects." J Cell Mol Med **5**(4): 378-387.

Stephen, T. L., M. Cacciottolo, D. Balu, T. E. Morgan, M. J. LaDu, C. E. Finch and C. J. Pike (2019). "APOE genotype and sex affect microglial interactions with plaques in Alzheimer's disease mice." Acta Neuropathol Commun **7**(1): 82.

Sturley, S. L., M. C. Patterson, W. Balch and L. Liscum (2004). "The pathophysiology and mechanisms of NP-C disease." Biochim Biophys Acta **1685**(1-3): 83-87.

Suzuki, E., K. Handa, M. S. Toledo and S. Hakomori (2004). "Sphingosine-dependent apoptosis: a unified concept based on multiple mechanisms operating in concert." Proc Natl Acad Sci U S A **101**(41): 14788-14793.

Tabas, I. (2004). "Apoptosis and plaque destabilization in atherosclerosis: the role of macrophage apoptosis induced by cholesterol." Cell Death Differ **11 Suppl 1**: S12-16.

Tai, L. M., S. Ghura, K. P. Koster, V. Liakaite, M. Maienschein-Cline, P. Kanabar, N. Collins, M. Ben-Aissa, A. Z. Lei, N. Bahroos, S. J. Green, B. Hendrickson, L. J. Van Eldik and M. J. LaDu (2015). "APOE-modulated Abeta-induced neuroinflammation in Alzheimer's disease: current landscape, novel data, and future perspective." J Neurochem **133**(4): 465-488.

Takamune, N., T. Kuroe, N. Tanada, S. Shoji and S. Misumi (2010). "Suppression of human immunodeficiency virus type-1 production by coexpression of catalytic-region-deleted N-myristoyltransferase mutants." Biol Pharm Bull **33**(12): 2018-2023.

Takeda, K., H. Miyatake, N. Yokota, S. Matsuyama, H. Tokuda and K. Miki (2003). "Crystal structures of bacterial lipoprotein localization factors, LolA and LolB." EMBO J **22**(13): 3199-3209.

Tangirala, R. K., W. G. Jerome, N. L. Jones, D. M. Small, W. J. Johnson, J. M. Glick, F. H. Mahlberg and G. H. Rothblat (1994). "Formation of cholesterol monohydrate crystals in macrophage-derived foam cells." J Lipid Res **35**(1): 93-104.

Tao, N., S. J. Wagner and D. M. Lublin (1996). "CD36 is palmitoylated on both N- and C-terminal cytoplasmic tails." J Biol Chem **271**(37): 22315-22320.

Tate, E. W., A. S. Bell, M. D. Rackham and M. H. Wright (2014). "N-Myristoyltransferase as a potential drug target in malaria and leishmaniasis." Parasitology **141**(1): 37-49.

Tharkeshwar, A. K., J. Trekker, W. Vermeire, J. Pauwels, R. Sannerud, D. A. Priestman, D. Te Vruchte, K. Vints, P. Baatsen, J. P. Decuypere, H. Lu, S. Martin, P. Vangheluwe, J. V. Swinnen, L. Lagae, F. Impens, F. M. Platt, K. Gevaert and W. Annaert (2017). "A novel approach to analyze lysosomal dysfunctions through subcellular proteomics and lipidomics: the case of NPC1 deficiency." Sci Rep **7**: 41408.

Thelen, A. M. and R. Zoncu (2017). "Emerging Roles for the Lysosome in Lipid Metabolism." Trends Cell Biol **27**(11): 833-850.

Thinon, E., R. A. Serwa, M. Broncel, J. A. Brannigan, U. Brassat, M. H. Wright, W. P. Heal, A. J. Wilkinson, D. J. Mann and E. W. Tate (2014). "Global profiling of co- and post-translationally N-myristoylated proteomes in human cells." Nat Commun **5**: 4919.

Thorne, R. F., K. J. Ralston, C. E. de Bock, N. M. Mhaidat, X. D. Zhang, A. W. Boyd and G. F. Burns (2010). "Palmitoylation of CD36/FAT regulates the rate of its post-transcriptional processing in the endoplasmic reticulum." Biochim Biophys Acta **1803**(11): 1298-1307.

Trinh, M. N., M. S. Brown, J. Seemann, J. L. Goldstein and F. Lu (2018). "Lysosomal cholesterol export reconstituted from fragments of Niemann-Pick C1." Elife **7**.

Tschantz, W. R., J. A. Digits, H. J. Pyun, R. M. Coates and P. J. Casey (2001). "Lysosomal prenylcysteine lyase is a FAD-dependent thioether oxidase." J Biol Chem **276**(4): 2321-2324.

Tybulewicz, V. L., M. L. Tremblay, M. E. LaMarca, R. Willemsen, B. K. Stubblefield, S. Winfield, B. Zablocka, E. Sidransky, B. M. Martin, S. P. Huang and et al. (1992). "Animal model of Gaucher's disease from targeted disruption of the mouse glucocerebrosidase gene." Nature **357**(6377): 407-410.

Underwood, K. W., N. L. Jacobs, A. Howley and L. Liscum (1998). "Evidence for a cholesterol transport pathway from lysosomes to endoplasmic reticulum that is independent of the plasma membrane." J Biol Chem **273**(7): 4266-4274.

Urnov, F. D. (2018). "Genome Editing B.C. (Before CRISPR): Lasting Lessons from the "Old Testament"." CRISPR J **1**(1): 34-46.

Uttamapinant, C., A. Tangpeerachaikul, S. Grecian, S. Clarke, U. Singh, P. Slade, K. R. Gee and A. Y. Ting (2012). "Fast, cell-compatible click chemistry with copper-chelating azides for biomolecular labeling." Angew Chem Int Ed Engl **51**(24): 5852-5856.

Valdez-Taubas, J. and H. Pelham (2005). "Swf1-dependent palmitoylation of the SNARE Tlg1 prevents its ubiquitination and degradation." EMBO J **24**(14): 2524-2532.

Valm, A. M., S. Cohen, W. R. Legant, J. Melunis, U. Hershberg, E. Wait, A. R. Cohen, M. W. Davidson, E. Betzig and J. Lippincott-Schwartz (2017). "Applying systems-level spectral imaging and analysis to reveal the organelle interactome." Nature **546**(7656): 162-167.

van Meer, G., D. R. Voelker and G. W. Feigenson (2008). "Membrane lipids: where they are and how they behave." Nat Rev Mol Cell Biol **9**(2): 112-124.

Vance, J. E. (1990). "Phospholipid synthesis in a membrane fraction associated with mitochondria." J Biol Chem **265**(13): 7248-7256.

Vanier, M. T., P. Gissen, P. Bauer, M. J. Coll, A. Burlina, C. J. Hendriksz, P. Latour, C. Goizet, R. W. Welford, T. Marquardt and S. A. Kolb (2016). "Diagnostic tests for Niemann-Pick disease type C (NP-C): A critical review." Mol Genet Metab **118**(4): 244-254.

Vanier, M. T. and G. Millat (2004). "Structure and function of the NPC2 protein." Biochim Biophys Acta **1685**(1-3): 14-21.

Vassilev, B., H. Sihto, S. Li, M. Holtta-Vuori, J. Ilola, J. Lundin, J. Isola, P. L. Kellokumpu-Lehtinen, H. Joensuu and E. Ikonen (2015). "Elevated levels of StAR-related lipid transfer protein 3 alter cholesterol balance and adhesiveness of breast cancer cells: potential mechanisms contributing to progression of HER2-positive breast cancers." Am J Pathol **185**(4): 987-1000.

Vega, M. A., F. Rodriguez, B. Segui, C. Cales, J. Alcalde and I. V. Sandoval (1991). "Targeting of lysosomal integral membrane protein LIMP II. The tyrosine-lacking carboxyl cytoplasmic tail of LIMP II is sufficient for direct targeting to lysosomes." J Biol Chem **266**(25): 16269-16272.

Verardi, R., J. S. Kim, R. Ghirlando and A. Banerjee (2017). "Structural Basis for Substrate Recognition by the Ankyrin Repeat Domain of Human DHHC17 Palmitoyltransferase." Structure **25**(9): 1337-1347 e1336.

Vieira, O. V., R. J. Botelho and S. Grinstein (2002). "Phagosome maturation: aging gracefully." Biochem J **366**(Pt 3): 689-704.

Visvikis, O., N. Ihuegbu, S. A. Labed, L. G. Luhachack, A. F. Alves, A. C. Wollenberg, L. M. Stuart, G. D. Stormo and J. E. Irazoqui (2014). "Innate host defense requires TFEB-mediated transcription of cytoprotective and antimicrobial genes." Immunity **40**(6): 896-909.

Vogelstein, B., D. Lane and A. J. Levine (2000). "Surfing the p53 network." Nature **408**(6810): 307-310.

Walther, T. C., J. Chung and R. V. Farese, Jr. (2017). "Lipid Droplet Biogenesis." Annu Rev Cell Dev Biol **33**: 491-510.

Wang, C. W. (2016). "Lipid droplets, lipophagy, and beyond." Biochim Biophys Acta **1861**(8 Pt B): 793-805.

Wang, J., J. W. Hao, X. Wang, H. Guo, H. H. Sun, X. Y. Lai, L. Y. Liu, M. Zhu, H. Y. Wang, Y. F. Li, L. Y. Yu, C. Xie, H. R. Wang, W. Mo, H. M. Zhou, S. Chen, G. Liang and T. J. Zhao (2019). "DHHC4 and DHHC5 Facilitate Fatty Acid Uptake by Palmitoylating and Targeting CD36 to the Plasma Membrane." Cell Rep **26**(1): 209-221 e205.

Webb, Y., L. Hermida-Matsumoto and M. D. Resh (2000). "Inhibition of protein palmitoylation, raft localization, and T cell signaling by 2-bromopalmitate and polyunsaturated fatty acids." J Biol Chem **275**(1): 261-270.

Wei, Y., Z. J. Xiong, J. Li, C. Zou, C. W. Cairo, J. S. Klassen and G. G. Prive (2019). "Crystal structures of human lysosomal EPDR1 reveal homology with the superfamily of bacterial lipoprotein transporters." Commun Biol **2**: 52.

Weill, U., G. Krieger, Z. Avihou, R. Milo, M. Schuldiner and D. Davidi (2019). "Assessment of GFP Tag Position on Protein Localization and Growth Fitness in Yeast." J Mol Biol **431**(3): 636-641.

Weinreb, N. J., R. O. Brady and A. L. Tappel (1968). "The lysosomal localization of sphingolipid hydrolases." Biochim Biophys Acta **159**(1): 141-146.

Widenmaier, S. B., N. A. Snyder, T. B. Nguyen, A. Arduini, G. Y. Lee, A. P. Arruda, J. Saksi, A. Bartelt and G. S. Hotamisligil (2017). "NRF1 Is an ER Membrane Sensor that Is Central to Cholesterol Homeostasis." Cell **171**(5): 1094-1109 e1015.

Wilhelm, L. P., C. Wendling, B. Vedie, T. Kobayashi, M. P. Chenard, C. Tomasetto, G. Drin and F. Alpy (2017). "STARD3 mediates endoplasmic reticulum-to-endosome cholesterol transport at membrane contact sites." EMBO J **36**(10): 1412-1433.

Wilkening, G., T. Linke, G. Uhlhorn-Dierks and K. Sandhoff (2000). "Degradation of membrane-bound ganglioside GM1. Stimulation by bis(monoacylglycero)phosphate and the activator proteins SAP-B and GM2-AP." J Biol Chem **275**(46): 35814-35819.

Winkler, M. B. L., R. T. Kidmose, M. Szomek, K. Thaysen, S. Rawson, S. P. Muench, D. Wustner and B. P. Pedersen (2019). "Structural Insight into Eukaryotic Sterol Transport through Niemann-Pick Type C Proteins." Cell **179**(2): 485-497 e418.

Wittig, I., H. P. Braun and H. Schagger (2006). "Blue native PAGE." Nat Protoc **1**(1): 418-428.

Wolozin, B. (2004). "Cholesterol and the biology of Alzheimer's disease." Neuron **41**(1): 7-10.

Won, S. J., M. Cheung See Kit and B. R. Martin (2018). "Protein depalmitoylases." Crit Rev Biochem Mol Biol **53**(1): 83-98.

Wright, M. H., B. Clough, M. D. Rackham, K. Rangachari, J. A. Brannigan, M. Grainger, D. K. Moss, A. R. Bottrill, W. P. Heal, M. Broncel, R. A. Serwa, D. Brady, D. J. Mann, R. J. Leatherbarrow, R. Tewari, A. J. Wilkinson, A. A. Holder and E. W. Tate (2014). "Validation of N-myristoyltransferase as an antimalarial drug target using an integrated chemical biology approach." Nat Chem **6**(2): 112-121.

Wu, H., P. Carvalho and G. K. Voeltz (2018). "Here, there, and everywhere: The importance of ER membrane contact sites." Science **361**(6401).

Xiong, X., C. F. Lee, W. Li, J. Yu, L. Zhu, Y. Kim, H. Zhang and H. Sun (2019). "Acid Sphingomyelinase regulates the localization and trafficking of palmitoylated proteins." Biol Open **8**(10).

Xu, C., C. Zhang, J. Ji, C. Wang, J. Yang, B. Geng, T. Zhao, H. Zhou, X. Mu, J. Pan, S. Hu, Y. Lv, X. Chen, H. Wen and Q. You (2018). "CD36 deficiency attenuates immune-mediated hepatitis in mice by modulating the proapoptotic effects of CXC chemokine ligand 10." Hepatology **67**(5): 1943-1955.

Xu, R., J. Jin, W. Hu, W. Sun, J. Bielawski, Z. Szulc, T. Taha, L. M. Obeid and C. Mao (2006). "Golgi alkaline ceramidase regulates cell proliferation and survival by controlling levels of sphingosine and S1P." FASEB J **20**(11): 1813-1825.

Xu, S., B. Benoff, H. L. Liou, P. Lobel and A. M. Stock (2007). "Structural basis of sterol binding by NPC2, a lysosomal protein deficient in Niemann-Pick type C2 disease." J Biol Chem **282**(32): 23525-23531.

Yamamoto, Y., Y. Chochi, H. Matsuyama, S. Eguchi, S. Kawauchi, T. Furuya, A. Oga, J. J. Kang, K. Naito and K. Sasaki (2007). "Gain of 5p15.33 is associated with progression of bladder cancer." Oncology **72**(1-2): 132-138.

Yamayoshi, S., S. Iizuka, T. Yamashita, H. Minagawa, K. Mizuta, M. Okamoto, H. Nishimura, K. Sanjoh, N. Katsushima, T. Itagaki, Y. Nagai, K. Fujii and S. Koike (2012). "Human SCARB2-dependent infection by coxsackievirus A7, A14, and A16 and enterovirus 71." J Virol **86**(10): 5686-5696.

Yamayoshi, S., Y. Yamashita, J. Li, N. Hanagata, T. Minowa, T. Takemura and S. Koike (2009). "Scavenger receptor B2 is a cellular receptor for enterovirus 71." Nat Med **15**(7): 798-801.

Yan, S. M., J. J. Tang, C. Y. Huang, S. Y. Xi, M. Y. Huang, J. Z. Liang, Y. X. Jiang, Y. H. Li, Z. W. Zhou, I. Ernberg, Q. L. Wu and Z. M. Du (2013). "Reduced expression of ZDHHC2 is associated with lymph node metastasis and poor prognosis in gastric adenocarcinoma." PLoS One **8**(2): e56366.

Yang, C., J. G. McDonald, A. Patel, Y. Zhang, M. Umetani, F. Xu, E. J. Westover, D. F. Covey, D. J. Mangelsdorf, J. C. Cohen and H. H. Hobbs (2006). "Sterol intermediates from cholesterol biosynthetic pathway as liver X receptor ligands." J Biol Chem **281**(38): 27816-27826.

Yang, W., D. Di Vizio, M. Kirchner, H. Steen and M. R. Freeman (2010). "Proteome scale characterization of human S-acylated proteins in lipid raft-enriched and non-raft membranes." Mol Cell Proteomics **9**(1): 54-70.

Yanjanin, N. M., J. I. Velez, A. Gropman, K. King, S. E. Bianconi, S. K. Conley, C. C. Brewer, B. Solomon, W. J. Pavan, M. Arcos-Burgos, M. C. Patterson and F. D. Porter (2010). "Linear clinical progression, independent of age of onset, in Niemann-Pick disease, type C." Am J Med Genet B Neuropsychiatr Genet **153B**(1): 132-140.

Yeagle, P. L. (2004). The structure of biological membranes, CRC press.

Yeste-Velasco, M., X. Mao, R. Grose, S. C. Kudahetti, D. Lin, J. Marzec, N. Vasiljevic, T. Chaplin, L. Xue, M. Xu, J. M. Foster, S. S. Karnam, S. Y. James, A. M. Chioni, D. Gould, A. T. Lorincz, R. T. Oliver, C. Chelala, G. M. Thomas, J. M. Shipley, S. J. Mather, D. M. Berney, B. D. Young and Y. J. Lu (2014). "Identification of ZDHHC14 as a novel human tumour suppressor gene." J Pathol **232**(5): 566-577.

Yokoi, N., Y. Fukata, A. Sekiya, T. Murakami, K. Kobayashi and M. Fukata (2016). "Identification of PSD-95 Depalmitoylating Enzymes." J Neurosci **36**(24): 6431-6444.

York, A. G. and S. J. Bensinger (2013). "Subverting sterols: rerouting an oxysterol-signaling pathway to promote tumor growth." J Exp Med **210**(9): 1653-1656.

Yount, J. S., B. Moltedo, Y. Y. Yang, G. Charron, T. M. Moran, C. B. Lopez and H. C. Hang (2010). "Palmitoylome profiling reveals S-palmitoylation-dependent antiviral activity of IFITM3." Nat Chem Biol **6**(8): 610-614.

Yu, F. P. S., S. Amintas, T. Levade and J. A. Medin (2018). "Acid ceramidase deficiency: Farber disease and SMA-PME." Orphanet J Rare Dis **13**(1): 121.

Zaballa, M. E. and F. G. van der Goot (2018). "The molecular era of protein S-acylation: spotlight on structure, mechanisms, and dynamics." Crit Rev Biochem Mol Biol **53**(4): 420-451.

Zachos, C., J. Blanz, P. Saftig and M. Schwake (2012). "A critical histidine residue within LIMP-2 mediates pH sensitive binding to its ligand beta-glucocerebrosidase." Traffic **13**(8): 1113-1123.

Zha, J., S. Weiler, K. J. Oh, M. C. Wei and S. J. Korsmeyer (2000). "Posttranslational N-myristoylation of BID as a molecular switch for targeting mitochondria and apoptosis." Science **290**(5497): 1761-1765.

Zhao, H. and G. A. Grabowski (2002). "Gaucher disease: Perspectives on a prototype lysosomal disease." Cell Mol Life Sci **59**(4): 694-707.

Zhao, Y., J. Ren, S. Padilla-Parra, E. E. Fry and D. I. Stuart (2014). "Lysosome sorting of beta-glucocerebrosidase by LIMP-2 is targeted by the mannose 6-phosphate receptor." Nat Commun **5**: 4321.

Zoncu, R., L. Bar-Peled, A. Efeyan, S. Wang, Y. Sancak and D. M. Sabatini (2011). "mTORC1 senses lysosomal amino acids through an inside-out mechanism that requires the vacuolar H(+)-ATPase." Science **334**(6056): 678-683.

Zunke, F.(2015). CHARACTERISATION OF THE LYSOSOMAL INTEGRAL MEMBRANE PROTEIN TYPE-2 (LIMP-2) AND ITS INTERACTION WITH β-GLUCOCEREBROSIDASE: IMPLICATIONS FOR PARKINSON AND GAUCHER DISEASE. PhD, Christian-Albrechts-University Kiel.

Zunke, F., L. Andresen, S. Wesseler, J. Groth, P. Arnold, M. Rothaug, J. R. Mazzulli, D. Krainc, J. Blanz, P. Saftig and M. Schwake (2016). "Characterization of the complex formed by beta-glucocerebrosidase and the lysosomal integral membrane protein type-2." Proc Natl Acad Sci U S A **113**(14): 3791-3796.

9. Appendix

9.1. List of Abbreviations

°C	Degree Celsius
-/-	Knockout
+/+	Wild type
µg	Microgram
µl	Microliter
µm	Micrometer
aa	Amino acid(s)
AP	adaptor protein complex
AMRF	Action Myoclonus Renal Failure Syndrome
ApoE	Apolipoprotein E
BCA	Bicinchoninic acid
CD36	cluster of differentiation 36
cDNA	Complementary DNA
Cer	Ceramide
Co-IP	Co-immunoprecipitation
CRISPR/Cas	Clustered regularly interspaced short palindromic repeats (CRISPR)/CRISPR-associated (Cas)
C.-t.	carboxy-terminus
Da	Dalton
DABCO	1,4-diazabicyclo[2.2.2]octane
DAPI	4-,6-diamidino-2-phenylindole
ddH_2O	double-distilled water
DHHC PAT	DHHC protein S-acyltransferase
DMEM	Dulbecco's modified Eagle Medium
DMSO	Dimethyl sulfoxide
DNA	Deoxyribonucleic acid
E. coli	*Escherichia coli*
EDTA	ethylenediaminetetraacetic acid
ER	Endoplasmic reticulum
ESCRT	endosomal sorting complex required for transport
EV71	Enterovirus71
FFAT	two phenylalanines (FF) in an acidic tract (AT)

GalChol	galactosyl-β-D-cholesterol
GCase	Lysosomal β-glucocerebrosidase (GBA1)
GlcSph	Glucosylsphingosine
GD	Gaucher disease
GFP	Green fluorescent protein
GluCer	Glucosylceramide
GlcChol	glucosyl-*β*-D-cholesterol/1-*O*-cholesteryl- *β*-D-glucopyranoside
h	Hour(s)
HeLa	Henrietta Lacks (cervical cancer cell line)
His	Histidine
HMGCR	3-hydroxyl-3-methylglutaryl (HMG-)-CoA reductase
IF	Immunofluorescence
INSIG1	insulin-induced gene 1
kDa	kilodalton
LAL	Lysosomal acid lipase
LAMP1/2	Lysosome-associated membrane protein 1/2
LBPA/BMP	Lysobisphosphaditic acid / bis-(monoacylglyceryl)-phosphate
LDL	Low-density lipoprotein
LDLR	Low-density lipoprotein receptor
LIMP-2	Lysosomal integral membrane protein type 2
LY	Lysosome
OD	optical density
OSBP	oxysterol-binding protein
M	Molar
MCS	Membrane contact site(s)
MEF	Mouse embryonic fibroblast
mM	Millimolar
mRNA	Messenger RNA
MVB	Multivesicular body
NaCl	Sodium chloride
NaOH	Sodium hydroxide
ng	Nanogram
nm	nanometer
nM	Nanomolar
NP-40	Nonidet P-40
NPC1/2	Niemann Pick Type C1/2 proteins
N.-t.	Amino terminus

PAGE	polyacrylamide gel electrophoresis
PB	Phosphate buffer
PBS	Phosphate-buffered saline
PCR	Polymerase chain reaction
PFA	Paraformaldehyde
PM	Plasma membrane
PtdIns(4,5)P2	Phosphatidylinositol-4,5-bisphosphate
PTM	post-translational modification
RNA	ribonucleic acid
rpm	Revolutions per minute
Sap	Saposin
SCAP	Sterol regulatory element binding protein cleavage activating protein
SCARB	scavenger receptor class B
SDS	sodiumdodecylsulfate
SEM	Standard error of the mean
siRNA	Small interfering ribonucleic acid
SREBP2	Sterol regulatory element binding protein
SR-BI	Scavenger receptor class B type I
STARD3	StAR Related Lipid Transfer Domain Containing 3
TAE	Tris-acetate-EDTA
TBS	Tris-buffered saline
TEV	Tobacco etch virus
TMD	Transmembrane domain
Tris	Tris(hydroxymethyl)aminomethane
U	unit
VAP A and B	vesicle-associated membrane protein-associated proteins A and B
v/v	volume per volume
Wnt	Wingless/in
WT	wild type
w/v	weight per volume

Generally used abbreviations are not listed.

9.2. List of Figures

9.3. List of Tables

9.4. Publications

Publications containing data or images depicted in this thesis:

Heybrock, S.*, K. Kanerva*, Y. Meng*, C. Ing, A. Liang, Z. J. Xiong, X. Weng, Y. Ah Kim, R. Collins, W. Trimble, R. Pomes, G. G. Prive, W. Annaert, M. Schwake, J. Heeren, R. Lullmann-Rauch, S. Grinstein, E. Ikonen, P. Saftig, and D. Neculai. 2019. 'Lysosomal integral membrane protein-2 (LIMP-2/SCARB2) is involved in lysosomal cholesterol export', *Nat Commun*, 10: 3521 https://doi.org/10.1038/s41467-019-11425-0

*Shared first authors

Meng, Y.*, **S. Heybrock***, D. Neculai, and P. Saftig. 2020. 'Cholesterol Handling in Lysosomes and Beyond', *Trends Cell Biol*, 30: 452-66 https://doi.org/10.1016/j.tcb.2020.02.007

*Shared first authors

Publications containing data not depicted in this dissertation:

Conrad, K. S., T. W. Cheng, D. Ysselstein, **S. Heybrock**, L. R. Hoth, B. A. Chrunyk, C. W. A. Ende, D. Krainc, M. Schwake, P. Saftig, S. P. Liu, X. Y. Qiu, and M. D. Ehlers. 2017. 'Lysosomal integral membrane protein-2 as a phospholipid receptor revealed by biophysical and cellular studies', *Nature Communications*, 8, 1908 DOI: 10.1038/s41467-017-02044-8

10. Acknowledgements

First of all, I would like to thank Prof. Dr. Paul Saftig for providing me with the opportunity to work in his research group on this exciting and challenging topic. His continuous advice, encouragement and support regarding all aspects of this work hugely contributed to an optimal working environment.

I would also like to thank Prof. Dr. Eric Beitz for reviewing this thesis.

I'd like to express my gratitude towards PD Dr. Markus Damme for his support and insightful & dynamic discussions.

I am grateful to have been part of a great group of scientists interested in LIMP-2 biology. I'm very happy I got to spend time in Prof. Dr. Elina Ikonen's lab in Helsinki and in Prof. Dr. Dante Neculai's lab in Hangzhou and work together with Dr. Kristiina Kanerva and Dr. Ying Meng. Girls, it was an honor to meet you, learn from and with you & to go on adventures with you. I sincerely hope we meet again someday!

I'd like to thank our other collaborators as well: Prof. Dr. Judith Klumperman and Dr. Nalan Liv from the University Medical Center Utrecht as well as Prof. Dr. Renate Lüllmann-Rauch from CAU Kiel for providing their EM expertise; PD Dr. Michael Schwake for the data on the LIMP-2 KI mice; Prof. Dr. Jörg Heeren and Sandra Ehret from UKE Hamburg for providing me with LDL and LPDS; Dr. Jan Michels from CAU Kiel for his microscopy expertise.

I am happy to have been part of the research units GRK1459 and FOR2625 through which I have met a bunch of fun students and scientists and learned a lot through the organized lectures and symposia. Thank you to the organizing committee, particularly Dr. Dorthe Labonté and Prof. Dr. Thomas Braulke.

During the nearly five years of my PhD thesis I was honored to meet numerous inspiring scientists. In particular, I would like to thank Prof. Dr. Sergio Grinstein and Prof. Dr. Johannes M.F.G. Aerts for sharing their knowledge and ideas and passion for science.

I'm glad to have shared the trials & tribulations of lab life as well as the celebrations, the sunny lunch breaks & beer tastings with a great group of co-workers and friends. To the former and present members of AG Saftig- thank you for a wonderful time. To my conference buddies Sandra, Adri, André, Cedric and David – cheers to great memories!

I'm indebted to Meryem, my lab twin, for keeping my head above water. I'm happy we got to share many laughs and the occasional sigh in R107. To my office and lab buddy Lisor: Thanks for all the encouragement and interesting discussions!

I had the opportunity to supervise and work with a great group of students: To Marie, Gerlis and Jessica- thanks for making supervising fun & all the best to you! To my trainee Sophie: Thanks so much for all your help! I'm very glad to have been part of your practical training.

Thank you to Prof. Dr. Danja Schünemann, Silke Funke and Dr. Beatrix Dünschede for introducing me to the world of protein biochemistry and teaching me how to science during my Bachelor's and Master's thesis.

Finally, I would like to express my deepest gratitude to my family and friends for the support and encouragement throughout the last five years. Special thanks to my husband Büßen for believing in me and always having my back.

11. Declaration

I hereby declare that apart from guidance from my supervisor, Prof. Dr. Paul Saftig, the content and design of this thesis is my own work. Contribution of other persons to generated data depicted in this thesis is explicitly indicated. Information derived from scientific publications is properly credited. I furthermore confirm the following:

- This thesis (partially or complete) has not been submitted elsewhere as a part of an examination procedure to obtain a doctoral degree.
- Parts of this thesis have been published in scientific journal articles (indicated in 9.4).
- This thesis was created according to the Rules of Good Scientific Practice of the German Research Foundation.
- No academic degree has been withdrawn.

Kiel, August 2020

Saskia Heybrock